Diss. ETH No. 13989

TRANSPORT AND TRANSFORMATION PROCESSES IN COMBINED SEWERS

A DISSERTATION SUBMITTED TO THE

SWISS FEDERAL INSTITUTE OF TECHNOLOGY
ZURICH

for the degree of

DOCTOR OF TECHNICAL SCIENCES

presented by

JACCO L. HUISMAN

Chemical Engineer (ir.)
Delft University of Technology
born on Januar 6, 1969
citizen of The Netherlands

accepted on the recommendation of
Prof. Dr. Willi Gujer, examiner
Prof. Dr. Peter Krebs, co-examiner

Zürich, 2001

Abstract

Introduction

Although most people regard the sewer system merely as the transport system for wastewater to the treatment plant, it is actually a biological, chemical and physical reactor. Traditionally, most research efforts in wastewater treatment were directed towards the design and control of wastewater treatment plants. The conversion processes that occur during sewer transport were essentially ignored.

The aim of this work

Recently, urban water management has gained much interest. Urban water management deals with facets of the water cycle related to urbanisation. However, quantitative information about sewer processes is scarce. The purpose of this project was to obtain a more fundamental understanding of the processes that underlie the changes in wastewater properties as this water flows to the wastewater treatment plant. The information is then used to develop a deterministic model. Emphasis is placed on the role of the biofilm or 'slime layer' growing on the sewer wall.

The question adressed by this research project is, 'What is the impact of the sewer system on the wastewater composition?'

Methodology

The full-scale investigations were mainly performed in a two kilometre main sewer. Firstly, the wastewater composition was determined in-line or after sampling and analysis. Secondly, the biofilm properties were determined. Thirdly, an *in situ* flow cell was used to quantify the biofilm activity directly in the sewer. And fourthly, these methods were extended with laboratory measurements of suspended and intact biofilm in a specifically designed flow cell. Finally, a new method for sewer system reaeration measurements based on the inert gas sulphur hexafluoride was introduced and tested. The results formed the foundation for a mechanistic model.

Wastewater concentration changes

The sewer proved to be a highly dynamic system. Concentration changes due to random variations in a time frame of minutes were often larger than the changes due to conversion processes. High frequency sampling (with an interval of two minutes) revealed that consistent and significant changes could be observed only for nitrate, nitrite and oxygen. It is therefore not recommended to quantify the sewer conversion processes by sampling and concentration changes.

Biofilm properties and activity

The sewer biofilm can maintain many physiological microbial groups. Most of the activity in the (aerobic) study reach can be attributed to heterotrophic biomass. The activity of sulphur reducing and oxidising bacteria could be quantified but proved to play only a minor role in the overall oxygen and COD* balance. The shear stress distribution, abrasive force of particles and fats floating on the water induced a clear radial profile of the biofilm biomass. However, the aerobic activity was constant and comparable with a trickling filter biofilm. Only the top layer of the biofilm relied on hydrolysed substrate from the wastewater. The deeper strata used trapped organic particles.

Oxygen balance

The validity of the methods that were adapted and developed was confirmed with a redundant oxygen balance. Further quantification under different hydrodynamic conditions showed that the contribution of the biofilm, wastewater and reaeration oxygen fluxes can vary extensively. The wastewater itself and biofilm contribute significantly to the aerobic conversions. The aerobic total in the study reach was 3%. However, when extrapolated to the entire sewer net of the connected town, the COD conversion was estimated as high as 30% of the dissolved COD during the night.

Sewer model

The experimental results were used to develop a deterministic hydrodynamic and biological sewer model. This model is based on the activated sludge model no. 3 (Gujer *et al.*, 2000). The biofilm mass transfer properties were modelled with the penetration depth approach. This allows for an accurate and fast calculation without many unknown parameters. The model was calibrated and validated for the study reach. It can easily be adapted for sewers with other conditions.

Conclusions

It is not justified to regard the sewers as a transport system only. The influence of the sewer cannot be denied when a large fraction of the wastewater is transformed before it reaches the wastewater treatment plant. Although it does not have the same capacity as the wastewater treatment plant, it should be seen as an extension that should be taken into account when a treatment plant is designed.

*Chemical Oxygen Demand

Zusammenfassung

Einführung

Die Kanalisation wird üblicherweise nur als blosses Transportsystem betrachtet, obwohl sie auch ein biologischer, chemischer und physikalischer Reaktor ist. Die Forschung in der Abwasserreinigung ist traditionell vor allem auf dem Entwurf und die Kontrolle von Kläranlagen ausgerichtet, weshalb quantitative Daten zur Kanalisation fehlen. Die Umwandlungen während des Transportes wurden nicht berücksichtigt. Im Moment steht das Urban Water Management, das das Gesamtsystem betrachtet, im Brennpunkt des Interesses. Die Hauptfrage lautet: "Wie stark beeinflusst die Kanalisation die Eigenschaften des Abwassers?"

Die Ziele dieser Arbeit

In diesem Projekt sollten die Umwandlungsprozesse, denen das Abwasser in der Kanalisation ausgesetzt, untersucht werden. Ziel der Arbeit war ein deterministisches Modell zu erstellen, mit dem die Prozesse in der Kanalisation beschrieben werden können. Besonderes Augenmerk wurde auf den Einfluss des Biofilmes an der Kanalwand gelegt.

Methodik

Die im Grossmassstab durchgeführten Untersuchungen fanden hauptsächlich in einem zwei Kilometer langen Kanal statt. Als erstes wurden die Änderungen in der Abwasserzusammensetzung über die Messstrecke untersucht. Danach wurden die Eigenschaften und Verteilung des Biofilms bestimmt. Als nächstes kam eine Messzelle zum Einsatz, mit welcher direkt die Aktivität des Kanalbiofilms bestimmt werden konnte. Im weiteren wurde im Labor unter kontrollierten Bedingungen die Aktivität der suspendierten Biomasse sowie mit Hilfe einer speziellen Messzelle auch jene des intakten Biofilms gemessen. Zuletzt wurde für die Bestimmung des Gasaustausches eine für die Kanalisation neue Methode eingeführt und überprüft. Die Ergebnisse bildeten die Grundlage für ein Modell im Simulationsprogramm AQUASIM.

Änderungen in der Abwasserzusammensetzung

Die Kanalisation hat sich als ein sehr dynamisches System erwiesen. Zufällige Konzentrationsänderungen waren oft grösser als die Änderungen über die Messstrecke. Probenahmen mit einer hohen Frequenz (in Intervallen von zwei Minuten) ergaben nur konsistente und signifikante Änderungen der Nitrat-, Nitrit- und Sauerstoffkonzentration.

Eigenschaften und Aktivität des Biofilms

Der Biofilm enthält viele physiologisch unterschiedliche mikrobielle Gruppen. Der Hauptanteil der aeroben Aktivität in der (aeroben) Messstrecke ist der heterotrophen Biomasse zuzuschreiben.

Die Aktivität von Schwefel reduzierenden und oxidierenden Bakterien konnte zwar quantifiziert werden, aber sie hatte nur einen kleinen Einfluss auf den gesamten Verbrauch an Sauerstoff und CSB[†]. Die kombinierten Effekte von Schubkraft, Reibung von Partikeln und Fetten im Abwasser verursachten eine klare Verteilung der Biomasse an der Wand über den Kanalquerschnitt. Die aerobe Aktivität war jedoch konstant und vergleichbar mit der eines Tropfkörpers. Nur die äussere Schicht des Biofilms war abhängig vom gelösten Substrat aus dem Abwasser. Die Biomasse in den tieferen Schichten zehrte die eingefangenen Schmutzstoffe.

Sauerstoffbilanzierung

Die Richtigkeit der angewandten Messmethoden wurde mit einer redundanten Sauerstoffbilanz überprüft. Weitere Quantifizierungen unter verschiedenen hydrodynamischen Bedingungen ergaben, dass sowohl der Beitrag des Biofilms, des Abwassers, als auch die Wiederbelüftung durch die Wasseroberfläche an der Gesamtbilanz ganz verschieden sein konnten. Sowohl die Biomasse im Biofilm als auch jene im Abwasser trugen zum Sauerstoffverbrauch bei. Der aerobe CSB-Abbau in der Messstrecke lag im Durchschnitt bei 3%. Wenn dieser jedoch auf das Gesamtnetz des angeschlossen Ortes extrapoliert wird, beläuft sich die CSB-Umwandlung auf bis zu 30% des gelösten CSBs während der Nacht.

Kanalisationsmodell

Mit der Versuchergebnisse wurde ein deterministisches Modell der hydrodynamischen und biologischen Vorgänge im Kanal entwickelt, welches auf dem "Activated Sludge Model No. 3" (Gujer *et al.*, 1999) beruht. Die Stofftransportvorgänge im Biofilm wurden mit dem Ansatz der Penetrationstiefe berechnet. Dieser erlaubt eine gute und schnelle Bestimmung der Vorgänge, ohne dass viele (unbekannte) Parameter berücksichtigt werden müssen. Dieses Modell wurde für die untersuchte Messstrecke kalibriert und validiert. Es kann leicht an andere Kanäle und Bedingungen angepasst werden.

Schlussfolgerungen

Die Kanalisation ist mehr als ein reines Transportsystem. Der Einfluss der Kanalisation auf das Abwasser kann nicht vernachlässigt werden, weil ein beträchtlicher Anteil der Abwasserinhaltsstoffe umgewandelt wird, bevor sie in die Kläranlage gelangen. Obwohl die Abbaukapazität sicher nicht diejenige der Kläranlage erreicht, sollte ihr Einfluss auf die Dimensionierung von Kläranlagen in Betracht gezogen werden.

[†]Chemischen Sauerstoffbedarf

Acknowledgements

A big ***thank you*** to all the people who contributed in one form or the other to this work:

the diploma students and trainees Cristhian Almeida-Rivera, Thomas Gasser, Claudio Gienal, Michele Hale, Liang Hao, Matthias Kühni, Christian Singeisen, Stefan Studer and Nicole Weber without whom many of the experiments would not have been possible.

Claudia Baenninger, Cecile Bernhard, Irene Brunner, Jack Eugster and Dea Vogt for their technical aid and analysis support.

Robert Berger and the EAWAG Workshop team who could always come up with a solution for my wishes.

The municipality of *Rümlang* and especially: Kurt Öhner and his colleagues from the fish farm who kindly supplied electricity, Jacob Keller from the town council and Ruedi Huber (waterworks of Rümlang). All other inhabitants are kindly thanked for supplying the substrate ....

The cantonal and airport police who decided not to arrest me when I was very suspiciously taking dirty water from deep holes during the night next to the airport.

Christian Fux, Ivana Kabelková-Jančárková, Dani Kobler, Gerri Koch, Max Maurer, Leiv Rieger, Donald Tillman and all other people of the Engineering department. Conrad Egli, Markus Hofer, Claude Jacques, Raoul Schaffner, Elisabeth Stuessi and last but not least Monika Zemp. of other departments of the EAWAG.

Peter Krebs for his supervision during the first one-and-a-half year and accepting the job of co-supervisor after his appointment as professor in Dresden.

Finally, I would like to thank Willi Gujer for supervising this doctoral studies. He gave me the freedom to express my own ideas but was always there when I needed help.

To Masako and my parents.

'It's possible to own too much [data]. A man with one watch knows what time it is; a man with two watches is never quite sure.'

-Lee Segall

This document was produced with LaTeX(Knuth, 1984; Lamport, 1986) and the editor WinEdt (written by Aleksander Simonič, http://wwww.winedt.com) and the compiler MiKTeX (port by Christian Schenk, http://www.miktex.org).

Contents, overview

chapter 1: Introduction	1
chapter 2: The sewer as a system	3
chapter 3: Sewer hydrodynamics	13
chapter 4: Sewer research toolkit	21
chapter 5: Wastewater composition changes	35
chapter 6: Biofilm distribution, development and activity	45
chapter 7: Gas-liquid mass transfer in open channels	69
chapter 8: Oxygen balancing in the sewer system	99
chapter 9: Hydrodynamic and biological sewer model	113
chapter 10: Interpretation, conclusion and outlook	137
Bibliography	141
appendix A: Additional Materials and Methods	151
appendix B: Oxygen Uptake Monitor program	163
appendix C: Additional data	165
appendix D: Dynamic biological sewer model	169
appendix E: Applied constants and definitions	173
appendix F: Curriculum Vitae	175
Nomenclature	177
Index	182

Contents

1 Introduction **1**
1.1 Current problems 1
1.2 Goals and questions 1
1.3 Methodology 2
1.4 Outline of this thesis 2

2 The sewer as a system **3**
2.1 Summary 3
2.2 The history of the sewer system 3
2.3 The system 'sewer' 4
2.3.1 Sewer compartments & Interactions 4
2.4 The wastewater 5
2.4.1 Origin and composition 5
2.5 The sewer biofilm 6
2.5.1 Biofilm morphology and mass transfer 6
2.5.2 Processes in the sewer biofilm 8
2.5.3 Biofilm erosion 10
2.6 The sewer as reactor 11
2.7 Sewer mass balance 12

3 Sewer hydrodynamics **13**
3.1 Summary 13
3.2 Selection of the hydrodynamic model 13
3.2.1 The Saint Venant equations 14
3.2.2 Flow equation 14
3.2.3 Wetted biofilm in relation to discharge 16
3.2.4 Biofilm distribution 16
3.2.5 Velocity distribution in open channel flow 17

4 Sewer research toolkit **21**
4.1 Problem description 21
4.2 Fast wastewater sampling 21
4.2.1 Sampling synchronisation 21
4.2.2 Amount of samples 22
4.3 Sewer biofilm sampling 22
4.3.1 Sewer balloon 23
4.3.2 Semi-invasive biofilm sampling: the 'Biofilm box´ 24
4.3.3 Intact Biofilm sampling 24

4.4 In-line measurements . . . 26
4.4.1 Protection of sensors . . . 26
4.4.2 Sensor calibration . . . 27
4.4.3 Flow measurement . . . 27
4.5 Respiration activity of suspended biomass . . . 27
4.5.1 Wastewater batch respiration measurements . . . 28
4.5.2 Continuous wastewater respiration measurement . . . 28
4.6 *In situ* sewer biofilm activity measurement . . . 30
4.6.1 Overall biofilm activity . . . 30
4.6.2 Measuring the benthic activity . . . 30
4.6.3 Sewer *in situ* flow cell . . . 31
4.7 Biofilm flow cell . . . 33
4.7.1 Biofilm Flow Cell (BFC) and supporting system . . . 33
4.8 Other materials and methods . . . 34

5 Wastewater composition changes 35
5.1 Summary . . . 35
5.2 Introduction . . . 35
5.3 Site descriptions . . . 35
5.3.1 Main sewer *Rümlang–Oberglatt* . . . 35
5.3.2 Main sewer *Remigen–Villigen* . . . 36
5.4 Residence time in the sewer . . . 36
5.4.1 The age of the *Rümlang* wastewater up to the measurement section . . 37
5.5 Changes in wastewater properties . . . 38
5.5.1 Sampling and Measurement . . . 38
5.5.2 Sampling with autosamplers . . . 38
5.5.3 Manual sampling . . . 39
5.6 Conclusions from the field sampling . . . 43

6 Biofilm distribution, development and activity 45
6.1 Summary . . . 45
6.2 Distribution of biofilm along the sewer wall . . . 45
6.2.1 Radial distribution . . . 46
6.2.2 Longitudinal distribution . . . 48
6.3 Biofilm growth and aerobic activity . . . 50
6.3.1 Biofilm erosion during a real and simulated rain event . . . 51
6.4 *in situ* sewer biofilm respiration rate measurements . . . 53
6.4.1 Introduction . . . 53
6.4.2 Data processing and results . . . 53
6.4.3 Sewer versus trickling filter biofilm . . . 56
6.4.4 Conclusion . . . 57
6.5 Storage materials in sewer biofilms? . . . 57
6.5.1 Introduction . . . 57
6.5.2 Results and conclusions . . . 58
6.6 Methanogenic and sulphidogenic bacteria in the sewer biofilm . . . 58
6.6.1 Introduction . . . 58
6.6.2 Methane production measurement . . . 58

6.6.3 Sulphur cycle activity 59
6.6.4 Conclusion 60
6.7 Hydrolysis 60
6.7.1 Introduction and background 60
6.8 Activity of hydrolysis enzymes 61
6.8.1 Sewer biofilm hydrolysis rate 62
6.8.2 Substrate limitation in the sewer system 64
6.8.3 Conclusion 65
6.9 Sewer biofilm denitrification 65
6.9.1 Introduction 65
6.9.2 Quantification of the denitrification 66
6.9.3 Conclusions 67
6.10 Other sewer biofilm properties 67
6.11 Conclusions sewer biofilm distribution, growth and activity 68

7 Gas-liquid mass transfer in open channels 69
7.1 Summary 69
7.2 The occurrence and fluxes of gases in the sewer 69
7.3 The physical background of interfacial mass transfer 70
7.3.1 Gas-liquid mass transfer 70
7.3.2 Water quality factors influencing interfacial mass transfer 71
7.3.3 Sherwood number for mass transfer 72
7.3.4 Boundary layer mass transfer models 72
7.3.5 Influence of turbulence on gas exchange 73
7.3.6 Temperature effect on gas-liquid mass transfer 75
7.4 Empirical reaeration equations for open channels 77
7.4.1 Stream reaeration 77
7.4.2 Previously proposed reaeration equations 77
7.4.3 New reaeration equation for open channel flow 80
7.4.4 Oxygen transfer measurement methods 80
7.5 Alternative gas exchange method 82
7.5.1 Experimental procedure of the sulphur hexafluoride (SF_6) method . . . 82
7.5.2 Applicability of SF_6 for the sewer system 83
7.6 Gas exchange calibration experiments 85
7.6.1 Introduction to the calibration experiments 85
7.6.2 General experimental procedure for the calibration experiments 85
7.6.3 Small channel: *'Schwamendinger Dorfbach'* 86
7.6.4 Large channel: *'Verbindungskanal'* 87
7.6.5 Modelling and discussion calibration experiments 91
7.7 Results of the SF_6 sewer measurements 93
7.7.1 Comparison with previously measured data 93
7.7.2 Parameter estimation of the alternative reaeration equation 97
7.8 Conclusion gas exchange experiments 98

8 Oxygen balance in the sewer system **99**
8.1 Summary 99
8.2 Introduction 99
8.3 The sewer oxygen balance 99
8.4 Longitudinal oxygen concentration variations 100
8.5 Wastewater respiration 100
8.5.1 Quantification of the wastewater biomass activity 100
8.5.2 Continuous wastewater respiration and concentration measurements . . 101
8.5.3 Estimate of biomass load 103
8.6 Validation of the sewer oxygen balance 103
8.6.1 Data collection 104
8.6.2 Resulting oxygen balances 105
8.6.3 Monte Carlo Simulation 106
8.7 Additional oxygen balances 107
8.7.1 Aerobic COD degradation and conversion 109
8.8 Conclusions 110

9 Hydrodynamic and biological sewer model **113**
9.1 Summary 113
9.2 Introduction 113
9.3 Sewer model structure 114
9.4 Physical model 115
9.4.1 Hydrodynamic model and gas exchange 115
9.5 Biological Model 115
9.5.1 Wastewater biomass 115
9.5.2 Biofilm biomass 115
9.5.3 Methane producing bacteria 117
9.5.4 Sulphur reduction, oxidation and cycling 117
9.5.5 Other taxa 120
9.6 Intact biofilm 120
9.6.1 Substrate flux based on diffusion and conversion: Effectiveness 120
9.6.2 Boundary layer 122
9.6.3 Biofilm thickness & TSS 123
9.6.4 Biofilm detachment 123
9.6.5 Biofilm attachment 124
9.6.6 Hydrolysis 124
9.7 Model implementation 125
9.8 Results modelling 125
9.8.1 Parameter identification with the suspended biofilm biomass 125
9.8.2 Sulphur cycle processes 126
9.9 Stoichiometric and kinetic constants of the biological model 127
9.9.1 The concept of the stoichiometric & composition matrix 127
9.9.2 The sewer model array 128
9.10 Calibration and validation of the sewer model 131
9.10.1 Assumption for the sewer model 131
9.10.2 Data for model calibration and validation 131
9.10.3 Calibration 132

9.10.4 Validation 132
9.10.5 Validation with in-line data 134
9.11 Conclusions 135
9.12 Recommendations 135

10 Conclusion, interpretation and outlook **137**
10.1 Conclusions 137
10.2 Interpretation of the results 138
10.3 Open questions and outlook 139

Bibliography **141**

A Additional Materials and Methods **151**
A.1 Enzyme activity measurements 151
A.1.1 α- and β-Glucosidases 151
A.1.2 Esterases 152
A.2 Search for a suitable biofilm substratum 153
A.3 Sewer *in situ* flow cell 154
A.3.1 Design of the measurement chamber 154
A.3.2 *In situ* flow cell supporting system 155
A.4 Biofilm Flow Cell (BFC) and supporting system 156
A.5 SF_6 gas exchange experiment methodology 157
A.5.1 Preparation and addition of the tracers 157
A.5.2 Sampling for the SF_6 method 158
A.5.3 Analysis of SF_6 158
A.6 Application and calibration of the oxygen meters 159
A.7 Other materials and methods 159
A.7.1 Alkalinity, TSS and TVS 159
A.7.2 Sewer biofilm TSS and TVS 160
A.7.3 Sewer biofilm density 160
A.7.4 Chemical Oxygen Demand 161
A.7.5 Nitrogen Components with FIA 161
A.7.6 Ionchromatographic analysis of anions 161
A.7.7 Analysis of urea 161

B Oxygen Uptake Monitor program **163**
B.1 Introduction 163

C Additional data **165**
C.1 Oxygen balances 165
C.2 Ammonium concentration changes - Urea hydrolysis 165
C.3 Easily degradable substrate in sewer 167

D Dynamic biological sewer model **169**
D.1 The simulation tool Aquasim 169
D.1.1 The sewer modelled as a river 169
D.1.2 Calculation of the stoichiomatrix matrix 170

E Applied constants and definitions **173**
E.1 Biomass 173
E.1.1 Temperature dependency of wastewater biomass 173
E.2 Water properties 173
E.3 Physical properties of oxygen 173
E.4 Physical properties of sulphur hexafluoride (SF_6) 174

F Curriculum Vitae **175**

Nomenclature **177**

Index **182**

1 Introduction

1.1 Current problems

The focus with regard to pollutant fluxes in the Urban Drainage System was traditionally on the wastewater treatment plant (WWTP). However, with the development of the integrated urban water management concept the system is no longer treated as separate units*, but as a whole. The current goal is to find an optimal solution with regard to the environment, costs and service to the public under the consideration of the mutual interactions.

The sewer system is by far the most expensive part of the urban wastewater system, though most people regard it only as a simple transport system. However, many biological, chemical and physical processes take place, thereby altering the properties of the wastewater as it flows to the WWTP (Boon and Lister, 1975; Pomeroy and Parkhurst, 1973). These processes may be advantageous because they reduce the amount of oxygen binding components in the wastewater, thereby relieving the WWTP. However, this self-purification might also be problematic, because it can remove the easily degradable material that is useful for more advanced wastewater treatment processes like nitrogen and phosphorus removal (Raunkjær *et al.*, 1994).

Furthermore, the sewer represent a potentially additional volume for wastewater purification because up to 90% of the sewer volume remains unused during dry weather conditions. The crux is, however, that the rates of sewer processes are not known at this moment.

The WWTP and to a lesser extend the receiving water have been given most attention with regard to the conversion processes. Practically all sewer related research was directed towards hydrodynamics, combined sewer overflows and sediment transport. Although the general nature of the chemical and biological processes in the sewer system are known, a more thorough understanding of the interactions and a quantification of the fluxes is still lacking.

1.2 Goals and questions

The underlying goal of this project is to obtain a more fundamental understanding of the processes that underlie the changes in wastewater properties as this water flows towards the treatment plant. The results should be used to develop a deterministic model describing biofilm growth and degradation processes in the sewer system. The following questions should be answered:

- How can the conversion rates for the main processes in a typical sewer be quantified?
- What are the limiting factors for the sewer conversion processes?
- What is the radial and longitudinal distribution of the sewer biofilm?
- What role does the sewer wall biofilm play in the degradation processes?
- Does the biofilm serve as particle trap, or is it the major source of biomass?

*The sewer system, wastewater treatment plant and receiving water

- What is the role of attachment and detachment of particles?
- What is the relationship between the biofilm and the wastewater biomass?
- What is the contribution of the gas transfer through the water surface to the overall oxygen mass balance?
- What are the biochemical constants for the growth of sewer biomass?
- How can the biochemistry and hydrodynamics in the sewer be modelled?
- Would such a model allow for the calculation of different sewer management scenarios?
- Can the management of the sewer system be adapted to support the wastewater treatment plant?

1.3 Methodology

Several individual aspects of the sewer system have been studied with laboratory and full-scale field experiments. Measurements were conducted on the wastewater, the gas exchange and especially the sewer wall biofilm. The acquired information has been used to develop and calibrate a deterministic model.

1.4 Outline of this thesis

The description of the sewer system from the viewpoint of interacting compartments together with a short literature overview will be given in the next chapter. Open channel hydraulics, which plays an important role in the sewer processes, is discussed in chapter 3. The techniques that were used during this study are described in chapter 4. The following two chapters (5 and 6) are devoted to the changes in wastewater properties and the biofilm properties in a sewer reach. Chapter 7 deals with the interactions between the sewer atmosphere and the wastewater. A safe and environmentally friendly method is introduced to quantify the gas exchange. This method and respiration measurements of the wastewater and of the intact biofilm are used in chapter 8 to set-up a redundant oxygen balance. Based on the experimental data of this study, a dynamic deterministic sewer degradation model is proposed in chapter 9. This work ends with an interpretation, conclusions and an outlook.

2 The sewer as a system

2.1 Summary

A description of the sewer as a system and a general sewer mass balance will be given. Furthermore, the origin and composition of wastewater will be shortly discussed. The rest of this section will introduce the biofilm morphology, biology and mass transfer.

2.2 The history of the sewer system

With the filth on the medieval streets in mind, we might think that the sewer system is a result of our modern thinking and ingenuity. This is however a misconception. The first sewer-like system had already been developed around 3000 b.c. as was discovered during excavations at Habuba al-Kabira at the site of the Assad Dam. Rectangular ducts had been installed for the major strands and prefab tubes had been used for the smaller pipes (see figure 2.1(a)). The Babylonians (2500 to 500 b.c.) even had seepage shafts and baked clay pipes (see figure 2.1(b)). Other well-known examples are the palace of Knosses on Crete in Greece and the Cloaca Maxima, a Roman sewer.

This ancient knowledge was lost for many centuries. The authorities started developing wastewater collection systems in the 18th century when the problems with hygiene and rainwater

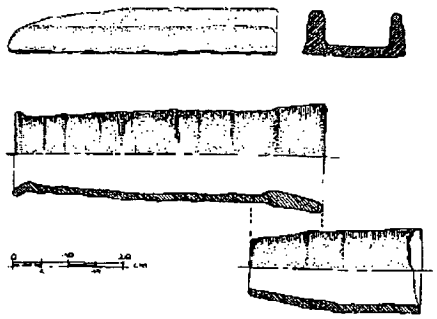

(a) Drawings of the rectangular ducts and prefab tubes that were used for the oldest known water supply and disposal system (≈ 3000 b.c.).

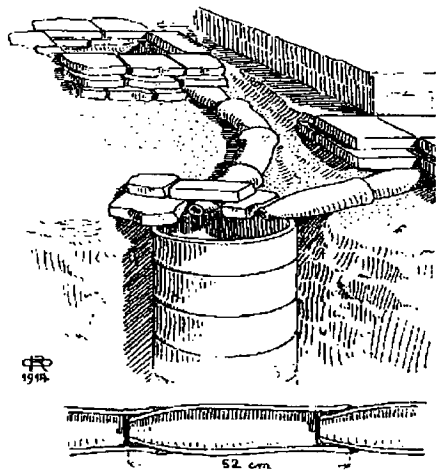

(b) The baked clay pipes and a seepage shaft that were build by the Babylonians (≈ 2500 to 500 b.c.).

Figure 2.1: Examples of old (waste-) water transport systems.

run-off in the metropolises London and Paris became unbearable. The initial purpose was the removal of excess water from the streets and houses, but the wide scale use of the flush lavatory (toilet)* led to the sewer system as it is today. It is convenient, but not very sustainable. Research is therefore going on to find alternative systems (e.g. Larsen and Gujer, 1996). But, for the time being a huge systems exists below our feet where more processes occur than just the transport of water.

2.3 The system 'sewer'

The sewer is a complex system with many degrees of freedom, which do not only change as a function of distance, but also of time. Changes can occur in a diurnal or weekly rhythm, or randomly due to rain.

2.3.1 Sewer compartments & Interactions

The sewer system can be subdivided in the following four interacting compartments (see figure 2.2):

- **Sewer atmosphere**. Swiss sewers are well aerated even under dry weather conditions. The composition of the sewer atmosphere is therefore similar to the outside atmosphere.
- **Wastewater**. The water phase normally accounts for only $\approx$ 10% of the total sewer volume. The flowing water transports the waste and contains active biomass.

*The flush lavatory was invented around 1595 by Sir John Harington, probably while translating an Italian Poem. He installed one for Queen Elizabeth in her palace at Richmond, Surrey (Anonymous, 1997).

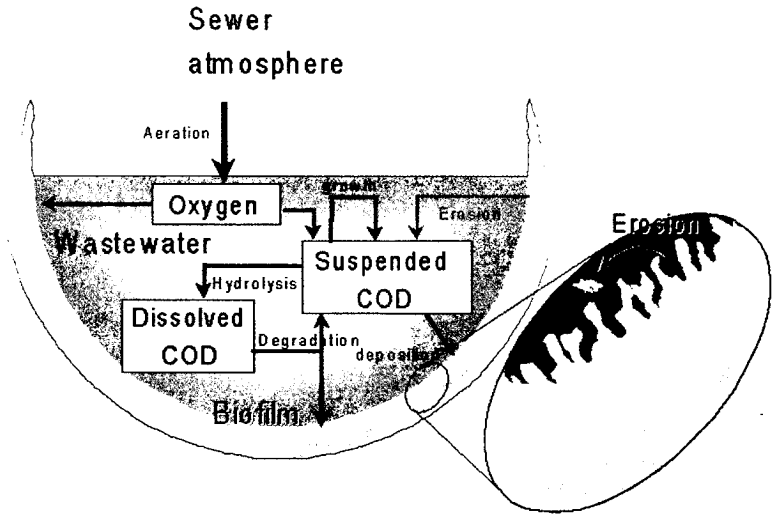

Figure 2.2: Sewer system compartments. See text for an explanation (After Anonymous (2000)).

- **Biofilm**. The sewer biofilm or slime layer covers the inside of sewer pipes. The biofilm prevents that the bacteria are flushed away and may further provide protection against environmental change, such as desiccation, antimicrobial agents and even against bacteriophages (Allison, 1993; Hughes *et al.*, 1998).
- **Sediments**. Sediments occur when the flow velocity drops below a certain value. They will not be discussed further because they were absent in the sewer under study. The absence of the sediments will not greatly affect the conclusions of this study.

The interactions between those compartments are affected by the following factors:

- **Physical properties**. The dimensions, slope and wall roughness of the sewer.
- **Hydrodynamic conditions**. These are determined by the influx of waste- and infiltration water, and rain runoff. They are strongly influenced by the physical properties of the sewer.
- **Environmental conditions**. These are mainly temperature and, although marginal, pressure (through its influence on the oxygen solubility).
- **Biological, chemical and physical processes**.

The wastewater and biofilm compartments are the most important for this project. In the next paragraphs they will be discussed separately.

2.4 The wastewater

The composition of 'fresh' wastewater with an age of only minutes to a few hours may be quite different from wastewater that has been under transportation for 20 hours or more. This is mainly due to microbial growth and respiration in the bulk water and the biofilm, solubilisation, enzymatic hydrolysis of macromolecules and hydraulic shear forces. Also sedimentation and resuspension may be important (Nielsen *et al.*, 1992).

2.4.1 Origin and composition

The combination of household wastewater, industrial wastewater and infiltration water determines the wastewater composition. Domestic wastewater usually has a very complex composition of both organic and inorganic compounds. The influence of industrial wastewater depends very much on the type and amount of industrial activity in the catchment area of the sewer. The main effect of the infiltration water is dilution. Furthermore, it will influence the temperature of the wastewater which affects the process rates. In addition, diurnal and seasonal variations, the design of the sewer system and the residence time have a considerable influence on the wastewater composition (Nielsen *et al.*, 1992).

The major wastewater components have been identified and quantified in the past (Heukelekian and Balmat, 1959; Painter and Viney, 1959; Hunter and Heukelekian, 1965). Attempts at measuring concentration changes in specific component pools like lipids, carbohydrates, proteins, organic acids and other substances have been made (Raunkjær *et al.*, 1995). However, such methods are expensive, laborious and do not coincide with the common praxis in wastewater treatment to use the overall chemical oxygen demand (COD). The total COD is split up in several dissolved and particulate fractions which are degradable or inert (see e.g. Henze (1992), Gujer *et al.* (1999)). A further important component are the active bacteria, which originate from faeces and from the sewer wall.

2.5 The sewer biofilm

A 'slime layer' or biofilm forms on the sewer wall. Biofilms are very common in nature. The slippery layer on the rocks in a river and the plaque on teeth are well-known examples. A broad definition of a biofilm is: '*A natural accumulation of microorganisms at an interface*' (Gjaltema, 1996). It consists of microorganisms embedded in a glycocalyx that is predominately composed of microbially produced exopolysaccharide (EPS) (Costerton *et al.*, 1994). But in the sewer it also contains a large fraction of inorganic material (sand, zeolite etc.), fats and higher species which can have a significant impact on the biofilm properties (Bouwer, 1987). Biofilms are highly heterogeneous with structures and streamers, water channels, stacks and fronts forming, depending on the prevailing conditions and environmental stresses (Keevil *et al.*, 1995). An electron microscope photograph of a sewer biofilm is shown in figure 2.3.

The bacteria have to invest energy and resources to produce the biofilm, which enables them to become settled in a system where they would otherwise be flushed away. This greatly increases the residence time ('sludge age') of the biomass in the sewer. As a result, slower growing bacteria like methanogenic or sulphur reducing bacteria can build up a significant population. Erosion of the biofilm adds to the biomass concentration of the wastewater.

Biofilms are very interesting but complex systems. Although great progress in understanding biofilms has been made over the last two decades, much less is known about biofilms in real systems, like the sewer system. Bishop (1997) therefore mentions that: 'The internal structure of wastewater biofilms is currently a mystery.'

2.5.1 Biofilm morphology and mass transfer

A mature biofilm in a heavily loaded system is complex with regard to the organisms present and the physicochemical microenvironments (Zhang and Bishop, 1994). The vertical zonation

Figure 2.3: A scanning electron microscope (SEM) picture of the sewer biofilm from the village Rümlang showing the entrapped sand and zeolite particles (photo by I. Weidmann, EAWAG).

of respiratory processes found on a centimetre or metre scale in sediments can be found within a few millimetre in the wastewater biofilm (Kühl and Barker-Jørgensen, 1992). The spatial gradients will lead to a change with biofilm depth of the structure, the composition and the conversion rates.

Heavily loaded biofilms contain all major physiological groups (see figure 2.4).

The commonly accepted viewpoint on the biofilm morphology is that it consists of a relatively firm and structured base layer and a less firm surface film with an extremely irregular topography. The surface film has macropores (also called water channels) and the biomass grows as cell clusters separated these interstitial voids (DeBeer *et al.*, 1996). These channels facilitate mass transfer through the biofilm. This effect can be lumped into an effective diffusivity as was done by Siegrist and Gujer (1985).

Gravity sewer biofilms are usually several millimetre thick and they are unique in growing at very high organic loading and at high water flow velocity (Norsker *et al.*, 1995). They usually have a pronounced filamentous surface, which enables higher mass transfer rates in comparison to compact biofilms. Furthermore, the oxygen consumption is almost independent of the oxygen concentration in the liquid in addition to a very high oxygen uptake rate (Nielsen *et al.*, 1992). Roth *et al.* (1994) determined a total oxygen penetration depth in a sewer biofilm of 1 mm.

It should be noted that biofilm not only grows on the sewer wall below the water surface, but also on the walls in the gas phase. The biofilm can maintain itself here due to the water-saturated air and the supply of nutrients by aerosols (Müller and Bartocha, 1978). Therefore, these biofilms are most pronounced near cascades or other aerosol producing constructions. Matthews (1976) measured a 5 mm or thicker gas phase biofilm near cascades over which cyclohexane-containing water flowed.

In the thirties of this century German engineers were discussing whether the 'Sielhaut' ('Slime layer') in sewer pipes could be protecting the pipe material against acids and bases in the (industrial) wastewater (Reye and Bleibtreu, 1940; May, 1939). This slime layer was even regarded as an enemy that should be constantly fought against because it imposed a constant danger for the workers and the general hygiene (Schnur, 1940).

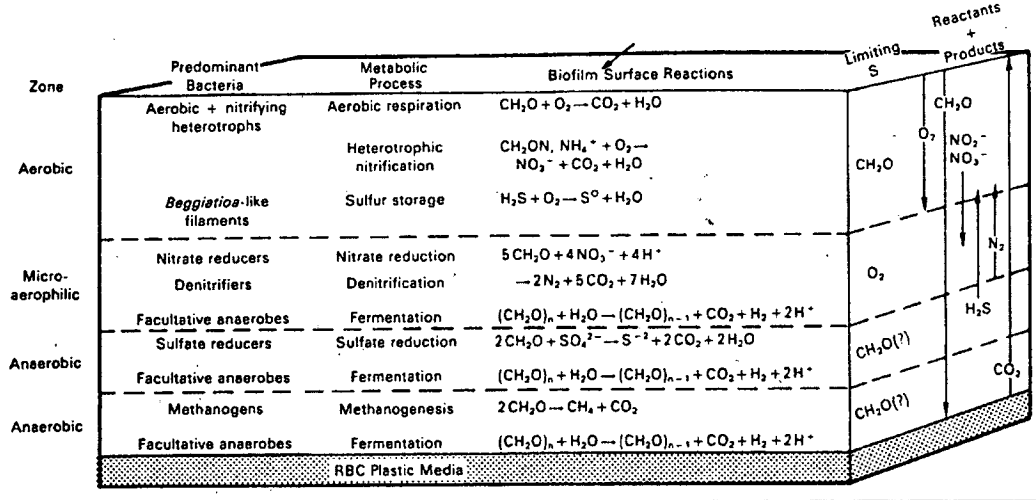

Figure 2.4: The redox zones in a heavily loaded biofilm (Arvin and Harremoës, 1990).

2.5.2 Processes in the sewer biofilm

Heterotrophic biomass

In the aerobic top layer of the biofilm mainly fast growing heterotrophic bacteria will be active.

Nitrification and denitrification

All reactions of the nitrogen cycle, except nitrogen fixation, can be found in a sewer biofilm (see figure 2.5). Nitrifying bacteria were found in a wastewater biofilm but their concentration was $\approx$ 1000x lower then the concentration of the heterotrophs that overgrew them (Lemmer *et al.*, 1994). Nitrification will therefore only play a minor role. But denitrification can very well occur as long as the wastewater contains nitrate, which must come from infiltrated groundwater or from drinking water. Kühl and Barker-Jørgensen (1992) showed with microelectrode measurements that the presence of nitrate did not effect the penetration depth of oxygen. Hydrolysis of urea and proteins are important sources of ammonium in the wastewater.

Sulphur reduction, oxidation and cycling

Sulphur compounds can serve as an electron donor or an acceptor in many processes (see figure 2.6(a)). It constitutes $\approx$ 1% of the dry mass of organisms where it serves many structural and enzymatic functions. However, sulphur in the sewer is mainly known for its role in concrete corrosion and odour problems. These are the main operational and maintenance problems in (flat) wastewater collection systems, which result from the production, transport and reaction of hydrogen sulphide (H_2S), as explained in figure 2.6(b) (Hao *et al.*, 1996).

Because gravity sewer biofilms are several millimeters thick, sulphate reduction can take place in the deeper biofilm strata. Reoxidation of sulphide with oxygen can take place in a stratum close to the biofilm surface, depending on the bulk water oxygen concentration (Norsker *et al.*, 1995). The relevance for the degradation in the sewer system is that COD is converted to CO_2 and biomass during the cycling of the sulphur compounds. This cycle effectively results in the conversion of COD to CO_2. The biomass production per amount of COD converted is however much lower than for the conversion with oxygen.

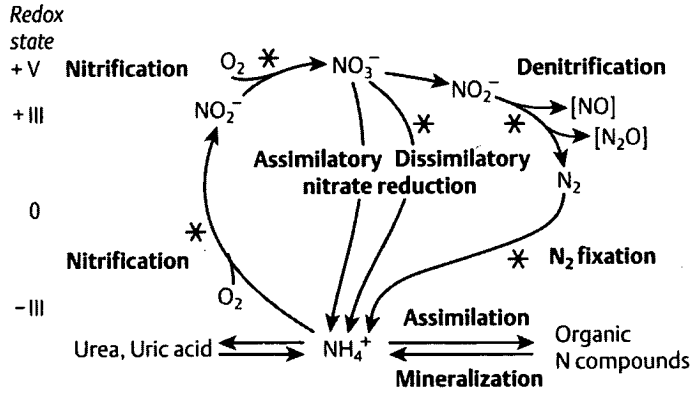

Figure 2.5: Key reactions in the cycling of nitrogen species. The redox state of nitrogen is displayed on the left. Reactions catalysed by prokaryotes are marked with an asterisk (Lengeler et al., 1999)

The Fe-sulphur cycle (not shown) will be neglected here since Okabe *et al.* (1999) found that it accounted for only 1% in the total sulphur cycle in a wastewater biofilm.

spatial distribution

The spatial distribution of the different physiological groups affects the activity. From laboratory research with a rotating drum reactor and synthetic wastewater, Zhang and Bishop (1994) concluded that heterotrophic bacteria in general outnumber autotrophs (mainly nitrifiers). The spatial distribution of heterotrophs was almost uniform. However, the facultative bacteria increased from 10^7-10^8 in the top layers to 10^9-10^{10} (CFU·cm^{-3}) near the substratum. The nitrifying population was about 10^4-10^6 MPN·cm^{-3} in a heterotrophic/autotrophic biofilm*. The bacteria at the top layers may all be metabolically active. However, at the bottom layers, only 15 to 25% of living bacteria were active; other living biomass could be dormant cells. About two thirds of the total biomass was inert. It should be mentioned that new molecular methods† that were developed during the last few years have shown that the classical methods do not give a correct estimation of the total number of bacteria.

The biofilm density increased with depth, from 14 in the top layers to 97 $kg_{TSS}\cdot m^{-3}$ in the bottom layers. Furthermore, Zhang and Bishop (1994) found that the porosity in thick biofilms (> 500 µm) changed from 83–92% at the top layers to 57–64% in the bottom layers.

The growth rate of bacteria is the major cause of the spatial distribution. Since fast growing bacteria tend to overgrow slower growing ones, they will accumulate in upper layers of a biofilm. Depending on the availability of substrate, other bacteria can grow deeper inside the biofilm. The bacterial population distribution is not static, but can adapt to changing substrate concentrations or other environmental conditions (Tijhuis, 1994).

*CFU = Colony Forming Units, MPN = Most Probable Number. Both are classical methods to estimate the viable number of bacteria in a sample.

†e.g. fluorescent in situ hybridisation (FISH).

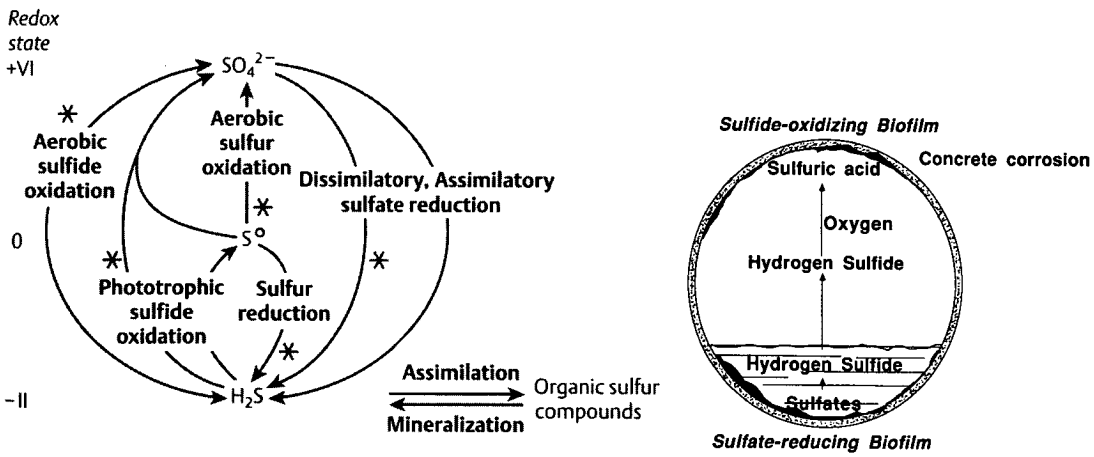

(a) Key reactions in the cycling of sulphur species. The redox state of sulphur is displayed on the left. Reaction catalysed by prokaryotes are marked with an asterisk (Lengeler *et al.*, 1999).

(b) The pathway of hydrogen sulphide induced concrete erosion in the sewer (Odom, 1993).

Figure 2.6: The sulphur cycle.

2.5.3 Biofilm erosion

The biofilm thickness is controlled by several factors (after Arvin and Harremoës, 1990):

- Growth of active biomass.
- Decay of active biomass.
- Accumulation of inert material as a result of the decay of active bacteria.
- Accumulation and/or degradation of extracellular polymers.
- Deposition and degradation of suspended particles from the bulk liquid.
- Erosion, abrasion, grazing and sloughing from the biofilm surface.
- 'Catastrophic events'.

Erosion is the gradual and continuous loss of biofilm, mainly influenced by the hydrodynamics of the liquid. Abrasion is analogous to erosion, but caused by particles in the flowing liquid. With sloughing, larger parts of the biofilm are periodically lost to the liquid. This is probably caused by processes inside the biofilm that either decrease the binding strength with the substratum or produce gases that break up the biofilm. Several types of ciliates 'graze' the biofilm. This causes loss of active biomass and can be regarded as biofilm decay. The catastrophic events are rain events that will erode much of the biofilm within a short time frame. Decay occurs due to the death of bacteria, for example due to lack of substrate. Finally, degradable particles that were trapped in the biofilm will be converted to soluble substances (hydrolysis) by enzymes released by the bacteria. These substances can serve as substrate for the biomass or diffuse out of the biofilm.

Gutekunst (1988) concluded that the magnitude of biofilm outgrowth is more determined by the hydrodynamics – mainly velocity and shear – than by the multiplication of bacteria. This is confirmed by the results of Norsker *et al.* (1995), who found that the biofilm growth rate of 80 $\mu m \cdot d^{-1}$ at 20°C in a model system (rotating drum reactor) could account for only 4 – 6% of the observed COD-removal. Apparently a significant part of biofilm growth was lost through detachment. Tijhuis (1994) found for a biofilm airlift reactor that biofilm detachment decreased drastically after the substrate supply was stopped.

A biofilm grown under low shear stress conditions detaches more readily upon an increased shear stress than a biofilm grown under high shear stress (Rittmann, 1989; Reiff, 1992). Furthermore, Gantzer *et al.* (1991) found for an artificial stream with cobbles that short-term water velocity changes effect the mass transfer, but that long-term changes led to changes in the biofilm biomass.

Reiff (1992) studied the growth and erosion of a biofilm in completely filled 44 and 63 mm tubes with presettled wastewater under variation of COD, oxygen concentration and shear stress and determined the removal of biofilm under increased shear stress. He observed several interesting phenomena:

- Neither the pipe material, nor the tube diameter influenced biofilm growth. This agrees with the results of Bland *et al.* (1975).
- Older biofilm (> 12 d) was more resistant to erosion than a younger film.
- The largest accumulation of biofilm was reached at a shear stress of 1.5 $N \cdot m^{-2}$.
- The oxygen and COD concentration affected the growth rate of the biofilm, but not the maximum amount per unit of surface area.
- The amount of biofilm eroded under increased shear stress depended on the magnitude of the applied shear stress.

- 90% of the removable biofilm at a certain increased shear stress was eroded within 1 to 2 minutes.
- The amount of biofilm removed under increased shear stress depends on the conditions under which the biofilm has grown. Higher shear stress during growth led to a more stable biofilm.
- Higher shear stress leads to non-uniform biofilm growth.

The above mentioned results indicate that the shear stress in the real sewer will strongly influence the biofilm properties. This is confirmed by the results of Dauber *et al.* (1982), who stated that the shear stress on the sewer wall at the insert is 15% higher than average, while near the water surface it is 55% lower. This non-uniform shear stress distribution might explain why an increased biofilm growth is often observed near the water surface (Schnur, 1940; Reye and Bleibtreu, 1940; Gutekunst, 1988; Dauber *et al.*, 1982; Reiff, 1992). The cause of this non-uniform shear stress profile as a result of the cross sectional velocity distribution will be discussed further in section 3.2.5.

2.6 The sewer as reactor

From the 1950's, scientists began to investigate the formation of hydrogen sulphide in pressure mains. To solve this problem, several authors proposed to inject oxygen or nitrate (Boon and Lister, 1975; Boon *et al.*, 1977). This led to research into the uptake rates of COD oxygen etc. by sewage.

The idea to use volume and length of the sewer as a support for the WWTP was probably first brought up by Stoyer (1970 in: Green, Shelef, and Messing, 1985). Pomeroy and Parkhurst (1973) recognised the potential of the sewer as a COD-removal reactor. They concentrated on respiration rates in the wastewater and noticed the importance of the biofilm on the sewer wall as a sink for oxygen and as a source for active biomass. The maximum *combined* oxygen uptake rate was 480 $g_{O_2} \cdot m^{-3} \cdot d^{-1}$. Furthermore, from wastewater respiration rates and by calculating the oxygen transfer from the gas phase with an empirical formula, they were able to estimate the biofilm uptake rate as $\approx$ 8.4 $g_{O_2} \cdot m^{-2} \cdot d^{-1}$. This was lower than the 29 to 43 $g_{O2} \cdot m^{-2} \cdot d^{-1}$ measured by Norsker *et al.* (1995) in a laboratory biofilm reactor with real wastewater.

Manandhar and Schroder (1995) tested the idea of recirculating synthetic wastewater in sewers by using a rectangular channel with a length of 90 m. They showed that the nitrification rate decreased from 1.5 to 0.5 $g_N \cdot m^{-2} \cdot d^{-1}$ when the COD and total nitrogen loading rate increased from 17 $g_{COD} \cdot m^{-2} \cdot d^{-1}$ and 1.8 $g_N \cdot m^{-2} \cdot d^{-1}$, to 62 $g_{COD} \cdot m^{-2} \cdot d^{-1}$ and 8 $g_N \cdot m^{-2} \cdot d^{-1}$. Furthermore, denitrification increased with increasing load from 0.09 $g_N \cdot m^{-2} \cdot d^{-1}$ to 0.5 $g_N \cdot m^{-2} \cdot d^{-1}$, with a maximum of 0.77 $g_N \cdot m^{-2} \cdot d^{-1}$ at a loading of 3.8 $g_N \cdot m^{-2} \cdot d^{-1}$. It should be noted that the temperature was tropical (30°C).

The somewhat different concept was followed by Cao and Alaerts (1995). They grew biofilm on polypropylene plates in a trickling filter treating sewage and subsequently installed them in a channel-type reactor with a length of 3 m. Because they used glucose as substrate the biofilm needed an adaptation time, after which the overall and the suspended biomass activity were measured. The activity of *suspended* biofilm biomass lay between 18 (20°C) and 25 $g_{O2} \cdot m^2 \cdot d^{-1}$ (28°C) when expressed per sampled biofilm area.

One step further than studying the natural processes in the sewer system is adding activated sludge at the beginning of a main sewer and injecting air or oxygen at several points (Green *et al.*, 1985). This way, the main sewer is converted into a plug-flow type wastewater treatment reactor, in contrast to the activated sludge WWTP, which is closer to a CSTR-type (Continuous

Stirred Tank Reactor). Because the bacteria are exposed to a higher substrate level compared to a CSTR the removal rates can be higher (Green *et al.*, 1985).

2.7 Sewer mass balance

Dynamic balance

A verbal mass balance for oxygen over a sewer reach consists of the following terms:

$$\overbrace{\text{accumulation}}^{\text{ACCUMULATION}} = \overbrace{\text{inflow} + \begin{bmatrix}\text{surface}\\ \text{reaeration}\end{bmatrix}}^{\text{IN}} + \overbrace{\text{outflow}}^{\text{OUT}} + \overbrace{\begin{bmatrix}\text{conversion}\\ \text{by biofilm}\end{bmatrix} + \begin{bmatrix}\text{conversion}\\ \text{in suspension}\end{bmatrix}}^{\text{CONVERSION}} \tag{2.1}$$

This can be converted into the following mathematical expression:

$$\left(\frac{\partial S_O}{\partial t}\right) = \bar{u} \cdot \left(\frac{\partial S_O}{\partial x}\right) + k_l \cdot \frac{w}{A_{cr}} \cdot (S_O^* - S_O) - r''_{O,f} \cdot \frac{P_w}{A_{cr}} - r_{O,w} \tag{2.2}$$

where S_O = oxygen concentration in liquid ($g_{O_2} \cdot m^{-3}$), t = time (s), $\bar{u}$ = average velocity ($m \cdot s^{-1}$), x = longitudinal coordinate (m), $r_{O,w}$ = conversion rate by suspended biomass ($g_{O_2} \cdot m_f^{-3} \cdot s^{-1}$), $r''_{O,f}$ = biofilm oxygen uptake rate per surface area ($g_{O_2} \cdot m_f^{-2} \cdot s^{-1}$), k_l = liquid-phase mass transfer velocity ($m \cdot s^{-1}$), w = surface width (m) and S_O^* = oxygen concentration in equilibrium with the atmosphere (saturation concentration) ($g_{O_2} \cdot m^{-3}$).

Steady state balance

A steady state mass balance can be a good approximation when the accumulation is small in comparison to the transport and conversion terms, and when the characteristic times of the measurements are much shorter than those of the changes in the fluxes. The resulting balance is:

$$\phi_{O,out} + \phi_{O,f} + \phi_{O,w} = \phi_{O,in} + \phi_{O,surf} + \phi_{O,gw} \tag{2.3}$$

where ϕ_O = oxygen flux ($kg_{O_2} \cdot d^{-1}$).

Groundwater infiltration is included because sewers often leak. This could affect the mass balance. Writing out equation (2.3) in full gives:

$$\begin{aligned} Q_{out} \cdot S_{O,out} + r''_{O,f} \cdot A_f + r_{O,w} \cdot \overline{Q} \cdot \tau \\ = \quad Q_{in} \cdot S_{O,in} + k_l a \cdot (S_O^* - \overline{S_O}) \cdot \overline{Q} \cdot \tau + Q_{gw,inf} \cdot S_{O,gw} \end{aligned} \tag{2.4}$$

where Q = discharge ($m^3 \cdot s^{-1}$), A_f = wetted biofilm area (m^2), τ_r = residence time (s), $\overline{Q}$ = average discharge ($m^3 \cdot s^{-1}$), $k_l a$ = reaeration coefficient (s^{-1}) with a = specific exchange surface area ($m^2 \cdot m^{-3}$) = w/A_{cr}. $Q_{gw,inf}$ = groundwater infiltration ($m^3 \cdot s^{-1}$) and $S_{O,gw}$ = groundwater oxygen concentration ($g_{O_2} \cdot m^{-3}$)

3 Sewer hydrodynamics

3.1 Summary

In this chapter the focus will be on the hydrodynamics and the shear stress distribution in the sewer. An appropriate hydrodynamic model for the sewer will be selected and literature data on the shear stress distribution will be summarised.

3.2 Selection of the hydrodynamic model

Time constants can be used to obtain information about the relative importance of different processes in a system. This method is applied here to decide on the type of hydrodynamic model.

The time scale for sewer processes is the wastewater residence time (the numbers are from the *Rümlang* study reach, which will be described in section 5.3.1):

$$\tau_r = L_{sect.}/\bar{u} \approx 2000/0.4 \approx \ 0.06 \text{ d} \tag{3.1}$$

where L = section length (m).

This is the lower boundary, τ_1. The higher boundary (τ_2) is one day because of the diurnal variation. A dynamic model is required when $\tau_1 < \tau_c < \tau_2$ where τ_c = time scale for reactions (d) taken as the invert of the maximum heterotrophic biomass growth rate: $1/\mu_{Het}^{max} = 0.5$ d (Gujer *et al.*, 1999). The conclusion is that a dynamic model is required in this reach.

Dimensionality may be selected by consideration of the length scales. Shanahan *et al.* (2000) gave the criterion that a one-dimensional model can be used when $L \gg l_l$ and $L \gg l_v$ where l_l and l_v are the length scales defined as for lateral and vertical mixing (with some typical numbers for the *Rümlang* main sewer):

$$l_l = \frac{w^2}{2 \cdot E_y} \cdot \bar{u} \approx \frac{w^2}{2 \cdot (0.6 \cdot u^* \cdot d_{mean})} \bar{u} \approx \frac{0.7^2}{2 \cdot 0.6 \cdot 0.03 \cdot 0.12} \cdot 0.4 \approx 45 \text{ m} \tag{3.2}$$

for lateral mixing where E_y = lateral dispersion ($m^2 \cdot s^{-1}$) and

$$l_v = \frac{h^2}{2 \cdot E_z} \cdot \bar{u} \approx \frac{h^2}{2 \cdot (0.067 \cdot u^* \cdot d_{mean})} \bar{u} \approx \frac{0.12^2}{2 \cdot 0.067 \cdot 0.03 \cdot 0.12} \cdot 0.4 \approx 13 \text{ m} \tag{3.3}$$

for vertical mixing. h = water depth (m), u^* = shear velocity (see equation (3.12); $m \cdot s^{-1}$) and d_{mean} = mean water depth (see equation (3.22); m). Clearly, a one-dimensional model is sufficient because the pipe diameter is only 0.9 m.

Dispersion may be neglected if (Shanahan *et al.*, 2000):

$$\tau_c \gg \frac{2 \cdot E_x}{\bar{u}^2} \approx \frac{2 \cdot 0.06}{0.4^2} \approx 0.75 \text{ seconds} \tag{3.4}$$

where $E_x^{\cdot}$ = axial dispersion ($m^2 \cdot s^{-1}$). This condition is fulfilled because τ_c was 0.5 d (see above).

3.2.1 The Saint Venant equations

The Saint Venant equations describe unsteady flow through open channels (e.g. Henderson, 1966; French, 1985). They are one-dimensional, which is sufficient for the sewer system (see previous section). The diffusive wave* and kinematic wave† are simplified approximations of the full Saint Venant equations. The kinematic approach is normally sufficient when there is no backwater. The diffusive approach can be used as long as the dynamics of the system are not too strong.

Ponce *et al.* (1978) published a method to check the validity of these approximations in an analytical way. They introduced the following combination of dimensionless numbers based on an analytical solution of a linearised form of the Saint Venant equations:

$$\frac{\hat{\tau}}{\mathbf{Fr}_0} = T_{sin} \cdot S_{f,0} \cdot \sqrt{g/h_0} \tag{3.5}$$

$$\hat{\tau} = T_{sin} \cdot \bar{u}_0 / L_0 \tag{3.6}$$

where $\hat{\tau}$ = dimensionless wave period of unsteady flow, **Fr** = Froude number (-), T_{sin} = wave period of sinusoidal perturbation (s), S_f = friction slope (see section 3.10; $m \cdot m^{-1}$), h = water depth (m) and L_0 = reference channel length (m). Index 0 indicates during steady uniform flow.

The diffusive approximation has $<$ 5% error in comparison with the full equations when $\hat{\tau}/\mathbf{Fr}_0 > 16$ for $0.1 \leq \mathbf{Fr}_0 \leq 0.4$, or when $\hat{\tau}/\mathbf{Fr}_0 \geq 35$ for $0.01 \leq \mathbf{Fr}_0 \leq 0.08$.

A rewritten form of equation (3.6) gives the criterion for the application of the kinematic wave approximation:

$$\hat{\tau} = \frac{T \cdot S_{f,0} \cdot \bar{u}_0}{h_0} \tag{3.7}$$

This approximation has less than 5% or 1% error when $\hat{\tau} \geq 171$ or $\hat{\tau} \geq 873$, respectively.

On the one hand, it has been shown previously with equation (3.5) to (3.7) that the diffusive approximation still remains valid for sewer calculations even when the discharge is suddenly increased by a factor of four (Huisman *et al.*, 2000). The full Saint Venant Equations are therefore not required. On the other hand, the culvert at the end of measurement section in *Rümlang* causes a backwater that excludes the use of the kinematic approach.

The diffusive wave approximation has therefore been used for all hydrodynamic calculations. Models of other systems were based on the same approximation (*Dorfbach* and *Verbindungskanal* in section 7.6.3 and section 7.6.4, respectively).

3.2.2 Flow equation

The Saint Venant equations or their simplified forms require the friction slope. The empirical equations for the friction slope under unsteady flow conditions can be written after French (1985) as:

$$S_f = \frac{1}{\Gamma^2} \cdot \frac{1}{R_h^{2 \cdot a}} \cdot \bar{u} \cdot |\bar{u}| = \frac{1}{\Gamma^2} \frac{1}{R_h^{2 \cdot a}} \cdot \frac{Q \cdot |Q|}{A^2} \tag{3.8}$$

*inertia terms are neglected relative to pressure, friction and gravity terms

†additionally pressure terms are neglected

where Γ = empirical resistance coefficient ($m^a \cdot s^{-1}$), R_h = hydraulic radius (m) and a = empirical exponent (-). A common flow equation can be deducted from equation (3.8) when $a = 1$ and Γ is replaced by the Darcy-Weisbach equation:

$$\Gamma = \sqrt{8 \cdot g/f} \tag{3.9}$$

where f = friction factor (-) and g = gravitational acceleration ($m \cdot s^{-2}$). The friction slope becomes:

$$S_f = \frac{f}{8 \cdot g} \cdot \frac{1}{R_h} \cdot \bar{u}_x \cdot |\bar{u}_x| \tag{3.10}$$

where $\bar{u}_x$ = cross-sectional average axial velocity ($m \cdot s^{-1}$).

The calculation of f depends on the hydraulic range: smooth, transitional or rough. These are distinguished by the amount of contact of the turbulent flow with the wall. The difference can be explained with the sand roughness that was introduced by Nikuradse (1933).

The hydraulic range of a channel can be estimated with (Henderson, 1966; Kölling, 1994)

$$\text{(smooth) } 5 < k^* = \frac{k_s \cdot u^*}{\nu} < 70 \text{ (rough)} \tag{3.11}$$

where k^* = dimensionless wall roughness (-), k_s = equivalent sand roughness (m) and ν = kinematic viscosity = η/ρ ($m^2 \cdot s^{-1}$), η = dynamic viscosity (Pa·s) and ρ = liquid density ($kg \cdot m^{-3}$). The shear velocity u^* ($m \cdot s^{-1}$) is calculated as:

$$u^* = \sqrt{g \cdot R_h \cdot S_f} \tag{3.12}$$

k_s is defined as the sand grain size which leads to same flow resistance as experienced by the flow under study. Because k_s includes all kind of influences it can deviate from the physical roughness of the channel wall.

The dimensionless friction factor is calculated after the Prandtl-Colebrook equation as:

$$\frac{1}{\sqrt{f}} = -2 \cdot \log\left(\frac{2.5}{\mathbf{Re} \cdot \sqrt{f}} + \frac{k_s/D}{3.7}\right) \tag{3.13}$$

where **Re** = Reynolds number (-)

$$\mathbf{Re} = \frac{\rho \cdot u \cdot D}{\eta} \tag{3.14}$$

where ρ = liquid density ($kg \cdot m^{-3}$) and D = pipe diameter (m) which can be substituted by

$$D = 4 \cdot R_h \tag{3.15}$$

where the hydraulic radius R_h (m) is calculated as

$$R_h = A/P_w \tag{3.16}$$

with P_w as the wetted perimeter (m)

$$P_w = D \cdot \alpha \tag{3.17}$$

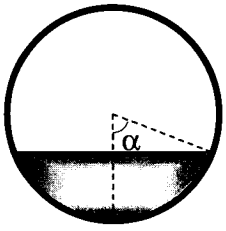

Figure 3.1: Definition of α

The angle α (rad) is the central parameter in the flow geometry calculations. It is calculated as (see also figure 3.1):

$$\alpha = \cos^{-1}\left((r - d_{max})/r\right) \tag{3.18}$$

where r = pipe radius (m) = $D/2$ and d_{max} = maximum water depth (m). But α may also be determined with an iterative procedure from

$$A_{cr} = 1/4 \cdot D^2 \cdot ((\alpha - \sin(\alpha) \cdot \cos(\alpha))) \tag{3.19}$$

The cross sectional area A_{cr} (m^2) is normally better known than d_{max} because it can be calculated as

$$A_{cr} = Q/\bar{u} \tag{3.20}$$

The method based on A_{cr} is therefore preferred to determine α. $\bar{u}$ can be calculated readily from the residence time of a tracer τ_r and the channel length L. Both can be determined accurately and the resulting A_{cr} gives an averaged value for the whole section. In the hydraulically rough range equation (3.13) can be simplified to:

$$f = \left[2 \cdot \log\left(\frac{14.8 \cdot R_h}{k_s}\right)\right]^{-2} \tag{3.21}$$

The mean water depth, d_{mean}, is calculated as:

$$d_{mean} = A_{cr}/w \tag{3.22}$$

Finally, the surface width w (m) can be calculated as

$$w = D \cdot \sin(\alpha) \tag{3.23}$$

3.2.3 Wetted biofilm in relation to discharge

A major part of the biological activity in the sewer is located on the sewer wall. The area in contact with the wastewater depends on the water height. This relation is shown in figure 3.2 for a pipe with Ø = 0.9 m.

3.2.4 Biofilm distribution

The biofilm is not uniformly distributed throughout the sewer (see page 11). Apart from heavy particles like sand that exert an abrasive force on the biofilm at the insert, the flow induces a

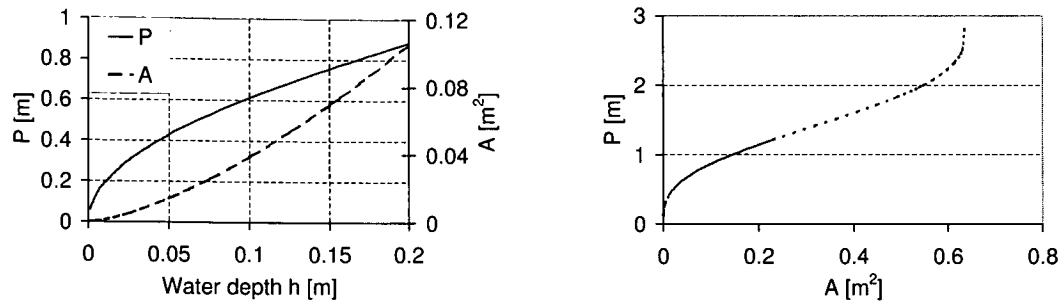

(a) As a function of the water depth.

(b) Wetted perimeter against the cross sectional area.

Figure 3.2: The changes of the wetted perimeter and cross section area.

shear stress that affects the biofilm surface. For uniform flow through a totally filled pipe the shear stress is given as:

$$\tau_w = \rho \cdot g_z \cdot R_h = \rho \cdot g \cdot S_f \cdot R_h = \rho \cdot (u^*)^2 \tag{3.24}$$

where τ_w = wall shear stress (N·m^{-2}) = (kg·m^{-1}·s^{-2}) and g_z = gravitational acceleration in the flow direction (m·s^{-2}). Equation (3.24) does not depend on the position along the (wetted) perimeter. It is common praxis to use this equation also for partly filled or even irregular channels. However, due to the boundary layer and the secondary currents this is an approximation, as will be shown in the following section.

3.2.5 Velocity distribution in open channel flow

Secondary currents and shear stress

A turbulent flow is always instationary, three-dimensional and has random deviations. This is even true when the statistically averaged velocity is constant (Nezu and Nakagawa, 1993). Such flows still produce large vortices. These are related to so-called bursts, which can have a large impact on gas transfer (see section 7.3.5). They are constantly produced in a random way, influence each other and disappear again, but they are not isotropic. This is in contrast with the high-frequency turbulent eddies.

Only a circular channel that is totally filled, is rotation symmetrical and has therefore a simple velocity profile. Measurements have shown that in any other form the velocity profile is distorted, as is shown for a partial filled open channel in figure 3.3. This is caused by secondary currents (SC) which flow perpendicular to the main flow. These have to be distinguished from the currents which are formed in bends in turbulent as well as laminar flow because these are the result of centrifugal forces and are normally much larger than the SC.

The SC are much more apparent in partly filled or open channels. They originate in general from anisotropy in the turbulence which are caused by the obstruction of the normal turbulent movements close to the wall and the free surface. The SC are therefore strongly influenced by the water level, the shape of the channel and the channel roughness. They cause a convective momentum transport that can influence the axial velocity profile, although their velocity is only 1 to 4% of the axial velocities. The surface vortex in open channel flow causes a strong horizontal flow directed from the wall towards the centre of the cross section which 'pushes down' the

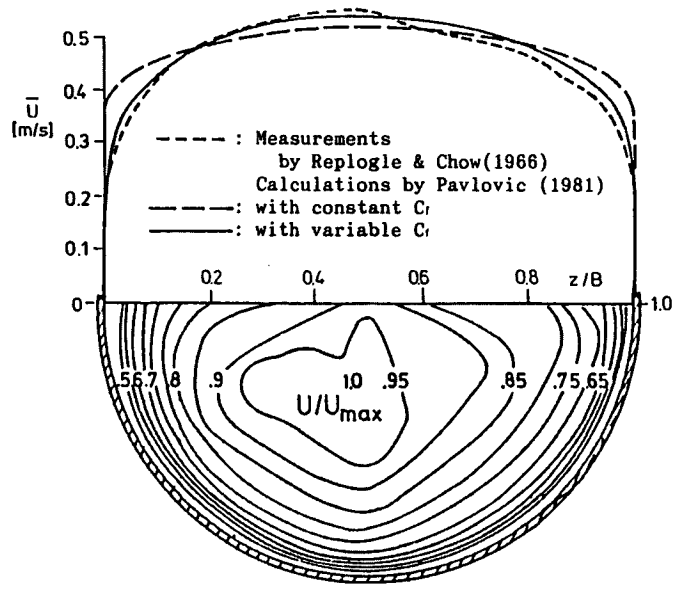

Figure 3.3: Measured velocity contours (lower part) and distributions of the depth-averaged velocity (upper part) for a semi-circular open channel (Nezu and Nakagawa, 1993).

isotachs: the 'velocity-dip.' Below the surface vortex is a return current at approx. half water height. This causes a horizontal momentum transport towards the wall and the typical deformation of the isotachs towards the channel wall. The precise location and effects of this vortex depend strongly on the channel geometry.

Kölling (1994) developed a model for the simulation of the axial and the SC in open channel flow. This numerical model was based on the mass and momentum balances that lead to the continuity and the three-dimensional Reynolds equation. He used a second order anisotropic turbulence model to calculate the correlations with the turbulence deviations of the Reynolds equation. This turbulence model describes the components of Reynolds stress tensors algebraically. The implementation of the universal logarithmic boundary layer equation makes it possible to use any kind of wall roughness. The cross section was made discrete with a finite elements method. This model allowed a changing wall shear stress along the perimeter of the channel.

The model of Kölling (1994) described the flow through a rectangular channel well in comparison with measured data. Figure 3.4 shows the velocity distribution for a circular open channel for three different fill grades ξ (-), expressed as:

$$\xi = d_{max}/D \tag{3.25}$$

where ξ = fill grade of the channel (-). Unfortunately, no precise measurements were available for a circular geometry.

One vortex perpendicular to the flow direction practically occupies the whole flow depth. The centre is close to the water surface, independent of ξ. The bend in the isotachs close to the water surface is a direct result of the SC that 'push' the isotachs to the centre. In all cases the SC are the strongest along the water surface because that is where most of the anisotropy is produced. From the middle of the water surface the normal velocity is directed downwards which will enhance the collection of particles at the insert as was observed by Wöhrle and

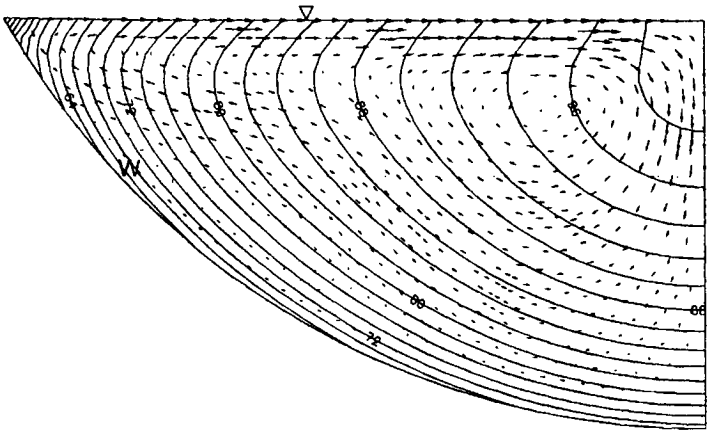

(a) A fill grade of 25%.

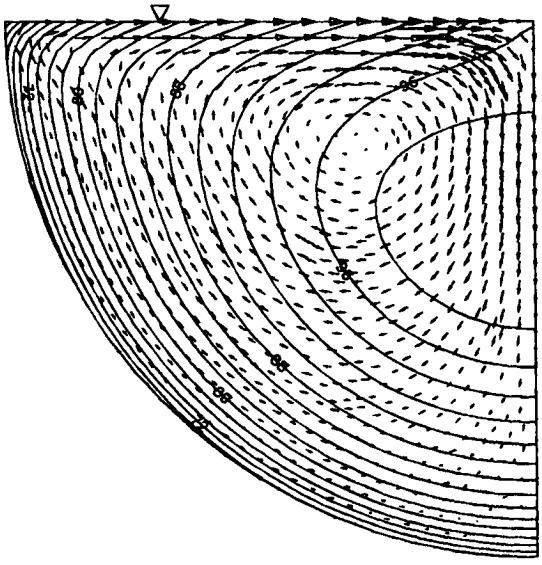

(b) A fill grade of 50%.

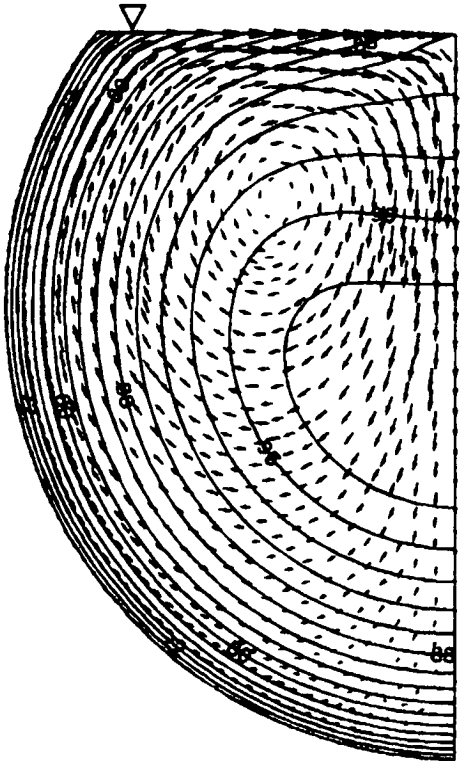

(c) A fill grade of 80%.

Figure 3.4: The velocity profile and SC in a circular channel with d=0.152 m and a slope of 0.05% (probably). The fill grades ξ are: 25, 50, and 80%. W = axial velocity, U = normal velocity. Note that the scales are different (Kölling, 1994)

Brombach (1991). This is the cause of the dense undercurrents in combined sewers that were described by Verbanck (1995). The SC close to the wall are directed parallel to the isotachs and are small in comparison to the ones near the surface. Therefore, they hardly affect the velocity profile, leaving it similar to the profile in a totally filled pipe. The simulation of a fill grade of 25% shows that the velocity maximum is located at the surface. Only at higher fill grades does this maximum move to below the water surface.

The α-angles under which the isotachs at the 25% fill grade reach the wall have been plotted against the relative longitudinal velocity (see figure 3.5). It can be expected that the wall shear stress follows a similar pattern.

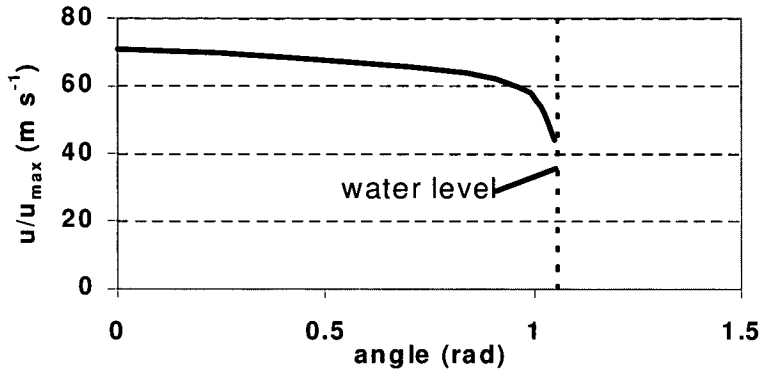

Figure 3.5: The flow velocity at the wall relative to the maximum velocity, as a function of the distance along the perimeter expressed as α (see section 3.1). The data have been taken from Kölling (1994).

4 Sewer research toolkit

4.1 Problem description

The sewer system has not been a central research topic in the past. Consequently, the applied techniques are even more basic than those used for wastewater treatment plant research. This is also related to the one major difference with the WWTP: the unsettled wastewater. Especially toilet paper has the strong tendency to stick to appliances, thereby covering sensors and clogging sampling tubes. Other factors that complicate experimenting in the sewer system are:

- The wastewater composition changes in the order of minutes or less.
- The diurnal changes in the discharge and in the wastewater composition.
- The influence of the sewer biofilm on the wastewater composition and on the conversion rates.
- The strong climatic influence.
- The difficult and localised access (only via manholes.
- The confined and branched structure of the sewer net.
- The dangerous environment (possibly toxic atmosphere, presence of pathogens, flowing water, darkness, and slippery, often invisible, inclined and uneven surfaces).

The following techniques that were adapted or developed are described in this chapter: wastewater sampling and analyses, biofilm sampling, in-line measurements and respiration rate measurements of wastewater and of biofilm. Whenever applicable a reference to appendix A is made where more detailed information is given.

4.2 Fast wastewater sampling

The changes in COD and other concentrations were determined by manually sampling at two locations. Samples were taken with the beaker opening pointing side ways to avoid that an unrepresentative amount of particles was collected.

The rapid composition changes of the wastewater meant that the samples at the inlet and outlet of a section should be taken from exactly the same water (synchronised). Unfortunately, the residence time depends on the flow rate and the state of the sewer wall and sediment. Therefore, the residence time cannot be predicted accurately and must be determined for each experiment.

4.2.1 Sampling synchronisation

Three tracer methods were therefore used to mark the wastewater:

Floating object. Polystyrene particles, tennis balls or even apples and potatoes can be used (Brombach, 1982). Although this method is easy, cheap and does not require much preparation, the wastewater must be constantly observed. Furthermore, the water surface velocity is

higher than average due to the velocity distribution (see section 3.2.5). Furthermore, neither the dispersion nor the discharge can be determined with this method. Floats were therefore used only to acquire a rough estimate of the residence time.

Dissolved colour tracer. Two coloured tracers are often used in studies of open channel flow. *Uranine* is a harmless, bright yellow-green fluorescing chemical of natural origin. Unfortunately, it is susceptible to biological and photochemical degradation. This makes it less suitable as a quantitative tracer. It is in principle possible to measure uranine directly in the water with a submersed fluorimeter, but that is not feasible in the sewer system (toilet paper). *Rhodamine* is much more resistant against degradation. This makes it less suited for the application in the urban hydrology system because it might not be completely degraded in the WWTP. Furthermore, it is difficult to judge the tracer arrival and the maximum concentration because the changes occur gradually and there is no easy reference because the whole wastewater will be coloured.

An estimation of the dispersion with either tracer can only be obtained when samples are taken with a high frequency.

Conductivity. Dissolved plain salt (sodium chloride) can be used as a tracer by measuring the conductivity. Although the required tracer concentration is in the range of 0.1 to 1 $g{\cdot}L^{-1}$, this is not problematic because it is cheap and has a high solubility of $\approx$ 300 $g{\cdot}L^{-1}$. Normally four kilograms dissolved in 20 L were added over 30 s when the discharge was 25 $L{\cdot}s^{-1}$. The tracer concentration (as conductivity) was easily measured in the field with a conductivity meter and was stored in a logger. The arrival, end and maximum in the tracer concentration could be determined accurately in the field by observing the display.

Salt is a conservative tracer. Therefore, later processing of the stored data allowed the determination of the actual discharge during the experiment (see section 4.4.3). Furthermore, salt is environmentally harmless and is invisible. This saves discussions with worried citizens and authorities. The only disadvantage is that extra equipment has to be used and that larger masses of tracer have to be prepared and carried around which is not feasible for large sewers.

The tracer was normally added 70 to 210 m before the first sampling site (see figure 5.1) and the sampling started 10 min. after the maximum had passed at the first sampling site . This procedure was followed to avoid that the sample would contain a significant amount of tracer. The previous discussion will have made clear that plain salt was the preferred tracer.

4.2.2 Amount of samples

A considerable number of samples (15 to 25) were taken at each site. In addition to the synchronisation, this allowed for a time shift of the resulting time series until their shapes matched. This way concentration changes could be determined accurately.

4.3 Sewer biofilm sampling

In this section the three techniques that were employed for biofilm sampling are presented. First, the use of a sewer balloon is described that can be used to lay bare a large biofilm area. Then, the use of a box to sample locally but destructively is described and finally the use of plates to obtain biofilm with an intact structure is explained.

4.3.1 Sewer balloon

Sewer balloons are drum-shaped, internally reinforced structures made out of rubber that can be blown up to approximately twice their uninflated diameter. They are normally used to prevent that contaminated water or other liquids spread through the sewer system. Another use is to block a sewer for maintenance work. The time the water can be held back depends on the sewer discharge, its slope and the location of the first critical point like a connection to a house or a combined sewer overflow. The section after the balloon will drain and samples can be taken from the whole cross-section of the sewer pipe.

Biofilm samples were taken as stripes with a width of 5 to 10 cm and a length of 50 cm. The location was measured as height from the insert, as shown in figure 4.1. The biofilm slowly released water from the time it was out of the water. However, this time was recorded and information about the biofilm water contents and biofilm density was obtained. This and the total suspended solids (TSS) and total volatile solids (TVS) analyses are described in appendix A.7.2. The sewer balloon method gives reproducible results for the biofilm characteristics as table 4.1 shows.

The major disadvantage of the sewer balloon method is that the collected water will create a wave when the balloon is removed. This will erode (an unpredictable amount of) the biofilm. Table 4.2 contains an overview of the advantage and disadvantages of this and the following sampling techniques.

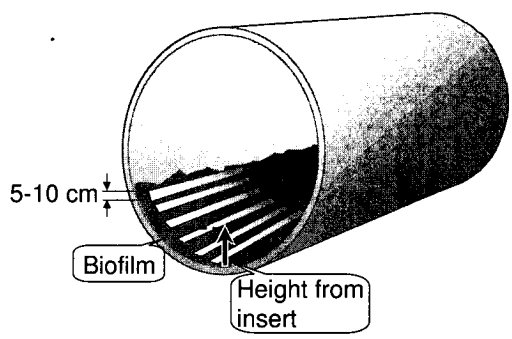

Figure 4.1: The definition of the height where biofilm samples were taken with the sewer balloon method.

Table 4.1: Triple measurement of sewer biofilm characteristics with the sewer balloon method. Areas of 0.05 m² were sampled.

		Average	Standard deviation	
			absolute	relative
thickness	[μm]	1375	132	9.6%
density	[kg·m³]	1082	0.8	0.1%
TSS	[g·m²]	245	32.5	13.2%
TVS	[g·m²]	84	13	15.0%
TVS:TSS	[%]	34	0.7	2.0%
COD:TSS	[%]	45	1.4	3.0%
COD:TVS	[%]	132	4.9	3.7%

Table 4.2: A list of the advantages and disadvantages of sewer biofilm sampling techniques.

	balloon	**box**	**plate**
disadvantages	• structure destroyed • biofilm erosion • heavy & bulky equipment	• structure destroyed • heavy equipment • localised • not for sediments • new box needed for every pipe diameter or shape	• time delay • artifacts possible
advantages	• large sampling area • sampling is easy • information about water contents of biofilm	• relatively quick • flexible • rest remains virtually unaffected	• structure intact • biofilm can returned • quick and easy

4.3.2 Semi-invasive biofilm sampling: the 'Biofilm box'

Another option to lay bare the biofilm is a box with an open bottom as depicted in figure 4.2. The curvature was equal to that of the sewer wall. Furthermore, a gasket ensured a tight seal. The construction to the right of the box in figure 4.2 was placed on top of the box and could be extended against the sewer wall to exert pressure.

The biofilm could be observed and sampled after the water had been carefully removed with a hand pump. A sample could be scraped from the wall, although the confinedness of the box made this difficult. A vacuum pump was therefore used in a set up as shown in figure 4.3. This enabled easy collection of the sample in 250 mL plastic bottles. The suction funnel had a width of one-third of the box. The box-area could therefore be divided over three samples. The TSS and TVS were determined as described in section A.7.2. Only the turbulence produced by the person standing in the water caused some minor damage to the biofilm downstream of the sampling location. See also table 4.2 for a comparison with the other sampling methods.

4.3.3 Intact Biofilm sampling

The two previous methods destroy the biofilm structure. This makes measurements with regard to biofilm mass fluxes impossible. To get intact biofilm samples, stainless steel rings with slots for thin plates were constructed (see figure 4.4). The local hydrodynamics have a significant effect on the formation and structure of a biofilm, as many authors found (e.g. Gjaltema, 1996). Therefore, several rings were installed in the sewer next to each other. Slits between the rings

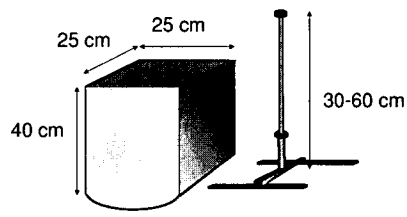

Figure 4.2: Set up for the collection of biofilm samples with the 'biofilm sample box.'

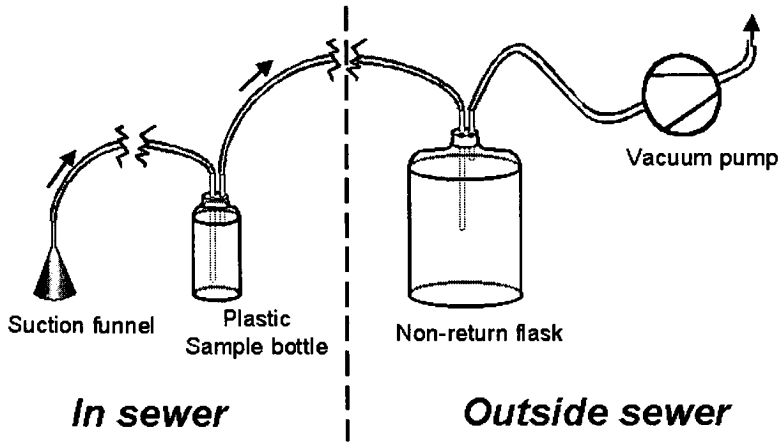

Figure 4.3: A diagram of the set up used to collect biofilm samples from the sewer wall. The non-return flask protects the vacuum pump against water.

were filled with Portland cement. Furthermore, the first three rings were not used for samples but only to stabilise the flow.

After a biofilm had developed, a ring was either released and turned so that the plates came out of the water, or it was removed as a whole. The plates were carefully removed and put into a container filled with wastewater. The container had slots to avoid that the plates would touch during transport and damage the biofilm. Experiments in the biofilm flow cell (see section 4.7) started within one hour after the plates had been removed. The plates could be returned after an experiment.

Plate material

The surface for biofilm growth, or substratum*, plays an important role in the initial phase of biofilm formation. Once the surface is covered with bacteria, the bond between the biofilm extracellular polymer substances and the substratum becomes most important. Apart from the material, attention should therefore be paid to the surface roughness. Several materials and surface treatments were tested (see appendix A.2 for details). The best results were obtained with polycarbonate (PC), treated with a rotating steel brush in the horizontal and vertical direction.

*the surface for biofilm growth

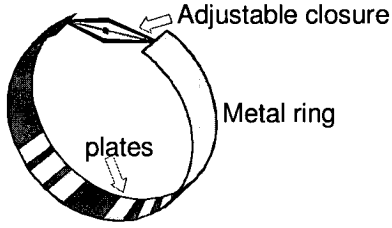

Figure 4.4: The stainless steel rings which served as the support for the biofilm substrata.

4.4 In-line measurements

Important variables like the oxygen concentration, temperature, conductivity and pH can be measured in-line* with sensors. The installation of these sensors and the logging equipment in the harsh sewer environment will be discussed in this section.

4.4.1 Protection of sensors

Autosamplers (Model 900Max, American Sigma, Medina, NY, USA) were equipped with an oxygen (galvanic type), a conductivity and a pH sensor. The accompanying manual proposes to simply hang the sensors from their wires into the water. However, soon the sensors were entangled with each other and totally covered by toilet paper etc. Furthermore, the cables and sensors were damaged as they hit the sewer wall, especially during rain events.

The sensors were therefore installed in protecting tubes (PVC) which were fixed to a frame by very flexible steel wire reinforced rubber tubing (see figure 4.5). This ensured that the sensors could follow the diurnal water level variation. Furthermore, they could swim up when the resistance to the flow due to attached toilet paper increased. Sharp edges were avoided, because these would trap floating material.

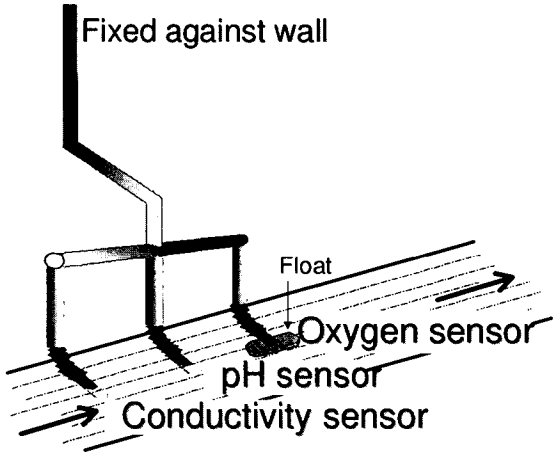

Figure 4.5: Construction for the protection of the sensors.

The **oxygen** sensor was especially susceptible to coverage. It was therefore equipped with an extra streamlined float of polystyrene that directed the coarse particles around the sensor and maintained a constant submergence for the oxygen sensor, independent of the water level. The sensor extended slightly and under a small angle from below the float, so that passing toilet paper could wipe the sensor surface clean. Otherwise, biofilm would cover the membrane within days and the oxygen reading dropped to half or even less of the actual concentration.

The **conductivity** sensor used an inductive measurement principle. Because this type has no electrodes in contact with the liquid, it was much more resistant against biofilm growth and coverage than the common sensors with two or four electrodes.

*__in-line__: the measuring device is placed in the reactor (e.g. oxygen sensor); **on-line**: the device is outside of the reactor, but connected with the medium (e.g. on-line ammonium analyser); **at-line**: the device is located near the reactor but there is no physical connection. However, a measurement can be conducted quickly (e.g. colourimetric ammonium test); **off-line**: samples are analysed later in the laboratory.

The **pH-sensor** was less susceptible to biofilm formation on its membrane than the oxygen sensor. The drift in this sensor was only $\approx$ 0.05 pH-units per week. However, the life span of this sensor was limited to approx. six months.

Each of the three sensors mentioned above contained a **temperature** sensor for the temperature correction. All four parameters were stored in the autosampler, which served as a logger with an interval of one minute.

4.4.2 Sensor calibration

Especially the oxygen sensor had to be cleaned and calibrated once a week. All sensor readings were checked with handheld meters to record the drift before they were taken out of the sewer. The sensors were only cleaned but not recalibrated when the difference between the atmospheric and the wastewater temperature was more than approx. 10°C. Otherwise, the recalibration was a lengthy and tedious task because of the time needed for temperature equilibration. Cleaning alone compensated for most of the drift. After reinstallation of the sewer sensors, their readings and those of handheld meters were compared again and differences were recorded.

4.4.3 Flow measurement

Continuous flow measurement with Doppler Ultrasound

The sewer discharge was measured with American Sigma 950 area velocity flow meters (American Sigma, Medina, NY, USA). The flow is calculated from the measurements of a Doppler ultrasound average velocity sensor, a bubbler water height measurement and the pipe geometry. The manufacturer claims an accuracy of 5%.

Dilution method

Occasionally, the discharge was accurately determined with the dilution method. This method is based on the addition of a known mass or mass flow of a tracer to the channel under study (e.g. ISO, 1983). Sodium bromide (analysed with an ionchromatograph, see A.7.6) and sodium chloride measured as conductivity have been used as tracer.

4.5 Respiration activity of suspended biomass

An important factor in the sewer conversion processes is the amount and activity of bacteria in the wastewater. Microbiological techniques like colony counting, in-cell DNA quantification or FISH* are interesting, but also very laborious and with a doubtful relevance for the actual conversion processes.

The respiration rate measurement is a common method in the WWTP research and gives a good indication of aerobic degradation (e.g. Kappeler and Gujer, 1992). The methodology is simple, although care has to be taken that the oxygen sensors are properly calibrated and handled (see appendix A.6). In the following two subsections the batch method and a continuous flow method will be described.

*Fluorescent in situ hybridisation

4.5.1 Wastewater batch respiration measurements

The method for the oxygen uptake rate measurement was adapted from the method presented by Pomeroy and Parkhurst (1973). A representative sample was taken from the sewer, aerated when the oxygen concentration was below 2 $mg_{O_2} \cdot L^{-1}$ and put in a closed container. The oxygen concentration was measured with a dissolved oxygen meter and stored on a computer with a custom-made oxygen uptake monitor program (OUM-program, see appendix B) written in LABVIEW (National Instruments, Austin, Texas, USA). Figure 4.6 shows the complete measurement system.

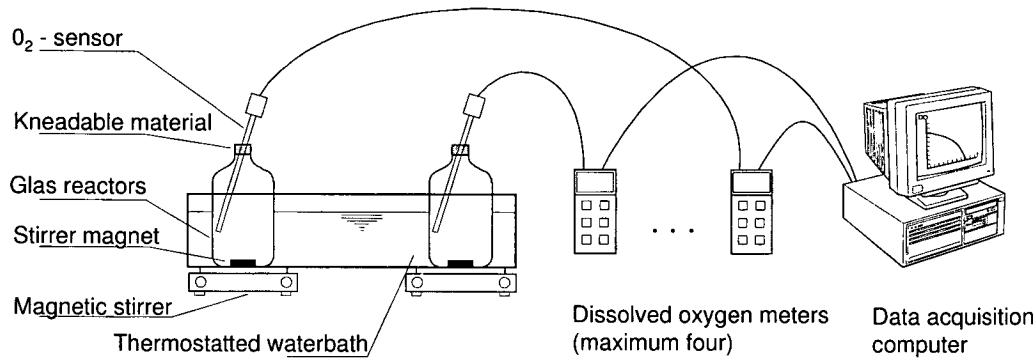

Figure 4.6: The experimental set-up for respiration measurement in wastewater samples (drawing by T. Gasser).

Representative wastewater samples were obtained from the sewer by scooping every 30 seconds for 10 minutes as described in section 4.2. The accuracy of the measurement system with properly calibrated oxygen sensors was very high; a test where the activated sludge respiration was measured with two oxygen meters on two separate channels gave 13.22±0.41 and 13.22±0.42 $g \cdot m^{-3} \cdot h^{-1}$ (30 measurements). The reproducibility when one sample was measured in two parallel reactors was 2%. An overall reproducibility of 7% was obtained when two successive samples where analysed.

For long-term experiments, stirred batch reactors as shown in figure 4.7 were used. These could be reaerated with either air (preferably) or pure oxygen. The OUM-program controlled the reaeration process.

4.5.2 Continuous wastewater respiration measurement

The batch respiration measurements as described in the previous section only result in the OUR* at the time of sampling. This rate might differ from the characteristic average rate at that time of the day due to the rapid changes in the wastewater composition.

A continuous flow respiration rate measurement made it possible to determine the average respiration rate over longer time periods. Wastewater was slowly pumped through one or more batch reactors. The decrease of the oxygen concentration in relation to the residence time gave the OUR.

A system based on a continuous-stirred tank reactor (CSTR) was used because it has a much smaller area-to-volume ratio than a plug-flow type reactor. Furthermore, the residence time characteristics of a CSTR smooth the incoming concentrations (see e.g. Levenspiel, 1972): a

*Oxygen uptake rate

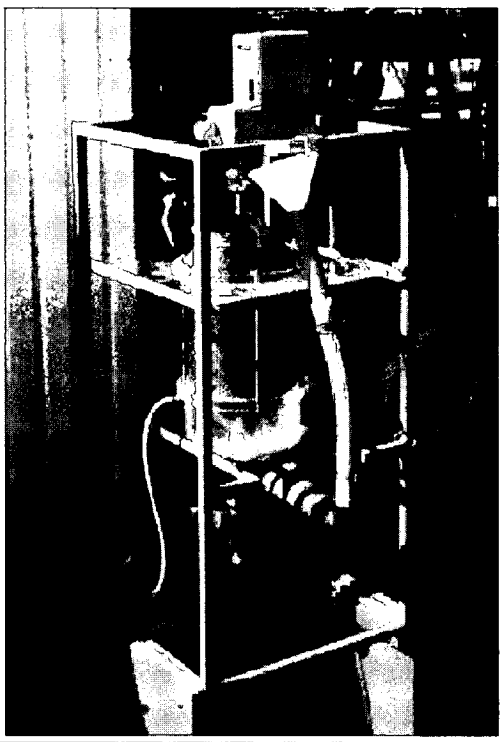

Figure 4.7: A photo of an 8–litre CSTR as used for the aerated batch experiments.

short pulse of a substance will be directly visible in the outlet and is then slowly washed out of the reactor. This behaviour is beneficial when dealing with the fast changes in the sewer system.

Figure 4.8 shows the set-up. The wastewater was taken from the sewer either at x = 0 m where the drop ensured complete cross sectional mixing, or at the culvert at x = 2015 m where turbulence was created with a temporary insert (see figure 5.1 for a map of the experimental). The strainer in the sewer was protected with a cap that directed toilet paper past it to avoid clogging. The wastewater was pumped from the sewer with a peristaltic pump (A) into a tall

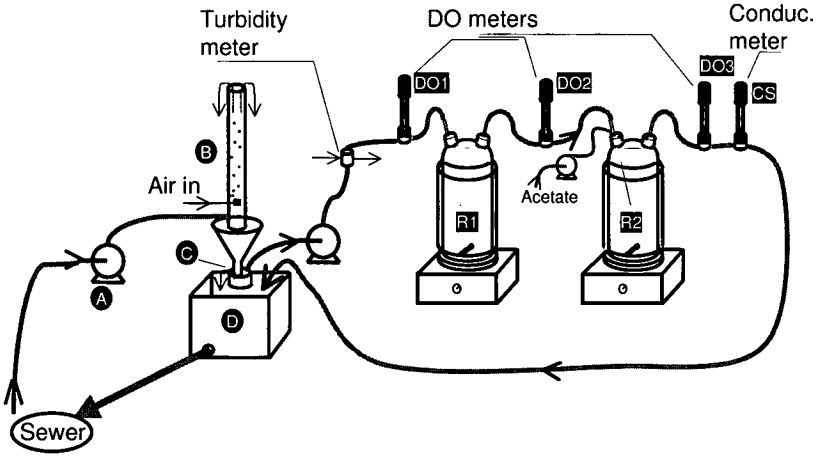

Figure 4.8: The experimental set up for the continuous flow respiration rate measurement.

aeration vessel (B) with a volume of 0.25 L. In (B), the wastewater oxygen concentration was raised by 4 to 6 mg·L^{-1}. The residence time was $\approx$ 2 minutes. The airflow from the bottom kept the particles in suspension and ensured complete mixing. Stripping of VFA* will have been negligible due to the high wastewater pH (8.0) and the short contact time. The wastewater flowed into the small container (C) (40 mL) from where a calibrated peristaltic pump transported it towards the first oxygen sensor (DO1). This way, the aeration air could escape and the flow of wastewater from the sewer and that through the reactors were decoupled. This was necessary because the wastewater flow from the sewer depended on the water velocity and height in the sewer, and on the degree of clogging of the strainer. The surplus water flowed back to the sewer via (D).

After the first oxygen sensor the wastewater flowed through the first stirred reactor (R1) with a volume of 5 L along the second oxygen sensor (DO2) into the second stirred reactor (R2) with a volume of 4 L. Here, acetate was added with 5 mL·h^{-1} to reach a concentration of 40 mg·L$^{-1}{}_{reactor}$ to activate the biomass present. The wastewater left the system past the third oxygen sensor (DO3) and a conductivity sensor (CS). It was returned to the sewer via (D). Samples (15 mL) were taken from the reactors on an hourly basis.

The sensors of oxygen meters (model OXI 340, WTW, Weilheim i. OB, Germany) were equipped with a clip-on magnetic stirrer (WTW) and installed in glass vessels (V_{dead} = 10 mL). They had been calibrated as described in appendix A.6. The data were logged and visualised on a PC (see appendix B). The glass reactors were thermostatted. All tubing was PVC.

4.6 *In situ* sewer biofilm activity measurement

The biofilm growing on the sewer wall is an important and interesting factor of the sewer system. Unfortunately, it is difficult to study due to its vulnerability and its location. Furthermore, the hydrodynamic conditions and the wastewater properties lead to an inhomogeniously distributed biofilm both in radial and longitudinal direction.

In the following sections two techniques for the sewer biofilm activity measurement are described.

4.6.1 Overall biofilm activity

The overall activity of the biofilm can be obtained from measurements of changes in the wastewater when a correction is made for the activity of the wastewater itself. For example, the respiration activity of the biofilm can be determined when the respiration activity of the wastewater (see section 4.5), the reaeration through the water surface (see chapter 7) and the incoming and outgoing oxygen concentration are known. Such results will be discussed in detail in chapter 8. However, it is not possible to detect the influence of local changes in hydrodynamic conditions on the biofilm properties.

4.6.2 Measuring the benthic activity

Methods to quantify the respiration activity of sediments have been developed in the past. Those *in situ* methods are direct measurements made in the field under ambient conditions (Bowman and Delfino, 1980). The applied devices should decrease the volume/surface ratio and prevent

*Volatile fatty acids

reaeration of the water. The result is the 'Sediment Oxygen Demand' (SOD) or 'Benthic (oxygen) Uptake Rate' (BUR) which consist of the biological respiration of all living organisms in the sediment and the chemical oxidation of reduced substances such as divalent iron and manganese, and sulphides (Bowman and Delfino, 1980). A review dealing with river and lake sediment oxygen demand has been presented by Bowman and Delfino (1980).

Several variants have been tested in the past. For example, James (1974) described a tunnel respirometer with a length of 30 m and a width of one metre that was constructed from steel hoops and plastic. The respiration in the bulk water and the change of the oxygen concentration in the tunnel were measured simultaneously. This method is unsuited for the sewer system because of the inaccessibility of the sewer. An alternative is to prevent reaeration by covering the water surface with a plastic sheet only. However, its installation is also troublesome.

Another option is the respiration chamber. This typically consists of a box open at the base that is pressed into the sediment. The decrease in the oxygen concentration is measured while the water is recirculated or stirred (Hickey, 1988). Care has to be taken that the natural hydraulic conditions are reproduced as well as possible within the chamber, especially with regard to the development of the boundary layer (Nowell and Jumars, 1984). The respiration chamber concept has been further developed for the sewer system as the sewer *in situ* flow cell.

4.6.3 Sewer *in situ* flow cell

An *in situ* flow cell that measures the biofilm activity directly in the sewer has several advantages:

- No time loss due to transport of samples into the laboratory.
- Flexible application since it can be used in any sewer as long as the curvature of the chamber fits the sewer diameter.
- No danger that the hydrodynamic conditions during biofilm growth were influenced by constructions in the sewer.
- No need to prepare and install a removable substratum (see section 4.7).

The disadvantages are:

- A lot of equipment has to be carried into the field.
- The sewer has to be large enough to make manoeuvring possible.
- The need to work with high voltage in a wet environment*.
- Longer exposure time to the sewer environment which increases the risk of accidents.
- The behaviour (especially erosion) of the biofilm cannot be checked visually due to the turbidity of the sewage that covers the flow cell.

A respiration chamber or *in situ* flow cell for the sewer systems needs a different design than its river equivalent because it cannot be pressed into the sediment but must be pressed against the wall. However, the flow cell height can be kept smaller because the wall has a smaller surface. This is beneficial for the volume ratio to surface area, V/A_f.

The main problem with benthic cells is the resuspension of sediment (Bowman and Delfino, 1980). In the sewer, thicker biofilm might be eroded. This would falsify the results because suspended biofilm has a much higher activity, as certain mass transfer limitations disappear. A careful design and proper flow control through the cell is therefore necessary to reproduce

*Only a 230 V pump could be used both submersed and in the open air, and had the right capacity.

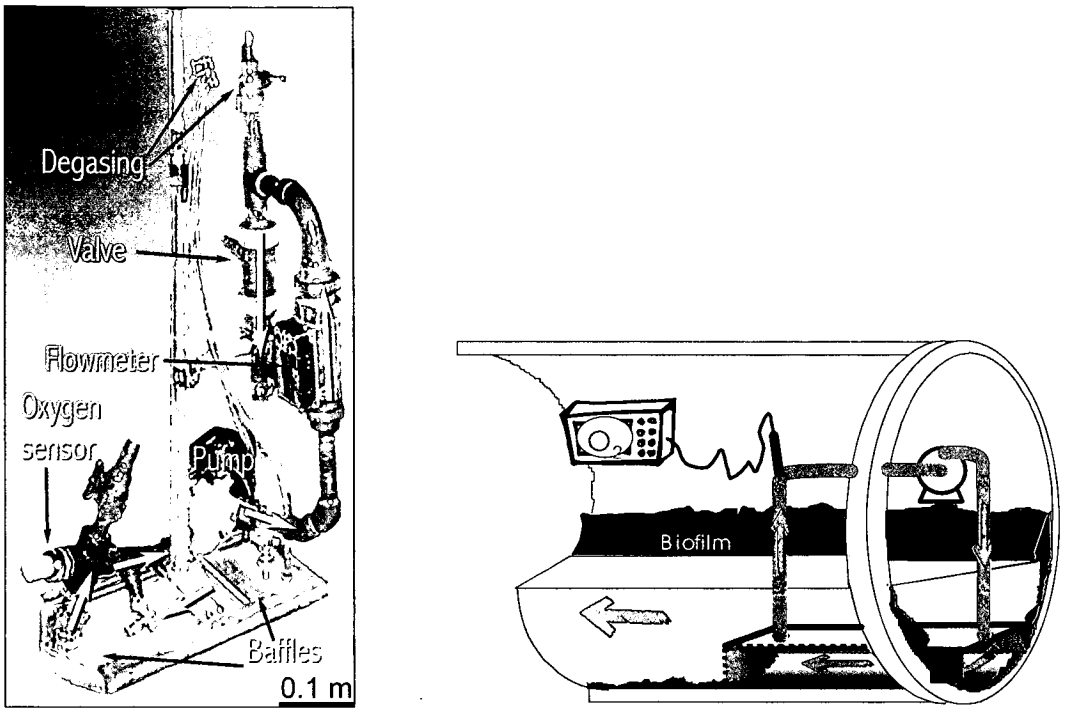

(a) Photograph of the *in situ* flow system.

(b) A schematic drawing of the in situ flow cell in the sewer.

Figure 4.9: The in situ flow cell.

the sewer hydrodynamic conditions as closely as possible. This is difficult because of the small chamber length in comparison to the length required for a sufficient boundary layer development (Nowell and Jumars, 1984).

A flume-like chamber with upstream and downstream baffles and diffusers that could be pressed onto the sewer wall was designed to obtain an even and unidirectional flow distribution over the entire measurement area (see figure 4.9(a) and 4.9(b)). Its dimensions were chosen so as to fulfill the following requirements with regard to the boundary layer thickness δ (m) (Nowell and Jumars, 1984): width $> 7 \cdot \delta$ to minimise the influence of the secondary circulation induced by the channel wall and length $> 50 \cdot \delta$ to allow the boundary layer to grow to its equilibrium thickness δ. At an average velocity of 0.3 $m \cdot s^{-1}$, δ is 5 mm, as calculated after the method presented by Cussler (1997). A chamber height of 18 mm was taken. The ratio of respirometer volume to active area V_T/A_f was 0.04 $m^3 \cdot m^{-2}$ ($A_f = 0.02$ m^2) The apparatus included an open-air/submersible circulation pump (30 $L \cdot min^{-1}$) and a flow meter. Either centrifuged raw wastewater (15 minutes at 4000 *g*) or river water (river Glatt) has been used as medium. With the latter the effect of an added carbon substrate (acetate) could be studied. Pure oxygen was occasionally injected to reoxygenate the medium. The oxygen readily dissolved due to the turbulence created by the pump and baffles. Details of the design and operation of the flow cell can be found in appendix A.3.

4.7 Biofilm flow cell

The *in situ* flow cell as described in the previous section is useful to measure the biofilm respiration in the film, but temperature or pH influences, or processes like nitrification etc. cannot be quantified. To study those influences and processes, the biofilm flow cell (BFC) was developed. This system allows for measurements under controlled conditions in the laboratory on biofilm that was grown in the sewer. The hydrodynamic conditions were mimicked as closely as possible to the sewer conditions.

4.7.1 Biofilm Flow Cell (BFC) and supporting system

The BFC-system is drawn in figure 4.10. The dimensions of the measurement cell are equal to those of the *in situ* system. The flow through the cell was turbulent. The resulting flat profile over the whole biofilm area is shown in figure 4.11. All data were collected in a computer equipped with a data acquisition card (model AT-MIO, National Instruments, Austin, Texas, USA). The oxygen uptake monitor program, custom programmed in LABVIEW (versions 3.0.1 up to 5.1, National Instruments), processed, stored and visualised the data of up to four independent systems. Furthermore, it controlled the oxygen concentration by periodic aeration with pure oxygen and the pH (see appendix B for details). The measurement was conducted within a DO-range of only 0.2 mg·L^{-1}. This resulted in a high resolution of the oxygen uptake rate measurement and

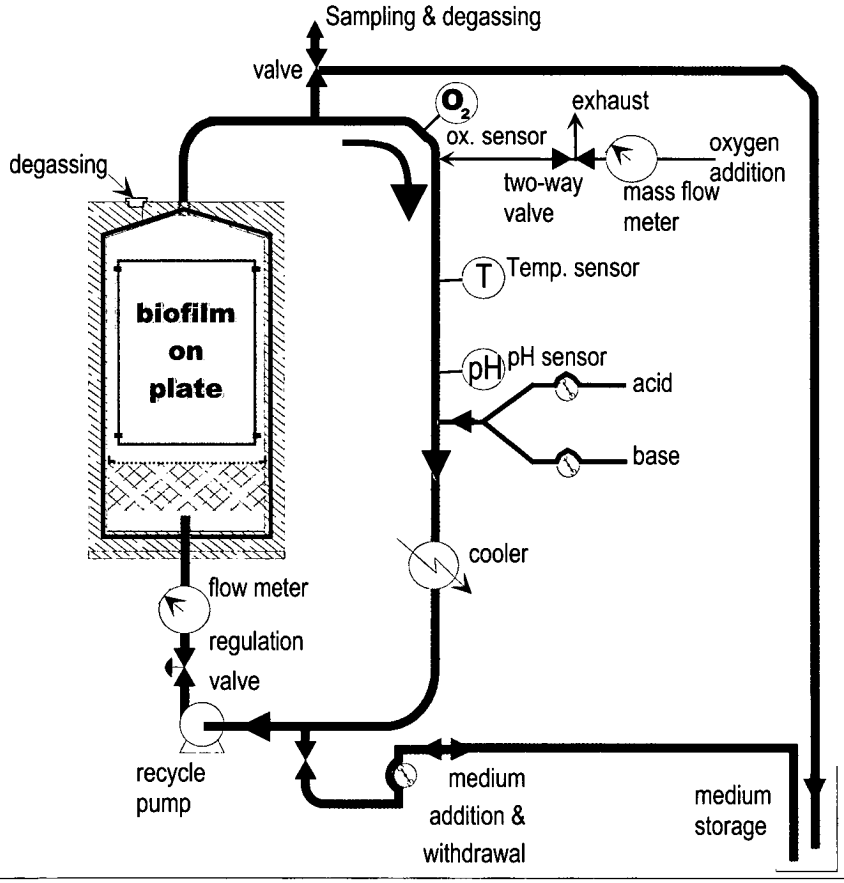

Figure 4.10: The laboratory Biofilm Flow Cell-system.

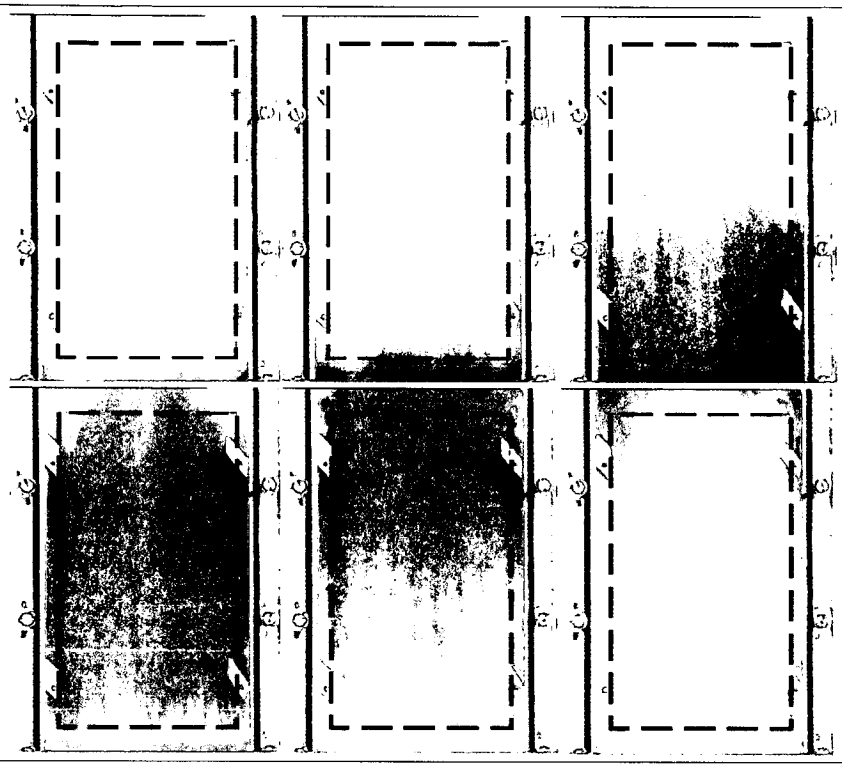

Figure 4.11: The flow profile through the BFC was visualised with a colour tracer. The rectangle indicates the location of the plate with biofilm. (many thanks to Raoul Schaffner for the camera work and the video editing).

kept the influence of the oxygen concentration on the biofilm negligible. However, the straightforward (feedback) DO-control with the oxygen meter output was impossible. Not only would the response time of the oxygen meter be too slow, but also would the plug flow character of the system with a residence time of $\approx$ 4 s hamper the response to an addition of oxygen. Therefore, the required oxygen mass was calculated and added while the oxygen flow was measured with a mass flow controller (Brooks Instruments, Veenendaal, The Netherlands). This corresponds with feedforward control.

The activity of one or two plates with biofilm that were obtained as described in section 4.3.3, was measured with centrifuged wastewater as the medium. Samples could be drawn from the system through the top valve while new medium was added at the bottom to compensate for the volume loss. More details about this system and its operation can be found in appendix A.4. Two parallel systems were available.

4.8 Other materials and methods

The common analysis methods for the COD etc. are described in appendix A.7.

5 Wastewater composition changes

5.1 Summary

The initiation of this study was the observation that the wastewater composition changes as it flows towards the wastewater treatment. To quantify these changes directly, samples were taken at the beginning and at the end of a two kilometre sewer section without connections. The following conclusions could be drawn:

- Automated samplers are of little use because of the composition fluctuations and the dependency of the wastewater residence time on the discharge.
- Manual, high frequency sampling showed that consistent significant changes only occurred for ammonium, nitrite, nitrate and oxygen.
- Trying to track down conversion processes by analysing wastewater samples is often a waste of resources, money and time.

5.2 Introduction

In this section measurements will be presented to quantify sewer conversion processes in the wastewater and biofilm. The emphasis lies on other compounds than oxygen, which will be treated in detail in chapter 8. Apart from concentration measurements at the inlet and outlet of a sewer section, the residence time of wastewater will be discussed. The chapter will start with a description of two sampling sites.

5.3 Site descriptions

5.3.1 Main sewer *Rümlang–Oberglatt*

The rural town of *Rümlang* near Zürich in Switzerland produces wastewater of 5000 population equivalents. Some information on the sewer system within the town is given in table 5.1. There is no predominant type of industry, although traces of a paint factory in the form of a solvent smell and colouration of the wastewater have been observed on some occasions. The town's wastewater is collected via three sewer strands that meet at the beginning of a main sewer (see figure 5.1). This is also the beginning of the measurement section. Table 5.1 contains the characteristics of this sewer. The section ended at a culvert with a diameter of 0.45 m that caused a small backwater effect which was of importantance only during rain events. Manholes did not influence the water flow up to a water level of 0.55 m because they had circular inverts. Most measurements were done in this sewer.

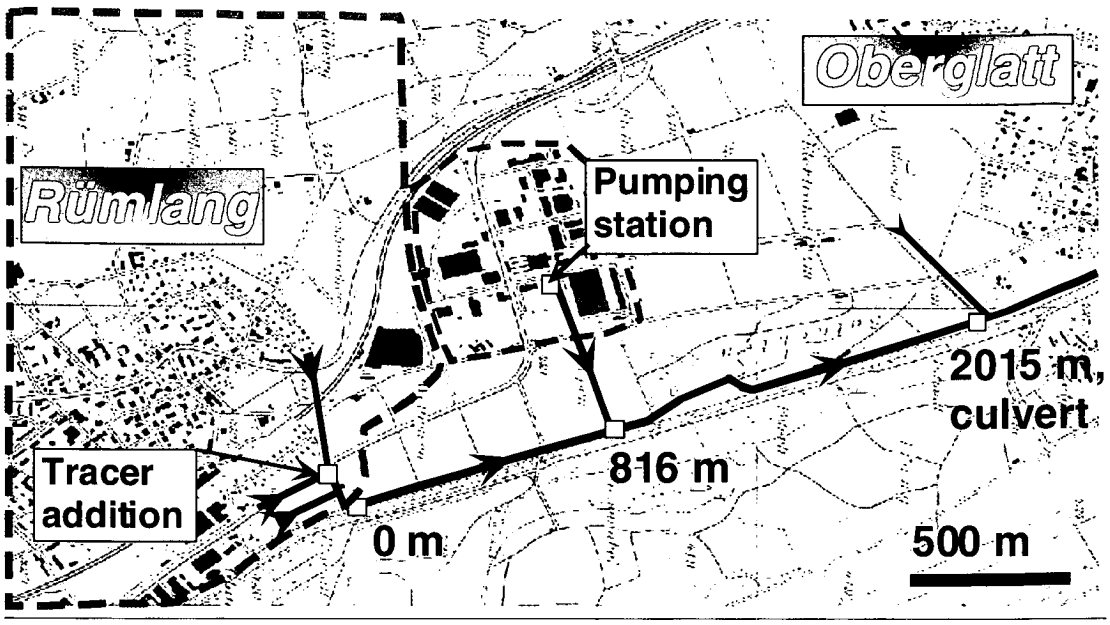

Figure 5.1: Top view of the location of the main sewer between the villages Rümlang and Oberglatt in the Canton of Zürich, Switzerland.

Table 5.1: Properties of the sewer system of Rümlang (left) and of the main sewer from Rümlang to Oberglatt (right) in the Canton of Zürich, Switzerland. D =sewer diameter (m), S_0 = sewer slope (%), $L_{sect.}$ = section length (m), Q_{DW}^{day}= daytime dry weather discharge (L·s^{-1})

Replacement value	SFr. 40,000,000		D	0.9	m
Total length	23.1	km	S_0	0.091±0.035	%
Total volume	800	m^3	$L_{sect.}$	2015	m
Wetted surface area	8000	m^2	Q_{DW}^{day}	25	L·s^{-1}

5.3.2 Main sewer *Remigen–Villigen*

The small main sewer between *Remigen* and *Villigen*, Canton Aargau in the north of Switzerland had been completed two months earlier when measurements were conducted there (see figure 5.2). The measurement section with a length of 1.56 km started directly after the village and ran to "*Hasel*", a small community. The average daytime discharge through this sewer with a diameter of 0.3 m was 2 L·s^{-1}.

5.4 Residence time in the sewer

A predominant factor for the sewer conversion processes is the wastewater residence time τ_r. Not only constant factors like the sewer design affect τ_r, but also the discharge and the biofilm properties. The wall material and its properties are however irrelevant because of the biofilm that covers it.

The residence time was mainly determined with plain salt as a tracer. It was measured directly in the field via conductivity. Bromide was used to accurately quantify the discharge.

The results of residence time measurements of several experiments in the *Rümlang* sewer are shown in figure 5.3. A wall roughness k_s of 5 mm gives a good general fit. Deviations from

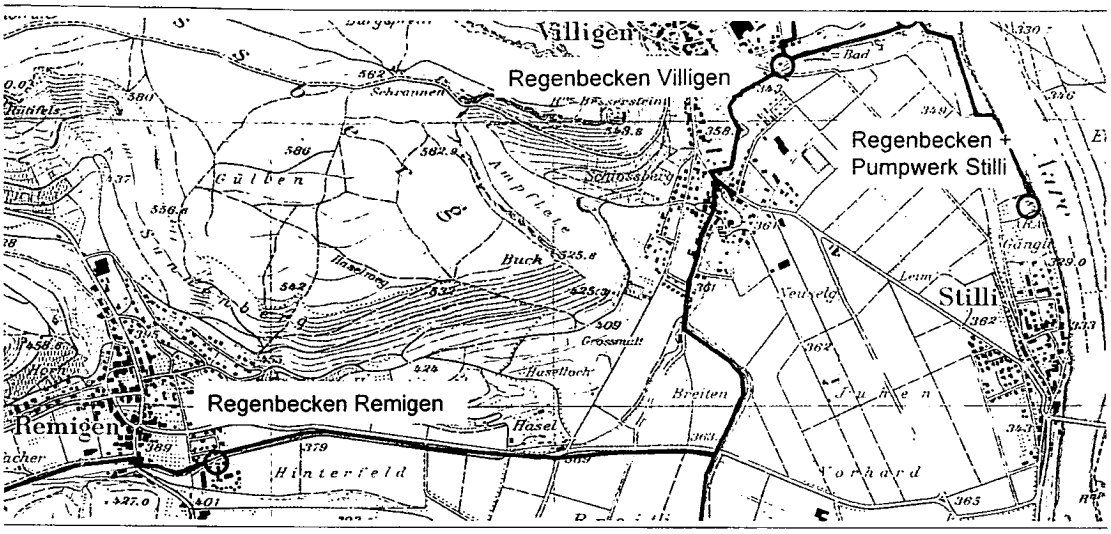

Figure 5.2: Experimental site between Remigen and Hasel, Canton Aargau, Switzerland.

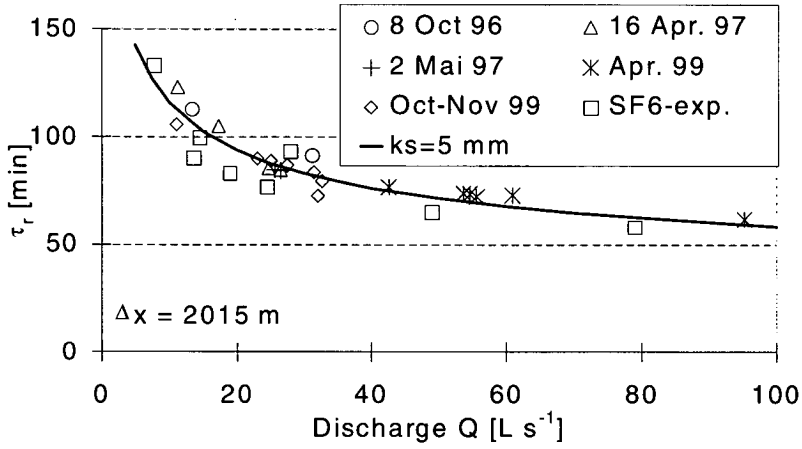

Figure 5.3: The residence time, τ_r, as a function of the discharge. The line for k_s = 5 mm was determined with the hydrodynamic model of chapter 3.

the predicted residence time will be predominately caused by variations in the biofilm surface and by discharge measurement errors.

With the relationship between Q and τ_r of figure 5.3, the residence time can be approximated from the flowrate (see figure 5.4). Variations of $\approx$ 40% due to the diurnal variations occur because the flowrate in this main sewer is directly linked to the activities in the town with its centre located on a low hill 0.7 km from the beginning of the section (see the map, figure 5.1).

5.4.1 The age of the *Rümlang* wastewater up to the measurement section

The age of the wastewater in *Rümlang* before it reaches the measurement section has been measured with plain salt as a tracer. The tracer was added at the beginning of two of the three major sewer strands. Conductivity, oxygen and pH meters were installed at several locations.

The results showed that the 'oldest' wastewater, which came from a hamlet 2.2 km away, had an age 65 min. It contributed however < 5% to the total discharge. The 'freshest' wastewater

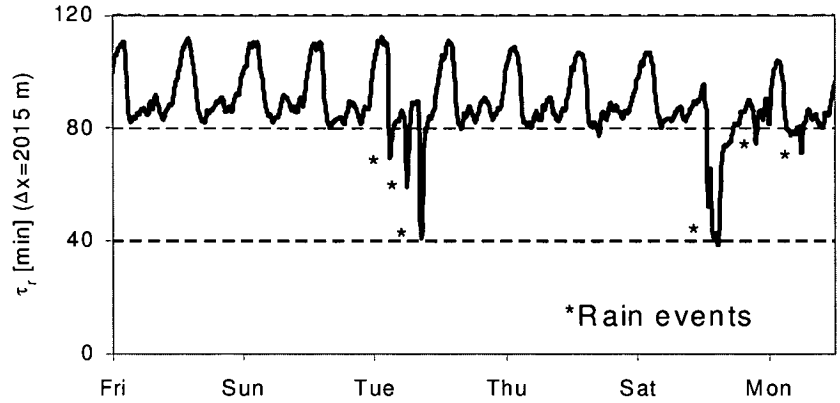

Figure 5.4: A typical residence time distribution with some rain events in the Rümlang sewer (starting May 30, 1997).

was 7 min. old. On average the age was 30 min. The initial oxygen concentration in the village of 4.5 $mg \cdot L^{-1}$ (in June 1999) had dropped to $\approx$ 3.0 $mg \cdot L^{-1}$ when the wastewater reached the main sewer. This showed that (biological) activity was present directly from the wastewater source. The pH remained constant at 8.0.

5.5 Changes in wastewater properties

5.5.1 Sampling and Measurement

The most obvious method to study the processes in the sewer system is to measure changes in the wastewater composition in a defined system (e.g. Raunkjær, 1993; Almeida *et al.*, 2000). However, due to the fast dynamics and the small concentration changes in the sewer system is seems doubtful whether the balancing of dissolved compounds will be helpful in the quantification of the processes. Several measurement campaigns were conducted to confirm this.

5.5.2 Sampling with autosamplers

Measurements in real sewers can either be manual and intensive*, or prolonged like a day or a week using an autosampler.

An example of the latter is shown in figure 5.5. The samplers started at the arrival of a conductivity peak (plain salt) which ensured initial synchronisation. Four samples per each of 24 bottles were taken. There are several drawbacks to this method:

The residence time changes with the flowrate. This could be partly corrected for because the flowrate was measured too. However, a shift of only a few minutes in the 'out' curves of figure 5.5 can mean the difference between a COD increase or a COD decrease over the sewer stretch.

The resolution is too low. A small rain event took place at 4:00 AM. The sampling interval was much too large to obtain a good resolution of this event. It would be possible to decrease the sampling interval during a (rain) event by connecting the sampler to a rain gauge, flow

*many samples within a short time frame (e.g. 30 min.)

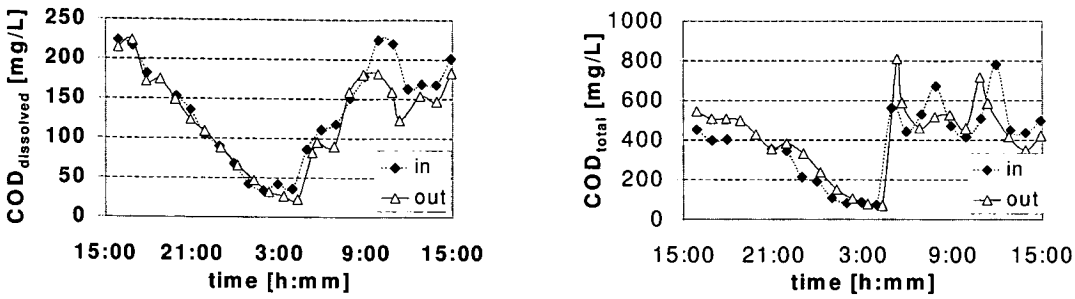

(a) (b)

Figure 5.5: The dissolved (a) and total (b) COD-concentration at x = 117 m (in) and 2015 m (out) of the Rümlang sewer on 2 to 3 June 1997. The curves of the second site have been shifted to compensate for the residence time.

meter or sensors, but the number of bottles would soon become limiting (unless several samplers are connected).

The strainer of the sample tube will lie at the insert. The reduced mixing at lower flow rates will lead to segregation and to a dense undercurrent. Wöhrle and Brombach (1991) clearly showed the existence of dense undercurrents, which contain a much higher concentration of particles. Therefore, only a high level of turbulence can prevent biased results. This requires a mixer at the sampling site, for example a bubbler.

5.5.3 Manual sampling

Manual, fast sampling —as was described in section 4.2— is a better option to quantify the wastewater changes than the autosamplers.

Some results from the *Rümlang* sewer are shown in figure 5.6 and figure 5.7. The samples were analysed in a random order. The same dissolved oxygen and conductivity meters were used at both locations. Therefore, systematic errors will not have led to false conclusions about the significance of changes. The conditions during the experiments are listed in table 5.2. These enable a calculation of the mass fluxes and the biofilm conversions per m^2. For example, the biofilm denitrified 0.7 and 1.9 $g_N \cdot m^2 \cdot d^{-1}$ during the 'night' and the 'day', respectively.

The clear shapes of the pollutographs due to the large number of points within a small time frame made it possible to correct for small errors in the residence time by shifting one of the curves until the shapes of the curves fitted. This was done during the 'day' (19:00) measurement.

Table 5.2: The conditions during the sampling campaigns. (Q = discharge, $L_{sect.}$ = section length, τ_r = residence time, T_m = water temperature, P_w = wetted perimeter, A_w = wetted biofilm area, A_{cr} = cross-sectional area)

		Q [$L \cdot s^{-1}$]	$L_{sect.}$ [m]	τ_r [min]	T_m [°C]	P_w [m]	A_w [m^2]	A_{cr} [m^2]
Rümlang	5:10 ('night')	28	1847	83	9.5	0.77	1420	0.072
	19:00 ('day')	50	1847	69	12.2	0.88	1630	0.10
Remigen-Hasel	11:30	1.9	1560	35.5	12	0.20	312	0.0041

A statistical evaluation of the results, as given in table 5.3, can identify whether changes are significant or not. A probability distribution showed that the time series at the beginning ('in') and at the end ('out') had a similar degree of diversity. A normal student's t-distribution test could have been used to test whether there is a significant difference between the 'in' and the 'out' time series. However, this test uses the averages and the standard deviations of each time series. Unfortunately, the concentration can change rapidly, as for example the phosphate measurement during daytime in figure 5.6 (right side, middle) shows. This leads to a large standard deviation (σ).

Because the sampling is synchronised and no external influences can be expected, it is allowed to test the samples from both time series pairwise. This results in the probability of table 5.3 that describes the chance of a valid zero-hypothesis. A difference is regarded as significant when the probability is less than 5%.

Only nitrite (NO_2^-), nitrate (NO_3^-), ammonium (NH_4^+) and dissolved oxygen (DO) clearly changed. The large difference in total COD during the 'day' was probably an artifact at the second sampling location because this difference was not observed during other campaigns.

Table 5.2 and table 5.4 contain the conditions and results of a similar experiment but in the connecting sewer between *Remigen* and *Villigen**. The results are comparable but no significant change in the alkalinity (HCO_3) was found.

Interpretation of the wastewater concentration changes

Some concentration changes over the measurement sections with a length of 1.6 to 2 km were significant but they are often unusable to draw conclusions on degradation rates:

Especially $\mathbf{NO_3^-}$ is degraded. The biofilm is responsible for this because the wastewater remained aerobic during all measurements. The source of nitrate is mainly drinking water, not nitrification.

*See section 5.3.2 for a site description.

Table 5.3: Statistical evaluation with a paired t-test of the concentration changes over the Rümlang sewer section on 18 and 19 March 1999. A negative average means a decrease. $\overline{\Delta}$ = the average difference between the points of two pollutographs, σ = the standard deviation based on a sample of the population and Pr = Probability (%) = the likely occurrence that the concentrations stayed unchanged over the measurement section.

'Night'	NO_2^- $g_N \cdot m^3$	NO_3^- $g_N \cdot m^3$	NH_4^+ $g_N \cdot m^3$	COD_{total} $g \cdot m^3$	$COD_{diss.}$ $g \cdot m^3$	SO_4^{2-} $g_{SO_4} \cdot m^3$	PO_4^{3-} $g_P \cdot m^3$	HCO_3^- mmol
$\overline{\Delta}$	0.02	-0.41	1.57	0.50	-1.23	0.10	0.04	0.11
σ	0.01	0.10	1.17	12.38	3.25	0.83	0.09	0.10
Pr [%]	0.0	0.1	2.3	87.4	24.1	100.0	100.0	0.0
signif.?	yes	yes	yes	no	no	no	no	yes
'Day'								
$\overline{\Delta}$	0.08	-0.70	2.41	75.90	-7.92	-0.01	0.01	0.08
σ	0.02	0.12	2.29	33.30	6.02	1.58	0.21	0.10
Pr [%]	0.0	0.0	0.1	77.9	0.0	100.0	100.0	0.0
signif.?	yes	yes	yes	no	yes	no	no	yes

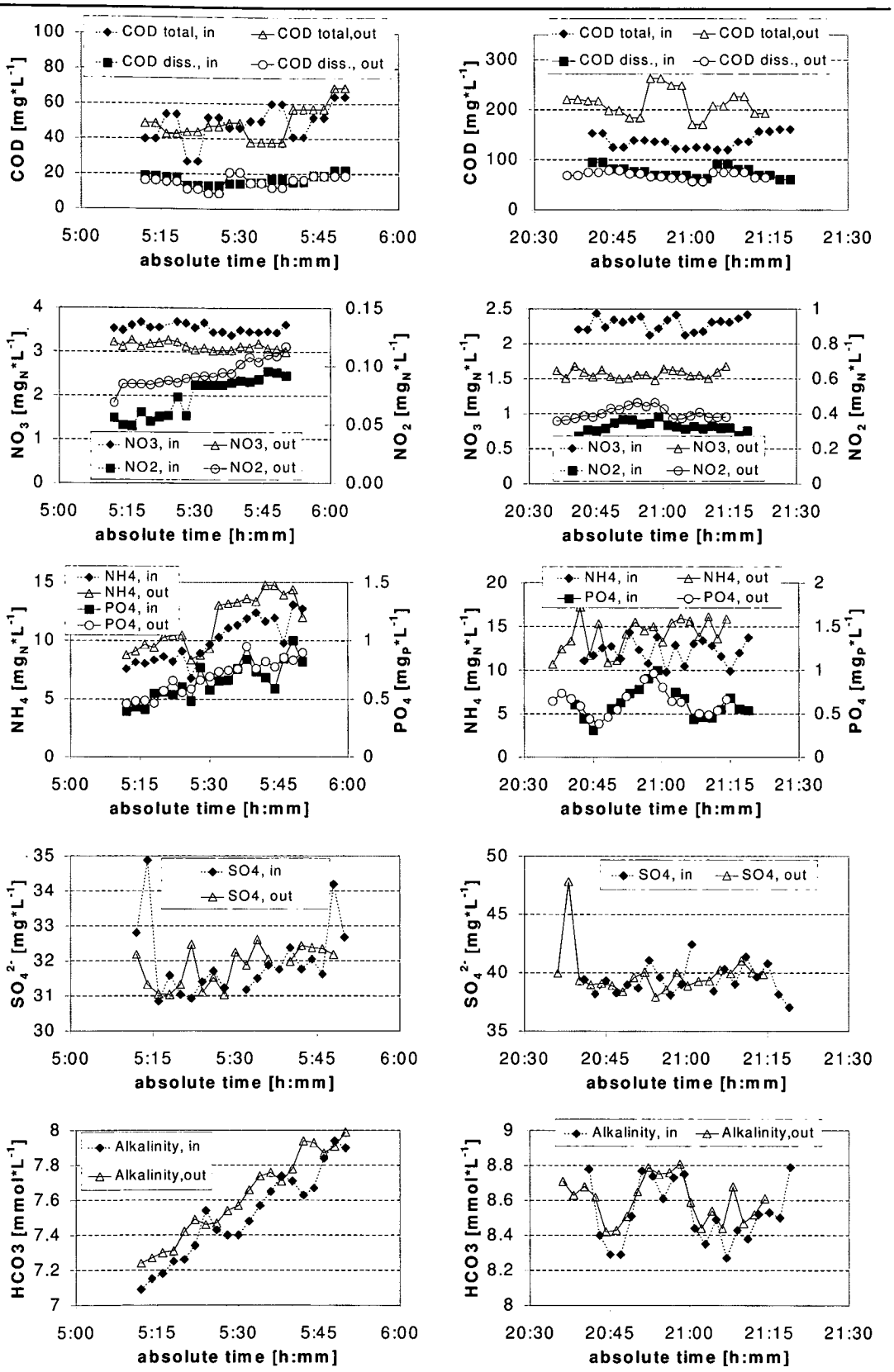

Figure 5.6: The results of fast sampling during the 'night' at 5:10 (left) and 'day' at 19:00 (right) in March 1999. The curves of the second site have been shifted to compensate for the residence time. See text for further comments.

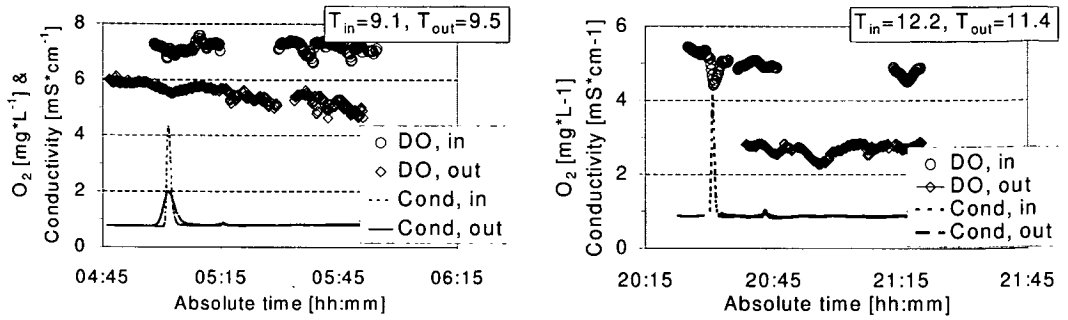

Figure 5.7: The DO-concentration and the conductivity before and during the fast sampling. The curves of the second site have been shifted to compensate for the residence time. ('night' = left, 'day' = right).

Table 5.4: The results of a measurement campaign in the connecting sewer between Remigen and Villigen in December 1997.

	NO_2^-	NO_3^-	NH_4^+	$N_{tot.}$	SO_4^{2-}	PO_4^{3-}	HCO_3^-
$\overline{\Delta}$	-0.09	-1.18	3.36	-0.80	0.64	-0.03	0.24
σ	0.02	0.22	1.40	3.34	6.32	0.22	0.44
t-value	8.26	20.26	4.56	0.68	0.60	0.66	2.00
Probability [%]	0.0	0.0	0.0	28.5	47.6	30.6	2.5
significant?	yes	yes	yes	no	no	no	yes

	TSS	TVS	$COD_{tot.}$	$COD_{diss.}$	DOC	TOC
$\overline{\Delta}$	20.96	13.34	-11.86	-34.33	-14.06	-2.19
σ	22.34	13.33	28.63	20.38	8.43	12.36
t-value	2.25	1.95	0.55	3.11	5.15	0.41
Probability [%]	0.1	0.0	7.2	0.0	0.0	42.7
significant?	yes	yes	no	yes	yes	no

NO_2^- is an intermediate and might either increase or decrease. Practically all NO_2^- will have been produced by denitrification. No data on the drinking water concentration were available, but it is too toxic to be allowed in a significant concentration. The increase in the nitrite concentration, despite a decrease of nitrate, is probably caused by the nitrate respiration of e.g. *E.Coli* that is known to have this pathway (Schlegel, 1986).

The increase in **NH_4^+** seems unexpected at first sight since a nitrification would be expected under aerobic conditions. This is however mainly caused by urea hydrolysis (see appendix C.2).

Changes in the **PO_4^{3-}** concentration were neither expected nor observed.

The **dissolved COD** is an intermediate between the hydrolysis of particulate material and biological degradation. One fraction is the easily degradable substrate (S_S), which is quantified in appendix C.3. A significant change in the total dissolved COD indicates that processes occur. But a degradation rate cannot be deduced from the data because dissolved COD is only an intermediate.

The **total COD** could be used for quantification but the dense undercurrent and the occurrence

of coarse particles* can easily falsify the results. Furthermore, the biofilm in the sewer section will erode which will contribute to the total COD. But the amount of erosion will depend on the biofilm growth rate, the age of the biofilm, the wastewater properties and the flow rate. The COD_{tot} is therefore not very suited to draw conclusion on the degradation or composition changes.

Biological processes can strongly influence the **alkalinity**. A significant change was sometimes observed. It seems not very suited as a parameter to quantify sewer processes because the effects of all processes from heterotrophic growth to methanogenesis are lumped into it.

Significant concentrations of **elementary sulphur** have been found in the *Rümlang* biofilm which indicates that a sulphur cycle must be active (see section 2.5.2 and 6.6.3). However, the net changes in the sulphur compound pools will be negligible compared with the mass flow of $\mathbf{SO_4^{2-}}$ through the sewer.

The **dissolved oxygen** (DO) concentration showed always a significant decrease as a result of biological processes. The converted oxygen is partly replaced with oxygen from the air by reaeration. A separate chapter has been dedicated to reaeration because it is important under all conditions, especially when the DO-concentration is low.

More specific analysis of pollutants e.g. carbohydrates and proteins as was done by for example Raunkjær (1993), have been tested during this study. The results of these laborious tests showed that such tests are not particularly useful. Furthermore, these substances would require an uncommon modelling approach.

5.6 Conclusions from the field sampling

A major problem when determining concentration changes over a sewer stretch is that the random variations at one sampling location are often larger than the absolute changes between the 'inlet' and 'outlet' of a section. The smaller the sewer the more disturbing this effect will be. The best method to obtain reliable data is manual sampling with a small interval (typically 2 minutes to allow for field filtration of the samples).

The manually taken samples were analysed in a random order to avoid systematic errors. In this light, the use of an automated analyser at the inlet and the outlet of a section must be strongly dissuaded. Systematic errors can easily occur due to the difference in the dense undercurrents at the sampling locations (see page 20 and 5.5.2), tube biofilm growth (especially for NO_2^- and NO_3^-) and machine depended factors because more than one sampler will be used. Apart from the normal operational difficulties of these machines, the peculiarities of the sewer system with its strong dynamics and the difficult sampling conditions (toilet paper and dental floss to name a few) should not be forgotten.

The sewer is built as a closed system, but with a life span of a century it is unlikely that it stays intact. Minor sewer infiltration of e.g. nitrate-rich groundwater in agricultural areas might strongly influence the results. Furthermore, undocumented or illegal connections can make all measurements worthless.

The quantification of sewer processes by the measurement of wastewater properties is only worth the effort when the residence time is clearly larger than one hour. Only changes in dissolved oxygen, nitrite and nitrate can be quantified with smaller residence times.

*In the range of millimeters, e.g. of broken up toilet paper.

The results show that it is a better option to study the causes of possible changes —the conversions by bacteria and other chemical processes— than the resulting concentration changes in the wastewater. The focus will be on those conversions in the following chapters.

6 Biofilm distribution, development and activity

6.1 Summary

The sewer biofilm has many unknown aspects. Its environmental conditions are different from those in rivers and in wastewater treatment plants because raw wastewater is nutrient rich and contains organic and inorganic particles with a wide range in sizes and properties.

In this chapter information about the biofilm characteristics is presented. Several experiments dealing with aspects of the biofilm are discussed. They seem unrelated but the acquired information in the form of parameters or the relative importance of processes will form the foundation for the sewer model that will be presented in chapter 9.

The following conclusions could be drawn from the measurements:

- The TSS and TVS are unevenly distributed along the perimeter. This does however hardly affect the aerobic activity of the intact biofilm.
- The total aerobic activity of young biofilm is proportional to the TSS and TVS.
- Older biofilm contains a considerable fraction of aerobically inactive organic material.
- A consistent effect of filaments on the aerobic activity was not found.
- Bacterial storage materials (PHA's, glycogen) were found.
- Methanogenic, sulphate reducing and sulphide oxidising activities were observed, but did not play a major role in the conversions.
- Hydrolysis took place in the bulk as well as in the biofilm.
- The sewer is not carbon and energy source limited during daytime.
- Biofilm can release easily degradable substrate (S_S) to the bulk liquid.
- The outer biofilm layer receives its easily degradable substrate mainly from the wastewater.
- Hydrolysis in the biofilm is comparable to the process as defined in the Activated Sludge Model no. 3 (Gujer *et al.*, 1999).
- The denitrification rate was not affected by the bulk oxygen and the nitrate concentration.
- The sewer biofilm activity of the town *Rümlang* with 5000 People Equivalents (PE) and the main sewer is comparable with a trickling filter volume of 110 m^3.

6.2 Distribution of biofilm along the sewer wall

The flow velocity and shear forces can have a large impact on the biofilm structure and properties (e.g. Gjaltema, 1996). The (hydrodynamic) conditions in the sewer system are divers and change both in longitudinal and radial direction. To what extend this affects the biofilm distribution and activity will be discussed in this chapter.

The structure is further influenced by the organic and inorganic particles transported through the sewer. These exert an abrasive force on the biofilm, but are also incorporated and might reinforce the biofilm (see figure 2.3). As a consequence, the biofilm amount, properties and activity can be expected to change in longitudinal as well as in radial direction. Some SEM* photo's of sewer biofilm are given in figure 6.1 and 6.2. Several bacterial morphologies can be observed. Inorganic material is clearly incorporated within the biofilm.

6.2.1 Radial distribution

At least three factors are responsible for the radial biofilm distribution:

- Firstly, the velocity distribution induces a shear stress field with a maximum at the insert and a minimum at the wall close to the water surface, as was explained in section 3.2.5. The shear becomes especially small close to the water surface. Furthermore, there is a small secondary current along the wall perpendicular to the flow.
- Secondly, the transport of sediment, which exerts an abrasive force on the biofilm.
- Lastly, fats and oil in the wastewater will float on the water surface and attach to that section of the wall where the water surface passes in the diurnal variation.†

The sewer balloon sampling method (see section 4.3.1) was employed to determine the radial biofilm distribution in the *Rümlang* sewer. The amount of TSS and TVS clearly increased along the perimeter and reached a maximum in the range of the diurnal water level variation (see figure 6.3). The biofilm density (figure 6.3(b)) was on average 1080 $kg \cdot m^{-3}$. It was higher close to the insert, as a result of a higher inorganic particle concentration in the biofilm, and above the water surface where the biofilm contains less water.

The aerobic activity in the biofilm samples was measured by suspending the samples in tap water and then measuring the respiration rate as described in section 4.5. Figure 6.4 shows that the biofilm above the water level had a much lower aerobic activity than the rest of the biofilm. This 'dry' biofilm section had a high amount of inactive organics, which was mainly

*Scanning electron microscope

†It was found by extraction of the fats with methylchloride that the biofilm around the water surface from the *Rümlang* sewer had a seven times higher fat content than below the surface

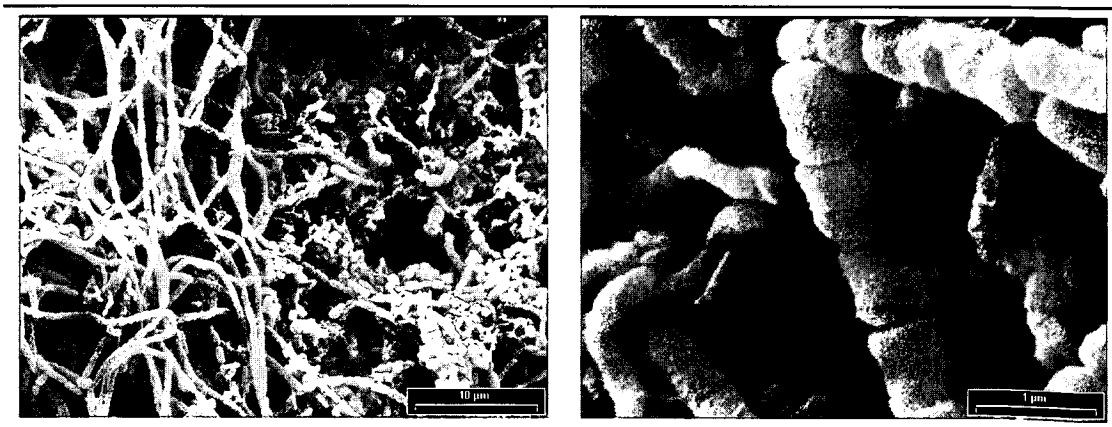

Figure 6.1: Two biofilm SEM pictures showing the occurrence of filamentous bacteria (photos by I. Weidmann, EAWAG).

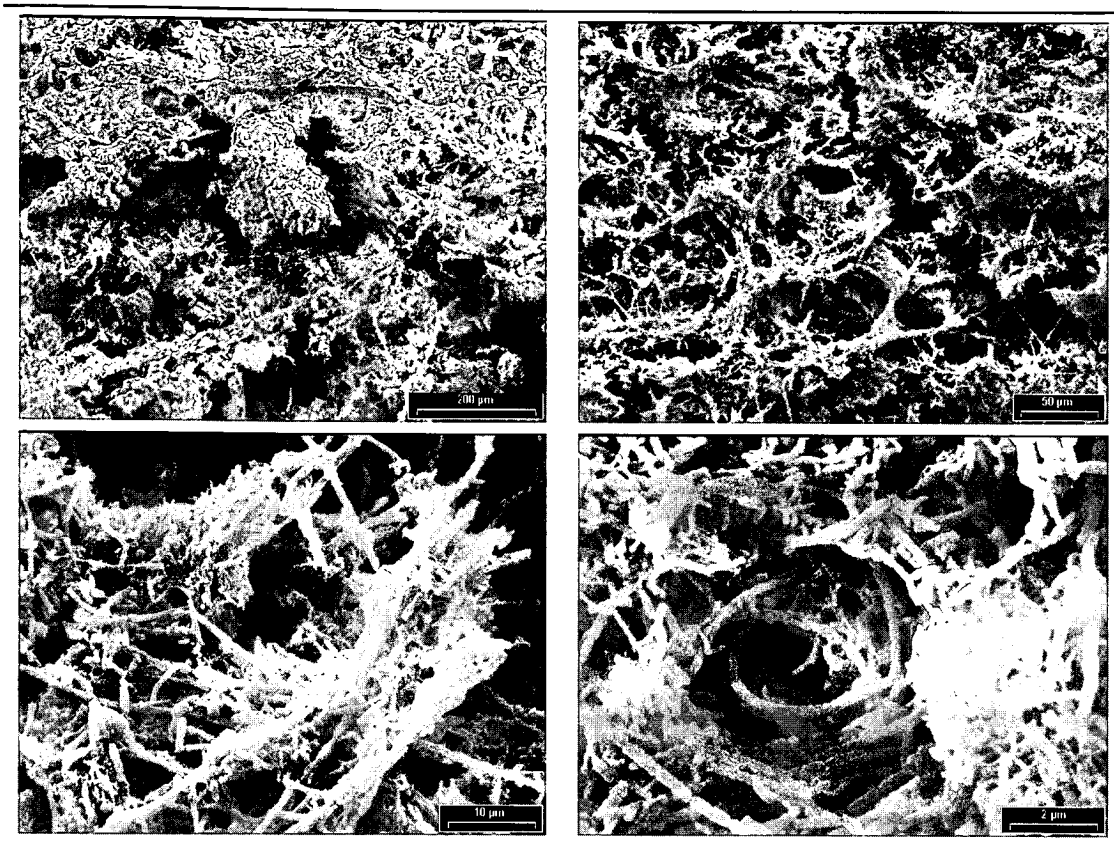

Figure 6.2: Scanning Electron Microscope pictures of the Rümlang sewer biofilm in increasing magnifications (photos by I. Weidmann, EAWAG).

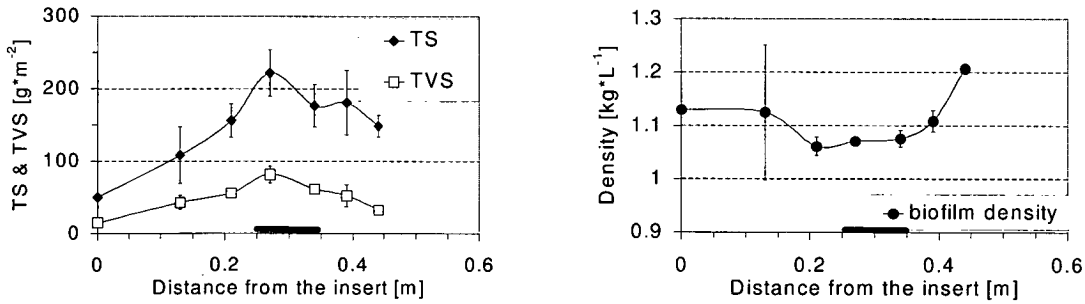

(a) The amount of total solids and total volatile solids per surface area.

(b) The biofilm density along the perimeter.

Figure 6.3: The radial distribution of the sewer biofilm. The values shown are the averages from the left and right side of the pipe wall. The bar indicates the range of the diurnal water level variations.

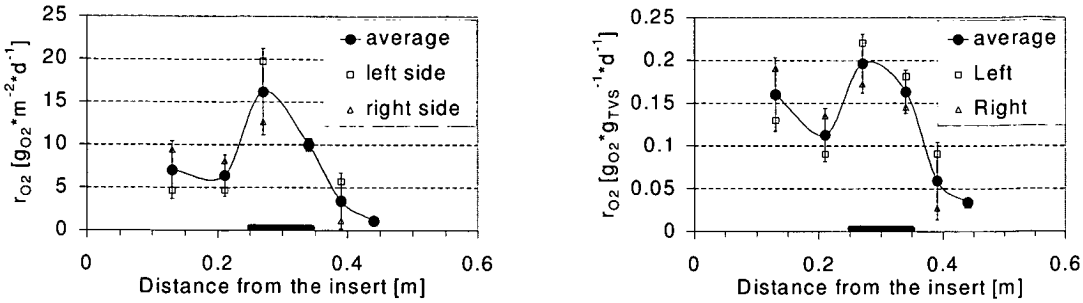

(a) The absolute respiration.

(b) The respiration relative to the amount of TVS.

Figure 6.4: The respiration rate r_{O_2} of suspended biofilm samples with added glucose to prevent substrate limitation to some extent.

fat. Furthermore, it proved to be more resistant against erosion; most of the submerged biofilm has eroded after three days with very heavy rain, but the fatty section remained (see figure 6.5).

6.2.2 Longitudinal distribution

Most conditions remained practically constant over the length of the *Rümlang* sewer. Biofilms are however known to be sensitive to small changes in the local (hydrodynamic) conditions (e.g. Gjaltema, 1996). The largest change was observed in the oxygen concentration that dropped on average 2 mg·L^{-1}.

Several samples were taken on the same day from several manholes. The TSS and TVS in the five subsequent manholes gave reproducible results (see figure 6.6(a) and 6.6(b)). Though a clear decrease can be observed when the averages of TSS and TVS per m^2 over the whole perimeter of each manhole are taken (see figure 6.6(c)). A clear reason for this effect could not be found. The TSS and TVS appear to be linearly related (see figure 6.6(d)). The offset is probably caused be small amounts of sand that were always present at the insert. Apart from a minor decrease in the oxygen concentration, a cause might be that these manholes are at the beginning of this sewer stretch after a drop. In the high turbulence wake of the drop coagulated particles might split up and adhere to the biofilm.

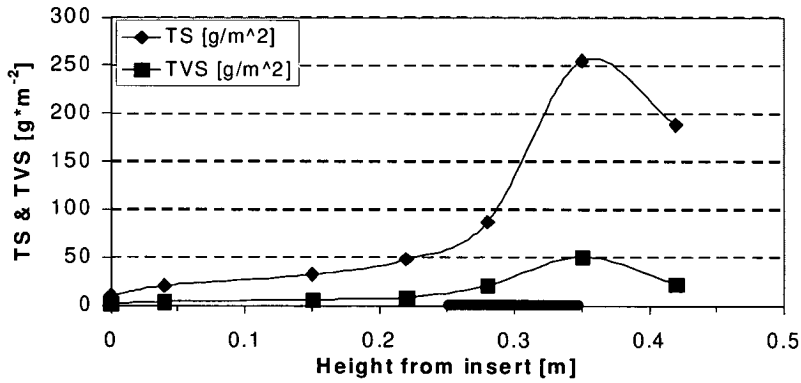

Figure 6.5: The solids on the sewer wall one day after very heavy rains on 15, 16 and 17 May 1999.

The amount of TSS and TVS did not show a continuous decrease along the whole length of the sewer (see figure 6.7). The manholes at 1670 and 2015 m had a 35% smaller slope than the average. This can explain the higher solids amounts at these locations.

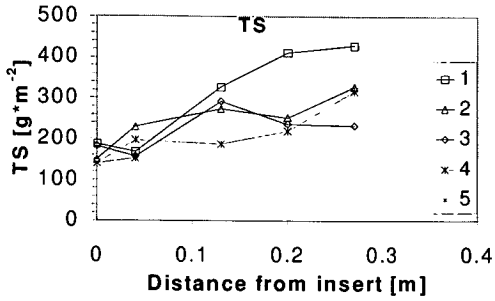

(a) The TSS per surface area for five manholes plotted as a function of the distance along the perimeter.

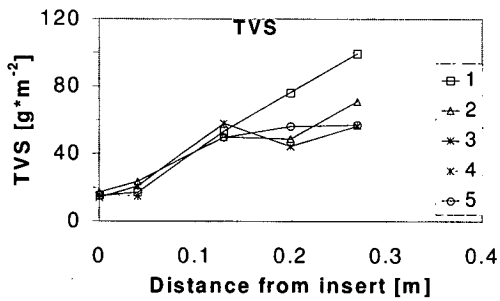

(b) The TVS per surface area for five manholes plotted as a function of the distance along the perimeter.

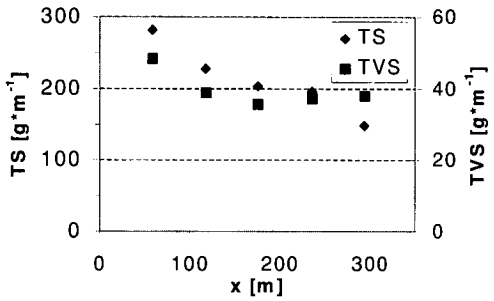

(c) The TSS and TVS per of channel summerised along the perimeter. x = distance from beginning of the section.

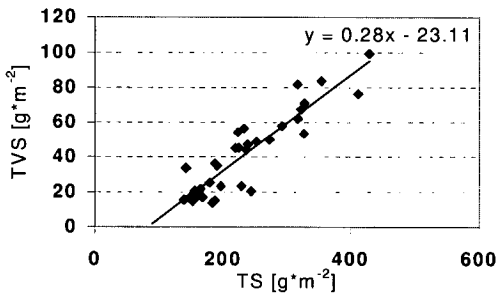

(d) The relation of TSS to TVS for the five manholes.

Figure 6.6: The biofilm dry solids in five subsequent manholes of the Rümlang sewer.

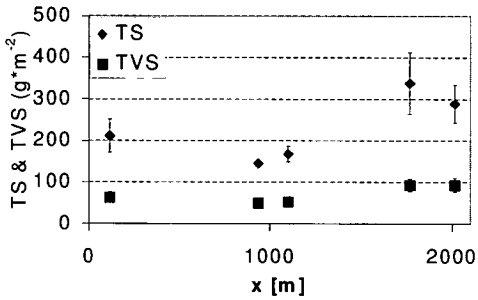

Figure 6.7: The amount of total solids at four locations along the whole Rümlang sewer (samples taken at another date than those of figure 6.6).

6.3 Biofilm growth and aerobic activity

The growth of sewer biofilm has been studied after the biofilm had been mechanically removed. The regrowth of biofilm was then followed over several weeks.

The regrowth in one manhole is shown in figure 6.8. The increase in TSS and TVS was the fastest close to the water surface as was expected from the radial distribution of figure 6.3(a) (results not shown). It rained several times during the measuring period and each sampling, for which the sewer balloon method was used, also produced a small wave. But still it can be presumed that it would take considerably longer than the measurement period to regain the original TSS and TVS amount.

The respiration measurements as depicted in figure 6.9(a) show that the TVS-fraction of the newly formed biofilm consisted of active biomass. However, the original biofilm that was removed on day 0 contained a significant fraction of aerobically inactive TVS. This was also found in other manholes (see figure 6.9(b)). Because the penetration depth of oxygen in the intact biofilm was much smaller than the actual thickness, this fraction of the TVS will have been anaerobic biomass like methanogenic and sulphur reducing bacteria, and other organic material. It is clear that anaerobic bacteria can only start growing when the biofilm is thick enough to allow for anaerobic conditions.

The above mentioned results show that the amount of oxygen respiring biomass that is released during a rain event is not automatically proportional to the amount of eroded TSS or TVS; it depends on the growth conditions, age and history of the biofilm.

The results from a similar experiment are shown in figure 6.10. Now subsequent manholes were sampled and the 'box' sampling method was used (see section 4.3.2). The arrow indicates a rain event of six times dry weather discharge during four hours. This had a clear effect on the ratio of TSS to TVS in the other uncleaned (control) manholes. The TVS was reestablished after almost four weeks, but the TSS was still smaller than in the controls.

Close to the water surface there are 'pockets' in the shear stress profile (see figure 3.4 and 3.5) where the shear is much lower. Shortly after a rain event, when the oxygen concentration is elevated and the available amount of substrate might be higher, a filamentous biofilm has been observed there. These filaments, which were up to two centimetres long, appear to be only a transitional state because they disappeared again within a few days.

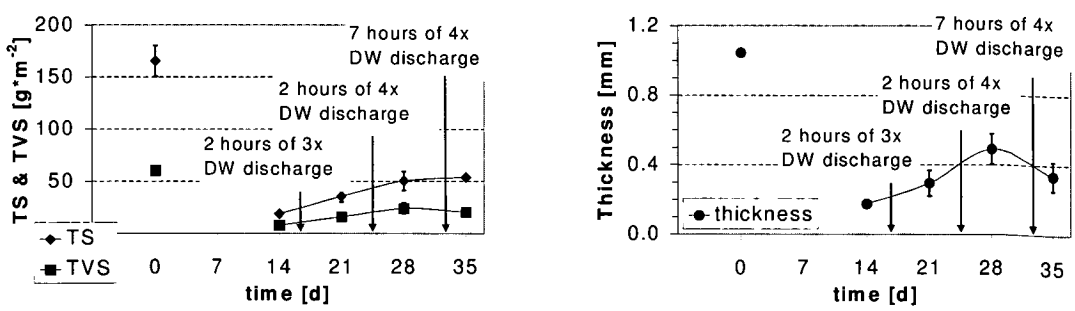

(a) The TSS and TVS during biofilm regrowth.

(b) The biofilm thickness during regrowth.

Figure 6.8: The regrowth of biofilm in the Rümlang sewer in the manhole at x = 1670 m. Samples between a height of 0.1 and 0.3 m from the insert have been taken from both sides. '4x DW discharge' = the discharge was increased to four times the dry weather discharge due to a rain event.

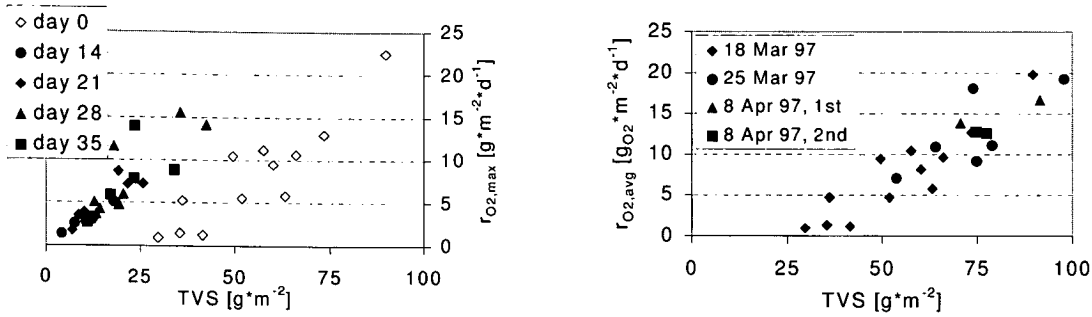

(a) Samples from day 0 before the biofilm was removed and on several occasions afterwards to study the regrowth.

(b) Samples taken on different days and from different manholes.

Figure 6.9: The respiration rate per g_{TVS} of suspended biofilm samples after the addition of glucose. Samples have been taken at a distance of 0.1 to 0.3 m from the insert and from both sides.

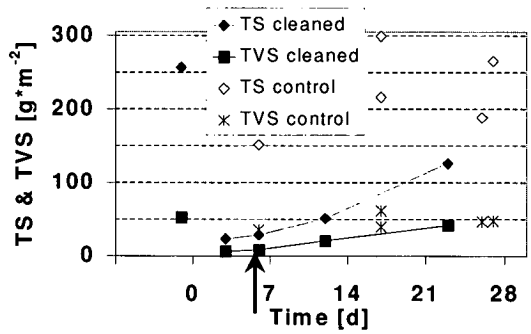

Figure 6.10: The results of samples taken from four subsequent manholes before and after removal of the biofilm on day 0. Control samples from manholes further downstream are also shown (open points). The arrow indicates a rain event. Day 0 was 3 April 1999.

6.3.1 Biofilm erosion during a real and simulated rain event

Biofilm erodes under dry weather conditions and during rain events. Quantification of the first type requires the use of particle tracers like fluorescent micro particles, coated magnetic nanoparticles or biomass traced with easily detectable rare earth metals. This was not within the scope of this study. The rain conditions have been on several occasions in the past (e.g. Dauber *et al.*, 1982). But there the scope was mainly on the effect of the eroded biofilm on the pollutant concentration of the wastewater. In this section, an experiment will be presented to study the effect of a simulated rain event on the *biofilm properties.*

Reiff (1991) studied the growth and erosion of biofilm that had been grown on presettled wastewater in a totally filled pipe (see also page 10). He observed that the amount of biofilm that eroded when the flow was suddenly increased, depended on the flow rate. Furthermore, 90% of the erodable biofilm at a certain flow rate was removed within two minutes.

The sewer biofilm proved to be more resistant to erosion during a modest rain event. After an event on April 9th, 1999 (300 $L{\cdot}s^{-1}$ for four hours), only about 30% of the TVS was removed from the side of the sewer wall. From the insert practically all biofilm had been removed due to the combined abrasive force of the water and larger inorganic particles. The velocity during the event was only ≈ 0.75 $m{\cdot}s^{-1}$ compared to 0.45 during dry weather.

The erosion behaviour of a real sewer biofilm was further studied with a simulated rain event by blocking the flow in the *Rümlang* sewer several times with the sewer balloon (see section 4.3.1). A biofilm strip of 0.1 m high and 0.2 m wide from the left and the right side of the sewer pipe was sampled after each release of the collected wastewater.

The flow velocity, which was up to two-times higher than normal for several minutes (see figure 6.11), resulted in a clear decrease of the amount of total and volatile solids on the sewer wall after each flush (see figure 6.12(a)). The density increased slightly (see figure 6.12(b)) but the ratio of TVS to TSS remained constant at 31±2.1%. This indicates that the biofilm density (in $kg \cdot m^{-3}$) increased towards the sewer wall and that the biofilm was more open near to the water side. These two observations are in agreement with the common observations of (laboratory) biofilms (e.g. Siegrist, 1985).

Another interesting observation was that the biofilm eroded during each flush, although all but the last had the same intensity. This contradicts a conclusion of Reiff (1991) who claims that 90% of the erodable biomass should have been removed within two minutes (see also page 10). Apart from the difference in experimental conditions, the high concentration of inorganic material in the sewer biofilm —which was lacking in the biofilm of Reiff (1992) because he used presettled water— might be responsible for this behaviour. This material can have acted as a reinforcement.

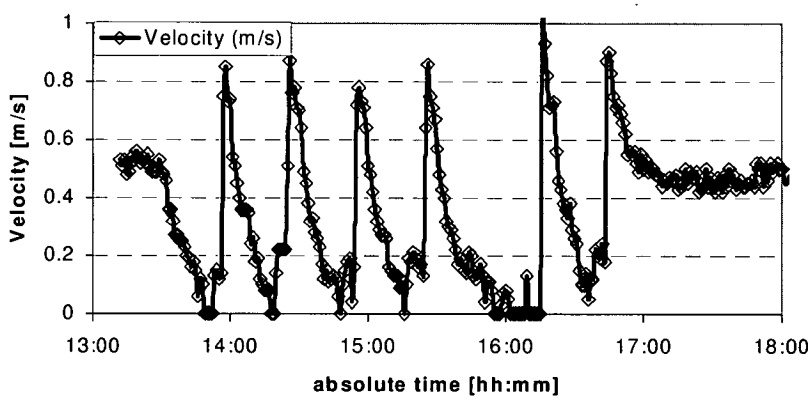

Figure 6.11: The velocity during the rain simulation experiment.

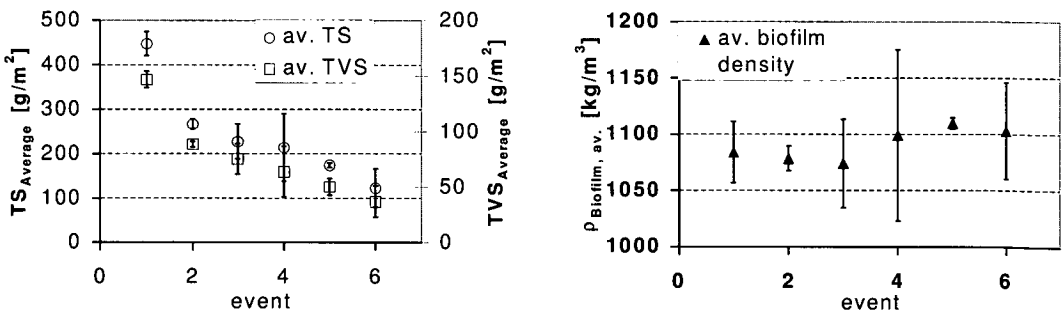

(a) The Total Solids and Total Volatile Solids.

(b) The biofilm density.

Figure 6.12: Results of the simulated rain event with the averaged values of the left and the right side of the sewer.

6.4 *in situ* sewer biofilm respiration rate measurements

6.4.1 Introduction

In the previous section, the respiration activity of a suspended biofilm was measured. The total aerobic activity correlated well with the amount of TSS and TVS on the sewer wall. However, mass transfer effects were excluded.

The question therefore is whether the activity of an intact biofilm is very different from the suspended one. To answer this, a sewer *in situ* flow cell was constructed (see section 4.6.3) that allowed the quantification of the biofilm activity in its natural surroundings. This has not been done before.

6.4.2 Data processing and results

The biofilm respiration activity ($r''_{O,f}$) can be expressed with the following equation under the assumption of a smooth and homogenous biofilm (Gujer and Boller, 1985):

$$r''_{O,f} = \sqrt{-2 \cdot \mathbb{D}_{O,f} \cdot \mu^{\max}_{Het,f} \cdot \gamma \cdot \nu_O} \cdot \sqrt{S_O^{surf.} - S_O^{base} - K_{O,f} \cdot \ln\left[\frac{S_O^{surf.} - K_{O,f}}{S_O^{base} - K_{O,f}}\right]} \quad (6.1)$$

where $r''_{O,f}$ = biofilm oxygen uptake rate per surface area ($g_{O_2} \cdot m^{-2} \cdot d^{-1}$), $\mathbb{D}_{O,f}$ = biofilm oxygen diffusion ($m^2 \cdot s^{-1}$), $\mu^{\max}_{Het,f}$ = max. specific growth rate of heterotrophic biofilm biomass (d^{-1}), γ = biomass density in biofilm ($g_{COD} \cdot m_f^{-3}$), ν_O stoichiometric parameter ($g_{O_2} \cdot g_{COD}{}^{-1}$), $S_O^{surf.}$ and S_O^{base} = oxygen concentration at the biofilm surface and base, respectively ($g_{O_2} \cdot m^{-3}$) and $K_{O,f}$ = biofilm oxygen half saturation constant ($g_{O_2} \cdot m^{-3}$).

Under the assumption that the boundary layer is negligible, $S_O^{surf.}$ is equal to bulk concentration, S_O^b. The sewer biofilm is normally deep, meaning that the biofilm thickness is larger than the penetration depth of oxygen and therefore $S_O^{base} = 0$. Equation (6.1) then becomes

$$r''_{O,f} = \sqrt{-2 \cdot \mathbb{D}_{O,f} \cdot \mu^{\max}_{Het,f} \cdot \gamma \cdot \nu_O} \cdot \sqrt{S_O^b - K_{O,f} \cdot \ln\left[\frac{S_O^b}{K_{O,f} - 1}\right]} \quad (6.2)$$

The temperature during the measurement, T_m (°C), strongly influences the measured uptake rate, $r''^{meas}_{O,f}$, via the cumulative effect on $\mathbb{D}_O$ and $\mu^{\max}_{Het}$. This is accounted for by using $\mathbb{D}_O^{T=T_m}$ and $\mu^{max,T=T_m}_{Het}$ according to equation (E.6) (page 174) and equation (E.1) (page 173), respectively. Filaments with a length of up to 2 cm were observed on the sewer biofilm several times after heavy rains, although they had disappeared again after a few days. These can have the characteristics of suspended biomass (Siegrist, 1985). Furthermore, biofilm can erode and behave like suspended biomass. Biofilm erosion is a natural process and can also occur before or during a measurement within the *in situ* flow cell. Even though the medium was exchanged several times after installation and before the measurement to remove most suspended biomass, it cannot be excluded that some remained and affected the respiration rate. The activity of suspended biomass is described as

$$r_{O,s} = \mu^{\max,T=T_m}_{Het} \cdot \frac{S_O}{S_O + K_O} \cdot X_{Het} \cdot \nu_O \quad (6.3)$$

Unfortunately, only the total activity can be determined; filamentous and eroded biofilm biomass cannot be distinguished.

A sensitivity analysis in AQUASIM* (Reichert, 1998) showed that the parameters γ, X_{Het} and $K_{O,f}$ can be identified with the combination of equation (6.2) and equation (6.3):

$$r_O^{meas.} = r_{O,f} + r_{O,s} \tag{6.4}$$

This is only possible when a large DO range —preferably down to zero— has been measured because these parameters are otherwise strongly correlated. Furthermore, a distinction between biofilm and suspended biomass can be made under the assumption that both have equal $K_{O,f}$ and μ_{Het}^{max}.

An example of a measurement is shown in figure 6.13(a). River water† was used during the first stage and had been replaced with centrifuged wastewater‡ during the second. The derivative of DO against time yields $r_{O,f}^{''\,meas.}$ that is fitted with equation (6.4) to obtain γ and X_{Het} (figure 6.13(b)). $\mu_{Het}^{max,T=20°C}$ has been taken as 5.6 d^{-1}. $K_{O,f}$ has been determined as 0.1 $g{\cdot}m^{-3}$ by fitting several experiments and has been kept constant for all measurements. The difference in γ between the centrifuged wastewater and the river water can have been related to the availability of substrate; only acetate was added to the river water but the centrifuged wastewater will have contained many different substrates. The latter can have enabled more bacteria to grow.

The results are listed in table 6.1. $\overline{\gamma} = 22400 \pm 7800$ $g_{COD}{\cdot}m_f^{-3}$was found for all measurements with centrifuged wastewater. The standard deviation of γ is large because $\gamma \propto r_{O,f}^2$. The errors in $r_{O,f}^{''\,meas.}$ are therefore squared too.

The $\overline{r_{O,f}^{''}}$ is of high practical relevance and can be calculated with γ at any temperature and DO-concentration. A value of 6.0 ± 1.0 $g{\cdot}m^{-2}{\cdot}d^{-1}$ at 20°C and DO = 2 $g{\cdot}m^{-3}$ was found.

Not for all experiments was $X_{Het} > 0$. A clear conclusion on the filament's activity is therefore not possible at this time and requires more research.

*See appendix D.1 for a short description.

†River water in *Rümlang* consists for up to 50% of WWTP's outflow.

‡The biomass activity is negligible after centrifuging, but the other properties remain the same.

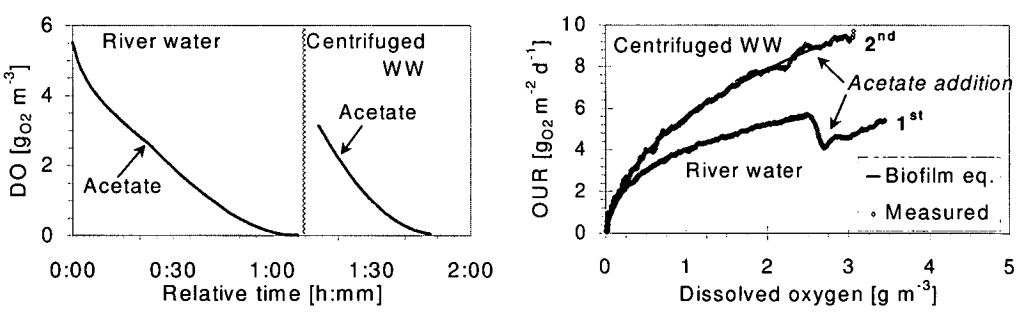

(a) The Dissolved Oxygen concentration as $f(t)$.

(b) The Oxygen Uptake Rate as a $f(DO)$ with the curves fitted with equation (6.4). River & wastewater: γ = 7700 & 31300 $g_{COD}{\cdot}m_f^{-3}$, and X_{Het} = 8.7 & 4.2 $g{\cdot}m^{-3}$

Figure 6.13: An example of the results of an in situ flow cell measurement. The flow cell was not moved between the measurements.

Table 6.1: The results of the in situ measurements. x = distance from the beginning of section, y = placement of flow cell = distance from the pipe insert along the sewer wall, negative and positive are left and right side, respectively.

Date	x (m)	y (m)	medium	$\overline{T_{meas}}$ (°C)	γ $\cdot 10^3$ g·m^{-3}	X_{Het} g·m^{-3}	$r_{O,f}$ † g·m^{-2}·d^{-1}	$r_{O,s}$ ♯ g·m^{-2}·d^{-1}
25-Jun-97	650	-0.24	RW	17	9.2	0	3.9	0
		-0.24	RW	17	14.1	0	4.8	0
1-Jul-97	59	-0.24	RW	17	19.0	0	5.6	0
18-Jun-98	643	0.24	CWW	18.9	11.5	0	4.4	0
		-0.24	CWW	17.2	14.5	0	4.9	0
		0	CWW	17.2	20.7	31.0	5.8	3.5
		0	CWW	17.2	18.3	21.9	5.5	2.5
11-Mar-99	235	0.24	CWW	12.1	16.6	0	5.3	0
		0.24	CWW	12.2	16.5	0	5.2	0
3-Apr-99	525	-0.24	CWW	14.7	17.0	0	5.3	0
		0.24	CWW	15.0	27.7	3.5	6.8	0.28
	584	-0.24	CWW	14.9	19.3	4.8	5.6	0.38
		-0.24	CWW	15.1	19.7	14.2	5.7	1.1
		-0.24	CWW	14.8	14.0	30.6	4.8	2.4
4-May-99	819	0.22	CWW	14.3	22.0	1.6	6.0	0.12
		0	CWW	14.2	38	0	7.9	0
15-May-99	1612	0.24	RW	14.1	21.5	0	6.0	0
25-May-99	1670	0	CWW	15.8	37.1	0	7.8	0
		0.22	RW↬	16	7.7	8.7	3.6	0.75
		0.25	↬CWW	16	31.3	4.2	7.2	0.36
		0	RW↬CWW	15.7	18.0	3.6	5.5	0.30
28-May-99	1788	0	CWW	16	18.3	0	5.5	0
		-0.24	CWW	15.5	28.7	1.2	6.9	0.10
		-0.24	CWW	15.6	29.7	7.7	7	4.8
		0.24	CWW	15.9	14.0	0	4.8	0
7-Jun-99	1847	0.24	CWW	16.5	19.4	8.0	5.7	0
		-0.24	CWW	16.5	15.8	0	5.1	0
		0	CWW	16.5	23.5	3.6	6.2	0
29-Oct-99	584	0.24	CWW	17.1	22.0	2.7	6.0	0.25
		0.24	CWW	17.2	35.8	20.9	7.7	2.0
		0.24	CWW	17.1	34.1	7.1	7.5	0.67

† $T = 20°C$, $DO = 2$ g·m^{-3}, ♯ The X_{Het} has been converted to (g·m^{-2}d^{-1}) with the area volume ratio (25.0 m^2·m^{-3}, see page 32) of the *in situ* respirometer. CWW = centrifuged wastewater, RW = river water and ↬ = the medium was changed.

The biofilm activity at the side of the sewer could be described very well with equation (6.4). The biofilm at the insert ($\approx$ 0.15 m wide) behaved differently (see figure 6.14). The highest heterotrophic biomass concentration (γ =29800 $\pm$ 9000) was found there, although the biofilm was the thinnest. The constant abrasion apparently leads to a highly active, compact, fast growing biofilm. This high activity was obtained only with the combination of centrifuged wastewater and added acetate. The biomass response of figure 6.14 is thought to be caused by the combination of a high biomass concentration but a small (external) substrate reserve. It can be expected that less easily degradable material will be produced within the biofilm because the deeper anaerobic strata are smaller or lacking. Therefore, during an experiment bacteria are first

carbon substrate limited before oxygen limitation sets in. This biofilm seems to depend largely on substrate input from the wastewater.

It seems unlikely that an $\approx$ 1 mm-thick sewer biofilm which is exposed to at most 3 $g_{O_2} \cdot m^{-3}$ and some nitrate will have a homogenous distribution of heterotrophs throughout its depth. The DO-data from an experiment confirmed this. Although the DO-data in figure 6.15 appear normal, the derivative ($\rightarrow r_{O,f}$ or OUR) in figure 6.15(b) remains practically constant above 3 $g_{O_2} \cdot m^{-3}$. Because no effect was observed after the addition of acetate, this indicates that the activity was biomass limited at higher oxygen concentrations (i.e. oxygen fully penetrated the biofilm).

6.4.3 Sewer versus trickling filter biofilm

A typical sewer biofilm activity is 5 $g_O \cdot m^{-2} \cdot d^{-1}$ at 20°C. This corresponds with a conversion of 15 $g_{COD} \cdot m^{-2} \cdot d^{-1}$ or 7 $g_{BOD_5} \cdot m^{-2} \cdot d^{-1}$ when a conversion of 2.1 $g_{COD} \cdot g_{BOD_5}{}^{-1}$ and a yield of 0.67 $g \cdot g^{-1}$ are assumed.

A typical trickling filter activity of $\approx$ 4 $g_{BOD_5} \cdot m^{-2} \cdot d^{-1}$ at 7°C (Gujer *et al.*, 1983) is practically equal to the observed sewer biofilm activity. A stone filling for a trickling filter has a surface area of 90 $m^2 \cdot m^{-3}$. The town of *Rümlang* ($\approx$ 8000 m^2) plus the main sewer (figure 5.1) ($\approx$ 1500 m^2) have a total wetted area of 9500 m^2. This is comparable with a trickling filter volume of 105 m^3. In that case, the sewer would degrade the sewage of $\approx$ 840 PE when a volumetric load of 8 $PE \cdot m^{-3}$ for the trickling filter is assumed. The major difference between the sewer and a trickling filter is that there is no secondary clarifier to remove the sludge. The

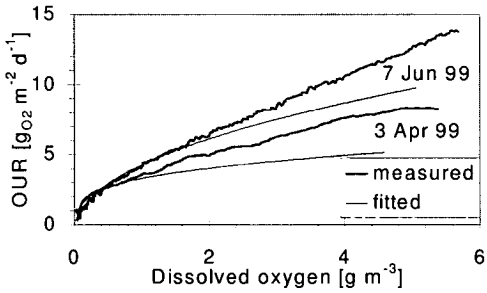

Figure 6.14: The biofilm activity at the insert against the dissolved oxygen concentration for two measurements.

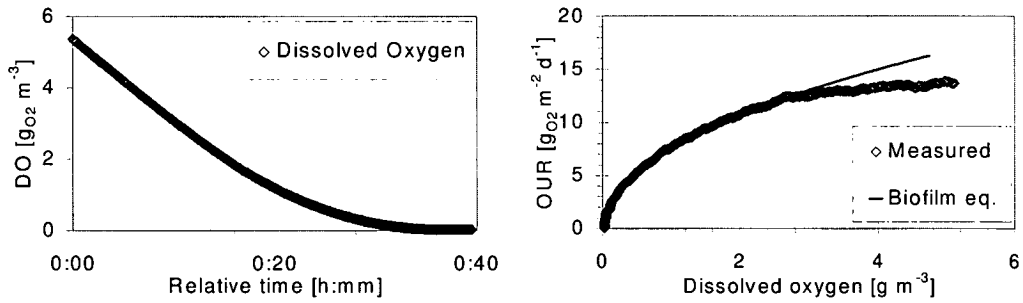

(a) The Dissolved Oxygen concentration as $f(t)$.

(b) The Oxygen Uptake Rate as a $f(DO)$ fitted up to 3 $g_{O_2} \cdot m^{-3}$.

Figure 6.15: Graphs showing the effect of biofilm biomass limitation on the $r''_{O,f}$.

biomass that is released from the biofilm due to erosion will reach the WWTP where a certain fraction will settle, or eroded biofilm might by released into the receiving water via combined sewer overflows during a rain event.

6.4.4 Conclusion

The *in situ* measurement was a useful technique to gain more insight into the sewer biofilm activity. It could be shown that aerobic activity was fairly constant along the perimeter and in time. Furthermore, the outermost layer of the biofilm depends on substrate from the wastewater, whereas the deeper strata fulfill their energy need either by hydrolysis of particles or by internal storage material which were also found in the sewer biofilm as will be discussed in the next section. The highest activity was found at the insert, but here extra substrate needed to be given, even with centrifuged wastewater. The role of filaments on the sewer biofilm remains unclear and requires more research.

6.5 Storage materials in sewer biofilms?

6.5.1 Introduction

The bacterial population in systems with cyclic changing substrate conditions can develop the ability to produce storage materials like glycogen and PHB. The presence of glycogen in a cell can prevent degradation of RNA and proteins because it can serve as an energy source under starvation conditions as Marr *et al.* (1963) showed experimentally. Glycogen is preferably produced when balanced growth is no longer possible due to some limitation (e.g. phosphate) (Preiss, 1989).

Sewer biofilms, especially in sewers with higher flow velocities and close to smaller towns, are exposed to a diurnal rhythm of their nutrient supply. Storage materials are bound to be present under such conditions. A complicating factor in comparison to a sequencing batch reactor is that substrate particles are thought to become trapped in the biofilm where they are slowly hydrolysed (Harremoës, 1983) (see also section 6.7).

The hypothesis is that storage components are present and that the maximum in their concentration will occur during daytime and the minimum at the end of the night.

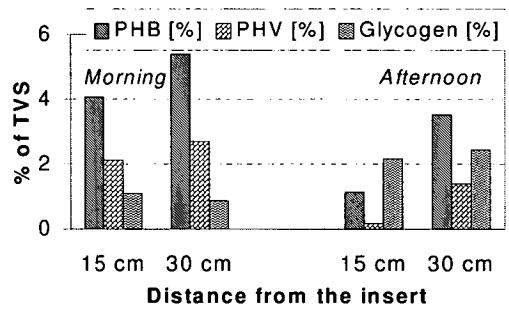

Figure 6.16: The polyhydroxybutyrate (PHB), polyhydroxyvalerate (PHV) and glycogen fraction in the sewer biofilm of Rümlang.

6.5.2 Results and conclusions

The hypothesis was tested by taking samples from a sewer biofilm and determining the PHB, PHV and glycogen concentrations*. The results, as shown in figure 6.16, are contradictory to the hypothesis for PHB and PHV, but do follow the expected trend for glycogen. It is difficult to draw conclusions on the nature of the bacteria involved because many microorganisms can synthesise storage components. However, the observed dynamic is similar to what is found in the wastewater treatment plant with biological phosphate removal. The diurnal variation of phosphate and dissolved oxygen in the sewer could have led to growth of such bacteria. It would be interesting to look for these bacteria with the newly developed FISH-probe (J. Keller, personal communication). When similar bacteria are present, the seeding into the wastewater treatment plant might be important.

6.6 Methanogenic and sulphidogenic bacteria in the sewer biofilm

6.6.1 Introduction

The sewer biofilm normally had a thickness of several hundred μm. This is more than the oxygen penetration depth, which makes the presence of anaerobic biomass likely. The methanogenic and sulphidogenic bacteria will be the prominent groups in the sewer biofilm.

Methane (CH_4) that is produced deep inside the biofilm will be converted to carbon dioxide (CO_2) when it reaches the aerobic zone (DiToro *et al.*, 1990). In the sulphur cycle hydrogen sulphide (H_2S) is produced which is reoxidised to sulphate (SO_4^{2-}) either chemically or biologically (see section 2.5.2).

In both cases, the final oxidant remains oxygen. Thus, these processes are not sinks for COD. However, their contribution to the overall COD conversion should be quantified to evaluate whether they should be included in the model structure.

6.6.2 Methane production measurement

The presence of archea, the group to which methanogenic bacteria belong, was confirmed with FISH measurements (figure 6.17). The CH_4 production by the sewer biofilm was determined in an anaerobic CSTR with biomass scraped from the sewer wall under the exclusion of oxygen. The DO-concentration and wastewater temperature at the moment of sampling were 1.4 mg·L^{-1} and 14.5°C. The CH_4-concentration in the wastewater was below the detection limit of 1 mg·L^{-1}. H_2S is known to inhibit methanogenic bacteria. Therefore, dissolved $FeCl_3$ was added to bind any produced H_2S . An iron concentration five times the sulphate concentration was added to compensate the production of H_2S due to the reduction of elementary sulphur. The pH was kept around 7.5 and the redox potential laid between -500 and -600 mV, depending on the pH, but was on average -560 mV.

The average gas production of three different samples was 0.14±0.04 $mL_{gas}\cdot(g_{wet\ biofilm}\cdot d)^{-1}$. The gas contained approx. 65% CH_4, 300 ppm H_2 and 15% CO_2. The rest was N_2 that was initially used to flush the headspace. The gas production was equivalent to 170 $mL_{CH_4}\cdot m^{-2}\cdot d^{-1}$ or 0.5 $g_{COD}\cdot m^{-2}\cdot d^{-1}$ (assuming 23 $L_{gas}\cdot mol^{-1}$ and 64 $g_{COD}\cdot mol^{-1}$ for CH_4). The effect on

*Many thanks to Janneke Beun and co-workers of the Delft University of Technology.

Figure 6.17: FISH measurement with a marker for archea bacteria. (Photo by C. Egli, Microbiology Department).

the oxygen balance will be negligible because the average oxygen conversion by an intact sewer biofilm is 9 $g_{O_2} \cdot m^{-2} \cdot d^{-1}$ (see section 6.1).

6.6.3 Sulphur cycle activity

As was pointed out theoretically in section 2.5.2, a sulphur cycle can exist in the biofilm of an aerobic sewer. Biofilm samples were taken from the *Rümlang* sewer in June 1998 to estimate the influence of the sulphur cycle on the overall conversion. The wastewater temperature was 18°C and the DO-concentration was 2.2 $g \cdot m^{-3}$. The samples were suspended in anaerobic wastewater and divided over several reactors. The sulphate reduction and sulphide oxidation were measured in an anaerobic and aerobic reactor after extra SO_4^{2-} (as dissolved $NaSO_4$) and H_2S (as dissolved Na_2S) had been added. The rates were determined from the uptake and production of SO_4^{2-}. The oxygen uptake rate (OUR) was measured in a reference reactor.

The results are shown in table 6.2. The OUR is clearly much larger than the X_{SRB}* and X_{SOB}† activity. A better comparison is possible when the uptake rates of easily degradable substrate (S_S) are compared. The rates in table 6.2 can be converted to S_S uptake rates with the help of the stoichiometric coefficients in table 9.8. The uptake of heterotrophic biomass (X_{Het})

*sulphate reducing bacteria
†sulphide oxidising bacteria

Table 6.2: The activity of the reduction and oxidation step in the sulphur cycle in comparison to the oxygen uptake rate. All rates are expressed per amount of biomass-COD (X). The removal and formation of SO_4^{2-} were measured.

Experiment	OUR $g_{O_2} \cdot g_X{}^{-1} \cdot d^{-1}$	r_{SRB} $g_{SO_4^{2-}} \cdot g_X{}^{-1} \cdot d^{-1}$	r_{SOB} $g_{S^{2-}} \cdot g_X{}^{-1} \cdot d^{-1}$
1	0.450	0.045	-
2	0.284	0.014	-
	0.256	-	-
3	0.229	0.018	0.018
4	0.230	0.026	0.031
	0.235	-	-

and X_{SRB} is 3.9 $g_{S_S} \cdot g_{O_2}$ and 0.79 $g_{S_S} \cdot g_{SO_4^{2-}}$ respectively. The resulting S_S uptake rates with the data in table 6.2 are therefore very far apart for X_{Het} and X_{SRB}. The sulphur cycle will therefore not play a significant role in the *Rümlang* sewer biofilm under aerobic conditions. However, this might not be true for other channels. Therefore, additional data and a modelling approach for the sulphur cycle is given in section 9.5.4.

6.6.4 Conclusion

Methanogenic, sulphate reducing and sulphide oxidising activities were found. The influence of this activity on the COD-balance was small because the wastewater was aerobic.

6.7 Hydrolysis

6.7.1 Introduction and background

The pollutants in wastewater range in size from less than 0.001 to well over 100 μm but bacteria can take up only molecules with a weight of less than 1000 Da* or $\approx 2 \cdot 10^{-4}$ μm (Levine *et al.*, 1985). Much of the large molecular mass material is broken down in size by the hydraulic shear forces and by solubilisation. But larger macromolecules can still constitute 50 to 60% of dissolved organic carbon (DOC) in wastewater (Confer and Logan, 1998). An extracellular hydrolysis is therefore required to make this fraction available for take up by cells.

Confer and Logan (1998) used fluorescent labelled substrates and found that in biofilm cultures, no more than 3% of the total hydrolysis activity was located in the cell-free bulk solution. Similar results were found for suspended cultures.

The observations of Confer and Logan (1998) coincide with the hypothesis for hydrolysis of particulate material by biofilm as published by Harremoës (1983) (see table 6.3). But Larsen and Harremoës (1994), who studied the hydrolysis of starch in a biofilm system, observed that bulk hydrolysis was the initial step. This lead to the second hypothesis in table 6.3. The measurements of Confer and Logan (1998) remain valid, because they quantified the final product of the hydrolysis process.

Based on the findings of Larsen and Harremoës (1994), the hypothesis for the sewer system is that hydrolysis mainly occurs in the wastewater and that only small organic fragments diffuse into the biofilm. In the Activated Sludge Model No. 3 (ASM 3) (Gujer *et al.*, 1999) the authors assume that the hydrolysis rate is similar under aerobic and anaerobic conditions. This will be tested for the sewer biofilm.

*Dalton. Also called Atomic Mass Units. A unit of mass, equal to 1/12 the mass of the carbon-12 atom.

Table 6.3: Summary of the hypotheses on the mechanisms of the degradation of non-biofilm-diffusible organic matter in biofilms (after Larsen and Harremoës (1994), see text for details).

Hypothesis No. 1 Harremoës (1983)	Hypothesis No. 2 Larsen and Harremoës (1994)
1. Adsorption onto the biofilm surface	1. Bulk liquid hydrolysis
2. Hydrolysis on the biofilm surface	2. Diffusion into the biofilm
3. Diffusion into the biofilm	3. Hydrolysis within the biofilm
4. Degradation within the biofilm	

Several experiments were conducted:

- Enzyme tests (next section, 6.8).
- *In situ* measurements with centrifuged wastewater and substrate poor water (section 6.4).
- Addition of easily degradable substrate into the sewer (section 6.8.2).
- Laboratory measurements with intact sewer biofilm (section 6.8.1 and 6.9).
- Quantification of storage polymers in biofilm bacteria (section 6.5).

6.8 Activity of hydrolysis enzymes

The activity of three types of enzymes, α-glucosidases, β-glucosidases and esterases was determined with fluorescent-labelled substrates as described in section A.1. α-Glucosidases split maltose and sucrose. β-Glucosidases split the disaccharide cellobiose, which is a product of the degradation of cellulose, with formation of glucose (Schlegel, 1986).

Wastewater and biofilm samples were taken. All samples were split up in a cell rich (centrifugate) and a cell poor fraction (supernatant) by centrifugation (four minutes at 3000 g). The cell rich fractions were diluted with tap water. Furthermore, a sample from the top and the bottom layer of the sewer biofilm were taken*. Biofilm and wastewater samples were taken at the end of the night (5:00 AM) and during daytime (1:00 PM). The results are shown in table 6.4.

The following conclusions could be drawn from these experiments:

- The activity per mg_{COD} of the supernatant of centrifuged biofilm is higher than that of centrifugate of wastewater.
- The activity of the biofilm sample is for approx. 75% associated with the centrifugate, but the biomass in the supernatant has a much higher activity per mg_{COD}. The supernatant, which

*The top layer was that part that could be easily removed. The bottom was the remainder.

Table 6.4: The main results of the hydrolysis measurements at 20°C with fluorescent-labelled substrates. BF = biofilm, WW = wastewater

in [μmol·(mg_{COD}· d)$^{-1}$]		COD	α-glucosidase		β-glucosidase		Esterase	
		[mg·L^{-1}]	average	σ	average	σ	average	σ
BF, bottom	morning	4100	1.00	0.09	0.86	0.07	0.12	0.02
BF, top	morning	3056	0.54	0.13	0.40	0.02	0.14	0.00
BF centrifugate	morning	4108	0.50	0.01	0.37	0.13	0.06	0.00
	afternoon	3772	1.69	0.16	1.44	0.32	0.17	0.02
BF supernatant	morning	1178	3.59	0.47	2.55	0.14	0.47	0.08
	afternoon	1309	2.34	0.07	2.49	0.11	0.26	0.03
WW centrifugate	morning	516	1.34	0.19	0.94	0.14	0.17	0.07
	afternoon	3760	1.52	0.16	0.74	0.12	0.07	0.03
WW supernatant	morning	55	1.23	0.18	-	-	0.22	-
	afternoon	342	0.75	-	0.14	0.02	-	-

in [μmol· (L· d)$^{-1}$]		COD [mg·L^{-1}]	α-glucosidase average	β-glucosidase average	Esterase average
WW	morning	66	82	22	14
	afternoon	469	459	150	-

was still turbid after centrifugation, apparently still contained cells or biofilm fragments with enzymes.

- The activity of the top layer (per mg_{COD}) is approx. twice that of the base layer, but only for the glucosidase. The esterase activity is approximately equal.
- The glucosidase activity per mg_{COD} of the biofilm centrifugate is three times smaller in the morning than in the afternoon.
- The esterase activity between the morning and the afternoon biofilm centrifugate is similar.
- The esterase activity of the biofilm supernatant is four times higher in the afternoon than in the morning.

6.8.1 Sewer biofilm hydrolysis rate

It could be shown that the enzymes for the final hydrolysis stage are present in the biofilm (see section 6.8). However, this does not mean that complete hydrolysis occurs. In this section the results of a macroscopic test in the biofilm flow cell (BFC-system, see section 4.7) are presented.

Anaerobic phase with S_S measurement

The goal was to measure the production and release of easily degradable substrate (S_S) from the sewer biofilm. The question is whether the sewer biofilm hydrolysis can be described with the approach of the ASM 3 (Gujer *et al.*, 1999).

A fully grown biofilm (L_f = 1.1 mm, 0.04 m^2) was put in the BFC-system and the system first ran aerobically for 2 hrs before the aeration was stopped. Under the assumption that the hydrolysis would continue under anaerobic conditions, samples from the medium (a phosphate buffer) were taken at a regular time interval. The amount of S_S that is shown in figure 6.18(a) was determined biochemically by mixing each sample with starved suspended sewer biofilm, as Kappeler and Gujer (1992) did with activated sludge. The sample volume was 2% of the BFC-system volume. Fresh buffer was added to compensate for the medium loss due to sampling because the BFC can only function properly when it is totally full. The actual release rate of S_S was therefore 8% higher, giving 2.5 $g_{COD}{\cdot}m^{-2}{\cdot}d^{-1}$. The dissolved COD increased somewhat stronger due to the apparent release of inert COD. The aeration of the BFC was started again after 5.75 hours. The respiration rate was elevated during the following 2 hours. (see figure 6.18(b)).

The area under the curve after the anaerobic phase (see figure 6.18(a)) represents the equivalent of 0.68 $g_{COD}{\cdot}m^{-2}$ as S_S after the 8% correction to compensate for sampling when a yield of 0.63 $g_X{\cdot}g_{COD}^{-1}$ is assumed. During the anaerobic phase of 3.5 hours, a total of 0.34 $g_{COD}{\cdot}m^{-2}$ was excreted by the biofilm into the medium. The difference to the total S_S amount was either present as storage material, as slow diffusing polymer fragments, or related to delayed hydrolysis and endogenous respiration of biomass.

The release rate of S_S was 4.5 $g_{COD}{\cdot}m^{-2}{\cdot}d^{-1}$ which is equivalent to a respiration of 1.7 $g_{O_2}{\cdot}m^{-2}{\cdot}d^{-1}$. The difference with the observed initial rate of 2.6 $g_{O_2}{\cdot}m^{-2}{\cdot}d^{-1}$ can be attributed to endogenous respiration*. The hydrolysis equation in ASM 3, which is independent of the presence of oxygen, is therefore supported.

*The plates with an area of 0.04 m^2 contained 48 g of wet biofilm. The biofilm density is 1070 $g{\cdot}m^{-3}$ (see figure 6.12(b)) which corresponds with $\approx$ 70 $g_{\text{dry solids}}{\cdot}m^{-3}$ when the density of the water is deducted. The wet biofilm therefore has 6.5 $g_{\text{dry solids}}{\cdot}g_{\text{wet biofilm}}^{-1}$, this equals 3.1 g_{TSS} or 1.6 g_{COD} (see section 6.10). Simulations showed that $\approx$15% of the total biofilm COD consist of heterotrophic biomass. The endogenous respiration then equals $b_{Het} \cdot X_{Het}$ = 0.2 · 0.24 =0.048 $g_{O_2}{\cdot}d^{-1}$ or **1** $\mathbf{g_{O_2}{\cdot}m^{-2}{\cdot}d^{-1}}$

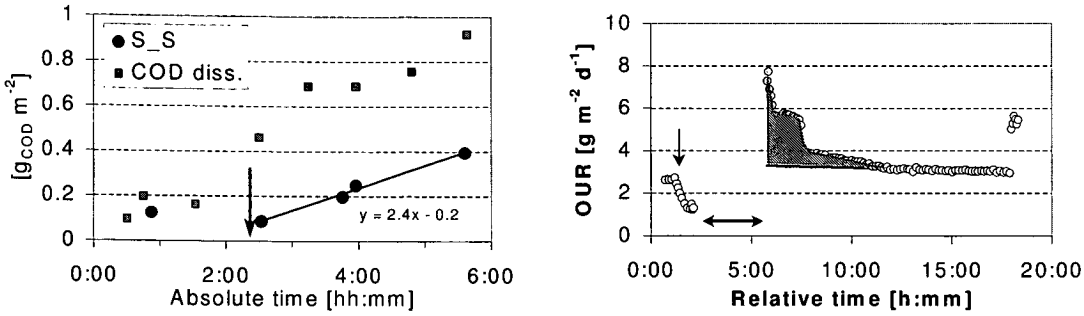

(a) The released amount of dissolved S_S and dissolved COD expressed per $m^2_{biofilm}$. The arrow indicates the start of the anaerobic phase.

(b) The OUR in the BFC-system before and after the anaerobic period indicated by the horizontal arrow. The vertical arrow indicates the reaeration stop.

Figure 6.18: Quantification of the release of S_S from a sewer biofilm. T = 19°C. Reaeration boundaries 2.0–2.2 $g_{O_2} \cdot m^{-3}$.

Anaerobic phase and medium replacement

In a similar experiment one day later with a fresh biofilm, the medium (phosphate buffer) was removed after the anaerobic phase under the exclusions of oxygen. The BFC-system was replenished with deoxygenated buffer solution. The goal was to determine whether easily degradable substrate (S_S) stays in the biofilm or is released into the bulk liquid.

The r_O is shown in figure 6.19. Acetate was added at the time indicated to check whether the previous peak was caused by S_S. The peak after the medium replacement (indicated with ↑) represented a S_S production of 0.6 $g_{COD} \cdot m^{-2} \cdot d^{-1}$ from the time that the medium became anaerobic. The concentration S_S in the removed medium was 11.4 $g_{COD} \cdot m^{-3}$. This is equivalent with 3.4 $g_{COD} \cdot m^{-2} \cdot d^{-1}$.

The total production of S_S (4.0 $g_{COD} \cdot m^{-2} \cdot d^{-1}$) was comparable with the previous experiment. Furthermore, only ≈ 15% of the S_S will have been present in the biofilm at the time of the medium replacement. At a biofilm thickness of 1.1 mm, this equaled a concentration of 57 $g_{COD} \cdot m^{-3}$. The difference between the bulk medium S_S and the biofilm S_S concentration will have been caused by the concentration gradient. Although most of the hydrolysed substrate will be oxidised within the biofilm under normal conditions, it shows that S_S produced within the biofilm can diffuse freely and can therefore be used within as well as outside of the biofilm.

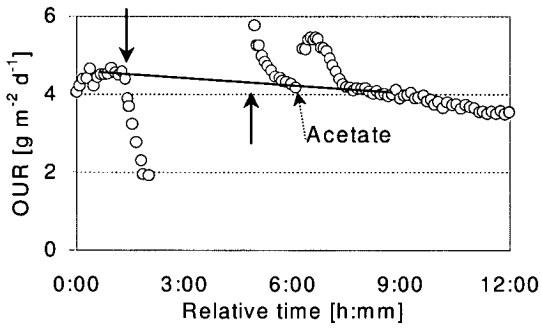

Figure 6.19: Quantification of S_S production by sewer biofilm. ↓ = stop of the reaeration, ↑ = medium replacement and reaeration start.

Particle addition

The influence of larger particles was studied by adding a concentrated solution of wastewater particulate material* to a BFC-system with centrifuged wastewater as medium to reach a particle concentration 5 times higher than in normal wastewater. The disappearance of the particles from the medium is depicted in figure 6.20. However, the oxygen uptake rate of the biofilm was not influenced. The system was therefore not limited by the particle concentration. It was observed that the system kept a constant respiration rate over a much longer time than without added particles.

The removal rate of particles from the bulk in the system with and without biofilm was similar. The biofilm apparently did not work as a strong scavenger. The absolute particle number was practically equal in both systems after addition of the particle solution.

6.8.2 Substrate limitation in the sewer system

Continuous respiration experiments (see section 8.5.2) indicated that the wastewater biomass is not substrate limited during daytime. A full-scale experiment was conducted to confirm this hypothesis. It consisted of raising the concentration of easily degradable substrates (S_S) by adding a mixture of acetate (2/3 on COD basis) and glucose (1/3) to the sewer. If the system were substrate limited then a drop in the oxygen concentration should be observed.

The measurements at both locations were synchronised by adding a salt pulse. The S_S addition started 5 min. later and lasted 20 min. Figure 6.21 shows the measured DO-concentrations and conductivities. The DO and conductivity at the second site has been shifted in time according to the residence time of the tracer peak. The difference between both DO curves does not show any significant change. Later, a Dirac-pulse of the substrate mixture was added (indicated by the small conductivity peak at 16:22), but no clear response was observed either. This confirms that this sewer section was not carbon-substrate limited during daytime.

*This solution was obtained by centrifugation and pasteurisation. For the latter the particles were pumped through a copper coil in a water bath at 70°C. The residence time was 2 min. The liquid was collected in a cooled beaker. No significant respiration was observed for at least 6 hours.

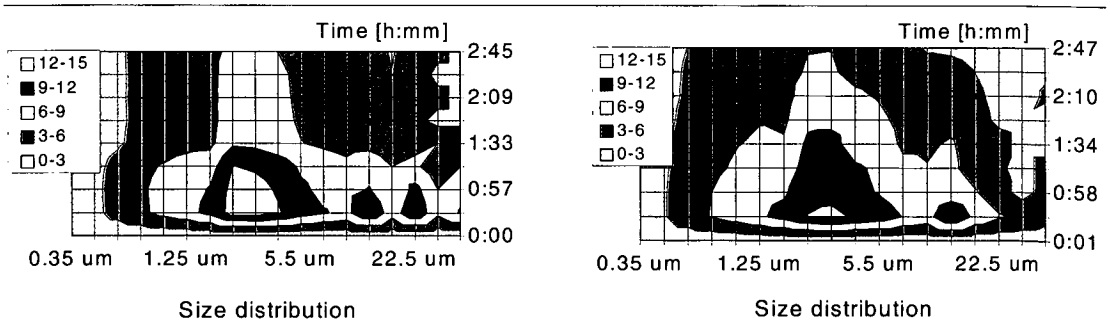

*Figure 6.20: The removal of particles from the medium in the BFC-system without biofilm (**left**) and with two plates containing biofilm (**right**). The 'z-axis' (legend) is the number of particles with a certain diameter at the time indicated on the right axis divided by the initial number at $t = 0:00$.*

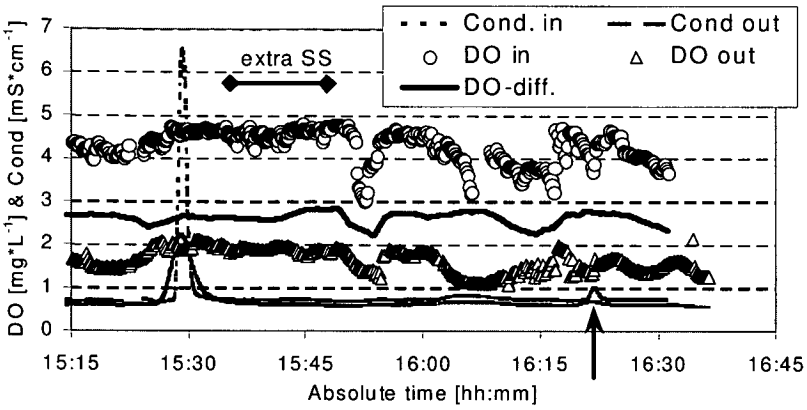

Figure 6.21: The measured conductivity and dissolved oxygen concentration after the continuous and pulse addition (arrow) of easily degradable substrate to the sewer.

6.8.3 Conclusion

The biofilm activity was measured directly with an *in situ* flow cell. The oxygen data made it possible to determine the biofilm biomass concentration γ. The highest concentration of 29800 $g \cdot m^{-3}$ was found at the insert where the biofilm is the thinnest. The highly active and compact biofilm is probably the result of the larger abrasion at this location. The average concentration along the wetted perimeter was 22400 $g \cdot m^{-3}$.

Extra substrate (20 $g_{COD} \cdot m^{-3}$ acetate) had no effect when centrifuged wastewater was taken as medium, but did lead to a higher activity with river or tap water. The sewer biofilm depended for at least one quarter on dissolved substrate from the wastewater.

The hypothesis that *only* the final stage of hydrolysis occurs in the biofilm could be confirmed for the top layers of the biofilm. Deeper strata seem to depend on hydrolysis. The hydrolysis rates under aerobic and anaerobic conditions were similar which showed that the ASM 3 approach for hydrolysis is also valid for this system.

6.9 Sewer biofilm denitrification

6.9.1 Introduction

Based on the common viewpoint on wastewater biofilms, denitrification must occur in the deeper strata (see figure 2.4). Indeed, it has been observed in several sewers that the nitrate concentration decreases with the flow distance (see for example figure 5.6). Due to the abundance of ammonium, which is preferred for biomass assimilation, it can be assumed that the nitrate is reduced by respiration. For example, the denitrification in the *Rümlang* main sewer on one occasion was quantified as 1.7 $g_N \cdot m^{-2} \cdot d^{-1}$ sewer*. This is equivalent to 3.0 $g_O \cdot m^{-2} \cdot d^{-1}$ when a conversion factor of 2.86 $g_{COD} \cdot g_N{}^{-1}$ is used. Denitrification could therefore contribute significantly to the conversion of COD in the sewer. The quantification of denitrification is also of importance for the pressurised sewer lines because nitrate is often added to raise the redox potential and prevent the formation of sulphides.

*0.4 $g_N \cdot m^{-3}$ (table 5.3) at a flowrate of 0.050 $m^3 \cdot s^{-1}$ and a biofilm area of 1630 m^2 (table 5.2) gives a conversion of 1.7 $kg_N \cdot d^{-1}$.

Based on the classical model, the nitrate must diffuse through the aerobic layer of the biofilm before denitrification can occur. The thickness of the aerobic layer is equivalent to the penetration depth of oxygen, which depends on the bulk oxygen concentration. The following questions arise:

- How strongly does the bulk oxygen concentration influence the denitrification rate?
- Does denitrification pose an effect on the oxygen uptake rate?
- Is the denitrification rate affected by the nitrate concentration?

6.9.2 Quantification of the denitrification

Several experiments were conducted with intact sewer-grown biofilm in the biofilm flow cell (described in section 4.7 and appendix A.4). The medium was centrifuged wastewater. The biofilm was several months old and had grown under an average sewer oxygen and nitrate concentration of 3 $g_O \cdot m^{-3}$ and 2 $g_N \cdot m^{-3}$, respectively.

One of the experiments was conducted under aerobic and anoxic conditions whereby the nitrate concentration was kept constant between 5 and 9 hours after the start of the experiment. The dissolved oxygen concentration (DO) was decreased stepwise (see figure 6.22(a)). The expectation was that the oxygen uptake rate (OUR) would decrease with an decreasing DO but that the denitrification rate would increase as the bacteria would switch from aerobic to anoxic respiration.

The result showed that the OUR followed a $1/2$-order relation with the dissolved oxygen concentration (see figure 6.22(a) and 6.22(b)). The denitrification rate, however, was hardly affected by the oxygen concentration. The accumulation of nitrite increased most strongly under anoxic conditions (see figure 6.22(c)).

A possible explanation is that the activity in the aerobic top layer is determined by the hydrolysis rate. Then, when the oxygen level decreases, the penetration depth of oxygen decreases and therefore the aerobic activity, which explains the 1/2-order dependency. The denitrification enzymes are apparently not induced in this previously aerobic layer. The denitrification remains limited to a deeper layer with a constant thickness where the rate is also determined by hydrolyses. Only at very low oxygen concentration when the aerobic activity decreases drastically, does the denitrification rate increase strongly. Furthermore, the induction of denitrification enzymes might have occured by then.

Several other denitrification experiments were conducted which showed that the denitrification rate was influenced by the biofilm thickness (see table 6.5).

Table 6.5: The denitrification and oxygen uptake rate for a thin (close to the insert) and a thick (close to the water surface) biofilm collected from the same manhole. (S_{NO_3} = 30–10 $g_N \cdot m^{-3}$, DO = 0.4 $g \cdot m^{-3}$, T = 20°C)

	thickness (μm)	TSS ($g \cdot m^{-2}$)	TVS ($g \cdot m^{-2}$)	$r_{NO_3^-}$ ($g_N \cdot m^{-2} \cdot d^{-1}$)	$r_{NO_3^-}$ # ($g_N \cdot m^{-2} \cdot d^{-1}$)	OUR ($g_O \cdot m^{-2} \cdot d^{-1}$)	OUR# ($g_O \cdot m^{-2} \cdot d^{-1}$)
thin	50	6.3	2.7	3.9	6.8	7	12
thick	350	52	23	2.4	4.1	8	15

#: Additional acetate added as carbon and energy source.

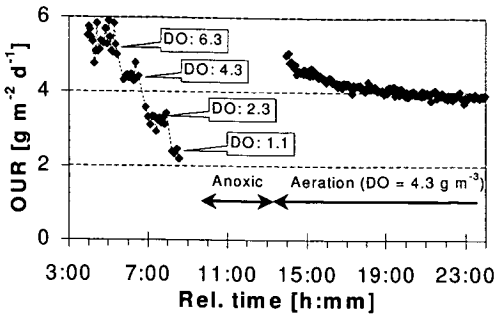

(a) Oxygen Uptake Rate at different oxygen concentrations DO.

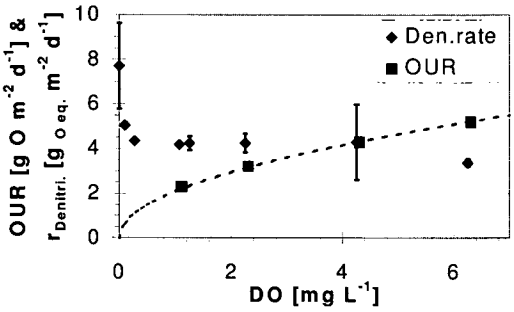

(b) The relation between DO and the OUR, fitted with a 1/2-order equation and the denitrification rate expressed in oxygen equivalents (1 mg-N $NO_3 \equiv 2.86$ mg O_2 and 1 mg-N $NO_2 \equiv 1.71$ mg O_2).

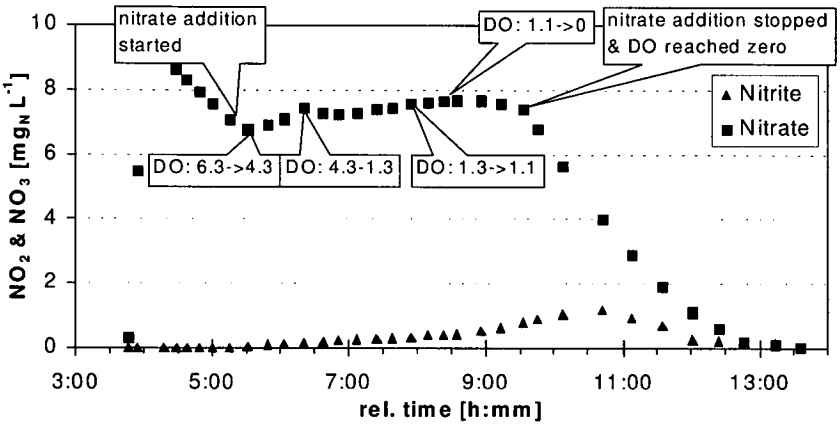

(c) The nitrite and nitrate concentration as a function of time.

Figure 6.22: The results of a denitrification experiment with intact sewer biofilm at 16°C and different oxygen concentrations (DO) in the presence of nitrate. At t = 5:10 a constant mass flow of nitrate into the BFC-system was started (65 $g_N \cdot m^{-3} \cdot d^{-1}$ or 2.1 $g_N \cdot m^{-2} \cdot d^{-1}$). The boxes indicate the DO concentration or a change in the DO-concentration (in $g \cdot m^{-3}$). The biofilm thickness was $\approx$ 200μm.

6.9.3 Conclusions

The DO level and the nitrate concentration in the bulk did not affect the denitrification rate. Furthermore, the denitrification did not affect the oxygen uptake rate. The model with the layered strata seems therefore not valid and the processes will be regarded as running parallel and independent.

6.10 Other sewer biofilm properties

The biofilm COD to TVS ratio was determined in biofilm samples taken from the plates before and after measurements in the biofilm flow cell. A value of 1.85 kg_{COD} per kg_{TVS} with a correlation coefficient $r^2 = 0.98$ was found. The ratio of COD to TSS was 0.49 $kg_{COD} \cdot kg_{TSS}{}^{-1}$ with $r^2 = 0.95$. Because there is also a linear relationship between the TVS and the (aerobic)

activity of the suspended biofilm, the COD as well as the TVS can be used as a measure for the amount of biomass. It should however be kept in mind that old biofilms from the *Rümlang* sewer contain an aerobically inactive organic fraction of $\approx$25 $g_{TVS}\cdot m^{-2}$ (see figure 6.9(a)).

The inactive fraction will mainly be located in the so-called base layer of the biofilm, when it is assumed that the biofilm consists of a strong base layer and a more fluffy top layer as was for example proposed by Siegrist (1985). The base layer has a larger resistance to erosion and will therefore survive modest rain events.

A separate COD-measurement of the 'top' and 'base' layer of the biofilm was possible by carefully scraping off the top layer. The 78 $mg_{COD}\cdot g_{wet\ biof.}{}^{-1}$ of the bottom layer was considerably lower than the 113 $mg_{COD}\cdot g_{wet\ biof.}{}^{-1}$ of the top layer. The total biofilm had 106 $mg_{COD}\cdot g_{wet\ biof.}{}^{-1}$. The difference is caused by the amount of inorganic material that collects in the older base film.

6.11 Conclusions sewer biofilm distribution, growth and activity

Several aspects of the sewer biofilm were analysed and discussed. The clear radial distribution of the biofilm mass along the perimeter was found with the minimum at the insert and the maximum in region of the diurnal water level variations. The total aerobic activity was proportional to the biofilm amount. No significant differences could be observed in the area specific activity of the intact biofilm. But the top layer of the biofilm depended on the wastewater for its substrate supply. The deeper strata are probably supplied with substrate through the hydrolysis of particulate material within the biofilm. A fraction of the substrate was stored as PHB and glycogen. Denitrification was unaffected by the bulk oxygen concentration.

Open questions

- What are the dynamics of the pools of storage materials?
- How strongly will different hydrodynamic conditions change the biofilm properties?
- Can the hypothesis be confirmed that the appearance and disappearance of the filaments after a rain event is caused by the temporarily increased oxygen and easily degradable substrate concentration?

7 Gas-liquid mass transfer in open channels

7.1 Summary

The reaeration of the wastewater in the sewer is an important component of the oxygen balance. The reaeration has been quantified in the past but a good and safe method to measure this in the sewer is lacking. The goal of the work presented in this chapter was to find an alternative reaeration measurement method for the sewer system.

The inert gas sulphur hexafluoride is used in rivers to quantify the reaeration. This method was adapted and tested for the sewer system. The conversion from tracer gas to oxygen was calibrated with field experiments in clean water pipes. Based on theoretical considerations, a new gas exchange equation was developed. Its parameters were found with experiments presented in this chapter and previously published results.

7.2 The occurrence and fluxes of gases in the sewer

The interest for gases in the sewer system is often either related to public uproar due to bad smells originating from the sewer or to the safety of maintenance personal. The problematic gases —methane, hydrogen sulphide and carbon monoxide— can be produced by biological processes under anaerobic conditions, for which especially pressure lines are notorious.

An obvious solution is to keep the sewage aerobic*. Therefore, engineers often design the sewers with a connection to the outside air. The drag of the water flow below and wind above will normally assure enough exchange of air to maintain a gas oxygen concentration in the sewer atmosphere close to that of the outside air (e.g. Pescod and Price, 1982). This also dilutes the odours. Whether enough oxygen will be transferred into the sewage depends on many factors like mean water depth, temperature etc. In Switzerland the oxygen mass transfer is often large enough to prevent anaerobic conditions.

Knowledge of the gas transfer rate in sewers is also of importance to determine the loss of volatile organic compounds (VOC) or toxic substances like chlorinated hydrocarbons or substrates for biological processes from sewers (e.g. Whitmore and Corsi, 1994).

Apart from the above mentioned problems, the dissolved oxygen concentration plays a cenral role in the degradation of pollutants. Especially the sewer biofilm activity is strongly affected by the oxygen concentration (see section 9 on page 113 and on). If the goal is to simulate or

*Although this does not mean that these noxious gases are not produced —that could still occur in sediments and other deadzones— but they would diffuse through an aerobic zone where they can be oxidised biologically and/or chemically.

model the processes in the sewer, then it is of uttermost importance that the reaeration* is described accurately.

In this chapter a theoretical background of mass transfer through the gas-liquid interface will be given, extended with an overview of empirical oxygen mass transfer equations and measurement methods for gas liquid mass transfer. The methods that have been applied in the sewer system up to now have some considerable disadvantages. A method has therefore been developed which is based on the gas sulphur hexafluoride (SF_6) as a tracer for gas transfer. Results will be presented of experiments that were done to calibrate this method under sewer conditions. Finally, the results of measurements in actual sewers will be presented.

7.3 The physical background of interfacial mass transfer

7.3.1 Gas-liquid mass transfer

The mass transfer rate through a gas-liquid surface is described by a transfer coefficient and a driving force (e.g. Skelland, 1974):

$$\phi_m = k_{o,l} \cdot A_S \cdot (c_l^* - c_{b,l}) \tag{7.1}$$

where ϕ_m = the mass flux across an interface (kg·s^{-1}), $k_{o,l}$ = overall mass transfer velocity related to the liquid-phase (m·s^{-1}), A_S = interfacial area (m^2), c_l^* = equilibrium concentration of solute in liquid phase (kg·m^{-3}) and $c_{b,l}$ = liquid-phase bulk concentration (kg·m^{-3}).

Under assumption of the two-film model of Lewis and Whitman (1924), $k_{o,l}$ is found from a combination of the liquid and of the gas side velocity (e.g. Skelland, 1974):

$$\frac{1}{k_{o,l}} = \frac{1}{k_l} + \frac{1}{k_g \cdot H_l} = \frac{1}{k_l} + \frac{\mathcal{R} \cdot T_K}{k_g \cdot H_g} \tag{7.2}$$

where k_l = liquid-phase mass transfer velocity (m·s^{-1}), k_g = gas-phase mass transfer velocity (m·s^{-1}), H_l = Henry coefficient related to liquid phase (kg·m^{-3})$_{gas}$/(kg·m^{-3})$_{liquid}$, H_g = Henry coefficient related to gas phase (Pa·m^3·mole^{-1}), $\mathcal{R}$ = ideal gas constant (J·K^{-1}·mole^{-1}) and T_K = absolute temperature (K). k_l and k_g depend on the prevailing turbulence level, which is determined by the water current and the wind, on the temperature, and on the properties of the solute such as the diffusivity and the molecular size (MacKay and Yeun, 1983). For many systems k_g/k_l has been reported to be greater than 100 since molecular diffusion processes are on average a factor 10^3 slower in liquids than in gases (Whitmore and Corsi, 1994). MacKay and Yeun (1980) showed that more than 99.8% of the resistance for oxygen transfer lies on the liquid side for typical stream flow conditions. Therefore, the k_{o,l,O_2} is in a good approximation equal to k_{l,O_2}. However, the liquid phase resistance controlled gas exchange rates in rivers are influenced by wind speed, since wind generates near-surface turbulence (MacKay and Yeun, 1980). Unfortunately, this effect is difficult to quantify, but it will be less important for the sewer system than for rivers because liquid and air flow in the same direction. Furthermore, the air velocity in the sewer is strongly related to the water velocity, which follows a predictable diurnal pattern. This effect is therefore accounted for when the gas exchange is measured with a method as presented in section 7.5.

The most common way to express mass transfer in technical systems is the product of k_l and the specific surface area a (m^2·m^{-3}): $k_l a$ (s^{-1}). Named K_2 it is also used to describe the

*colloquial name for the oxygen flux through the gas-liquid interface into flowing water

reaeration of streams. The one notation is easily transformed in the other as long as there is no entrainment of air resulting in bubbles:

$$K_2 = k_l a = k_l \cdot \frac{A_S}{V} = k_l \cdot \frac{w}{A_{cr}} = k_l \cdot \frac{1}{d_{mean}} \tag{7.3}$$

where V = volume (m^3) and d_{mean} = mean hydraulic depth (m).

7.3.2 Water quality factors influencing interfacial mass transfer

Very small amounts of impurities in the water (surfactants, fats and oils) which concentrate on the interfacial area can have a measurable effect on the oxygen mass transfer (ASCE Standard, 1993). This can be expressed with the empirical $\alpha_{k_l a}$-factor. Pomeroy and Parkhurst (1973) mention a value for $\alpha_{k_l a}$ of 0.3 to 0.4 for open channel flow. In contrast to this, Jensen (1995) found a value around unity, based on laboratory experiments with wastewater and tap water with commonly used detergents. In the latter case even *increases* were observed: 6% without foam, 44% with $\leq$ 2 mm foam and 104% with > 2 mm foam. These findings are remarkable because surfactants collect at the gas-liquid interface and occupy surface area, hampering the exchange of liquid elements at the surface (Kögel *et al.*, 1981). Consequently, the gas transfer rate is lower. In the experiments of Jensen, the foam will probably have led to an increased exchange area. Or, the decreased surface tension due to the surfactants might have led to a larger mass transfer area in the stirred vessel that Jensen (1995) used for his measurements, because the turbulence at the surface would have been damped less. Consequently, the exact effect of surface-active impurities on open channel gas transfer still remains unclear.

Often, tabulated values for the saturation concentration of a gas like oxygen are used. This can however lead to a significant error due to several reasons:

water vapour the air at gas-liquid interface is saturated with water, which lowers the air oxygen fraction. Equation (E.8) is an empirical relationship for this.

oxygen uptake oxygen dissolves in the sewage, which lowers the sewer atmosphere oxygen fraction. The influence depends on the gas exchange with the outside air.

dissolved salts and other impurities the interface mass transfer can be affected by dissolved salts and other impurities because they lower the solubility of the gas in the liquid. The effect is small at a salt concentration of < 0.1 $g.L^{-1}$ chloride-equivalents (An oxygen saturation concentration decrease of < 0.3% (APHA, 1985)). However, also other impurities can lower the oxygen solubility, for which the empirical β-factor can account. β can be approximated as 0.95 (Jensen, 1995) for wastewater, although Hanel (1982) gives a value between 0.97 and unity.

The saturation concentration c_l^* can be calculated with the Henry coefficient H:

$$c_l^* = \underbrace{\beta \cdot \frac{c_{b,g}}{H_l}}_{liquid} = \underbrace{\beta \cdot \frac{p_x}{M_x \cdot H_g}}_{gas} \tag{7.4}$$

where p_x = partial pressure of a solute in the atmosphere (Pa) and M_x = molecular mass of the solute ($g{\cdot}mol^{-1}$).

Whenever possible c_l^* should be measured with the actual liquid instead of using a tabulated value. But care has to be taken that badly calibrated oxygen sensors (see appendix A.6) and biological and chemical processes do not falsify the results.

The mass transfer rate with the empirical correction factors is written as:

$$r_{O,m} = \alpha_{k_l a} \cdot k_l a \cdot \left(\beta \cdot \frac{p_x}{M_x \cdot H_g} - c_{b,l} \right) \tag{7.5}$$

where $r_{O2,m}$ = specific oxygen mass transfer rate (kg·m^{-3}·s^{-1}), $\alpha_{k_l a}$ = ratio of $k_l a$ under practical conditions to that in clean water (-) and β = ratio of solubility under practical conditions to that in clean water (-).

7.3.3 Sherwood number for mass transfer

The gas liquid mass transfer can be expressed with the dimensionless Sherwood number* (**Sh**) as a function of the Reynolds number (**Re**)† and the Schmidt (**Sc**)‡ numbers (e.g. Bennett and Myers, 1962):

$$\mathbf{Sh} = c \cdot \mathbf{Re}^{1/2} \cdot \mathbf{Sc}^{1/3} \qquad \text{valid for } \mathbf{Sc} > 0.6 \tag{7.6}$$

where c = proportionality constant (-).

The **Sc**-number is a constant for a given solute/solvent system, but is strongly influenced by the temperature, especially for liquids. The exponent of **Sc** in (7.6) is based on the ratio of the thicknesses of the hydrodynamic and the thermal boundary layers in common process equipment (Bennett and Myers, 1962). It depends on the water phase turbulence level at the gas-liquid interface as Dobbins (1964) showed experimentally.

This exponent should be expressed as $(1-n)$ instead of $(1/3)$ where the constant n depends on the interfacial turbulence which is approximated with a boundary layer model, as will be shown in the next section.

When (7.6) is rewritten with the definitions of the dimensionless numbers it transfers into:

$$\frac{k_l \cdot L}{\mathbb{D}} = c \cdot \left(\frac{u \cdot L}{\nu} \right)^{1/2} \cdot \left(\frac{\nu}{\mathbb{D}} \right)^{1-n} \tag{7.7}$$

where L = characteristic length (m) and $\mathbb{D}$ = diffusion coefficient (m^2·s^{-1}). When all non-temperature dependent parameters and variables of (7.7) are lumped into the proportionality variable c_2, the following equation is obtained:

$$k_l^{\mathbf{Sh}} = c_2 \cdot \mathbb{D}^n \cdot \nu^{1/2-n} \tag{7.8}$$

where $k_l^{\mathbf{Sh}}$ = k_l based on the Sherwood number (m·s^{-1}) and c_2 = system constant (s$^{1/2}$·m^{-1}).

7.3.4 Boundary layer mass transfer models

Researchers have developed three basic models for mass transfer through the boundary layer (see e.g. Dobbins, 1964). These are listed in table 7.1 with the corresponding value for the exponent n in (7.8). In all cases the bulk fluids are completely mixed.

*The Sherwood number is the ratio of overall mass transfer to the molecular diffusivity = R_h/δ_c.

†The Reynolds number is the ratio of inertial force to viscous force in a flow system.

‡The Schmidt number is the ratio of mass transport by turbulence and by diffusion.

Table 7.1: The three classical boundary layer models with the corresponding value for the exponent n.

model	Reference	n
film-theory	Lewis and Whitman (1924)	1
penetration theory	Higbie (1935)	1/2
surface renewal theory	Danckwerts (1951)	2/3

7.3.5 Influence of turbulence on gas exchange

Although numerous theoretical models and empirical formulations have been proposed over the years, there is still no general agreement on the calculation of the gas transfer rate. The main reason is that the relation between the liquid turbulence and interfacial mass transfer still remains unresolved (Chu and Jirka, 1991).

Most authors agree that turbulence is a key parameter in oxygen interfacial transport. Turbulence is produced due to the conversion of kinetic energy in the bulk of the liquid and at the walls of the channel.

Scales in mass transfer

The classical two-film model as presented in section 7.3.1 implies that only one layer with a defined thickness at the liquid side of the interface controls the mass transport. In reality, however, several length scales are thought to have an impact. Figure 7.1 shows these lengths for a moderate (**Re***). This number is defined as:

$$\mathbf{Re}^* = \frac{\rho \cdot u^* \cdot d_{mean}}{\eta} \tag{7.9}$$

where u^* = shear velocity (m·s^{-1}) as defined in equation (3.12).

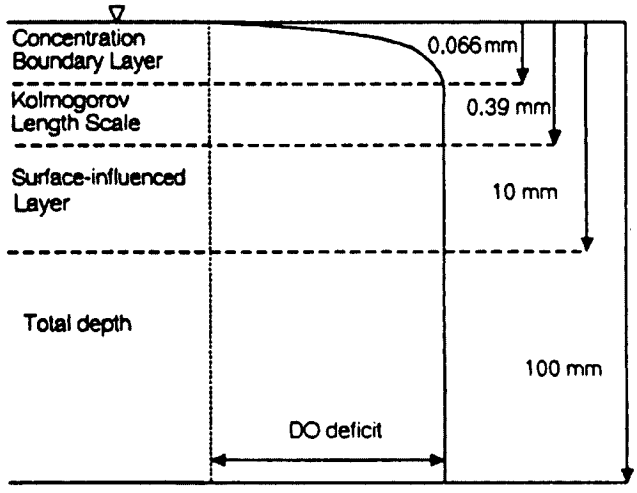

*Figure 7.1: Typical length scales in smooth channel reaeration for **Re*** = 2300, as calculated by Moog and Jirka (1999).*

An eddy cannot approach the free surface closer than roughly its length scale, which is given by the Kolmogorov length* l_k (m) (Moog and Jirka, 1999):

$$l_k = \left(\frac{\nu^3}{\varepsilon}\right)^{\frac{1}{4}} \tag{7.10}$$

where ε = near-surface turbulent energy dissipation rate (J·s^{-1}):

$$\varepsilon = \frac{u^{*3}}{d_{mean}} \tag{7.11}$$

The mean concentration boundary layer is the mean distance over which the gas concentration varies form the surface to nearly the bulk value. Its thickness is estimated by:

$$\delta_c = \frac{\mathbb{D}_{O_2}}{k_l} \tag{7.12}$$

Surface renewal

Higbie (1935) first introduced the concept that the surface is periodically replaced by bulk liquid. This process is controlled by eddies which penetrate the concentration layer and renew the concentration boundary layer. Contamination of the free surface can prevent that eddies break through the concentration layer and reach the surface. This can explain the detrimental effect of a surfactant (Hunt, 1984). The surface renewal model was generalised by Danckwerts (1951) when he introduced random replacement times at a mean frequency r:

$$k_l = \sqrt{\mathbb{D} \cdot r} \tag{7.13}$$

The problem is to estimate r. The choice of one of the two following eddy models is hereby of importance:

Large eddy model the dominating eddies are large 'roll cells' with a length scale proportional to for example the flow depth and a velocity proportional to the shear velocity, i.e. $r \propto u^*/d_{mean}$ (Fortescue and Pearson, 1967). Inserting this in (7.13) results in

$$\frac{k_l}{u^*} \propto \mathbf{Sc}^{-1/2} \cdot (\mathbf{Re}^*)^{-1/2} \tag{7.14}$$

small eddy model the smallest eddies are dominating. The length scale is based on the Kolmogorov length l_k. Lamont and Scott (1970) found that $r \propto (\varepsilon \cdot \nu)^{1/2}$ which leads to

$$\frac{k_l}{u^*} \propto \mathbf{Sc}^{-1/2} \cdot (\mathbf{Re}^*)^{-1/4} \tag{7.15}$$

Both models only differ in the shear Reynolds number exponent. They can therefore be generalised as

$$\frac{k_l}{u^*} \propto \mathbf{Sc}^{-1/2} \cdot (\mathbf{Re}^*)^{m} \tag{7.16}$$

*The Kolmogorov scale approximates the size of the smallest turbulent motions.

where m = exponent of $\mathbf{Re}^*$ (-). The dominating model can be found by determining m experimentally. Theofanous *et al.* (1976), however, proposed that the dominating model should depend on $\mathbf{Re}^*$ too. They assumed that the large eddy model would prevail at $\mathbf{Re}^* < 500$. Therefore, the outcome of an experiment in a certain channel cannot be extrapolated to the whole flow range because there might be a shift as the flow changes from the large eddy to the small eddy model or vice versa.

Bursts

Up to now, the assumption was that the turbulence is horizontally homogenous. However, in reality coherent turbulent motion occurs, which one can see in open channel flow as patches of upwelling water. These 'bursts' are large-scale motions that lift water from the wall towards the free surface, causing an acceleration and downward motion of the surface liquid. As shown in direct numerical simulation, these bursts can attach to the surface for a limited time, creating patches below which lie greatly elevated vortices (Banerjee, 1992; Pan and Banerjee, 1995). This is in contradiction with the renewal theory. These patches strongly contribute to the mass transfer. As a result, the dependency of k_l on $\mathbf{Re}^*$ decreases, which is reflected in a reduction of the exponent m in (7.16). Moog and Jirka (1999) presented results of several researchers that implied that m can be -0.15 or even 0 for $\mathbf{Re}^* \approx 4500$ (the *Rümlang* sewer $\mathbf{Re}^*$ is $\approx$ 1500 to 10000).

7.3.6 Temperature effect on gas-liquid mass transfer

The gas exchange rate at a reference temperature is converted to the rate at another temperature —or vice versa— with the help of a temperature correction function. The most often used empirical equation was originally published by Elmore and West (1961):

$$\mathrm{f}_T[\text{Elmore}] = \frac{k_{l,T}}{k_{l,T_{ref}}}[\text{Elmore}] = \theta^{(T-T_{ref})} = 1.0241^{(T-20)} \tag{7.17}$$

where f_T = temperature factor for k_l, θ = exponential temperature coefficient (-), T = temperature (°C) and T_{ref} = reference temperature (normally 10 or 20°C). The ASCE Standard (1993) now recommends this equation for oxygen mass transfer in clean water.

Equation (7.8) provides a way to take the temperature influence into account through the effect on $\mathbb{D}$ and ν:

$$\mathrm{f}_T[\text{Sherwood}] = \left(\frac{\mathbb{D}_T}{\mathbb{D}_{T_{ref}}}\right)^n \cdot \left(\frac{\nu_T}{\nu_{T_{ref}}}\right)^{1/2-n} \tag{7.18}$$

Figure 7.2 shows a comparison between (7.17) and equation (7.18) for the penetration and the film theory. The conversion factor becomes practically equal to equation (7.17) of Elmore and West (1961) when $n = 0.77$ in equation (7.18).

The conversion to a reference temperature introduces a small error as long as the temperature is close to the reference temperature, as Whitmore and Corsi (1994) state. However, in the sewer and many other systems the temperature might be 10°C or lower. Two error sources can be introduced when equation (7.17) is used for the temperature correction from for example 10 to 20°C:

1. the choice of an inappropriate boundary model (the exponent n in equation (7.18)) could introduce an error of up to 30% (see figure 7.3).

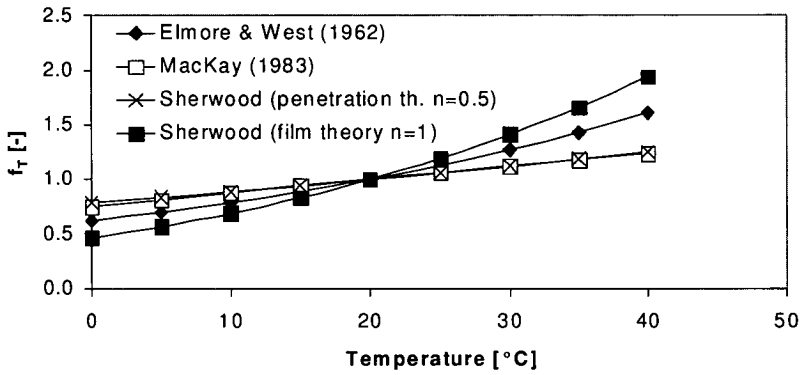

Figure 7.2: The conversion factor for O_2 mass transfer as a function of temperature for the different temperature correction approaches. 'Sherwood' refers to (7.18). The temperature dependencies of $\mathbb{D}$, ρ and η have been taken according to the equation in appendix E.2

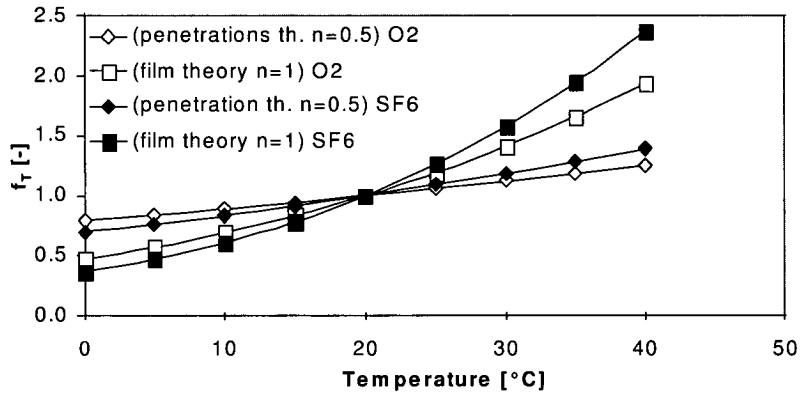

Figure 7.3: Comparison between the temperature conversion factors of oxygen and of sulphur hexafluoride (SF_6) for two different boundary layer models.

2. the use of a temperature conversion calibrated for oxygen for another gas results in an unnecessary error of 7% for example for krypton in comparison to a conversion with the diffusion coefficient of Jähne *et al.* (1987):

$$\mathbb{D}_{Kr} = 6.936 \cdot 10^{-6} \cdot \exp\left(-2.02 \cdot 10^4/(8.3144 \cdot T_K)\right) \tag{7.19}$$

The ratio of (7.18) as a function of temperature is shown in figure 7.4. The error even becomes 14% for the sulphur hexafluoride that was used in this study.

These errors can become significant in systems where the flow, the oxygen concentration, the geometry and the temperature can be measured accurately, like in laboratory or sewer systems.

The clearly described solvent/solute specific temperature dependency in equation (7.18) is a major improvement over the common praxis to use equation (7.17) for oxygen as well as all other gases. It can easily be adapted for other combinations because the $\mathbb{D}$ and ν are often known.

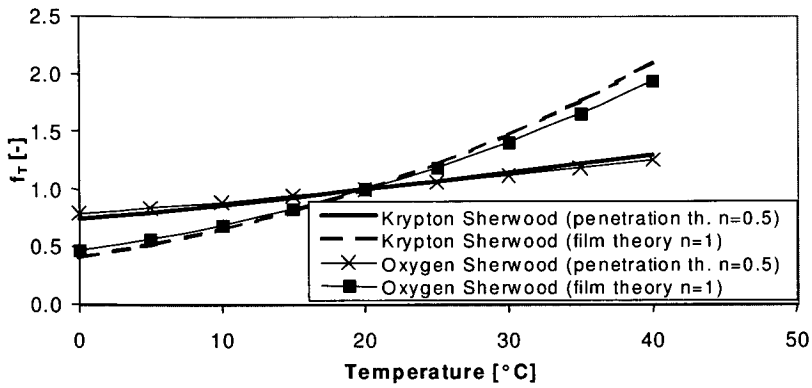

Figure 7.4: The conversion factor, equation (7.18), for krypton and oxygen mass transfer compared when either the penetration or the film theory is used.

7.4 Empirical reaeration equations for open channels

7.4.1 Stream reaeration

The process of oxygen mass transfer in the sewer is comparable with the reaeration in streams and rivers which has been studied frequently (e.g. Streeter and Phelps, 1925; O'Conner and Dobbins, 1958; Tsivoglou, 1968; Owens *et al.*, 1964; Parkhurst and Pomeroy, 1972). Detailed information concerning sewers has been presented only by Pomeroy and Parkhurst (1973), Jensen and Hvitved-Jacobsen (1990, 1991), Jensen (1995), Whitmore and Corsi (1994). Krenkel and Orlob (1962) and Bålmér and Tagizadeh-Nasser (1995) performed studies under controlled conditions in a variable slope channel with a rectangular and a circular cross section, respectively.

Although some fairly good equations exist for the oxygen gas transfer in sewers (see next section), it is often advisable to measure the actual transfer rate, since local conditions as well as the wastewater properties and the geometry of the sewer will have a significant influence on the gas transfer. This has been clearly shown with oxygen mass transfer measurements in wastewater treatment plants (e.g. Doyle and Boyle, 1986) and the above mentioned sewer measurements.

7.4.2 Previously proposed reaeration equations

Several researchers have proposed equations for oxygen mass transfer in open channels, which are listed in table 7.2. Jensen (1995) compared the equations (7.20) to (7.24) for which he used the data of Jensen and Hvitved-Jacobsen (1991), Taghizadeh-Nasser (1986) and Pomeroy and Parkhurst (1973). He came to the conclusion that (7.22) had the optimal structure and re-estimated the coefficients to obtain equation (7.26).

However, the observations of Balmér and Tagizadeh-Nasser (1995) were left out, because they did not follow the trend of the experiments performed in sewers. There are several possible reasons for this:

- *The laboratory equipment or procedure introduced a substantial systematic error* (Jensen, 1995). This is not unlikely since the water was recycled and aeration at the in- and outflow might have occurred.

Table 7.2: An overview of reaeration equations for open channel flow from literature sources expressed as $k_l a$ (in h^{-1}). If necessary they were converted from k_l to $k_l a$ by dividing by d_{mean}.

A	$7.235 \cdot (S_0 \cdot u)^{0.408} \cdot d_{mean}^{-2/3}$	Krenkel and Orlob, 1962	(7.20)
	$0.222 \cdot u^{0.67} \cdot d_{mean}^{-0.85} / d_{mean}$	Owens *et al.*, 1964	(7.21)
B	$0.96 \cdot (1 + 0.17 \cdot \mathbf{Fr}) \cdot (S_0 \cdot u)^{3/8} \cdot / d_{mean}$	Parkhurst and Pomeroy, 1972	(7.22)
	$720 \cdot u \cdot S_0$	Tsivoglou and Neal, 1976	(7.23)
	$0.4 \cdot u \cdot (d_{mean}/R_h)^{0.613} / d_{mean}$	Taghizadeh-Nasser, 1986$^{\diamond}$	(7.24)
	$0.96 \cdot (1 + 0.17 \cdot \mathbf{Fr}) \cdot (S_0 \cdot u)^{0.75} \cdot d_{mean}$	Jensen and Hvitved-Jacobsen, 1991	(7.25)
	$0.86 \cdot (1 + 0.20 \cdot \mathbf{Fr}) \cdot (S_0 \cdot u)^{3/8} / d_{mean}$	Jensen, 1995	(7.26)
C	$2.10 \cdot (S_0 \cdot u \cdot g)^{3/8} \cdot (d_{mean}/D)^{0.4} / d_{mean}$	Balmér and Tagizadeh-Nasser, 1995	(7.27)

where A = simulated stream, B = sewer and C = simulated sewer
$^{\diamond}$ in: Jensen (1995).
S_0 = sewer slope (%), u = velocity (m·s^{-1}), d_{mean} = mean water depth (m), R_h = hydraulic radius (m), g = gravitational acceleration = 9.81 (m·s^{-2}), D = pipe diameter (m) and **Fr** = the Froude number as defined in equation (7.28).

- *The artificial open channel consisted of concrete pipe sections of one metre.* These will probably have created more turbulence than in a real sewer where biofilm and sediments smoothen the joints, which are further apart too because the sections are longer.
- *Tap water was used instead of wastewater.* The data of Balmér and Tagizadeh-Nasser could be integrated with the other data when an $\alpha_{k_l a}$-factor of 0.3 would be introduced. This is clearly lower than the common $\alpha_{k_l a}$-factor of 0.6 that was given on page 71 for bubble aerated systems, but remarkably similar to the value 0.3 as estimated by Pomeroy and Parkhurst (1973). The impurities of the wastewater will not only have influenced the k_l but also the bubble size and therefore the exchange area. Though the exchange area in open channel flow remains practically constant. As far as known, only Jensen (1995) tried to measure $\alpha_{k_l a}$ for surface aeration and found a value around unity, but the experimental procedure seems questionable (see section 7.3.2).

  Another indication that the water quality plays an important role is that the data of Balmér and Tagizadeh-Nasser are consistent with the outcome calibration experiments with clean water instead of wastewater. These experiments will be presented in section 7.6. The gas exchange was also approx. twice as high as was predicted by (7.22).
- *The experiments were conducted at high Froude numbers* (**Fr**). The **Fr**-number describes the influence of gravity on fluid motion:*

$$\mathbf{Fr} = \frac{\bar{u}}{\sqrt{g \cdot L}} \tag{7.28}$$

where $\bar{u}$ = average velocity (m·s^{-1}), g = gravitational acceleration (m·s^{-2}) and L = characteristic length (m). The mean depth (d_{mean}) is taken as the characteristic length. Figure 7.5

*This is the version used in this work. Unfortunately, there is also a squared variant: $\mathbf{Fr} = \bar{u}^2 / g \cdot L$

shows that **Fr** was larger than unity during almost all of their experiments. The influence of the **Fr** number on the Parkhurst and Pomeroy equation is based only on a relatively small number of measurements in a small range. However, equation (7.22) could not be adjusted to fit the data of Balmér and Tagizadeh-Nasser.

The equation proposed by Balmér and Tagizadeh-Nasser (equation 7.27) does predict their data rather well (see figure 7.6), but not the other data. Balmér and Tagizadeh-Nasser (1995) explain the difference of the predictions of equation (7.27) in comparison to equation (7.22) with the uncertainties in the experimental conditions of Pomeroy and Parkhurst (1973) like incompletely inhibited respiration. However, it is remarkable that the data with clean water are different from the other data. Therefore: *The data of Balmér and Tagizadeh-Nasser has been left out in the following evaluations, although the data is shown in the graphs.*

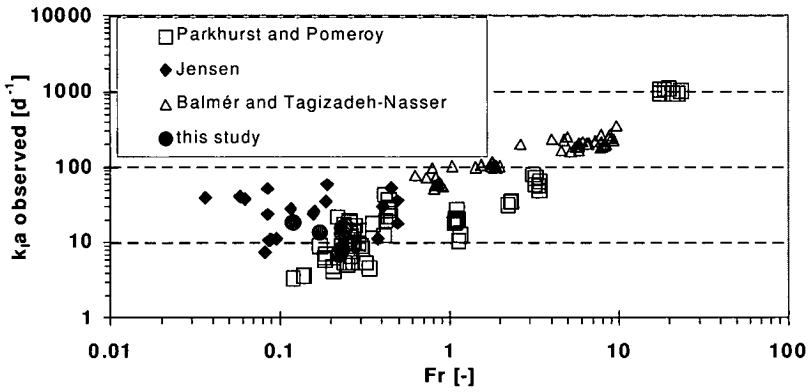

*Figure 7.5: The **Fr**-number against the observed $k_l a_{20,O_2}$.*

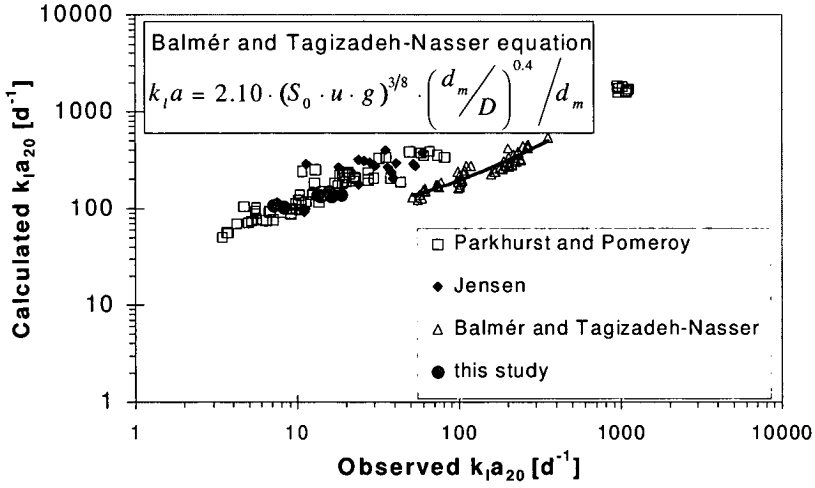

Figure 7.6: The observed against the calculated $k_l a_{20,O_2}$ with equation equation (7.24) as was proposed by Balmér and Tagizadeh-Nasser.

7.4.3 New reaeration equation for open channel flow

Parkhurst and Pomeroy (1972) developed a reaeration equation based on the assumption that the dissipation of potential energy is related to the gas transfer rate. Although their empirical approach described the data quite well, the data acquired during this study will be fitted with the more fundamental approach based on the **Sc** and **Re*** as given in (7.16). This equation is extended with a term that contains **Fr** to take the effect of an increased interface roughness at higher flow velocities into account:

$$k_l a_{20,O_2} = \frac{k_{l,20,O_2}}{d_{mean}} = a_{reaer.} \cdot \frac{u^* \cdot Sc^0 \cdot (\mathbf{Re}^*)^{0.004} \cdot (1 + b_{reaer.} \cdot \mathbf{Fr})}{d_{mean}} \tag{7.29}$$

$$= 33 \cdot \frac{u^* \cdot (1 + 0.41 \cdot \mathbf{Fr})}{d_{mean}} \tag{7.30}$$

where $a_{reaer.}$ = proportionality constant (-) and $b_{reaer.}$ = proportionality constant for the influence of **Fr**. The calculation of the proportionality constants will be explained in section 7.7.2.

7.4.4 Oxygen transfer measurement methods

Experience with the quantification of the reaeration during open channel flow has been collected over a period of many decades. Two fundamentally different principles are used:

Indirect method This was first applied in open channel flow by Streeter and Phelps (1925). It is based on the oxygen mass balance over a channel section and requires knowledge or elimination of all other processes with regard to oxygen but the reaeration. Parkhurst and Pomeroy (1972) used this method to measure reaeration in the sewer system by first cleaning the sewer wall mechanically with the common sewer cleansing methods and chemically with sodium hydroxide. During the experiment, hypochlorite was added to inhibit biological processes. The oxygen levels of the incoming water can be lowered with sodium sulphite (Chapra, 1997). The major uncertainties are the residual and unknown oxygen sinks (Jensen, 1995). Furthermore, the application of such large amounts of aggressive chemicals is nowadays hardly acceptable.

Direct method The basic assumption behind this technique is that the ratio between the desorption of a tracer gas and the adsorption rate of oxygen from the liquid is constant. Normally, an inert gas with similar physical properties as oxygen is dissolved in the water. The concentration difference of the tracer gas in the liquid between the start and end of a channel section is a measure for the gas exchange. The properties the tracer gas should have are: non-toxic, no ad- or absorption, accurate and sensitive analysis, and easy handling. Because the driving force of gas transfer is the partial pressure difference between the gas in the atmosphere and that dissolved in the water, tracers should be chosen that have no significant atmospheric component. Thus, measurements can be made under assumption of a saturation concentration of zero.

Direct gas exchange measurements

The first efforts to develop tracer alternatives to the indirect method resulted in the use of radioactive krypton-85 (^{85}Kr) (Tsivoglou *et al.*, 1965). The Kr-gas was injected in the river and its desorption was measured along the river reach. The ratio of the tracer gas transfer rate to the oxygen transfer rate was determined through laboratory experiments involving the simultaneous

transfer of both gases. This technique worked well, however, with regard to the environment, authorities and personnel, it is undesirable to use radiotracers. In spite of this, they were still applied recently (Jensen and Hvitved-Jacobsen, 1991; Jensen, 1995).

Other gas tracers like ethylene and propane have been tested (Rathbun *et al.*, 1978; Friedmann and Blanc, 1991). These had the disadvantage of a low solubility and possible degradation. Later, other gases have been used to overcome problems with the solubility and potential of degradation of these hydrocarbons. These were methyl chloride (Wilcock, 1984), sulphur hexafluoride (Wanninkhof *et al.*, 1991) and non-radioactive krypton (Whittemore and Krause, 1991). Non-radioactive krypton, which is a mixture of 6 stable isotopes, would be a good alternative to ^{85}Kr considering the amount of experience and data regarding ^{85}Kr. However, the analysis is difficult and laborious.

Sulphur hexafluoride has many desirable features as a deliberate tracer, most notably its low detection limit, its long-term stability in water, the ability to preserve water samples containing SF_6, and ease of analysis. A drawback of this gas for gas transfer studies is that its fat solubility is higher than that of oxygen. This will be further discussed in section 7.5.2. Furthermore, its Schmidt number (**Sc**) is higher than that of gases of environmental interest such as O_2 and CO_2 (Wanninkhof *et al.*, 1991) (see figure 7.7). Therefore, under highly turbulent conditions when bubbles contribute to gas transfer, SF_6 transfer will be enhanced to a greater extend than transfer of gases with higher solubilities (Ascher *et al.*, 1991).

Tracer addition

The tracer can either be added as a pulse, or continuously. In rivers pulse-addition is almost always used due to the large flows that would otherwise require a large amount of tracer. However, when the tracer is added as a pulse, a non-volatile dispersion tracer has to be added also because the tracer peak will decrease and widen due to dispersion. A dispersion tracer can either be radioactive ^3H (tritium) (Tsivoglou *et al.*, 1965; Jensen and Hvitved-Jacobsen, 1991; Jensen, 1995) or an inert salt like bromide. Often a third easily detectable tracer like rhodamine is released first to synchronise sampling.

In the sewer system, where the flows are generally smaller, continuous addition of a gas tracer is often necessary because the dispersion is so small that otherwise very fast sampling is required to resolve the tracer peak. This could hardly be done manually, so that extra infras-

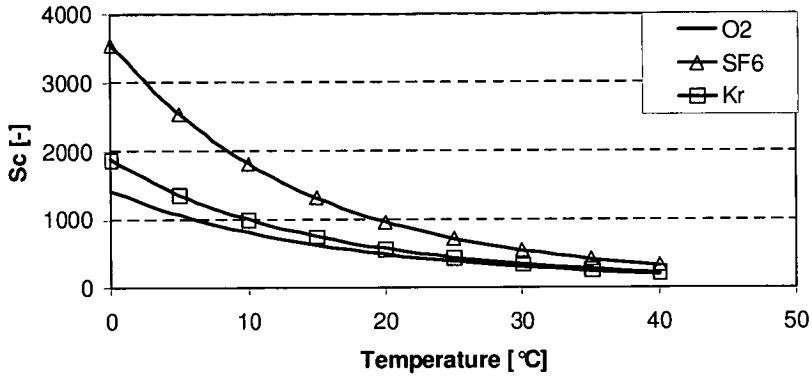

*Figure 7.7: The **Sc**-number for sulphur hexafluoride (SF_6) and krypton (Kr) in comparison to oxygen (O_2).*

tructure would be required (see for example Jensen and Hvitved-Jacobsen, 1991) which could give rise to an extra error and complicates fields experiments. In contrast, continuous addition allows sampling over prolonged periods of time, but care has to be taken that the assumption that the gas has no atmospheric component still remains valid. An easily detectable tracer is also required for synchronisation purposes as is described in section 4.2.1. The residence time is found by deducting the times of the maximum in both tracer curves. A dispersion tracer is no longer needed. The gas tracer concentrations are therefore easier to process because a correction for dispersion is not necessary. Finally, if infiltration is expected then a non-volatile tracer like bromide can be added continuously to quantify the amount of dilution.

All above mentioned gas tracers have the disadvantage that they require injection, which comprises the potential problem of incompletely cross-sectional mixing and low concentrations. This can be circumvented when gases are used that are already abundant in the water. Tsivoglou *et al.* (1965) already used radioactive radon-222 (^{222}Rn), for which these authors went to wells containing high concentrations of this gas. Methane, which is produced due to anaerobic processes in the benthic layer of streams and lakes, has also been used lately because of the improved analytical techniques (McDonald and Gulliver, 1991). Unfortunately, its use is limited because in many systems its consumption or production might introduce a considerable error.

Conversion of tracer gas to oxygen exchange

The equation for the conversion of the tracer gas mass transfer coefficient to the coefficient for oxygen can be based on (7.8). All system parameter like flow and boundary layer thickness and solute properties are equal and therefore cancel out when the quotient of the mass transfer equation (7.8) for the tracer and for oxygen is taken:

$$\frac{k_{l,tracer}}{k_{l,O_2}} = \left(\frac{\mathbb{D}_{tracer}}{\mathbb{D}_{O_2}}\right)^n \tag{7.31}$$

Equation (7.31) also coincides with the observation of Tsivoglou *et al.* (1965) that the ratio of gas exchange rates of two gases is independent of the degree of turbulence of the water. Tsivoglou *et al.* (1965) further claim that the ratio of the overall mass transfer coefficients is independent of temperature. According to equation (7.31), however, this can be true only when the temperature dependencies of the diffusion coefficients of oxygen and the tracer are equal.

7.5 Sulphur hexafluoride as an alternative sewer reaeration tracer

In this section an alternative to the before mentioned gas exchange method with radioactive krypton will be presented. The inert gas sulphur hexafluoride (SF_6) was selected for this method. The advantages of this gas were mentioned already in section 7.4.4.

7.5.1 Experimental procedure of the sulphur hexafluoride (SF_6) method

The SF_6 was dissolved in water and added into the sewer together with bromide as a tracer for groundwater infiltration, which dilutes the sewage. 15 to 20 samples were taken at two or three locations. More details can be found in section A.5. The sampling was synchronised with an easily detectable tracer (see section 4.2.1). The analysis of SF_6 and bromide were done with a gas chromatograph (see section A.5.3) and an ionchromatograph (see section A.7.6).

7.5.2 Applicability of SF_6 for the sewer system

Pulse or step addition?

Tracers are either added as a pulse or as a step. The concentration of a gas exchange tracer added as a pulse will change due to loss to the atmosphere, absorption and dispersion. The dispersion must be quantified with an additional tracer which increases the error of the overall determination (see page 81). Absorption and storage might occur when the tracer has an affinity for material in the channel or when large deadzones like stagnant water or a biofilm are present.

In this study, the SF_6 was added as a step to circumvent such problems. Therefore, a higher accuracy could be obtained than with a pulse addition. A possible problem is the accumulation of SF_6 in the sewer atmosphere. However, if the maximum gas tracer amount added during an experiment ($\approx$ 20 mg SF_6) would collect in the sewer atmosphere, which is approx. 90% of the total volume, this would have resulted in a concentration of 17 $ng{\cdot}L_{gas}^{-1}$. The Henry coefficient for SF_6 is 132 at 15°C (Cirpka *et al.*, 1993). Hence, the gaseous SF_6 is in equilibrium with 0.1 $ng{\cdot}l_{liquid}^{-1}$, which is negligible compared with the applied tracer concentration of 50 to 100 $ng{\cdot}l_{liquid}^{-1}$. Furthermore, the sewers are normally ventilated to the free atmosphere by applying either slotted manhole covers or ventilation shafts. Sewer aeration is promoted by the drag force that the water exerts on the gas phase (Pescod and Price, 1982). As a result, the assumption of a zero tracer concentration in the gas phase is valid.

Absorption by the sewer biofilm?

The high octane-water partition coefficient of SF_6 (though $<$ 1000 as estimated by Cirpka *et al.*, 1993) bares the danger that the tracer is enriched in the fat-containing deposits on the sewer wall, thereby decreasing the concentration in the water phase. Batch reactor and real sewer control experiments were therefore conducted.

Batch reactor control experiments 0.1 ppm SF_6 was bubbled through a laboratory batch reactor with a magnetic stirrer and demineralised water or wastewater at 17.5°C (1.35 L). At the time indicated in the graphs, 0.13 L clean water, wastewater or a biofilm suspension leading to a five-fold higher biofilm-to-water ratio than in the sewer, was added. Figure 7.8 shows the results. The data were fitted with an exponential function. Only in the case of the biofilm two fits were made neglecting the effect of the dilution in the other two reactors. The exponent of e of the exponential curves fitted through the points is similar for all three cases, indicating that neither wastewater nor suspended biofilm drastically changed the gas exchange. The lowest gas exchange rate was observed with the suspended biofilm but this can be explained as a result of the particles reducing the gas exchange.

Real sewer control experiments A mixture of SF_6 and bromide (Br) has been added in the *Rümlang* sewer (see section 5.3.1) for $1\frac{1}{2}$ hours. Samples have been taken at x = 1964 m. Figure 7.9(a) shows that SF_6 and Br behave similarly. The rise and fall of the curves is equal. A plot of the normalised concentrations(figure 7.9(b)) also confirms this; only a few points are slightly away from the theoretical line.

It can be concluded that the sewer biofilm will not affect the gas exchange rate of the tracer gas SF_6, especially when the tracer is added as a step.

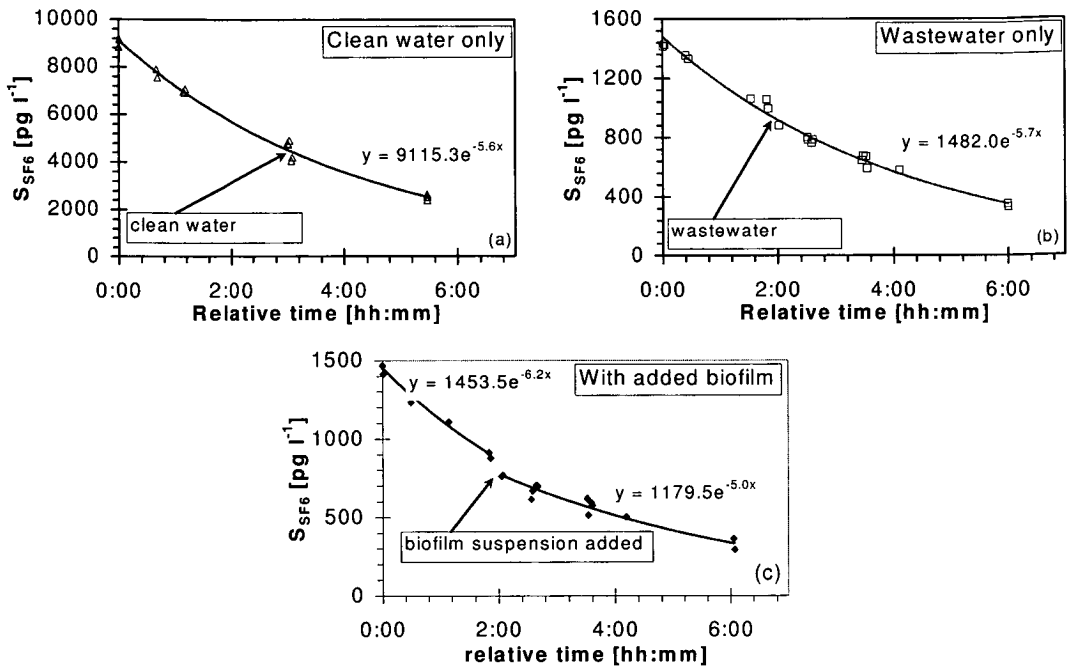

Figure 7.8: The results of the control experiments with clean water (a), wastewater (b) and clean water with added biofilm (c).

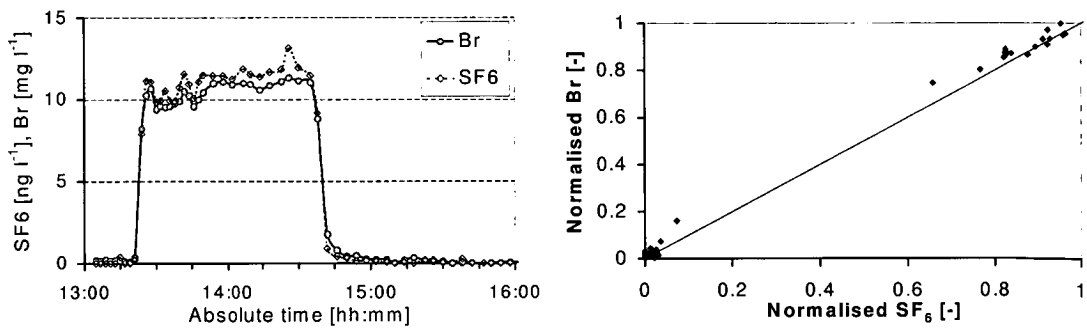

(a) The SF_6 and Br concentrations against the absolute time.

(b) The normalised concentrations of SF_6 and Br plotted against each other. A concentration of 12 $ng \cdot L^{-1}$ of SF_6 and 11 $mg \cdot L^{-1}$ of Br were used for the normalisation.

Figure 7.9: The results of the SF_6 control experiment in the Rümlang sewer.

7.6 Gas exchange calibration experiments

7.6.1 Introduction to the calibration experiments

The direct method (gas tracer) is more reliable than the indirect method (oxygen balance), as was written in section 7.4.4. The exponent n of equation (7.31) that converts the tracer transfer rate to oxygen is not a constant as Dobbins (1964) showed experimentally. It can be approximated by choosing one of three boundary layer models of table 7.1. The influence of the exponent on the conversion increases as the ratio of diffusion constant of oxygen and the tracer gas increases. Figure 7.10 shows the ratios of oxygen and sulphur hexafluoride*. An error of up to 30% can be introduced when the wrong boundary layer model is assumed. After the conversion of the tracer to an oxygen exchange rate, the rate has to be converted to a reference temperature as was described in section 7.3.6.

Tsivoglou *et al.* (1965) already advised to determine the transfer properties of oxygen and the tracer gas. In this section the results from the experiments to determine the relation between the gas exchange of oxygen and SF_6 for flow in smooth open channels and under real conditions are presented.

7.6.2 General experimental procedure for the calibration experiments

The calibration experiments were done at two different sites. They differed mainly in the pipe diameter (0.3 and 2.2 m) and the discharge (2 and 12 $l \cdot s^{-1}$).

The experimental procedure was to a large extent the same at both locations. Sodium sulphite (Na_2SO_3) was mixed with the water to lower the oxygen concentration. The amount was estimated with the theoretical deoxygenation of 7.9 $mg_{Na_2SO_3}$ per mg_{O_2}. However, as already indicated in the ASCE Standard (1993), an excess is needed, especially when re-oxygenation can be expected. Cobalt chloride ($CoCl_2 \cdot 6H_2O$) was added as a catalyst to enhance the reaction rate. The Co concentration was kept well below the maximum concentration of 0.5 $mg_{Co} \cdot L^{-1}$ for the discharge of industrial water into rivers and lakes as allowed under Swiss law (Anonymous, 1998). A saturated SF_6 stock solution was obtained by bubbling pure SF_6 (99.5%, Carbagas, Switzerland) through water during several minutes.

*The diffusion coefficients as a function of temperature are listed in appendix E.

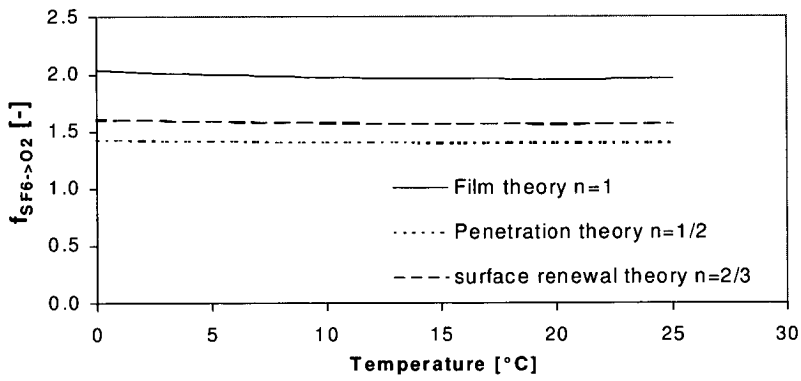

Figure 7.10: The ratio of the diffusion coefficients of SF_6 and O_2 needed for the conversion of the tracer gas exchange measurement to oxygen for the three boundary layer models as a function of temperature.

7.6.3 Small channel: *'Schwamendinger Dorfbach'*

Experimental site

A creek in Schwamendingen, located in the outskirts of Zürich, was restored in 1997 after having been connected to the sewer system for many decades. However, due to the changed surroundings, the water now initially flows through a new clean water pipe with a length of 500 m as shown in figure 7.11.

There were two deadzones. The first was a large filled manhole near the inlet (x = 1 m, volume = 1.8 m^3). The second was a totally filled section (x = 179–189 m, volume = 4.1 m^3). The actual measurement section started at x = 189 m and ended at x = 307 m (section length $L_{sect.}$ = 118 m). The material up to the measurement section was vitrified clay pipe (Ø = 0.250 m), in the section itself it was high density polyethylene (Ø = 0.315 m). No oxygen consumption must be expected because COD of the water was low and it contained no ammonium.

Experimental procedure in the *'Dorfbach'*

A pulse and a step experiment were done in the *Dorfbach.* During the pulse experiments the sodium sulphite, catalyst and tracer were added over a period of 15 s. During the step experiment, the sodium sulphite and catalyst were added with a peristaltic pump at x = 1 m after a float that closed of the pipe inlet to prevent nitrogen gas from entering. This nitrogen was bubbled in the first deadzone to ensure complete mixing and to enhance the removal of oxygen.

The oxygen concentrations before and after the second deadzone were compared to ensure that all Na_2SO_3 had reacted. The residence time up to x = 189 m was approx. ten minutes. The sampling was synchronised with the help of a pulse of dissolved sodium chloride added at x = 23 m. The sampling commenced ten minutes after the conductivity maximum at a site had been detected. The oxygen concentration and conductivity were measured with WTW OXI 340 oxygen meters (see also section A.6) and WTW LF 96 conductivity meters (WTW, Weilheim i. OB, Germany) and stored with an interval of 2 seconds.

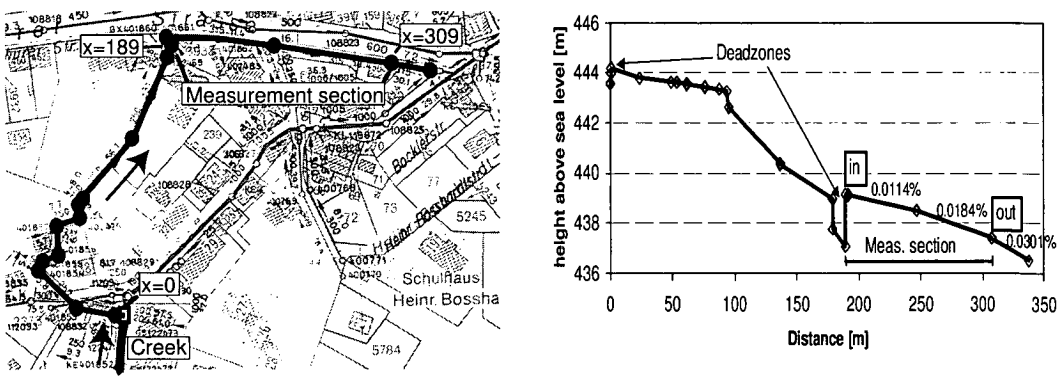

(a) Top view. (b) Side view.

Figure 7.11: A situation sketch of the clean water pipe running underground in the suburb Schwamendingen of Zürich, Switzerland.

Table 7.3: The experimental conditions during the Dorfbach and the Verbindungskanal experiment, and the resulting saturation concentration for oxygen.

Date		*Dorfbach* Pulse 17 Aug. 1999	*Dorfbach* Step 20 Aug. 1999	*Verbindungskanal* 2 July 1999
$T_{Air,\ outside}$	(°C)	17	19	23
T_{water}	(°C)	14.3	14.1	14.2
Q	(L·s^{-1})	2.0	4.0	see figure 7.17(a)
$p_{atmosphere}$	(Pa)	96200	96800	96900
$p_{H_2O,\ 1\ atm}$ †	(Pa)	1625	1604	1614
$X_{H_2O,\ p_0}$ $	(-)	0.0169	0.0166	0.0167
$X_{H_2O,p=p}$	(-)	0.0160	0.0158	0.0159
$S_{O,\ sat,\ p=p}$ ‡	(mg·L^{-1})	9.68	9.78	9.77
$S_{O,\ sat,\ p=p,\ X_{H_2O}}$	(mg·L^{-1})	**9.53**	**9.63**	**9.62**

† Calculated with equation (E.8), ‡ Calculated with equation (E.5), $ $X_{H_2O,\ p_0} = p_{H_2O}/(1\ \text{atm})$.

Results *'Schwamendinger Dorfbach'* experiment

During the *pulse experiment* the measurement sites were at x = 92 m, x = 189 and x = 307 m. The experimental conditions are listed in table 7.3. The results of the in-line measurements are shown in figure 7.12(a) and 7.12(c). The discharge was calculated from the first conductivity peak in figure 7.13, which has already been corrected for the background conductivity. The sodium chloride concentration was obtained by multiplying with a factor of 0.53 as described in the ISO handbook on flow measurement (ISO, 1983). Integrating and comparing with the total amount of sodium chloride added (0.37 kg) gave the discharge. The second peak in figure 7.13 was a result of the deoxygenating agent and its products. The measured SF_6-concentrations are shown in figure 7.12(e). The major difference between the first and the consecutive two peaks is caused by the second deadzone.

The experimental conditions of the *step experiment* are listed in table 7.3. The results of this experiment are shown in figure 7.12(b), figure 7.12(d) and figure 7.12(f). The interference of the Na_2SO_3 conductivity with the NaCl conductivity during the 'step experiment' (see figure 7.14) was removed with the linear relationship between the conductivity and the oxygen concentration decrease before the arrival of the NaCl at 15:43.

7.6.4 Large channel: *'Verbindungskanal'*

Experimental site

The *Verbindungskanal* was a newly constructed circular sewer pipe (Ø = 2.2 m) with a length of 245 m and a constant slope of 0.45% (see figure 7.15). The measurement section started at a construction shaft (L·W·H = 12.9 · 2.8 · 5 m) which was flooded by groundwater after heavy rainfall. The entrance to the pipe section was closed off with a steel plate. A valve had been mounted at the bottom. The water level stood at 3.2 m and was in equilibrium with the groundwater level. The section ended at a large construction shaft. A small brick wall had been built at the exit with a pipe as outlet for leakage water. This pipe was mounted higher than the section's insert by a distance h_{offset} (m) (see also site description in section 7.6.4).

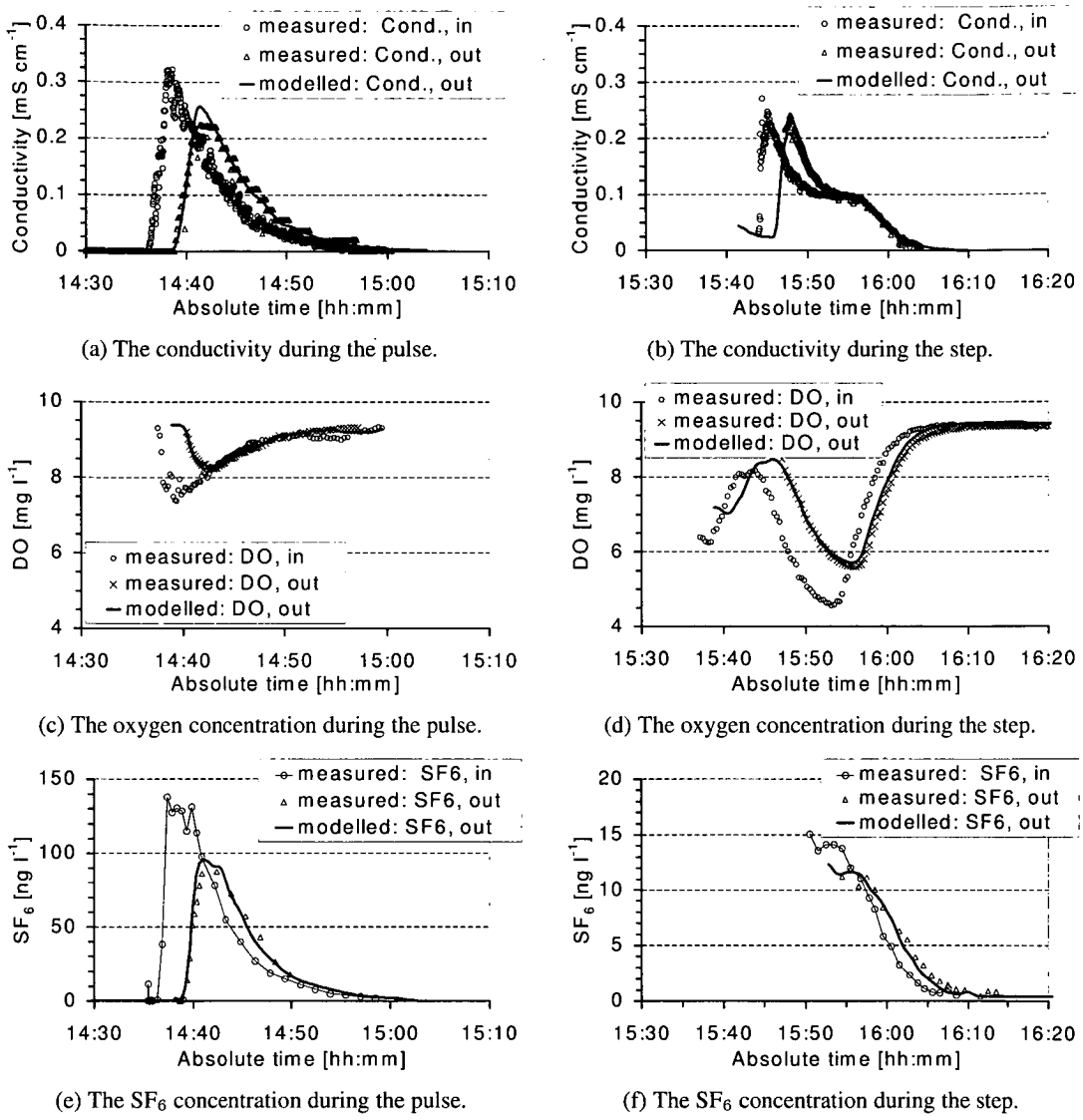

(a) The conductivity during the pulse.

(b) The conductivity during the step.

(c) The oxygen concentration during the pulse.

(d) The oxygen concentration during the step.

(e) The SF_6 concentration during the pulse.

(f) The SF_6 concentration during the step.

Figure 7.12: The measured and modelled results of the Dorfbach-experiments. 'in' = 189 m, 'out' = 307 m.

Experimental procedure in the *'Verbindungskanal'*

In the *Verbindungskanal*, 16 hours prior to the experiment, 7 kg Na_2SO_3 and 0.25 kg $CoCl_2 \cdot 6H_2O$ were dissolved in 100 L of water. This solution and 2 L of SF_6 saturated water were pumped into the flooded shaft. The amount of Na_2SO_3 was theoretically enough to lower the oxygen concentration to 0 $mg \cdot L^{-1}$. But, due to reaeration during the mixing, the final concentration would be larger than zero, ensuring that all sodium sulphite would react. Three pumps (15 $L \cdot s^{-1}$ each) circulated the water from the bottom of one side to the top at the other to ensure complete mixing. The water level in the shaft was measured with a pressure transducer and stored with one-minute intervals.

Measuring and sampling sites were installed at 20 and 220 m from the valve and were equipped with an oxygen (WTW, Weilheim i. OB, Germany, model OXI 340), a conductiv-

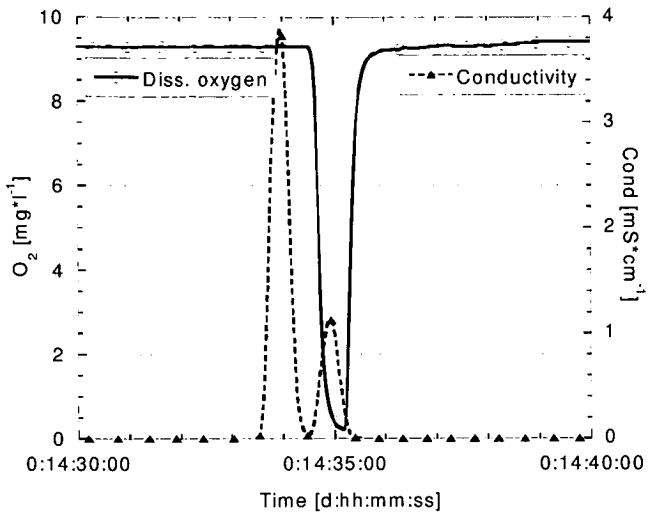

Figure 7.13: The oxygen concentration and conductivity during the pulse addition in the Dorfbach at x = 92 m.

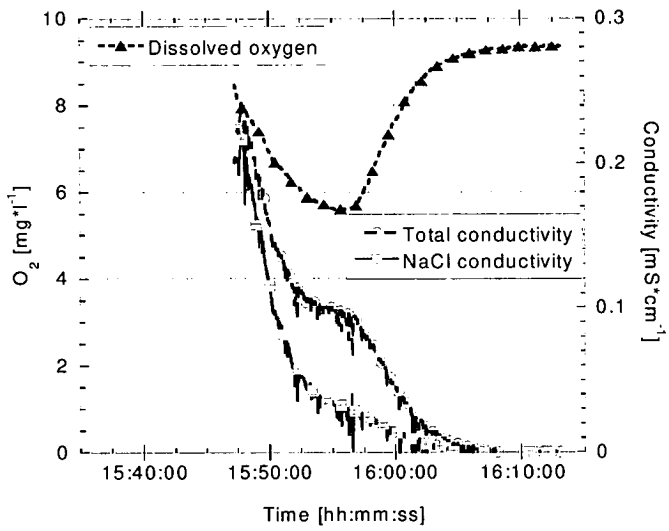

Figure 7.14: The conductivity and the oxygen concentration during the step addition in the Dorfbach.

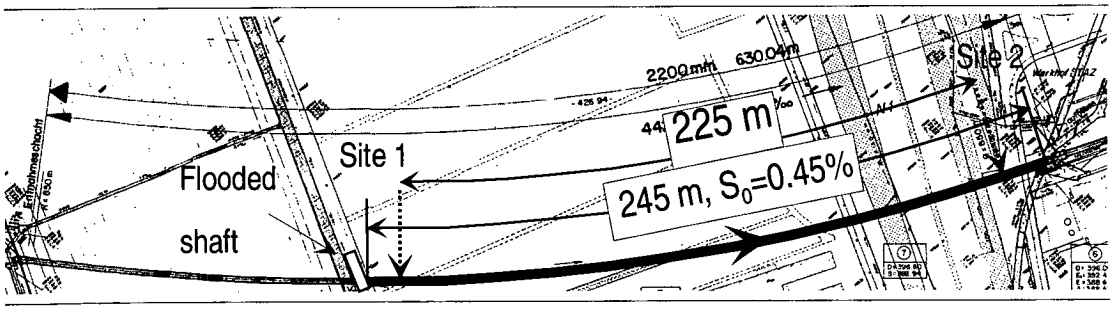

Figure 7.15: A situation sketch of the new connecting sewer in the city of Zürich, Switzerland.

ity (WTW, LF 96) and a flow meter (Sigma 950, American Sigma, Medina, NY, USA). Per site, two persons alternately took 25 mL. samples in 50 mL. glass syringes for the SF_6 analysis. The samples were analysed for SF_6 within 8 hours as described in section A.5.3.

A concentrated sodium chloride solution ($\approx$ 5 L with 250 g·L^{-1} NaCl) to synchronise the sampling was added ten minutes after the valve had been opened. The sampling with intervals of 30 s started at each site 5 minutes after the maximum in the conductivity had been detected and went on for 10 minutes.

Results 'Verbindungskanal' experiment

The steel plate did not completely close off the pipe. This resulted in a base flow of 2.1 L·s^{-1}. The groundwater infiltration in the construction shaft was a function of the water level. It could be described with a function calibrated with the exponential increase of the water level after the experiment had been stopped (see figure 7.16):

$$Q_{gw,inf} = 0.0021 + 0.00547 \cdot \left(1 - e^{0.657\cdot(h-3.22)}\right) \tag{7.32}$$

where $Q_{gw,inf}$ = groundwater infiltration (m^3·s^{-1}) and h = water level in the shaft (m).

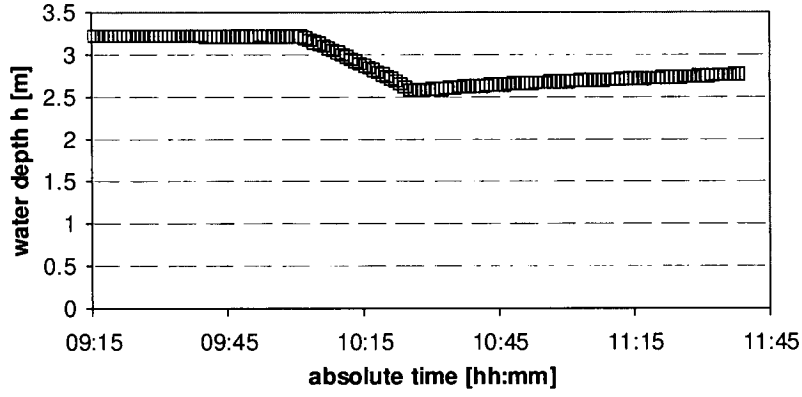

Figure 7.16: The measured water level in the flooded shaft before, during and after the Verbindungskanal calibration experiment as a function of the absolute time.

The infiltration flow equation (7.32) and the water level change Δh (m·s^{-1}) in figure 7.16 were the basis for the discharge calculation:

$$Q = Q_{gw\,inf} + A_{shaft} \cdot \Delta h = 0.00209 + 0.00547 \cdot (1 - e^{0.657\cdot(h-3.22)}) + 12.9 \cdot 2.8 \cdot \Delta h \tag{7.33}$$

where A_{shaft} = area of the shaft in the horizontal plane (m^2). The resulting discharge is displayed in figure 7.17(a). The discharge increased at the end of the experiment because the valve had been opened further. The level measurement at site 2 shows the build up of a backwater at the outlet (see figure 7.17(b)). This had an effect on the residence time and the gas exchange, as will be shown in the next section (7.6.5). The oxygen concentration at the start of the experiment was 2.1 mg·L^{-1}. The oxygen concentration and the SF_6 concentrations are shown in figure 7.18(a) and figure 7.18(b). Other conditions are listed in table 7.3

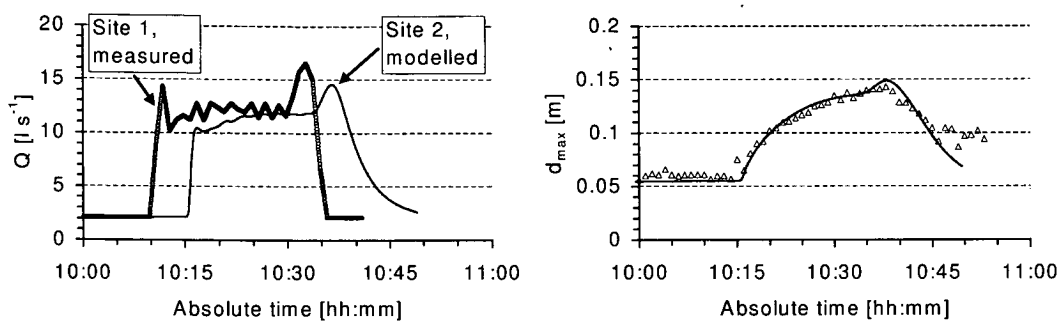

(a) The calculated discharge from the level measurement in the flooded shaft and the flow at the 2nd site.

(b) The measured and modelled water level at the 2nd site.

Figure 7.17: The main hydrodynamic measurement and modelled results of the Verbindungskanal experiment.

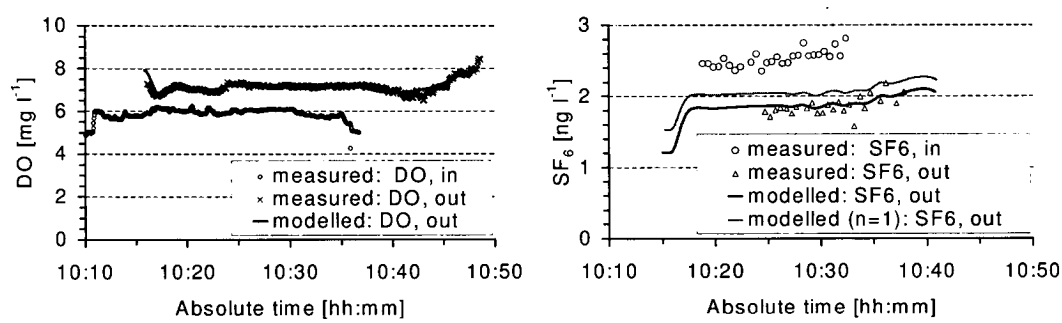

(a) The measured and modelled O_2 concentration.

(b) The measured and modelled SF_6-concentration.

Figure 7.18: The model results of the Verbindungskanal experiment.

7.6.5 Modelling and discussion calibration experiments

Introduction

In this section the results of the numerical modelling will be presented and discussed. Numerical modelling gave more accurate results than an analytical approach because the discharge and the incoming concentrations varied during the before mentioned calibration experiments.

The oxygen flux was calculated with equation (7.30). The equations (7.18) and (7.31) were used for the temperature conversion and the conversion of oxygen to SF_6, respectively. A grid size of 2 m was taken for the *Dorfbach* and 1 m for the *Verbindungskanal*. Details about the hydrodynamic model are given in section 9.4.1.

Modelling of the *'Dorfbach'* experiment

The results of the experiments at x = 189 m as presented in figure 7.12 were used as the model input concentrations for SF_6, O_2 and the conductivity in the *Dorfbach*. The residence time of the conductivity pulse was used to adjust to wall roughness k_s. A value of 1.6 mm was found. The proportionality parameter $a_{reaer.}$ of equation (7.30) was refitted to describe the oxygen

data, which led to an increase from 33 to 53. Because the creek water is much cleaner than wastewater, the $\alpha_{k_l a}$-factor will be closer to unity (see page 71). Figure 7.12(c) and 7.12(d) show the measured and modelled results for oxygen at x = 307 m with the optimised $a_{reaer.}$. Table 7.4 lists the average $k_l a$ and other parameters.

The $k_l a_{O_2}$ can be converted to SF_6 with equation (7.31). The ratio of the diffusion coefficients of oxygen to sulphur hexafluoride was taken according to the data in appendix E. n was identified as 0.45. It was therefore concluded that the penetration theory ($n = 0.5$) prevailed over the film theory ($n = 1$). The modelled results for $n = 0.5$ are shown in figure 7.12(e) and 7.12(f).

Modelling of the *'Verbindungskanal'* experiment

The concentration and conductivity data measured at the 1st site and the discharge as calculated from the level change in the flooded shaft (figure 7.17(a)) were taken as input for the model.

The brick wall at the end of the channel caused a backwater at the 2nd site (see figure 7.17(b)). This affected the residence time and flow velocity, and therefore the gas exchange. It was taken into account by using the diffusive wave approximation of the Saint Venant equations and using the following end level equation at x = 245 m for the model:

$$d_{endlevel} = z_B + h_{offset} + A_{Q\to h} \cdot Q^{B_{Q\to h}} = z_B + 0.17 + 57 \cdot Q^{1.45} \tag{7.34}$$

where $d_{endlevel}$ = water height at the end of the section (m), $A_{Q\to h}$ = coefficient (m) and $B_{Q\to h}$ = coefficient (-). These coefficients where determined with a fit procedure for the water level and conductivity at the 2nd site. During the same procedure, a wall roughness k_s of 1 mm was found based on the residence time of the conductivity peak (graph not shown). This corresponds well with the value of 0.8 mm for new concrete (Hager, 1995). The physical dispersion was smaller than the numerical dispersion and was therefore neglected (see Huisman *et al.*, 2000).

To model the oxygen mass transfer rates of this experiment it was also necessary to change the first parameter of equation (7.30) from 33 to 60. Again, this is expected because clean groundwater was used. This way the measured oxygen concentration could be predicted very well (see figure 7.18(a)). The decrease in SF_6-concentration could then be predicted accurately with an exponent $n = 0.5$ (see figure 7.18(b)). Again, this corresponds with the penetration model.

Table 7.4: The modelled results of the Dorfbach (at x = 290 m) and the Verbindungskanal experiment.

Date		*Dorfbach* Pulse 17 Aug. 1999	*Dorfbach* Step 20 Aug. 1999	*Verbindungskanal* 2 July 1999
$\bar{u}$	($m \cdot s^{-1}$)	0.76	0.90	0.58
d_{mean}	(m)	0.026	0.036	0.05
u^*	($m \cdot s^{-1}$)	0.06	0.07	0.04
Re	(-)	$5.3 \cdot 10^4$	$7.9 \cdot 10^4$	$6.4 \cdot 10^4$
Fr	(-)	1.5	1.5	1.0
$k_l a_{O_2}$	(d^{-1})	181	146	86
$k_l a_{SF_6}$	(d^{-1})	70	55	61

7.7 Results of the SF_6 sewer measurements

Several gas exchange measurements have been done in *Rümlang* and *Bauma**. In the *Rümlang* sewer (see section 5.3.1), the SF_6 was always added as a step (see section 7.5.2).

Sampling commenced approx. one hour later to ensure saturation of the biofilm with SF_6 and Br and was synchronised according to the method described in section 4.2.1.

Figure 7.19 shows the SF_6 and tracer concentration during the gas exchange experiments in the *Rümlang* and *Bauma* sewers. The experiment at 16-Apr-99 was conducted in between rain events to obtain an exchange rate at a high flow rate (see figure 7.20 and 7.21). The conditions during the experiments, the variables necessary for the conversion and the numerical values of the gas transfer rates are listed in the tables 7.5 to 7.7. The $k_l a_{SF_6}$ was converted to $k_l a_{O_2}$ with (7.31) with $n = 0.5$ because the penetration theory is most appropriate is will be discussed later.

7.7.1 Comparison with previously measured data

The most extensive studies are those of Parkhurst and Pomeroy (1972) who performed 73 measurements based on the indirect method and Jensen and Hvitved-Jacobsen (1991) who used the direct tracer method with a pulse addition of the tracers (see section 7.4.4). These data are shown in figure 7.22 together with the data from an artificial channel (Balmér and Tagizadeh-Nasser, 1995) and those acquired during the present study.

The data of Parkhurst and Pomeroy (1972) appear to be reliable although they have considerable scattering. The authors blame this on the small oxygen concentration differences and the limitations of the measurement techniques that were available. They also had problems with the water depth measurement due to the high water velocities. Furthermore, residual oxygen sinks might have influenced their results.

The data of Jensen (1995) have more scatter than those of Parkhurst and Pomeroy. For example, two experiments with a discharge difference of only 25% showed a difference in $k_l a$ of a factor three. According to the author, this might be caused by the influence of the wall rough-

*The *Bauma*-sewer, which was located in a rural area, had a slope of 0.008 $m \cdot m^{-1}$ (0.8%) on average and a diameter of 0.5 m.

Table 7.5: An overview of the hydrodynamic conditions and $k_l a_{SF_6}$ for the experiments in Rümlang and Bauma (23-Aug-98). τ_r = tracer residence time.

Date	Q [L·s-1]	$L_{sect.}$ [m]	τ_r [hh:mm:ss]	$\overline{u}$ [$m \cdot s^{-1}$]	T [°C]	$k_l a_{SF_6}$ [d^{-1}]	$S_{O,\,in}$ [$mg \cdot L^{-1}$]	$S_{O,\,out}$ [$mg \cdot L^{-1}$]
Rümlang								
12-Sep-97	28.1	1964	1:30:56	0.36	20.1	5.4	-	-
14-Oct-97	24.6	1906	1:12:32	0.44	17.4	8.3	4.5	2.1
17-Oct-97	14.5	1847	1:31:21	0.34	16.5	7.1	4.5	3.8
16-Dec-97	13.6	1906	1:25:15	0.37	14.0	8.0	-	-
07-Jan-98	49	1847	0:59:45	0.53	13.1	3.6	-	-
13-Aug-98	18.9	1788	1:13:46	0.40	20.1	6.8	1.3	0.3
21-Aug-98	7.7	1788	1:58:15	0.25	19.4	9.5	2.4	2.1
16-Apr-99	79	1906	0:55:00	0.58	14.0	4.4	2.4	2.1
Bauma								
23-Aug-98	11.7	1246	0:25:30	0.81	17.2	45	2.0	2.1

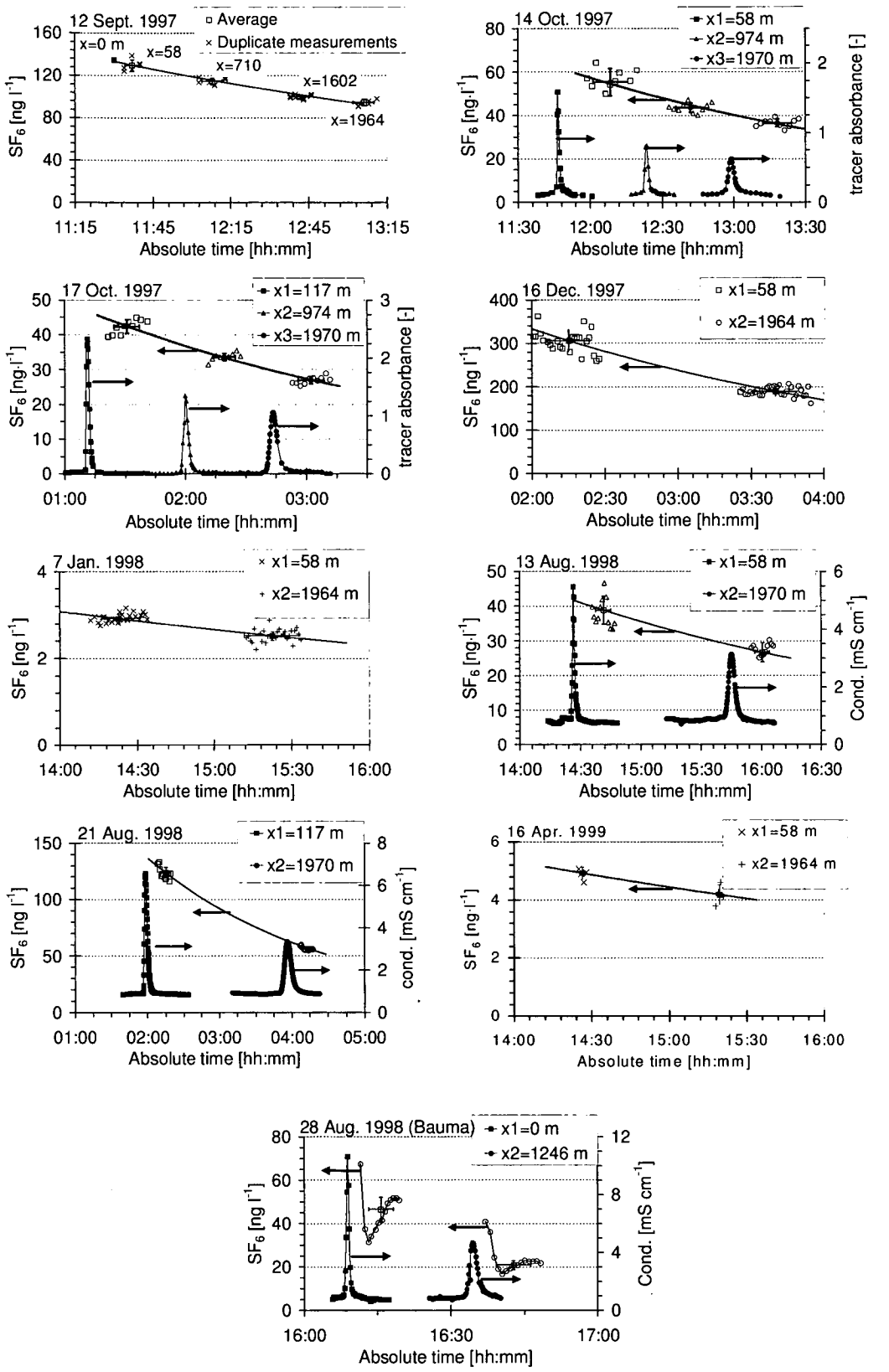

Figure 7.19: The SF_6 and tracer concentration during gas exchange measurements in Rümlang and in Bauma. 'Tracer absorbance' refers to the light absorbance of rhodamine in the samples.

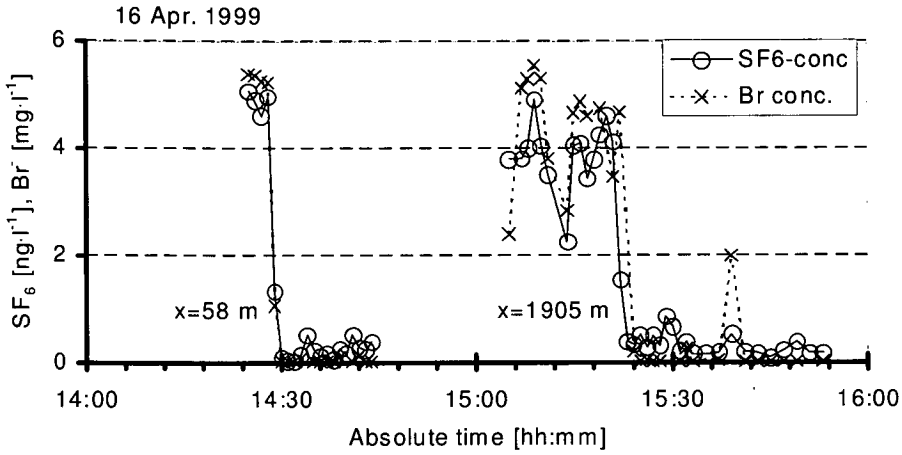

Figure 7.20: The SF_6 compared with the bromide (Br)-concentration on 16 April 1999.

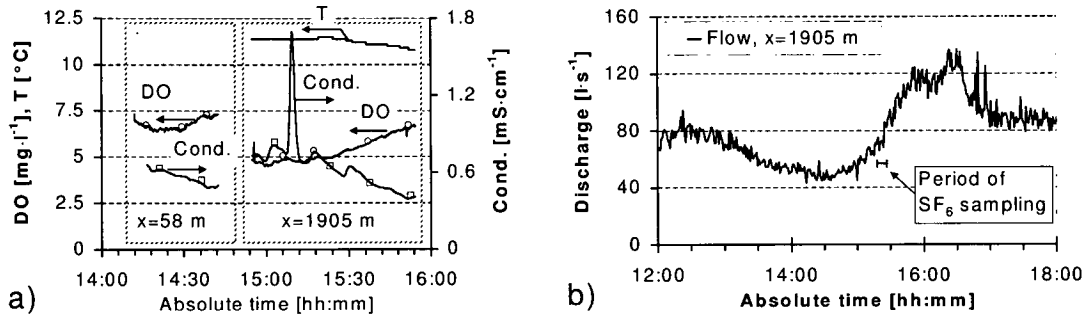

Figure 7.21: The temperature (T), conductivity (Cond.) and oxygen concentration (DO) (figure a), and the discharge and sampling interval (figure b) during the experiment on the 16-Apr-99.

Table 7.6: An overview of the diffusion constant etc. for the experiments in Rümlang and Bauma (23-Aug-98).

eq. nr. → date ↓	$\mathbb{D}_{SF_6}$ equation (E.9) [m²·s⁻¹] ·10⁻⁹	$\mathbb{D}_{O_2}$ equation (E.6) [m²·s⁻¹] ·10⁻⁹	$\frac{\mathbb{D}SF_6}{\mathbb{D}_{O_2}}$ [-]	$k_l a_{O_2,T=T}$ equation (7.31) [d⁻¹] $n = 0.5$	ν equation (E.4) [m²·s⁻¹] ·10⁻⁶	$k_l a_{O_2,T=20°C}$ equation (7.18) [d⁻¹] $n = 0.5$
Rümlang						
12-Sep-97	1.06	2.07	0.511	7.55	1.00	7.6
14-Oct-97	0.983	1.92	0.511	11.5	1.07	11.1
17-Oct-97	0.959	1.88	0.511	9.90	1.10	9.4
16-Dec-97	0.895	1.76	0.510	11.1	1.17	10.3
7-Jan-98	0.872	1.71	0.509	5.09	1.20	4.6
13-Aug-98	1.06	2.07	0.511	9.51	1.00	9.5
21-Aug-98	1.04	2.03	0.511	13.3	1.02	13.2
16-Apr-99	0.895	1.76	0.510	6.22	1.17	5.7
Bauma						
23-Aug-98	0.978	1.91	0.511	63.0	1.08	45

Table 7.7: Overview of the calculated hydrodynamic conditions and the resulting **calculated** $k_l a_{O_2}$ *for the experiments in Rümlang and Bauma (23-Aug-98). There are no results for 16-Apr-99 because the conditions were unsteady during that experiment which required numerical modelling.*

eq. nr.→ Date	A_{cr} (3.20) [m^2]	α (3.19) [-]	w (3.23) [m]	P_w (3.17) [m]	d_{mean} (3.22) [m]	R_h (3.16) [m]	u^* (3.12) [m s^{-1}]	**Fr** (7.28) [-]	$k_l a_{O_2,calc.}$ (7.30) [d^{-1}]
Rümlang									
12-Sep-97	0.078	0.88	0.69	0.79	0.113	0.099	0.030	0.34	8.11
14-Oct-97	0.056	0.78	0.63	0.70	0.080	0.080	0.027	0.49	10.83
17-Oct-97	0.043	0.71	0.58	0.64	0.068	0.068	0.025	0.41	11.48
16-Dec-97	0.036	0.67	0.56	0.60	0.061	0.061	0.023	0.48	12.40
7-Jan-98	0.092	0.93	0.72	0.84	0.110	0.109	0.031	0.51	9.30
13-Aug-98	0.047	0.73	0.60	0.65	0.071	0.071	0.025	0.48	11.43
21-Aug-98	0.031	0.63	0.53	0.56	0.054	0.054	0.022	0.35	12.50
Bauma									
23-Aug-98	0.014	0.49	0.34	0.62	0.023	0.016	0.032	1.69	64

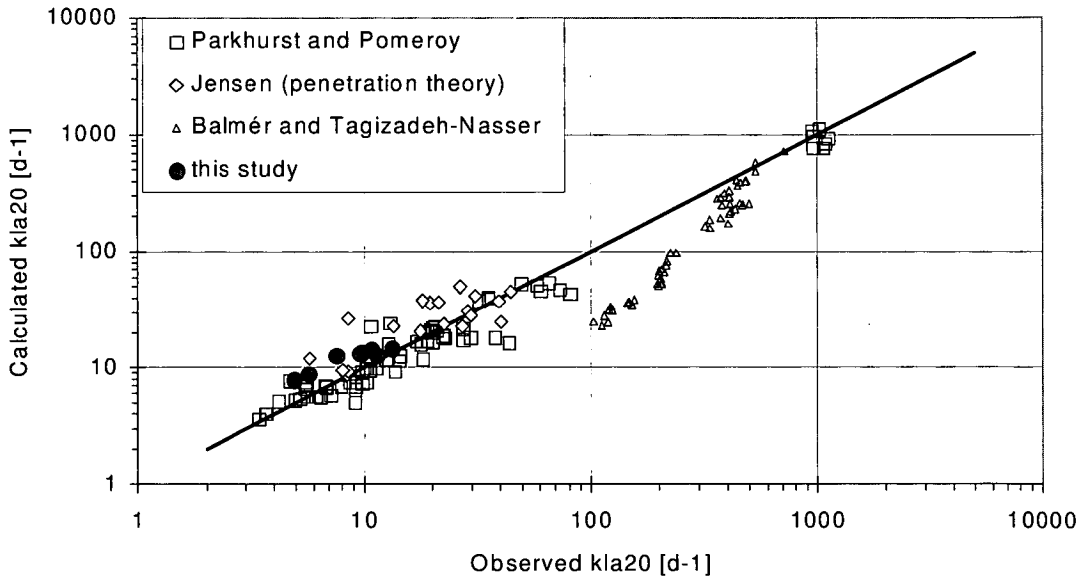

Figure 7.22: The observed $k_l a_{O_2}$ against the value calculated with equation (7.35). The line is the diagonal.

ness, since uncleaned gravity sewers were used. However, some of the experimental procedures are questionable:

- The flow rate, which is important for the calculation of k_l from hydraulic data, has been measured either before or after the experiment (section with a diameter of 0.6 m), or from the measured water depth and the mean residence time (section with a diameter of 0.153 m). In the first case, the strong flow fluctuations in smaller sewers leads to unreliable results. In the second case, apart from the flow fluctuations, an accurate water depth measurement in such small sewers is difficult.
- The tracer was added as pulse. As a result, the actual flow at the moment of tracer addition has a large influence on the experiment.

- The tracer was pumped from the manhole to the surface. However, Schlatter (1991) mentions a loss of up to 6% of a gas tracer (sulphur hexafluoride) through the tube wall, depending on the type of material used.
- No test was made for dilution of the wastewater by undocumented side connections or groundwater infiltration.

Balmér and Tagizadeh-Nasser (1995) performed gas exchange measurements in a concrete pipe (24 m long and 0.225 m diameter) through which tap water was recirculated. The data show little scatter, but appears incompatible with the other results, as was explained on page 77.

The results from the present study are overestimated when $k_l a_{O_2}$ is calculated with the Pomeroy and Parkhurst equation (equation (7.22) in table 7.2). This is mainly caused by the conversion of the SF_6 to the oxygen transfer rate with the penetration theory instead of the film theory. The penetration theory should be used in circular open channel flow as was shown in section 7.6. The data of Jensen who originally used the film theory, are more similar to the data of the present study when his results are converted with the penetration theory (see figure 7.22).

7.7.2 Parameter estimation of the alternative reaeration equation

The dimensionless coefficients of (7.30) were fitted with all available data but those of Balmér and Tagizadeh-Nasser (1995):

$$k_l a_{20,O_2} = \frac{k_{l_{20,O_2}}}{d_{mean}} = 33 \cdot \frac{u^* \cdot (1 + 0.41 \cdot \mathbf{Fr})}{d_{mean}} \tag{7.35}$$

The residual sum of squares (SS_{res}), in comparison with equation (7.22) of Parkhurst and Pomeroy (1972), decreased from $3.1 \cdot 10^{-5}$ to $2.5 \cdot 10^{-5}$.

Figure 7.22 shows the resulting agreement with the measured data. The krypton exchange rate of Jensen has been reconverted to oxygen under the assumption of the penetration theory. Most results are predicted well, including the data of Balmér and Tagizadeh-Nasser at the higher values (although these data were left out during the fitting procedure).

The exponent of **Sc** was set to zero because all measurements had already been converted to a reference temperature of 20°C. It was mentioned in section 7.3.5 that the value of the $\mathbf{Re}^*$ affects its exponent m in equation (7.16). The $\mathbf{Re}^*$ of most data is larger than 2000; thus an exponent close to zero can be expected. Especially the results of Jensen have a low $\mathbf{Re}^*$ because these measurements were done in small channels. Most deviation from the diagonal is found with these data.

Bursts probably control the gas exchange in sewers (see section 7.3.5). Because bursts mostly originate from the wall, the wall properties and sediments will play an important role in their formation. Thus, in real sewers the surface properties of the sewer biofilm are important, apart from larger structures like uneven links between pipe sections and rough sediments.

Rümlang sewer

For the reaeration of the *Rümlang* sewer another fit will be used that has been made exclusive with data from this sewer:

$$k_l a_{20,O_2}[\textit{Rümlang}] = 23.5 \cdot \frac{u^* \cdot (1 + 0.41 \cdot \mathbf{Fr})}{d_{mean}} \tag{7.36}$$

The $k_l a_{20,O_2}[\textit{Rümlang}]$ against the flowrate is shown in figure 7.23.

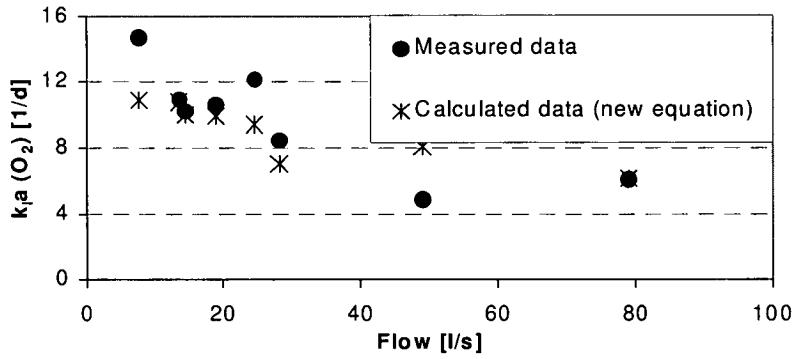

Figure 7.23: The measured and the calculated (with equation (7.36)) $k_l a_{20,O_2}$ against the flowrate for the Rümlang sewer.

7.8 Conclusion gas exchange experiments

The gas exchange and especially the reaeration play an important role in the conversion processes in the sewer system. In this chapter, an introduction to the physical processes of gas transfer, the currently available measurement methods and the empirical reaeration equations was given.

An alternative method based on the non-toxic inert gas SF_6 (sulphur hexafluoride) has been presented that lacks the disadvantages of the current methods. Furthermore, a general temperature conversion function based on the diffusion and kinematic viscosity has been used:

$$\mathrm{f}_T[\mathrm{Sherwood}] = \left(\frac{\mathbb{D}_T}{\mathbb{D}_{T_{ref}}}\right)^n \cdot \left(\frac{\nu_T}{\nu_{T_{ref}}}\right)^{1/2-n} \tag{7.18}$$

A simultaneous measurement of the tracer and oxygen gas exchange in clean water pipes showed that the *penetration theory* should be used to convert the tracer to the oxygen gas exchange. Exponent n in (7.18) is therefore equal to 0.5. Furthermore, it was shown that the commonly used empirical temperature correction factor of Elmore and West (1961) is only an approximation for oxygen at an average turbulence level.

Measurements with the SF_6 method in two sewers were presented. The present results and those of former studies by other researchers were used to determine the coefficients of a new sewer reaeration equation based on the shear velocity:

$$k_l a_{20,O_2} = \frac{k_{l_{20,O_2}}}{d_{mean}} = 33 \cdot \frac{u^* \cdot (1 + 0.41 \cdot \mathbf{Fr})}{d_{mean}} \tag{7.35}$$

This equation predicted the $k_l a_{20,O_2}$ better than equation (7.22) of Parkhurst and Pomeroy (1972).

8 Oxygen balance in the sewer system

8.1 Summary

The oxygen fluxes in the sewer system were quantified with different methods. The validity of these methods was verified with redundant oxygen balances over the study reach. Additional oxygen balances under different hydrodynamic conditions showed that the relative contribution of the biofilm, the wastewater, the reaeration and the in- and outflow with the water can vary considerably. However, all contribute significantly. The COD-conversion in the sewer could be determined from the aerobic activity.

8.2 Introduction

Concentration changes in wastewater fractions like carbohydrates, nitrogen compounds, lipids and fats (Raunkjær, 1993; Almeida, 1999 and this study) indicate conversion processes in the sewer, though they do not provide us with conclusive information about the fate of the products. Balancing of suspended or dissolved components should also involve sedimentation and fixation in the form of biomass (either sessile or suspended). At the present level of knowledge, the most informative variable to collect information about conversion in the sewer system is the turnover of oxygen since this variable plays a central role and can be readily measured.
The aim in this chapter is to identify the main terms of a sewer oxygen balance and to verify the validity of the methods with a redundant balance based on full-scale measurements. Several measurements of the oxygen fluxes under different sewer conditions are presented and the resulting COD-conversion and degradation are estimated.

8.3 The sewer oxygen balance

A verbal steady state oxygen mass balance over a sewer reach with groundwater infiltration but no accumulation can be expressed as:

$$\overbrace{\text{inflow} + \left[\begin{array}{c}\text{surface}\\ \text{reaeration}\end{array}\right] + \left[\begin{array}{c}\text{groundwater}\\ \text{infiltration}\end{array}\right]}^{\text{INLET}} = \overbrace{\text{outflow}}^{\text{OUTLET}} + \overbrace{\left[\begin{array}{c}\text{respiration}\\ \text{by biofilm}\end{array}\right] + \left[\begin{array}{c}\text{respiration}\\ \text{in suspension}\end{array}\right]}^{\text{CONVERSION}} \tag{8.1}$$

The mathematical expression of this mass balance is given in equation (2.4) on page 12. In the following sections the quantification of the respiration and groundwater infiltration terms will be discussed.

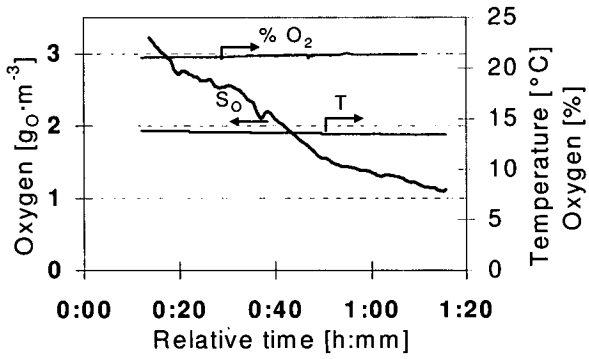

Figure 8.1: The profiles of the wastewater temperature and the oxygen concentrations in the wastewater in ($g \cdot m^{-3}$) and in the sewer atmosphere in %.

8.4 Longitudinal oxygen concentration variations

A float with a dissolved and a gas oxygen meter was constructed to record longitudinal oxygen and temperature profiles in the *Rümlang* sewer. Figure 8.1 shows an example of the results. The changes in the sewer atmosphere are negligible, whereas the DO (dissolved oxygen) concentration decreased exponentially.

8.5 Wastewater respiration

8.5.1 Quantification of the wastewater biomass activity

Wastewater from the sewer has an aerobic activity which can be quantified with a respirometer in a 'batch experiment' as the *oxygen uptake rate* (OUR or r_O). This methodology, which was in its basic form applied by Pomeroy and Parkhurst (1973), is described in section 4.5.1.

The suspended biomass in the wastewater will initially grow. But, as the amount of available substrate declines, the rate decreases as can be seen in figure 8.2. After one day an equilibrium was reached. Such behaviour can be modelled easily with the activated sludge model nr. 3 that was published by Gujer *et al.* (1999) with heterotrophs as the only biomass (results not shown).

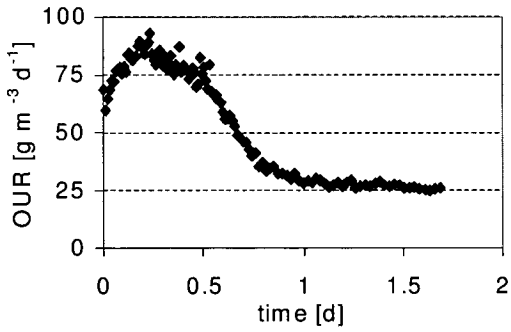

Figure 8.2: A characteristic wastewater respiration curve with wastewater from the Rümlang sewer. (T_{meas} = 20°C)

8.5.2 Continuous wastewater respiration and concentration measurements

It seems likely that the strong diurnal variation of the wastewater composition (see figure 5.5) will also affect the wastewater respiration ($r_{O,w}$). This was tested with the continuous respiration rate method described in section 4.5.2. Batch respiration experiments were used to check the continuous measurement. The respiration of the wastewater indeed had a strong diurnal variation (figure 8.3(a)). Acetate was added to the second stage of the respiration measurement and led to a higher $r_{O,w}$, but only during the night*. The variations of the turbidity that was measured at the input coincided with the $r_{O,w}$ (figure 8.3(b)). Their relation is, however, somewhat disturbed by the turbidity fluctuations that were caused by larger particles like toilet paper fragments in the measurement cell.

Concentrations of dissolved compounds were measured in the inflow. The Dissolved Organic Carbon (DOC) variation coincided with the $r_{O,w}$ (figure 8.3(c)). The nitrate concentration showed a remarkable increase during the night (figure 8.3(d)). However, the most obvious process, nitrification, was not responsible. In contrast, the nitrate originated from the drinking water. *Rümlang* has two drinking water sources: nitrate poor water from the lake of Zürich that is the major source during daytime and nitrate rich water from a local groundwater well that is the primary source during the night. Furthermore, infiltrated groundwater will constitute a larger fraction of the wastewater during the night because the household discharge is much lower. As a result, the nitrate concentration in the wastewater is higher during nighttime. The ammonium

*The residence time in the CSTR's was 30 and 20 minutes for the first and second stage, respectively.

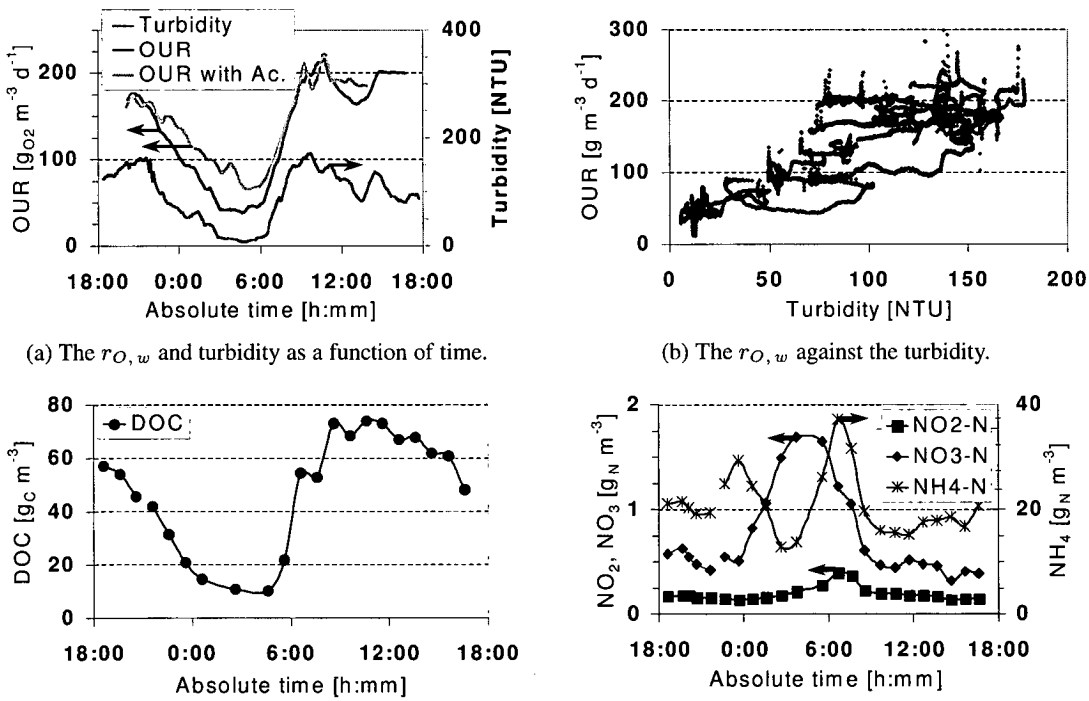

(a) The $r_{O,w}$ and turbidity as a function of time.

(b) The $r_{O,w}$ against the turbidity.

(c) The Dissolved Organic Carbon concentration.

(d) The concentration of N-components.

Figure 8.3: The results of the continuous respiration rate measurement at x = 0 m on 20 to 21 October 1998. ($T_{meas.}$ = 18°C)

concentration peaked —as espected— during the morning hours. The nitrite peak did not coincide with the nitrate peak but with the one from ammonium. This could have been caused either by a delayed response of the biomass on the nitrate, or by nitrate respiration by *E. Coli*; a higher *E. Coli* concentration can be expected to coincide with the ammonium peak.

To investigate whether large changes occurred within sewer section, the experiment was repeated shortly afterwards at the section end (the culvert). The measurements were done in the open air (see figure 8.4). The pumping station was switched off during this time. Unfortunately, the experiment was interrupted by a heavy storm. The results that were obtained up to that moment are shown in figure 8.5.

The experiment was repeated at a later time. The results are shown in figure 8.6. The peak in the $r_{O,w}$ between 2:00 and 3:00 was caused by a small rain event where the discharge increased from 25 to 100 $L{\cdot}s^{-1}$. This clearly led to sediment transport and biofilm erosion. The eroded biofilm not only contained bacteria, but also substrate because the added acetate did not affect the $r_{O,w}$. The continuous rates were checked with two batch experiments. The first at 10:00 confirmed the continuous measurement, but the second at 19:00 gave a rate of 650 $g_{O2}{\cdot}m^{-3}{\cdot}d^{-1}$. Because this was much higher than normal, the experiment was stopped. According to the water colour and the texture of particles, the cause was probably a farmer cleaning a manure storage.

Figure 8.4: Open air experiment for the continuous measurement of the wastewater respiration.

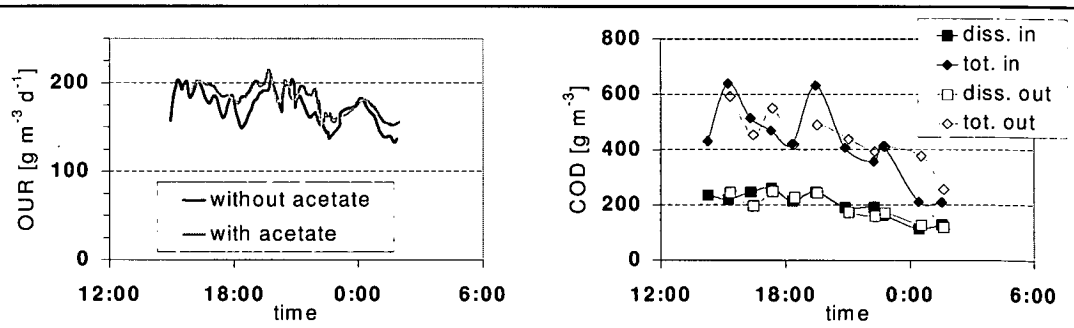

Figure 8.5: The results of the continuous respiration rate measurement at x = 2015 m from 23 to 24 October 1998. 'in' and 'out' refer to the respirometer. ($T_{meas.}$ = 18°C)

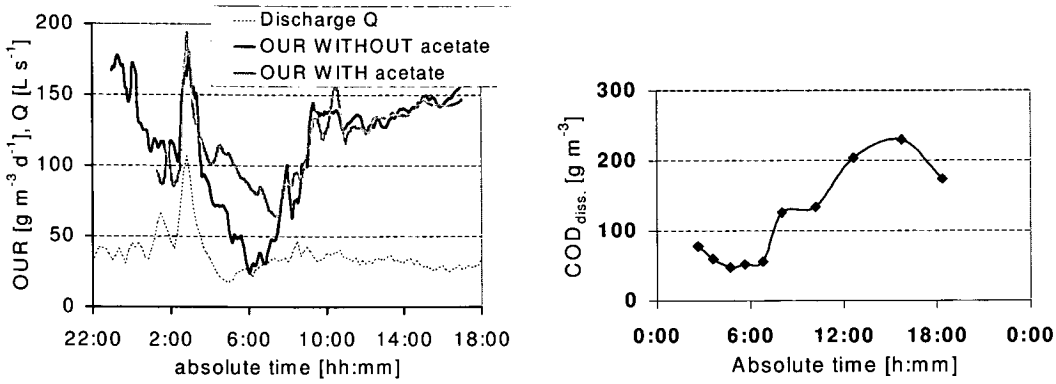

Figure 8.6: The continuous respiration rate with and without added substrate and dissolved COD from 19 to 20 October 1999. (x = 0 m, T_{meas} = 19°C)

8.5.3 Estimate of biomass load

The suspended sewer biomass will originate not only from eroded biofilm, but also from faeces. During the night, however, eroded biofilm will form the major part. A $r_{O,w}$ of 50 $g_O \cdot m^{-3} \cdot d^{-1}$ at 18°C was observed at that time (compare with figure 8.3(a)). A heterotrophs concentration (X_{Het}) of $\approx$ 17 $g_{COD} \cdot m^{-3}$ is required for this activity*. At a flowrate of 0.012 $m^3 \cdot s^{-1}$ this results in a biomass flow of 21 $kg_{COD} \cdot d^{-1}$ which accounts for one third of the particulate COD (X_{part}) during the night. This roughly corresponds with a detachment rate of 5 $g_{COD} \cdot m^{-2} \cdot d^{-1}$ when A_f of $\approx$ 4000 m^2 is assumed. Growth during transport through the sewer will not contribute significantly because the average residence time of the wastewater in the sewer system before the sampling location is only 30 minutes, as was discussed in section 5.4.1 on page 37.

The biomass concentration during daytime is $\approx$ 55 $g_{COD} \cdot m^{-3}$ which corresponds with $\approx$ 20% of X_{part}. At a flowrate of 0.035 $m^3 \cdot s^{-1}$ this results in a load of 170 $kg_{COD} \cdot d^{-1}$. Unfortunately, it is impossible to estimate the amount of biofilm biomass during daytime because the relative contributions of faeces and biofilm biomass are unknown. However, because the flow velocity and wetted surface area are larger it can be expected that the biofilm erosion will have increased to for example 50 $kg_{COD} \cdot d^{-1}$.

Furthermore, these continuous measurements showed that the wastewater biomass is substrate limited during the night. This was related to the ratio of X_{Het} to X_{part}, which is 1:6 during the day but 1:3 during the night.

8.6 Validation of the sewer oxygen balance

The validity of a steady state sewer oxygen balance was checked three times during daytime and once during the night by measuring all terms, which resulted in a redundant balance. The applied methods were described in the sections 4.5 and 4.6.3, and in chapter 7.

*The observed respiration rate is equivalent to a biomass growth rate of 83 $g_{COD} \cdot m^{-3} \cdot d^{-1}$, when a Y_{Het} of 0.63 is assumed. With a μ_{Het}^{max} of 4.8 d^{-1} at T=18°C, which has been determined for the wastewater heterotrophic biomass, the above mentioned biomass concentration is found.

8.6.1 Data collection

Concentration changes

In table 8.1, the flow, concentration and temperature data are listed. The average oxygen concentrations were found by assuming an exponential concentration decrease over the sewer reach.

Suspended biomass

A simple and well-known method was applied. This consisted of measuring the $r_{O,w}$ in wastewater samples from two to four locations. The sampling start was synchronised (see section 4.2.1) and the samples were taken over a 10-minute period. The wastewater at the sampling locations was mixed with an obstacle that was placed in the sewer and produced turbulence. The measured $r_{O,w}$ are listed in table 8.2. The respiration rate during the night is significantly lower than during daytime as was also found with the continuous respiration rate measurements (see section 8.5.2). The daytime rates are lower because the experiments were done in winter when the sewer temperature is lower.

Biofilm respiration activity

Figure 8.7 shows the *in situ* biofilm respiration measurements against the distance along the wall in the radial direction. Each data point consists of two measurements performed closely together in the same manhole. Due to the limited number of data points that could be obtained for a single balance and the assumption that the biofilm activity had not changed strongly between the different experiments it was decided to approximate the biofilm activity with a polynomial equation. These are similar to the rates in section 6.4.

Table 8.1: Flow properties at four sites within the reach. Site 1 and 4 are 'in' and 'out' respectively. See the nomenclature page 177 and further for a description of the variables.

Date	Q	d_{mean}	u^*	Q_{inf}	flow time [s]			
	[L·s^{-1}]	[mm]	[m·s^{-1}]	[L·s^{-1}]	St. 1-2	St. 2-3	St. 3-4	total [min]
27/11/97	24	81	0.026	0$^{\#}$	1650	1710	1710	84.5
02/12/97	32†	83	0.026	0.5	1510	1600	1650	79.3
06/12/97	14	64	0.023	0.21	2040	2130	2130	105
09/12/97	36	89	0.027	0$^{\#}$	1425	1545	1560	75.5

	T	S_O^*	S_O [g_{O_2}·m^{-3}]				$S_{O,avg}$
	[°C]	[g·m^{-3}]	St. 1	St. 2	St. 3	St. 4	[g·m^{-3}]
27/11/97	14.4	9.7	2.9	-	-	1.3	1.7
02/12/97	14.8	9.6	3.28	2.03	1.33	0.95	1.8
06/12/97	13.1	10.0	4.69	3.83	3.37	3.05	3.4
09/12/97	13.9	9.8	3.13	1.93	1.24	0.67	1.6

† Determined by a mass balance of the added mass flux of bromide and the measured wastewater bromide concentration, $^{\#}$ No significant change observed

Table 8.2: The suspended biomass respiration in ($g_{O_2} \cdot m^{-3} \cdot d^{-1}$) measured at the average sewer temperature.

Date	Site 1 x = 117 m	Site 2 x = 816 m	Site 3 x = 1623 m	Site 4 x = 1964 m	average
27/11/97 (day)	37.7 ±3.1	48.2± 0	42.7±1.9	43.2± 1.2	43.4
02/12/97 (day)	40.8	55.4±1.4	-	90.5±2.88	71.7
06/12/97 (night)	15.1	-	12	14.9	14.0
09/12/97 (day)	80.2 ±3.4	88.1±3.1	91.2±7.0	103± 0.7	82.3

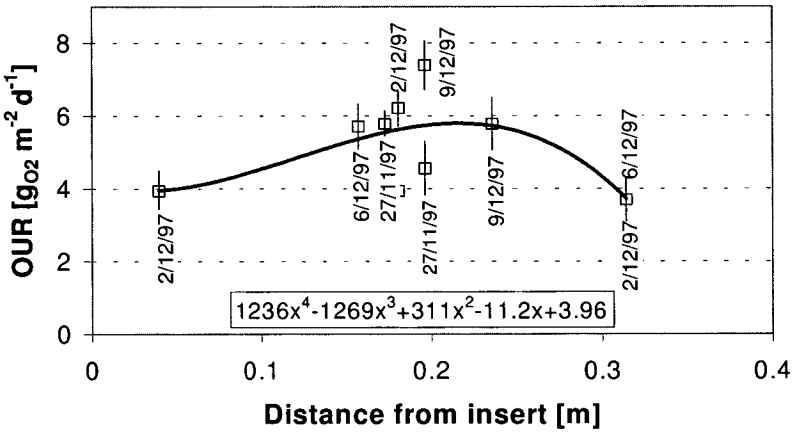

Figure 8.7: in situ biofilm respiration rates in the radial direction along the wall starting from the insert. The measurement date has been listed with every data point. The temperature was 14°C.

Groundwater infiltration

Groundwater infiltration often occurs in older sewers (Jensen and Hvitved-Jacobsen, 1991), either caused by leaking pipe joints, cracks in the pipe wall, or by ill-connected drainage lines. The infiltrated quantity in a sewer section can be found by measuring the dilution of a conservative tracer like bromide over a sewer section. Exfiltration of wastewater is more difficult to quantify, but it will have a smaller effect on the oxygen balance.

The oxygen concentration of the groundwater was measured in samples collected from a crack in a manhole where groundwater infiltrated. The infiltration flow was calculated from the measured decrease in the bromide concentration. It could be visually observed that the groundwater infiltration depended strongly on the rainfall during the previous days.

The groundwater infiltration could be identified during the night and was very small relative to the main flow (see table 8.1). An infiltrate oxygen concentration of 7 $g_{O_2} \cdot m^{-3}$ was found.

8.6.2 Resulting oxygen balances

Based on the data presented above, four redundant oxygen balances could be set up according to equation (2.4), which are depicted in figure 8.8. The surface reaeration rates were computed

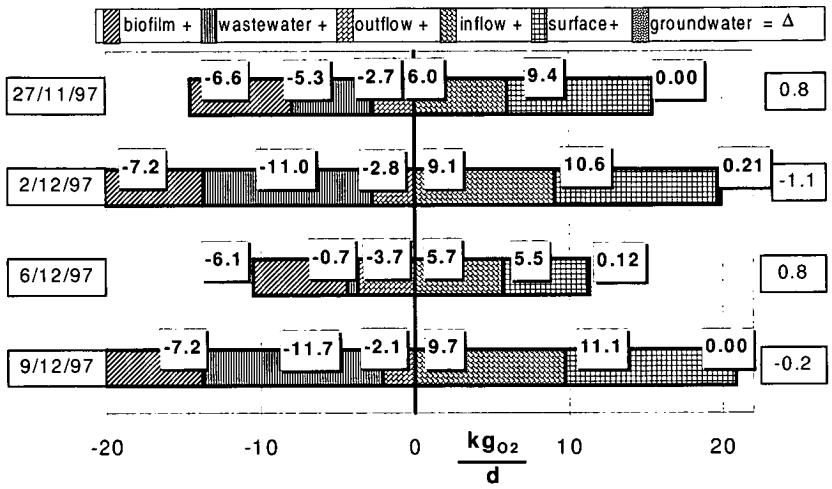

Figure 8.8: An overview of the oxygen mass balances as obtained after applying all data to equation (2.4). *Δ = the difference between all 'out' (left side) and all 'in' (right side) terms. (in $kg_{O2} \cdot d^{-1}$)*

with equation (7.36). The biofilm respiration rates were calculated by integrating the equation given in figure 8.7.

All terms of the oxygen balance appear to be significant, except for the groundwater infiltration. During daytime the respiration rates of biofilm and wastewater were similar. During the night, the biofilm oxygen uptake decreased slightly, as the wetted biofilm area became smaller*. The wastewater respiration rate, however, decreased strongly. This was partly caused by the smaller discharge during the night, but also by reduced biofilm erosion, by a reduced amount of faeces, and by a lack of substrate (see section 8.5.2). The relative contribution of the surface reaeration indicates that this parameter should be determined accurately with a suitable method like the sulphur hexafluoride method used in this study (see chapter 7).

8.6.3 Monte Carlo Simulation

An error estimation of the oxygen balance is not straightforward because the variables and parameters are not independent. Instead of calculating the error propagation, the result of the balance with a set of realistic input variables can be determined. This is basically a Monte Carlo simulation.

Monte Carlo simulation is a statistical technique by which a quantity is calculated repeatedly, using randomly selected input parameters and variables for each calculation. Not the exact value of an input variable is given but a value is randomly taken from the error distribution around a variable. This is done for all input parameters and variables and the balance is calculated. The result will be somewhere around the exact answer. When this process is repeated numerous times it approximates the full range of possible outcomes from which the standard deviation can be deduced.

In other words: the overall standard deviation is estimated by calculating a mass balance j times with randomised input variables $\widehat{M_i}$ according to

$$\widehat{M_{i,j}} = M_i + Z_{i,j} \cdot \widehat{\sigma_{M_i}} \cdot M_i \tag{8.2}$$

*The biofilm activity remains high for several hours even without any substrate in the wastewater, probably due to the presence of storage material and particulate substrate

where M_i = variable (e.g. discharge Q) and $\widehat{\sigma_{M_i}}$ = estimated (relative) standard deviation for the variable M_i. The vector of random numbers Z_j has been determined according to

$$Z_j \sim N(0,1) \tag{8.3}$$

$\widehat{M_{i,j}}$ therefore has a standard normal distribution. The estimated relative standard deviations $\widehat{\sigma_{M_i}}$ of the variables M_i are listed in table 8.3.

Each of the four steady state mass balances was calculated 2000 times. A $\widehat{\sigma}$ was calculated for each balance from the results. These are listed in table 8.4 together with the sum of the mass balance, $\sum r_O$, which should be zero for a redundant balance. The absolute value of $\sum r_O$ is always smaller than $\widehat{\sigma_{OB}}$ which shows that these redundant balances are valid and that all major terms of the oxygen balance have been identified.

8.7 Additional oxygen balances

As was shown in section 8.6, all significant terms are included in the mass balance (equation (2.1)). Furthermore, they can be quantified properly with the methods applied in this study.

More oxygen balances were measured over a two-week period with rainy weather. This led to an ever-increasing discharge that resulted in interesting shifts in the relative importance of the different terms, as can be seen in table 8.5. The biofilm respiration was an unknown term here. Under normal dry weather flow, all terms (except groundwater infiltration that has been neglected here) contribute approx. equally to the oxygen mass balance. The main results from the oxygen balance measurement from two additional measurement campaigns are listed in table 8.5. A '✓' indicates that the resulting $r_{O,f}$ is valid with regard to $\widehat{\sigma}$. The remaining data can be found in appendix C.1.

Table 8.3: The estimated relative standard deviations of the measured input variables for the oxygen balance. The assumption is that σ is constant over the whole range of M_i. (p = atmospheric pressure (Pa), S_0 = channel slope (m·m^{-1}). The other nomenclature can be found from page 177 and further.

Variable	$\widehat{\sigma}$	Variable	$\widehat{\sigma}$	Variable	$\widehat{\sigma}$
k_la	10%	Q	10%	$S_{O,gw.\ inf.}$	20%
$L_{sect.}$	0.1%	$Q_{gw.\ inf.}$	10%	T	5.0%
$r_{O,f}$	17%	S_0	0.5%	τ_r	2.0%
$r_{O,w}$	7.0%	$S_{O,in}$	2.0%		
p	1.0%	$S_{O,out}$	2.0%		

Table 8.4: A comparison between the sum of the redundant oxygen balance ($\sum F_O$) and its estimated absolute standard deviation ($\widehat{\sigma_{OB}}$ (kg·d^{-1})).

Date	$\sum F_O$	$\widehat{\sigma_{OB}}$
27/11/97 11:10	0.8	1.5
2/12/97 9:30	-1.1	1.7
6/12/97 2:20	0.8	1.2
9/12/97 13:00	-0.2	1.8

Table 8.5: An overview of the hydrodynamic and respiration rate data of the additional oxygen balances. More details can be found in appendix C.1. $L_{sect.}$ = 1906 m, $F_{COD,tot.}$ and $F_{COD,diss.}$ = total and dissolved COD-load at the section inlet ($kg_{COD} \cdot d^{-1}$)

	Unit	7/6	9/6	10/6	11/6	12/6	13/6	14/6	22/10	28/10	28/10	28/10	29/10	29/10	01/11
t_{start}	h:mm	10:50	10:00	10:00	10:00	10:40	10:20	10:00	15:20	17:09	19:39	22:08	0:40	11:38	9:18
τ	h:mm	1:09	1:09	1:12	1:08	1:09	0:58	0:51	1:20	1:23	1:19	1:24	1:39	1:22	1:08
Q	$m^3 \cdot s^{-1}$	0.054	0.055	0.043	0.055	0.061	0.095	0.120	0.03	0.024	0.032	0.023	0.011	0.031	0.032
$\overline{S_O}$	$g_{O_2} \cdot m^{-3}$	3.2	4.2	5.2	6.2	7.2	8.2	9.2	0.9	1.65	1.05	1.44	1.85	1.28	2.20
$\overline{T}$	°C	16.3	16.1	16.2	16.2	16.7	16	15.7	17.1	16.7	17.5	17.4	16.5	16.9	16.7
$F_{O_2,in}$	$kg_{O_2} \cdot d^{-1}$	21.2	26.5	24.3	36.0	45.0	78.3	110	3.7	5.0	5.3	4.4	2.1	5.5	9.2
$F_{O_2,surf}$	$kg_{O_2} \cdot d^{-1}$	10.6	9.0	6.5	5.5	3.8	2.6	0.6	11.2	9.3	11.4	9.4	6.4	11.2	9.4
$F_{O_2,out}$	$kg_{O_2} \cdot d^{-1}$	8.8	13.8	14.4	23.3	31.0	56.4	82.2	1.01	1.69	0.45	1.27	1.46	1.32	2.98
$r_{O,WW}$	$kg_{O_2} \cdot d^{-1}$	11.0	11.1	9.1	11.1	12.8	15.9	17.5	13.8	11.5	22.9	9.5	2.4	14.6	8.7
$r_{O,f}^{bal}$	$kg_{O_2} \cdot d^{-1}$	11.9	10.5	7.3	7.1	5.1	8.5	10.9	0.06	2.1	-6.3	3.9	5.4	1.5	8.9
$r''^{bal}_{O,f}$	$g_{O_2} \cdot m^{-2} \cdot d^{-1}$	6.8	5.9	4.5	4.0	2.8	4.1	5.1	0.04	1.5	-4.2	2.8	4.8	1.0	6.2
$\widehat{\sigma_{OB}}$ †	$kg_{O_2} \cdot d^{-1}$	1.6	1.6	1.4	1.6	1.9	2.1	2.6	1.7	1.3	2.4	1.2	0.7	1.7	1.2
OK?♯		✓	✓	✓	✓	✓	✓	✓	✓	✓		✓	✓	✓	✓
$\sum r_O$ ♠	$kg_{O_2} \cdot d^{-1}$	23	22	20	22	27	24	26	14	13	–	13	7	16	16
$F_{COD,tot}$	$kg_{COD} \cdot d^{-1}$	1791	1381	1377	1679	2152	1889	1746	–	–	–	–	–	–	
$F_{COD,diss.}$	$kg_{COD} \cdot d^{-1}$	659	614	590	452	600	560	734	–	–	–	–	–	–	

† the input variables of each balance have been randomised 2000 times according to their individual standard deviation. $\widehat{\sigma_{OB}}$ is calculated from the 2000 resulting $r_{O,f}$ (see text),

♯ A checkmark indicates that the balance is possible ($r_f^{bal.} > 0$)

♠ The sum of $r_{O,w}$ and $r_{O,f}$.

A graphical comparison between the balances (figure 8.9) clearly shows the effect of the increased flow rate during the first campaign. Most remarkable is that the wastewater contribution decreases but that this is compensated by an increased biofilm uptake. During the second campaign the weather was quiet which led to a low discharge and low oxygen concentrations with the result that the biofilm contributed less to the overall balance.

The biofilm activity determined from the balance, $r_{O,f}^{bal}$, for June and October seem remarkably variable at first sight. However, when the data are plotted against the DO (see figure 8.10(a)), there appears to be a clear dependency as would be expected for a biofilm system, except for an offset in the DO*. This contradicts a conclusion of Nielsen *et al.* (1992) who claimed that the wastewater biofilm activity is practically independent of the oxygen concentration due to the filamentous structure. As can be expected, the OUR increases as the wetted perimeter (P_w) increases (see figure 8.10(b)).

The balance of 28/10/99 19:39 is an outlier because the measured $r_{O,w}$ was much larger than normal, probably due to the dumping of manure. In the sewer itself however, the biomass will have been DO-limited because the DO was practically zero at the outlet. Furthermore, the estimation of the biofilm activity could be more accurate when the exponential DO decrease (see e.g. figure 8.1) is taken into account. Such phenomena that have more influence at a lower DO-concentration are difficult to describe with these simple balances and require numerical modelling as will be presented in chapter 9.

8.7.1 Aerobic COD degradation and conversion

The sums of $r_{O,w}$ and $r_{O,f}$ ($\sum r_O$), which equal the actual degradation in the main sewer, are compared in table 8.5 and 8.6 with the COD-loads (F_{COD}) during the experiments (not accumulated over the whole day!). The aerobic biological processes clearly influence the wastewater composition. The effect will probably be strongly enhanced by the available wetted surface area

*The influence of the reaeration on the oxygen balance is thought to be causing the offset because the reaeration was calculated based on the average oxygen concentration.

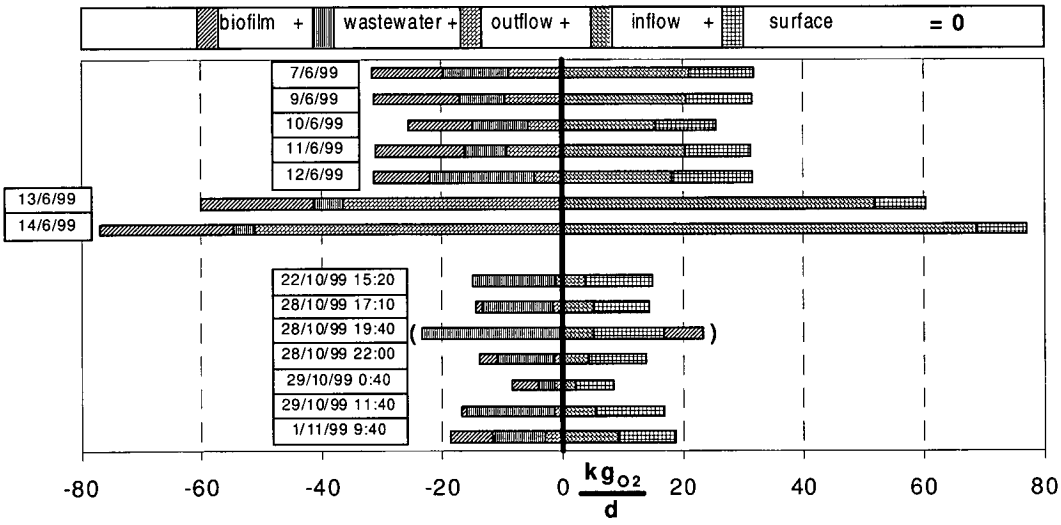

Figure 8.9: The oxygen mass fluxes during two measurement campaigns. See also table 8.5 and appendix C.1.

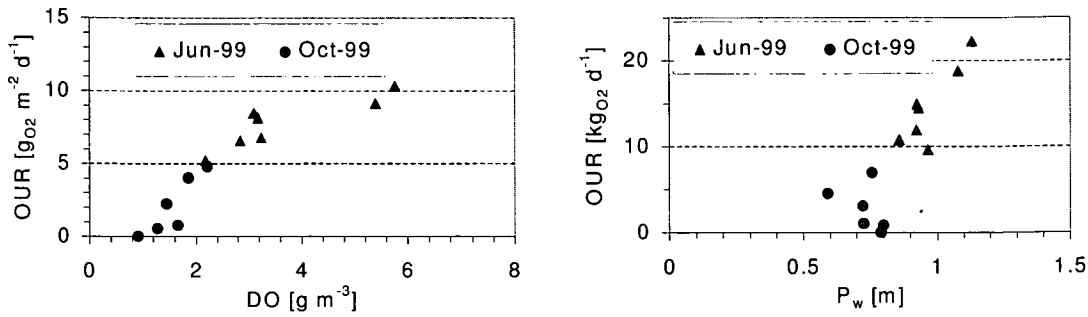

(a) The effect of the dissolved oxygen concentration (DO).

(b) The effect of the wetted parimeter (P_w).

Figure 8.10: Relationships between two variables and the biofilm oxygen uptake rate OUR_f.

within the town connected to the main sewer, which was estimated at 8000 m^2 during daytime. Assuming a biofilm activity of 5 $g_{O2}\cdot m^{-2}\cdot d^{-1}$ (see figure 8.7), this would result in an extra degradation of 40 $kg_{COD}\cdot d^{-1}$. In the main sewer 20 $kg_{COD}\cdot d^{-1}$ is degraded on average (see table 8.5) giving a total of 60 $kg_{COD}\cdot d^{-1}$ during daytime for the town plus 2 km main sewer. The actual aerobic biological turnover is even a factor three higher, based on a yield of 0.67, and approximates 180 $kg_{COD}\cdot d^{-1}$. This is $\approx$ 30% of the dissolved COD-flow during the day.

Denitrification will also occur. During several occasions a decrease of 0.5 $g_N\cdot m^{-3}$ was observed (e.g. figure 5.6). An extra $\approx$ 25% COD-degradation and conversion can therefore be expected.

8.8 Conclusions

The processes involved in the oxygen fluxes are among the most important in the sewer system. These were investigated by setting up an oxygen balance over a sewer section that was successfully validated with redundant balances. This showed that all major terms —wastewater and biofilm respiration, surface reaeration, in- and outflow and groundwater infiltration— could be identified and quantified. The sewer biofilm as well as the wastewater respiration contributed substantially to the COD-conversion of wastewater. Furthermore, the surface reaeration plays an important role (see chapter 7).

Table 8.6: The measured degradation rates ($r_{O,f}^{meas}$ and $r_{O,w}^{meas}$) and their sum ($\sum r_O^{meas}$) compared with the total and dissolved measured COD-fluxes at the time of sampling ($\phi_{COD,tot}^{meas}$ and $\phi_{COD,diss}^{meas}$, respectively). (in $kg\cdot d^{-1}$).

Date and time		$r_{O,w}^{meas}$	$r_{O,f}^{meas}$	$\sum r_O^{meas}$	$\phi_{COD,tot}^{meas}$	$\phi_{COD,diss}^{meas}$
27/11/97	11:10	5.3	6.6	12	1300	370
2/12/97	9:30	11.0	7.2	18	1550	490
6/12/97	2:20	0.7	6.1	7	250	91
9/12/97	13:00	11.7	7.2	19	1730	470

Continuous respiration measurements showed that the wastewater respiration has a clear diurnal variation. A biomass concentration of 17 $g_{COD} \cdot m^{-3}$ (35% of the particulate COD) was observed during the night when the biomass was substrate limited, but this increased to 55 $g_{COD} \cdot m^{-3}$ (20% of the particulate COD) during the day. It was deduced that the biofilm biomss erosion lies in the range of 5 $g_{COD} \cdot m^{-2} \cdot d^{-1}$. Finally, the biomass released during a small nightly rain event was, at least initially, not substrate limited.

The oxygen balances showed that the wastewater respiration is the most variable. During daytime it could be more than 12-times larger than during the night. Furthermore, the relative contribution of the in- and outgoing wastewater varied strongly as the discharge and oxygen concentrations fluctuated.

The results indicated that 3% of the dissolved COD-load from a town with 5000 PE was degraded in the sewer study reach with a length of 2 km. When the results were extrapolated to the whole sewer system of this town an aerobic turnover of up to 30% of the dissolved COD-load can be expected.

9 Hydrodynamic and biological sewer model

9.1 Summary

A deterministic sewer model based on the Activated Sludge Model no. 3 (ASM 3, Gujer *et al.* (1999)*) is presented. The original ASM 3 is used for the wastewater biomass. This is extended with the penetration depth approach for biofilm mass transfer. This approach allows for fast calculation, requires only a limited number of parameters and gives good results. The most important sewer specific parameters are the attachment rate of particles and the biofilm erosion. These were calibrated with the help of full-scale measurements. The other model parameters were calibrated with the help of laboratory experiments. Furthermore, an approach to model the sulphur cycle is presented. The resulting model described the data well.

9.2 Introduction

A deterministic model is a useful way to bundle knowledge about a system in a compact and transferable form. The first attempt at modelling the biomass growth and BOD degradation in a sewer with oxygen or air injection was made by Koch and Zandi (1973). They calculated that it would take 40 km to obtain 30% reduction in biological oxygen demand (BOD). However, they took only suspended biomass into account.

Conversions in the sewer system are optional in for example the water quality module MOUSETRAP of the sewer system simulation program MOUSE. The approach is based on the BOD and is very coarse (Garsdal *et al.*, 1995). A similar but more refined approach was presented by Almeida (1999). Bjerre *et al.* (1998) adapted ASM 1 for use in a strongly polluted river (open sewer) but neglected the influence of biofilm biomass which accounted for approx. 20%. Several studies were presented by Tanaka and Hvitved-Jacobsen (1998), Vollertsen *et al.* (1999a, 1999b) and Vollertsen and Hvitved-Jacobsen (1999). These were all based on transferring ASM 1 to the sewer system. Only very limited attention was paid to the peculiarities of the sewer biofilm. Finally, up to three different fractions of X_S were required to explain the respiration curves which is hardly suited for practical use.

The sewer as a river?

Dozens of river conversion models were developed in the past†. The major differences in comparison with the sewer system are:

*An updated version has been published: Gujer *et al.* (2000).

†Many are however based on QUAL2E of the US-EPA (see Jørgensen *et al.* (1996) and http://dino.wiz.uni-kassel.de/ecobas.html) for an overview of river models.

- The suspended biomass concentration is much higher than in rivers.
- The concentration of COD and other substances is much higher; the processes will not be limited by the concentration of trace substances.
- Nitrification will barely take place because nitrifiers will be overgrown by heterotrophic biomass.
- There is often a clear diurnal variation in the hydrograph and the pollutograph.
- There is no primary production from algae or macrophytes because light is lacking.
- The system geometry is on the one hand much more defined because the channel diameters and length are known, but on the other the system is much more branched.

The sewer as a wastewater treatment plant?

The activated sludge models 1 to 3 (Henze, 1987; Henze *et al.*, 1995; Gujer *et al.*, 1999) are the standard in WWTP-modelling. These models cannot be used directly for sewer modelling because:

- The hydrodynamic conditions are totally different.
- The conversion occurs in suspension as well as in a thick biofilm.
- Anaerobic processes can play a significant role.
- The wastewater is not settled.
- There is a stronger impact of rain events on the system.
- Reaeration through the water surface and the oxygen inflow with the water are the main oxygen sources.

The goals for the sewer model

In this chapter a model will be presented that can be described as a WWTP model with biofilm properties in a river situation. It should fulfill the following goals:

- Simple hydrodynamic model, but accurate with regard to the residence time.
- Aerobic and anoxic conversions.
- Conversions in the wastewater and in the sewer biofilm.
- Erosion and attachment of particles.
- Biofilm mass transfer implemented.
- Gas exchange with the sewer atmosphere.
- Fast calculation so that it can be implemented in an overall urban hydrology model.
- Compatible in state variables, processes and model structure with ASM no. 3.
- Extendable for anaerobic processes.

9.3 Sewer model structure

The sewer system can be divided in three compartments when sediments are regarded as a thick biofilm. A reactor model with plug flow has been chosen for the simulations (figure 9.1). The biofilm mass transfer will be modelled with penetration depth for the important components; models involving one or more dimensional biofilm modelling would introduce many unknown parameters and would increase the calculation time drastically.

The different parts of the resulting model will be discussed in the following sections.

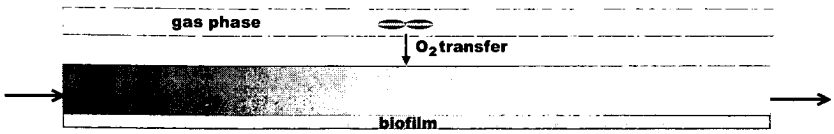

Figure 9.1: The sewer system modelled as a tubular reactor.

9.4 Physical model

9.4.1 Hydrodynamic model and gas exchange

The water phase hydrodynamics can be simulated with the diffusive wave approximation of the Saint Venant equations (see section 3.2.1). This one-dimensional model is sufficient. However, calibration is required because of the model yields the wetted biofilm area and the wastewater residence time which are very important variables. Tracer experiments have been conducted for this which resulted in an average wall roughness (k_s) for the *Rümlang* sewer section of 5 mm (see figure 5.3). The reaeration is added as a gas transfer process based on equation (7.36).

9.5 Biological Model

The biological conversion rates will be discussed for wastewater biomass, suspended biofilm and intact biofilm. Experiments with suspended biofilm have been conducted to obtain kinetic and stoichiometric parameters without mass transfer limitations.

The biofilm and the wastewater biomass are assumed to have the same properties. The major difference might be the occurrence of enterobateria* in the wastewater that will probably not grow well in the sewer biofilm because their optimal growth temperature lies around 37°C.

9.5.1 Wastewater biomass

The biological model for wastewater biomass is equal to the ASM 3 and will therefore not be further discussed. The processes (1 to 12) are however listed in table 9.1 to present the complete model. The major difference is that the Monod terms for ammonium and alkalinity are left out to speed up the execution of the model. These compounds will normally not be limiting in the sewer.

9.5.2 Biofilm biomass

In the biofilm of an aerobic sewer, the redox potential can range from +200 to -500 mV. This creates niches for many types of microorganisms. Apart from the aerobic and anoxic conversions as defined in ASM 3, anaerobic processes like sulphur reduction, fermentation and melanogenesis can also take place.

The modelling of the anaerobic processes is much more of an open field than the aerobic and anoxic processes. These conversions and the resulting model structure will therefore be discussed in the following sections.

*The nitrate respiration of *E. Coli* might cause the increase of the nitrite concentration over the sewer section (see page 42).

Table 9.1: The kinetic rate expressions for the model. Row 1 to 12 are slight simplifications of the ASM 3 rate expressions (after Gujer et al., 1999). The constants are declared in table 9.5 on page 128.

j	Process	Process rate equation ρ_j, all $\rho_j \geq 0$
		STANDARD ASM 3 PROCESSES
1	Hydrolysis	$k_H \cdot \frac{\frac{X_S}{X_{Het}}}{K_X + \frac{X_S}{X_{Het}}} \cdot X_{Het}$
	Heterotrophic organisms	
2	Aerobic storage of COD	$k_{Sto} \cdot \frac{S_O}{K_O+S_O} \cdot \frac{S_S}{K_{S,Het}+S_S} \cdot X_{Het}$
3	Anoxic storage of COD	$k_{Sto} \cdot \eta_{NO} \cdot \frac{K_O}{K_O+S_O} \cdot \frac{S_{NO}}{K_{NO}+S_{NO}} \cdot \frac{S_S}{K_{S,Het}+S_S} \cdot X_{Het}$
4	Aerobic growth	$\mu_{Het}^{max} \cdot \frac{S_O}{K_O+S_O} \cdot \frac{\frac{X_{Sto}}{X_{Het}}}{K_{Sto}+\frac{X_{Sto}}{X_{Het}}} \cdot X_{Het}$
5	Anoxic growth	$\mu_{Het}^{max} \cdot \eta_{NO} \cdot \frac{K_O}{K_O+S_O} \cdot \frac{S_{NO}}{K_{NO}+S_{NO}} \cdot \frac{\frac{X_{Sto}}{X_{Het}}}{K_{Sto}+\frac{X_{Sto}}{X_{Het}}} \cdot X_{Het}$
6	Aerobic endogenous respiration	$b_{O,Het} \cdot \frac{S_O}{K_O+S_O} \cdot X_{Het}$
7	Anoxic endogenous respiration	$b_{NO,Het} \cdot \frac{K_O}{K_O+S_O} \cdot \frac{S_{NO}}{K_{NO} \cdot S_{NO}} \cdot X_{Het}$
8	Aerobic respiration of X_{Sto}	$b_{O,Sto} \cdot \frac{S_O}{K_O+S_O} \cdot X_{Sto}$
9	Anoxic respiration of X_{Sto}	$b_{NO,Sto} \cdot \frac{K_O}{K_O+S_O} \cdot \frac{S_{NO}}{K_{NO}+S_{NO}} \cdot X_{Sto}$
	Autotrophic organisms, nitrification	
10	Nitrification	$\mu_{Aut}^{max} \cdot \frac{S_O}{K_{O,Aut}+S_O} \cdot X_{Aut}$
11	Aerobic endogenous respiration	$b_{O,Aut} \cdot \frac{S_O}{K_O+S_O} \cdot X_{Aut}$
12	Anoxic endogenous respiration	$b_{NO,Aut} \cdot \frac{K_O}{K_O+S_O} \cdot \frac{S_{NO}}{K_{NO}+S_{NO}} \cdot X_{Aut}$
		SULPHUR CYCLE PROCESSES
	Sulphur Reducing Bacteria	
13	Growth on SO_4^{2-}	$\mu_{SRB}^{max} \cdot \frac{S_{SO_4}}{K_{SO_4,SRB}+S_{SO_4}} \cdot \frac{K_{O,SRB}}{K_{O,SRB}+S_O} \cdot \frac{K_{NO,SRB}}{K_{NO,SRB}+S_{NO}} \cdot \frac{S_S}{K_{S,SRB}+S_S} \cdot X_{SRB}$
14	Growth on S^0	$\mu_{SRB}^{max} \cdot \frac{X_{S^0}}{K_{S^0,SRB}+X_{S^0}} \cdot \frac{K_{O,SRB}}{K_{O,SRB}+S_O} \cdot \frac{K_{NO,SRB}}{K_{NO,SRB}+S_{NO}} \cdot \frac{S_S}{K_{S,SRB}+S_S} \cdot X_{SRB}$
15	Decay	$b_{SRB} \cdot X_{SRB}$
	Sulphur Oxidising Bacteria	
16	Aerobic growth ($HS^- \rightarrow S^0$)	$\mu_{SOB}^{max} \cdot \frac{S_O}{K_{O,SOB}+S_O} \cdot \frac{S_{HS}}{K_{HS,SOB}+S_{HS}} \cdot X_{SOB}$
17	Aerobic growth ($S^0 \rightarrow SO_4^{2-}$)	$\mu_{SOB} \cdot \frac{S_O}{K_{O,SOB}+S_O} \cdot \frac{X_{S^0}}{K_{S^0,SOB}+X_{S^0}} \cdot X_{SOB}$
18	Anoxic growth ($HS^- \rightarrow S^0$)	$\mu_{SOB}^{max} \cdot \frac{S_{NO}}{K_{NO,SOB}+S_{NO}} \cdot \frac{K_{O,SOB}}{K_{O,SOB}+S_O} \cdot \frac{S_{HS}}{K_{HS,SOB}+S_{HS}} \cdot X_{SOB}$
19	Anoxic growth ($S^0 \rightarrow SO_4^{2-}$)	$\mu_{SOB}^{max} \cdot \frac{S_{NO}}{K_{NO,SOB}+S_{NO}} \cdot \frac{K_{O,SOB}}{K_{O,SOB}+S_O} \cdot \frac{X_{S^0}}{K_{S^0,SOB}+X_{S^0}} \cdot X_{SOB}$
20	Decay	$b_{SOB} \cdot X_{SOB}$

9.5.3 Methane producing bacteria

Methane was produced by biofilm biomass from the study reach. But the amount did not affect the COD and oxygen balance significantly (see section 6.6.2). Furthermore, data are lacking to calibrate this process. It will therefore not be discussed further.

9.5.4 Sulphur reduction, oxidation and cycling

The sulphur cycle was explained in section 2.5.2. In this section available kinetic, stoichiometric data and interactions will be discussed.

sulphur reduction

The sulphur reducing bacteria (SRB, chemoorganoheterotrophs) are anaerobes that use mainly low-molecular-weight organic acids and alcohols (e.g. acetate, lactate, malate, ethanol, etc) as carbon and energy source and use ammonium as nitrogen source (Hao *et al.*, 1996). The overall reduction of sulphate (SO_4^{2-}) is written as (Hao *et al.*, 1996):

$$SO_4^{2-} + 8\,H^+ \rightarrow S^{2-} + 4\,H_2O \tag{9.1}$$

Although anaerobes, they can withstand oxic periods (VandenEnde *et al.*, 1997). For example, a combined heterotrophic and SRB biofilm on steel only grew when SRB and heterotrophs were inoculated simultaneously under aerobic conditions (O. Wanner, EAWAG, personal communication). Aerobic periods in the sewer system might occur during the diurnal variations and rain events.

The idea that SRB will reduce only SO_4^{2-} to H_2S is rather simplistic because they can also perform a partial reduction to S^0 or thiosulphate ($S_2O_3^{2-}$). Some species can use iron, manganese and even O_2 as electron acceptors and can oxidise H_2S, sulphite (SO_3^{2-}), $S_2O_3^{2-}$ and S^0 with oxygen, nitrate or nitrite as electron acceptor. Finally, some can carry out a disproportionation of S^0 (Fuseler *et al.*, 1996):

$$4\,S^0 + 4\,H_2O \rightarrow SO_4^{2-} + 3\,H_2S + 2\,H^+ \tag{9.2}$$

This reaction will occur only in the presence of H_2S sulphide scavengers like $FeCO_3$ (Ehrlich, 1996). Such scavengers will probably not be present in sufficient quantities in the sewer system. However, Okabe *et al.* (1999) indicated that the high S^0 concentration they observed in a wastewater biofilm might make disproportionation thermodynamically as favourable as sulphate reduction.

A nearly constant SRB-activity was found in sediments throughout the active zone with low levels of organic substrate in the medium. This indicated that SRB received their electron donor from endogenous sources within the biofilm (Kühl and Barker-Jørgensen, 1992). These sources will probably include disintegrating bacteria as well as hydrolysis of organic particles. Addition of glucose led to an increased SRB activity in the upper part of the active layer (Kühl and Barker-Jørgensen, 1992).

Inhibition of SRB can occur due to H_2S, which is toxic even to the SRB themselves. The inhibition is direct and is caused by the undissociated form. It is reversible and not due to Fe-limitation (Cooney *et al.*, 1996; Visser *et al.*, 1996).

Nielsen (1987) reported a Q_{10} of 3.4 for the temperature range of 9 to 20°C.

Sulphide oxidation

The sulphur oxidising bacteria (SOB, mainly chemolithoautotrophs) are most likely obligate and facultative chemolithoautotrophic colourless sulphur bacteria like *Beggiatoa* or *Thiobacillus*. From an engineering viewpoint the oxidation process proceeds in two stages (Buisman *et al.*, 1991):

$$S^{2-} + 2\,H^+ + 0.5\,O_2 \rightarrow S^0 + H_2O \quad \text{and} \tag{9.3}$$

$$S^0 + H_2O + 1.5\,O_2 \rightarrow SO_4^{2-} + 2\,H^+ \tag{9.4}$$

It is unclear whether these conversions are done by one or two microorganisms. Buisman *et al.* (1991) had strong indications that the first stage proceeded faster than the second, while Ehrlich (1996) found that a lower oxygen tension leads to S^0 accumulation. Presumably, this is caused via the influence on the rate of the second reaction step. At sulphide loading rates above 10 $mg_S \cdot mg_N \cdot h^{-1}$ mainly (> 80%) S^0 was produced (Buisman *et al.*, 1991). The produced S^0 is stored either intra- or extracellularly as hydrophilic liquid sulphur droplets (Steudel, 1996). Because the sewer biofilm will normally be exposed to a low oxygen concentration that quickly drops within the biofilm, it seems likely that the oxidation will primarily go to S^0.

Certain SOB can use nitrate as an electron acceptor (Hines *et al.*, 1997; Okabe *et al.*, 1999):

$$4\,NO_3^- + H_2S \rightarrow 4\,NO_2^- + SO_4^{2-} + 2\,H^+ \tag{9.5}$$

The mechanism will probably also run via S^0 as intermediate.

Many reduced S compounds are highly reactive and the SOB must therefore often compete with abiotic reactions (chemical oxidation). The oxidation rate at pH 8 and 20°C was (Buisman *et al.*, 1991):

$$r_{S_{tot}^{2-}}^{chemox} = \left(0.41 \cdot {S_{tot}}^{0.39} \cdot {S_O}^{0.57 \cdot \log(S_{tot})}\right) \cdot 24/32 \tag{9.6}$$

where $r_{S_{tot}^{2-}}^{chemox}$ = chemical oxidation rate of sulphide ($mol \cdot m^{-3} \cdot d^{-1}$), S_{tot} = total sulphide concentration $= S_{S^{2-}} + S_{HS^-} + S_{H_2S}$ ($mol \cdot m^{-3}$).

Buisman *et al.* (1990) showed that the biological oxidation of sulphide is 7 (high H_2S concentration) to 75 (low concentration) times faster than in a chemical non-catalysed system. The chemical oxidation will therefore be neglected.

Interactions between SRB and SOB

The sulphur cycle seems to account for 10% in a laboratory grown biofilm (Norsker *et al.*, 1995) to more than 50% in a rotating biofilm contactor (Okabe *et al.*, 1999) of the oxygen consumption of a wastewater biofilm.

The classical assumption is that SRB are dependent upon the development of anaerobic strata in the deeper biofilms and sediments. Reoxidation of sulphide with oxygen would take place in a stratum close to the biofilm surface, depending on the oxygen penetration depth (Norsker *et al.*, 1995). The highest SRB activity would then typically be close to the interface between aerobic and anaerobic microenvironments (Hamilton, 1995). This was confirmed by microelectrode measurements that showed that the SOB activity based on gradients of H_2S, was restricted to a narrow zone (100 to 300 μm) within the biofilm (Kühl and Barker-Jørgensen, 1992). Rates calculated from these measurements indicated that turnover times of the substrates involved in

the sulphide oxidation were short (in the range of seconds) in comparison to the time required for chemical oxidation (minutes to hours) (Kühl and Barker-Jørgensen, 1992). It seems therefore valid to neglect chemical oxidation for biofilms.

More recent research of for example VandenEnde *et al.* (1997) showed that even in suspended cultures SRB and SOB can live in symbiosis. The SRB could grow only if the SOB kept the oxygen concentration low (VandenEnde *et al.*, 1997). The yield of the SRB on lactate was *doubled* in comparison to the growth in pure culture because they used S^0 instead of SO_4^{2-}. Nielsen (1991) also observed that SRB prefer more reduced substrates ($S_2O_3^{2-}$ and SO_3^{2-}) than SO_4^{2-} and have a higher H_2S production rate when more reduced sulphur compounds than sulphate are available. The SOB produced more S^0 because the local H_2S concentration was higher, although their yield per mole converted H_2S decreases.

Okabe *et al.* (1999) found an approx. constant SRB concentration through the whole depth of a wastewater biofilm by counting FISH-marked cells. Although this does not prove SRB-activity throughout the whole biofilm, it seems unlikely that this distribution would be just be the result of cell movement due to biofilm growth and detachment. The SOB must be able to compete well with heterotrophic organism because no H_2S could be detected in the bulk liquid, even under slight aerobic conditions (Kühl and Barker-Jørgensen, 1992; Norsker *et al.*, 1995).

In the sewer study reach, patches rich in sulphur were found in the sewer biofilm with X-ray scattering in an ESEM*. Subsequently, S^0 concentrations in the range of 10 to 50 $mg_{S^0} \cdot L^{-1}$ were found in biofilm samples. Furthermore, the sewer biofilm was on occasions covered with whitish filaments which is characteristic for *Beggiatoa* (Kühl and Barker-Jørgensen, 1992). Another indication that S^0 can be an important intermediate is that it accounted for $\approx$ 75% of the total sulphur pool in a wastewater biofilm grown under low DO (1.3 $g \cdot m^{-3}$) (Okabe *et al.*, 1999). This confirms the observation of Buisman *et al.* (1991) that S^0 accumulates at low DO.

The pH is known to influence the growth rates of SRB due to its effect on the H_2S-equilibrium (Visser *et al.*, 1996). The undissociated H_2S is toxic, even to SRB's themselves. This effect will however be neglected due to a lack of information about the pH in the biofilm.

Based on this literature survey a model for the sulphur cycle in the spirit of the ASM 3 is proposed, as shown in figure 9.2. As this figure indicates, it will be assumed that the SOB can use oxygen and nitrate in a similar manner as the heterotrophs do. The resulting process rates (14 to 21) are listed in table 9.1. The degradation of SRB and SOB biomass has been described with a simple first order rate equation.

*Environmental scanning electron microscope

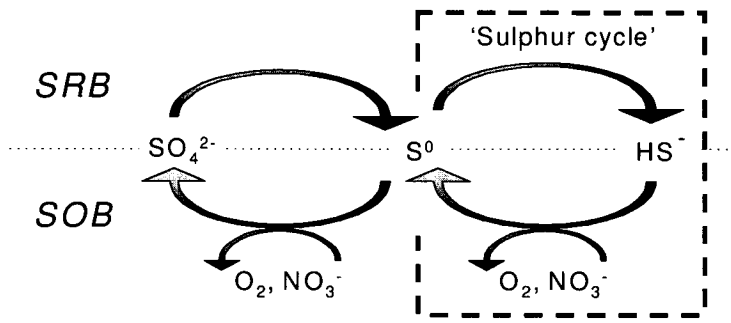

Figure 9.2: A model for the oxidation and reduction of sulphur by the sewer biomass.

9.5.5 Other taxa

The biofilm environment in real systems like a sewer contains also fungi, protozoa* and metazoa† (Gutekunst, 1988). The latter two groups actively feed on the biofilm and on each other. Many of these organisms were observed in the biofilm of the study reach. It will however be presumed that their effect on the biofilm is included in the endogenous respiration and erosion.

9.6 Intact biofilm

An intact biofilm adds mass transfer phenomena to the processes discussed in the previous section. Biofilm models exist from 0 to 3 dimensional. An overview of biofilm models and related processes can be found in Chaudhry and Beg (1998). But, as was discussed in section 9.3, the model should preferable contain a limited number of calibratable parameters and require a limited calculation time. A pseudo first order model based on penetration depths was therefore chosen (see figure 9.3). Consequently, the radial variation in biofilm thickness and activity (see section 6.4) cannot be taken into account. However, the variation in the activity was limited. Thus, this assumption will not introduce a major error.

9.6.1 Substrate flux based on diffusion and conversion: Effectiveness

An effectiveness factor, η, is commonly used in chemical engineering to describe the reduced activity of a catalyst particle due to transport limitation. η is the ratio of actual flux to that flux that would occur if particle were fully penetrated with the reagents. This concept was adapted

*Any of a subkingdom of microscopic animals made up of a single cell or a group of more or less identical cells and living in water or as parasites, including ciliates, flagellates, rhizopods, and sporozoans.

†Any of the very large subkingdom made up of all animals whose bodies, originating from a single cell, are composed of many differentiated cells arranged into definite organs.

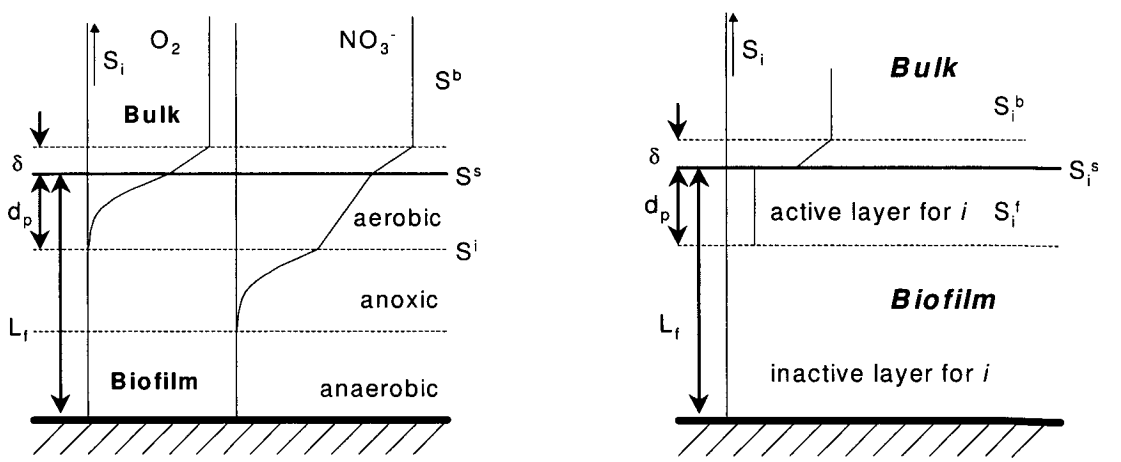

(a) The original concept for the biofilm showing the transport through the boundary layer and the subsequent consumption. Nitrate has a an extra diffusion layer because it is consumed in the anoxic layer.

(b) The simplified diffusion model when applying the effectiveness approach.

Figure 9.3: A sketch of the boundary layer and penetration depth.

for biofilms in the early seventies and later further refined by Rittmann and McCarty (1981) which resulted in:

$$r_i = a_f \cdot J_i = a_f \cdot \eta_f \cdot \mu^{max} \cdot X_i^f \cdot L_f \cdot \frac{S_i^f}{K_i + S_i^f} \tag{9.7}$$

where r_i = consumption rate of substrate i (g·m^{-3} ·d^{-1}), J_i = flux of compound i into the biofilm (g·m^{-2}·d^{-1}), a_f = specific biofilm area (m^2·m^{-3}), η_f = effectiveness factor for the biofilm activity (-), X_i^f = biomass concentration active for component i in the biofilm, L_f = biofilm thickness (m), S_i^f = substrate concentration in the active layer of the biofilm and K_i = half-saturation constant (g·m^{-3}).

Calculation of the effectiveness and biofilm activity

The substrate concentration and biofilm thickness can be made dimensionless:

$$S_i^* = \frac{S_i}{K_i} \qquad\qquad L_f^* = \frac{L_f}{\tau_f} \tag{9.8}$$

where τ_f = standard biofilm depth dimension (m) (changed in comparison with the original equation of Rittmann and McCarty (1981) by replacing the constant bacteria density γ with M_{X_X}/L_f):

$$\tau_f = \sqrt{\frac{2 \cdot K_i \cdot \eta_{\mathbb{D}} \cdot \mathbb{D}_i}{q_{S_i}^{max} \cdot M_{X_X}/L_f}} = \sqrt{\frac{2 \cdot K_i \cdot \eta_{\mathbb{D}} \cdot \mathbb{D}_i}{\nu_{j,i} \cdot \mu_X^{max} \cdot M_{X_X}/L_f}} \tag{9.9}$$

where M_{X_X} = amount of bacterial biomass X_X on the surface (g$_{COD}$·m^{-2}), $\eta_{\mathbb{D}}$ = factor describing biofilm diffusion reduction or enhancement (-) and $q_{S_i}^{max}$ = max. specific substrate uptake rate (g$_S$·g$_X{}^{-1}$·d^{-1}) and $\nu_{j,i}$ = stoichiometric coefficient for compound i and process j (-). η_f can now be written as (Rittmann and McCarty, 1981):

$$\eta_f = \begin{cases} 1 - \frac{\tanh\left(\sqrt{2}\cdot L_f^*\right)}{\sqrt{2}\cdot L_f^*} \cdot \left[\frac{\phi}{\tanh\phi} - 1\right] & \text{if } \phi \leq 1 \text{ kinetic limitation} \\ \frac{1}{\phi} - \frac{\tanh\left(\sqrt{2}\cdot L_f^*\right)}{\sqrt{2}\cdot L_f^*} \cdot \left[\frac{1}{\tanh\phi} - 1\right] & \text{if } \phi \geq 1 \text{ diffusion limitation} \end{cases} \tag{9.10}$$

in which ϕ = biofilm modulus (-):

$$\phi = \sqrt{2} \cdot \frac{L_f^*}{\sqrt{1 + 2S_i^*}} \tag{9.11}$$

An effectiveness from (9.10) is chosen based on ϕ.

This concept requires the assumption of a homogeneous biofilm*. The fraction of active biomass (in g$_{COD}$·m^{-3}) is presumed equal to the effectiveness factor:

$$M_{X_X}^{active} = \eta_f \cdot M_{X_X} \tag{9.12}$$

The penetration depth is calculated as:

$$d_{p,i} = \eta_f \cdot L_f \tag{9.13}$$

*The density and composition is constant throughout the biofilm.

This analytical approach allows for an approximation of the aerobic activity when S is oxygen. However, processes like denitrification also took place in the sewer biofilm. The effectiveness concept was therefore extended for nitrate.

Initially, the anoxic layer was defined as lying under the oxic layer (see figure 9.3(a)). However, the denitrification rate obtained with this model was too small. Furthermore, experiments had showed that the denitrification rate was unaffected by the oxygen concentration (see section 6.9.2). An extra aerobic biofilm layer between the boundary and anoxic layer was therefore omitted (see figure 9.3(b)).

9.6.2 Boundary layer

The mass-transport resistance from the bulk to the biofilm surface can be expressed with the effective diffusion concept. The entire resistance is located in a layer with a thickness δ through which the mass transport can be described by molecular diffusion only (Rittmann and McCarty, 1981) (see also figure 9.3):

$$J_i = -\mathbb{D}\frac{d\,S_i}{d\,z_f} = \mathbb{D}\frac{S_i^b - S_i^s}{\delta_c} \tag{9.14}$$

where J_i = flux of compound i into the biofilm (g·m^{-2}·d^{-1}), $\mathbb{D}$ = diffusion coefficient (m^2·s^{-1}), S_i^b = bulk concentration of component i (g·m^{-3}), S_i^s = concentration of component i on the biofilm surface (g·m^{-3}), z_f = distance from the biofilm substratum (m) and δ_c = depth of concentration boundary layer (m).

The penetration theory is used to approximation of the biofilm mass transfer processes. As a consequence, not the substrate concentration *on* the biofilm surface is of relevance, but the concentration *within* the biofilm as a result of the flux through the boundary layer. The active layer of the biofilm —determined by the penetration depth d_p— is regarded as a mixed reactor (see figure 9.3(b)). The resulting stoichiometric matrix for mass transfer of dissolved components and particles through the boundary is given in table 9.2.

Dawson and Trass (1972) determined the following equation for mass transfer in a rectangular duct for the dimensionless Sherwood number:

$$\mathbf{Sh} = R_h/\delta_c = 0.0153 \cdot \mathbf{Re}^{0.88} \cdot \mathbf{Sc}^{0.32} \tag{9.15}$$

where **Sh** = Sherwood number (-), **Re** = Reynolds number (-) and **Sc** = Schmidt number (-) (see page 72 for a definition).

DeBeer *et al.* (1996) measured the thickness of a mass transfer boundary layer around biofilm patches with microsensors and found 80 and 30 µm while the velocity was 0.0078 and 0.12 m·s^{-1}. Concentration changes in the boundary layer due to conversions are presumed negligible.

Table 9.2: The rate equation and stoichiometry for boundary layer transport. S_i^b = substrate concentration in the bulk liquid.

mass flux (g·m^{-2}·d^{-1})	S_i^b (g·m^{-3})	S_i^f (g·m$^{-3}_{biofilm}$)
equation (9.14)	$-\frac{P_w}{A_{cr}}$	$\frac{1}{d_p}$

9.6.3 Biofilm thickness & TSS

The biofilm thickness is determined from the sum of all compounds in the biofilm:

$$L_f = \frac{M_i^{inorg.}}{\rho_{inorg.}} + \frac{M_S + M_{Het} + M_{SOB}}{\rho_{Het}} + \frac{M_{S^0}}{\rho_{S^0}} + \frac{M_I + M_{Aut} + M_{SRB}}{\rho_{Aut}} \tag{9.16}$$

where ρ_n = density of compound group i. Subscript i is: $inorg.$ = inorganic (sand, zeolite) material, S = degradable particulate material, Het = heterotrophs, SOB = sulphur oxidising bacteria, S^0 = elementary sulphur, I = inert COD, Aut = nitrifiers, SRB = sulphur reducing bacteria.

The particulate compounds are divided over the density groups based on the assumption that slow growing bacteria form biomass with a higher density which has been set equal to that of nitrifiers. Attached particles are presumed to contribute as low density material.

The amount of TSS on the surface is calculated by converting the total COD, assuming a conversion factor of 1.85 as was determined in (section 6.10):

$$M_{TSS} = \frac{\sum M_i}{1.85} + M_{S^0} \cdot MW_S \tag{9.17}$$

where MW_S = molecular weight of sulphur = 32 g·mol^{-1} and M_i = amount of a particulate compound i on the surface (g·m^{-2}). The TSS is a state variable (and an 'observable') in the model.

9.6.4 Biofilm detachment

Despite the importance of detachment for the formation and stability of biofilms, the detachment process is one of the most studied but least understood phenomenon in biofilm research. As a result many equations for biofilm loss due to erosion have been developed, but none was found to be appropriate for this work. Therefore, another equation is proposed.

During dry weather, the wastewater exerts a constant shearing force on the sewer biofilm, which leads to a continuous loss of biomass. Periodically the biofilm is exposed to a higher shear stress due to rain events. Although the increase in the average shear stress, as calculated with 3.24, is only approx. a factor three, much of the biofilm is removed and only a base biofilm remains (Dauber *et al.*, 1982). However, in other sewers a biofilm might grow normally under the same shear conditions. This confirms the observation that biofilm structure and strength adapts to the shear conditions (Gjaltema, 1996) (see also 2.5.3). Tijhuis (1994) found for a biofilm airlift reactor that biofilm detachment decreased drastically after the substrate supply was stopped.

Shear does play an important role in biofilm erosion. It is only possible to present a more general erosion equation when the conditions under which the biofilm has grown are included. The following equation that includes the above mentioned observations is therefore proposed:

$$r_{X_i}^{det} = k_{det} \cdot \mu_{Het} \cdot \left(\frac{\tau_w - \tau_{min}}{\tau_{min}}\right)^{2.5} \cdot (L_f)^2 \tag{9.18}$$

where $r_{X_i}^{det}$ = detachment rate of i (g·m^{-3}·d^{-1}), k_{det} = rate coefficient for detachment (g·m^{-5}), τ_w = current wall shear stress (N·m^{-2}) and τ_{min} = minimal shear stress under dry weather conditions (N·m^{-2}).

The growth rate for heterotrophs (μ_{Het}) is included because these bacteria form the weakest biofilms and grow on the outside of the biofilm (Tijhuis, 1994). The term $(\tau_w - \tau_{min})/\tau_{min}$ introduces the 'history' of the biofilm. The effect of a rain event on the biofilm is accounted for with the coefficient 2.5. Therefore, an extra 'catastrophe erosion' is not required. The factor $(L_f)^2$ is often used in erosion equations and ensures that the biofilm does not grow unlimited. Furthermore, it prevents that all biofilm is lost during a rain event, which would be in contradiction to the field observations. The observation that an old biofilm is less susceptible to erosion than a young one has not been included at this stage. In the real biofilm this is related to the increase of the amount of inorganic material in the biofilm. This cannot be readily included in this pseudo 1-dimensional biofilm model. The detachment rate is enhanced with a tanh-term which ensures that the coefficient will slowly approach zero as the M_i becomes smaller than 1. This simulates that some bacteria will remain in niches in the surface and makes the simulation more stable by avoiding discontinuities. The stoichiometry of the detachment is given in table 9.3.

Table 9.3: The rate equation and stoichiometry for biofilm detachment and attachment.

process rate ($g \cdot m^{-3} \cdot d^{-1}$)	X_i ($g \cdot m^{-3}$)	M_i ($g \cdot m^{-2}$)
detachment		
$r_{X_i}^{det} \cdot \tanh\left(\frac{M_i}{M_{TSS} \cdot f_{COD}}\right)$	1	$-\frac{P_w}{A_{cr}}$
attachment		
$r_{X_i}^{att}$	-1	$-\frac{P_w}{A_{cr}}$

9.6.5 Biofilm attachment

Just like biofilm detachment (erosion), the attachment of particles to a biofilm and the subsequent transport is still being studied. As was shown with laboratory experiments during this work with intact biofilm, hydrolysis does occur within the sewer biofilm (see section 6.8.1). An attachment process must therefore be included in the model to supply the biofilm with particulate substrate, X_S, for hydrolysation. Due to a lack of better information, attachment is described by a simple rate law (Tijhuis, 1994; Wanner and Reichert, 1996):

$$r_{X_i}^{att} = k_{att} \cdot X_i \tag{9.19}$$

where $r_{X_i}^{att}$ = attachment rate of any particle i ($g \cdot m^{-3} \cdot d^{-1}$) k_{att} = specific attachment rate (d^{-1}) and X_i = bulk concentration of particulate substrate i ($g \cdot m^{-3}$). The stoichiometry is given in table 9.3.

9.6.6 Hydrolysis

Particulate matter has to be hydrolysed to dissolved material first before it is available for biological breakdown. In ASM 3 it is assumed that hydrolysis is associated with (heterotrophic) biomass and independent of the redox conditions (Process 1 in table 9.1 on page 116). Laboratory experiments with intact sewer biofilm did not show a different behaviour (see section 6.7). The hydrolysis rate constant k_H was also comparable to values published for the ASM 3 (Koch *et al.*, 2000) but will be adapted during the calibration of the model.

9.7 Model implementation

The simulation tool AQUASIM was used to model the batch and sewer experiments. A short description of the program and the implementation of the sewer as a 'river compartment' are given in appendix D.1.

9.8 Results modelling

9.8.1 Parameter identification with the suspended biofilm biomass

The aerobic conversion, nitrification, denitrification, sulphide oxidation and sulphur reduction by suspended biofilm were measured on four occasions in six parallel reactors. Parameters for the sewer model were checked and determined. The biofilm was measured as soon as possible after sampling. When the suspended biofilm would be aerated for several days, large shifts in the population can be expected making any parameter fit useless.

Heterotrophic activity

A parameter fit and the validation for the aerobic condition are shown in figure 9.4. The total COD was measured, but the different biomass and substrate fractions were adapted to describe the measurements. These data are shown in table 9.4.

Table 9.4: An overview of the initial data for the calibration and validation experiments. (f_{X_i} = fraction of total COD (-) and $m_{X_{S0}}$ = initial concentration of elementary sulphur ($mol_S \cdot m^{-3}$))

Experiments	X_{tot} $g_{COD} \cdot m^{-3}$	$f_{X_{Het}}$ -	$f_{X_{Sto}}$ -	$f_{X_{Aut}}$ -	$f_{X_{SRB}}$ -	$f_{X_{SOB}}$ -	$m_{X_{S0}}$ $mol_S \cdot m^{-3}$
calibration, no acetate	4060	0.25	0.01	0.0012	0.16	0.01	0.07
calibration, acetate added	5400	"	"	"	"	"	"
Exp 1	3850	0.14	0.04	0.0012	0.18	0.04	0.04
Exp 2	4540	"	"	"	"	"	"
S-cycle, aerobic	4980	0.14	0.04	0.0012	0.18	0.04	0.04
S-cycle, anaerobic	5090	"	"	"	"	"	"

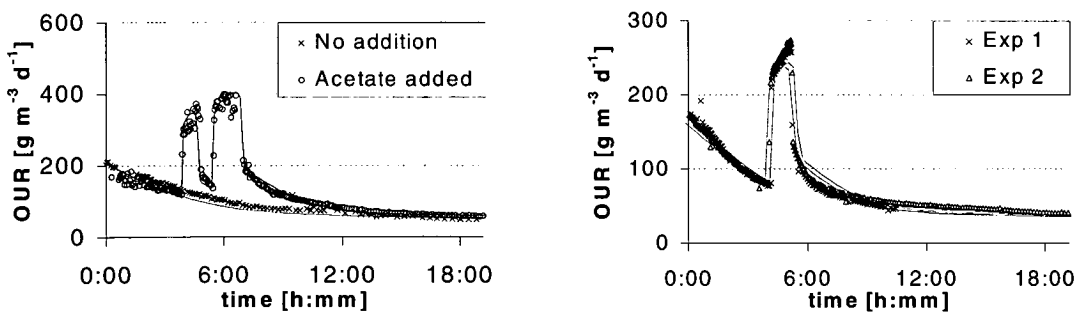

(a) Measured and modelled OUR after a parameter fit (3 July 1998, T=18°C).

(b) Validation of the model 6 Aug. 1998, T18°C.

Figure 9.4: The calibration and validation of the model with suspended biofilm.

Nitrification

The nitrification cannot be quantified by changes in the ammonium concentration because other processes can also consume or produce ammonium. Therefore, the activity of the nitrifiers was inhibited with allylthiourea (ATU; 20 mg·L^{-1}) in one reactor while another reactor served as control. A small decrease in the respiration rate was observed (see figure 9.5). A model fit indicated that the fraction of nitrifiers would be < 0.1% of the total biomass when the small response is fully attributed to nitrification.

Denitrification

Different values have been published for the anoxic reduction factor for growth, η_{NO}:

- 0.5 in a calibrated ASM 3 (Koch *et al.*, 2000),
- 0.6 in the original ASM 2 (Henze *et al.*, 1995), 0.75 for a Swiss wastewater (Roeck and Rufer, 1994) and
- 1.29 for a moving bed with biofilm on porous carriers Maurer *et al.* (1999).

A denitrification rate of for example 190 $g_N \cdot m^{-3} \cdot d^{-1}$ ($\equiv$ 540 $g_O \cdot m^{-3} \cdot d^{-1}$) was found while the OUR in the aerobic reactors was 930 $g_O \cdot m^{-3} \cdot d^{-1}$. The anoxic reduction for growth and storage η_{NO} has therefore been taken as 0.6.

9.8.2 Sulphur cycle processes

The activity of the sulphur cycle was measured in six parallel reactors with suspended biofilm biomass from the same sewer sample. The conditions in each reactor were chosen such that the following conversion could be studied in separate reactors: oxygen uptake, nitrification, denitrification, sulphide oxidation and sulphate reduction. The sixth reactor served as a control and was only aerated. The biofilm samples for the sulphur cycle activity were taken in August when the conditions in the sewer were favourable: low oxygen concentration and high temperature. The results of a measurement are shown in figure 9.6. The conversion rate was 0.6 mol SO_4^{2-} $m^{-3} \cdot d^{-1}$. It could be shown that:

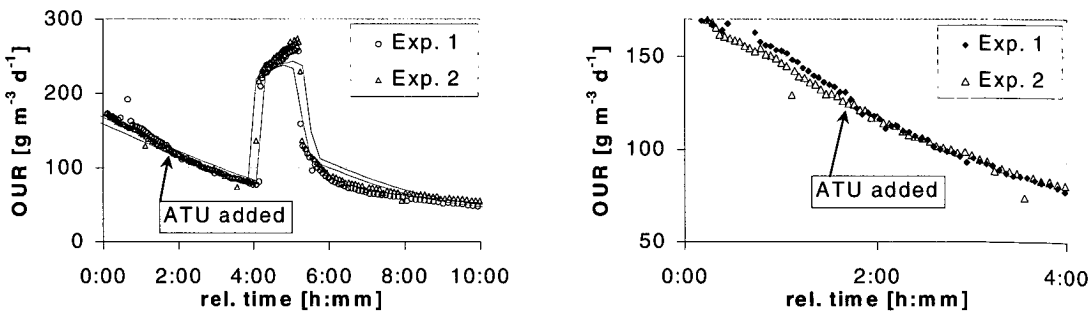

(a) Overview of the OUR as a function of the time.

(b) Enlargement around the time where the ATU was added.

Figure 9.5: A comparison between two paralellel reactors with regard to the nitrification activity. The nitrification was inhibited in the first experiment (Exp. 1) while the other served as control. (6 Aug 1998, T=18°C)

- Elementary sulphur (S^0) and SOB were present because the SO_4^{2-} increased under aerobic conditions in the control and nitrification reactors. This could be detected by measuring the S^0 concentration.
- S^0 oxidation with nitrate is considerably slower than with oxygen (no SO_4^{2-} increase under anoxic conditions).
- SRB were inactivated by nitrate because the SO_4^{2-} concentration in figure 9.6(b) does not decrease after the anoxic phase.

The model for the sulphur cycle as proposed in section 9.5.4 was applied to model the results (see figure 9.6). The model described the data very well after the initial biomass concentrations were adapted.

These results show that the sulphur cycle can be successfully modelled, but that the processes will not play a large role in the uptake of COD and oxygen (compare also with section 6.6).

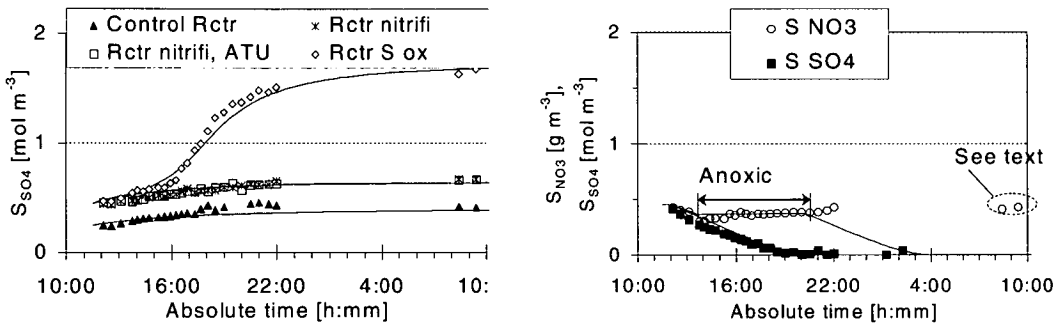

(a) The sulphate concentration in the aerobic reactors.

(b) The sulphate concentration in the anaerobic/anoxic reactors.

Figure 9.6: Measured and modelled results of the sulphur cycle. Six parallel reactors at T=17.5°C. Control Rctr = *biofilm suspended with tap instead of wastewater,* Rctr S ox = *sulphide oxidation,* Rctr nitrifi = *nitrification,* Rctr nitrifi,ATU = *nitrification with added allylthiourea,* Rctr denitrifi = *denitrification,* Rctr S red = *sulphate reduction.*

9.9 Stoichiometric and kinetic constants of the biological model

9.9.1 The concept of the stoichiometric & composition matrix

The biological model will be expressed in compounds (index i) and processes (index j). The amount of change in a component concentration due to a process is given by the stoichiometric coefficient $\nu_{j,i}$. The complete set of coefficients is represented in the stoichiometric matrix. The composition of the compounds in the model is represented by the composition matrix $\iota_{k,i}$ where k is the number of a conservative variable. All process rates form the vector ρ_j. This convention has for example been used for the Activated Sludge Models (Henze, 1987; Henze *et al.*, 1995; Gujer *et al.*, 1999) and is explained in Gujer and Larsen (1995).

9.9.2 The sewer model array

The kinetic constants and the array of the model compounds, stoichiometric matrix and composition matrix for the model are shown in the tables 9.5, 9.6 and 9.7. They are compared with the examples for the constants as given in the original ASM 3 publication and the results for a Swiss municipal WWTP as obtained by Koch *et al.* (2000). Table 9.8 contains the resulting stoichiometric matrix. The equations for the calculation of the stoichiometric coefficients are listed in appendix D.

*Table 9.5: A comparison between the kinetic constants for the ASM 3 processes given by Gujer et al. (1999) (**A**) and Koch et al. (2000) (**B**), and those used and obtained (boldface) for this study (**C**). All values at 20°C.*

Symbol	Kinetic parameter	A	B	C	Unit
k_H	Hydrolysis rate constant	3	9.0	**14**	$g_{X_S} \cdot g_{X_{Het}} \cdot d^{-1}$
K_X	Hydrolysis saturation constant	1	1	1	$g_{X_S} \cdot g_{X_{Het}}$
Heterotrophic biomass (X_{Het})					
k_{Sto}	Storage rate constant	5	12	**4.9**	$g_{S_S} \cdot g_{X_{Het}} \cdot d^{-1}$
η_{NO}	Anoxic reduction factor	0.6	0.5	0.6	-
K_O	Saturation constant of S_O for X_{Het}	0.2	0.2	**0.1**	$g_{O_2} m^{-3}$
K_{NO}	Saturation constant for S_{NO}	0.5	0.5	**0.2**	$g_{NO_3^- - N} \cdot d^{-1}$
K_S	Saturation constant for S_S	2.0	10	**5**	$g_{COD} \cdot d^{-1}$
K_{Sto}	Saturation constant for X_{Sto}	1	0.1	**0.2**	$g_{X_{Sto}} \cdot g_{X_{Het}}^{-1}$
μ_{Het}^{max}	Heterotrophic max. growth rate	2.0	3.0	**2.5**	d^{-1}
K_{NH}	not used				
K_{HCO}	not used				
$b_{O,Het}$	Aerobic endogenous resp. rate of X_{Het}	0.2	0.3	**0.25**	d^{-1}
$b_{NO,Het}$	Anoxic endogenous resp. rate of X_{Het}	0.1	0.15	0.2	d^{-1}
$b_{O,Sto}$	Aerobic resp. rate for X_{Sto}	0.2	0.3	0.2	d^{-1}
$b_{NO,Sto}$	Anoxic resp. rate for X_{Sto}	0.1	0.15	0.1	d^{-1}
Nitrifying autotrophic biomass (X_Aut)					
μ_{Aut}^{max}	Autotrophic max. growth rate	1	1.3	1	d^{-1}
$K_{O,Aut}$	Saturation constant of S_O for X_{Aut}	1	1.4	1	$g_{O_2} m^{-3}$
$K_{NH,Aut}$	not used	0.5	0.5	0.5	
$K_{HCO,Aut}$	not used	0.5	0.5	0.5	
$b_{O,Aut}$	Aerobic endogenous resp. rate of X_{Aut}	0.15	0.2	0.15	d^{-1}
$b_{NO,Aut}$	Anoxic endogenous resp. rate of X_{Aut}	0.05	0.1	0.05	d^{-1}

Table 9.6: The kinetic constants for the sulphur cycle. All values at 20°C unless stated otherwise.

Sulphur Reducing Bacteria (X_{SRB})				
μ_{SRB}^{max}	SRB max. growth rate	0.1	d^{-1} (30°C)	(Visser *et al.*, 1996)
$K_{O,SRB}$	Saturation constant	0.5	$gO_2 \cdot m^{-3}$	(estimated)
$K_{SO_4,SRB}$	Saturation constant for SO_4^{2-}	0.033	$mol_S \cdot m^{-3}$	(Omil *et al.*, 1998)
$K_{S^0,SRB}$	Inhibition constant for growth on X_{S^0}	0.01	$mol_S \cdot m^{-3}$	(estimated)
$K_{S,SRB}$	Saturation constant for S_S	11.1	$g_{COD} \cdot m^{-3}$	(Visser *et al.*, 1996)
$K_{NO,SRB}$	Inhibition constant for NO_3^-	0.1	$g_{NO_3^- - N} \cdot d^{-1}$	(estimated)
b_{SRB}	Decay rate of SRB	0.005	d^{-1} (30°C)	(Alphenaar, 1994)
a_{SRB}	Increment factor for oxygen tolerance	10	-	(estimated)
Sulphide Oxidising Bacteria (X_{SOB})				
μ_{SOB}^{max}	SOB max. growth rate	2	d^{-1}	(estimated)
$K_{O,SOB}$	Saturation constant for O_2	0.05	$g_{O_2} m^{-3}$	(estimated)
$K_{HS,SOB}$	Saturation constant HS^-	0.1	$mol_S \cdot m^{-3}$	(estimated)
$K_{S^0,SOB}$	Saturation constant for X_{S^0}	2.9	$mol_S \cdot m^{-3}$	(estimated)
$K_{NO,SOB}$	Saturation constant for NO_3^-	0.5	$g_{NO_3^- - N} \cdot d^{-1}$	(estimated)
b_{SOB}	Decay rate of SOB	0.1	d^{-1}	(estimated)

Table 9.7: Similar to table 9.5, but for the stoichiometric parameters.

Symbol	Stoichiometric parameter	A	B	C	Unit	
Y_Het	Aerobic yield of heterotrophic biomass	0.63	0.8	**0.7**	$g_{X_H} \cdot g_{X_{Sto}}^{-1}$	
Y_{HetNO}	Anoxic yield of heterotrophic biomass	0.54	0.65	0.54	$g_{X_{Het}} \cdot g_{X_{Sto}}^{-1}$	
Y_A	Yield for autotrophic biomass per NO_3^-	0.24	0.24	0.24	$g_{X_A} \cdot g_{S_{NO}}^{-1}$	
Y_{StoO}	Aerobic yield of heterotrophic biomass	0.85	0.8	0.85	$g_{X_{Sto}} \cdot g_{S_S}^{-1}$	
Y_{StoNO}	Anoxic yield of heterotrophic biomass	0.8	0.7	0.8	$g_{X_{Sto}} \cdot g_{S_S}^{-1}$	
$Y_{SOB,HS}$	Yield for SOB while growing on H_2S	–	–	5.7	$g_{X_{SRB}} \cdot mol_S^{-1}$	*
Y_{SOB,S^0}	Yield for SOB while growing on S^0	–	–	2	$g_{X_{SRB}} \cdot mol_S^{-1}$	*
Y_{SRB,S^0}	Yield for SRB with S^0 as oxidiser	–	–	0.44	$g_{X_{SRB}} \cdot g_{S_S}^{-1}$	#
Y_{SRB,SO_4}	Yield for SRB with SO_4^{2-} as oxidiser	–	–	0.22	$g_{X_{SRB}} \cdot g_{S_S}^{-1}$	#
i_{NBM}	N contents of biomass (X_x)	0.07	0.07	0.07	$g_N \cdot g_{X_x}^{-1}$	
i_{NXS}	N contents of X_S	0.04	0.03	0.04	$g_N \cdot g_{X_S}^{-1}$	
i_{NXI}	N contents of X_I	0.02	0.04	0.02	$g_N \cdot g_{X_I}^{-1}$	
i_{NSS}	N contents of S_S	0.03	0.03	0.03	$g_N \cdot g_{S_S}^{-1}$	
i_{NSI}	N contents of S_I	0.01	0.01	0.01	$g_N \cdot g_{S_I}^{-1}$	
f_{SI}	Production of S_I in hydrolysis	0	0	0	$g_{S_I} \cdot g_{X_S}^{-1}$	
f_{XI}	Production of X_I in endo. resp.	0.2	0.2	0.2	$g_{X_I} \cdot g_{X_x}^{-1}$	
i_{TSSXS}	TSS to COD ratio for X_S	0.75		0.75	$g_{TSS} \cdot g_{X_S}^{-1}$	
i_{TSSBM}	TSS to COD ratio for biomass (X_x)	0.9		0.9	$g_{TSS} \cdot g_{X_x}^{-1}$	
i_{TSSXI}	TSS to COD ratio for X_I	0.75		0.75	$g_{TSS} \cdot g_{X_I}^{-1}$	
$i_{TSSXSto}$	TSS to COD ratio for X_{Sto}	0.6		0.6	$g_{TSS} \cdot g_{X_{Sto}}^{-1}$	

*: Buisman *et al.* (1991)
#: VandenEnde *et al.* (1997)

Table 9.8: The array of model compounds, stoichiometric matrix and composition for the dynamic model. See also appendix D.

	COMPOUNDS →	S_O	S_I	S_S	S_{NH}	S_{NO}	S_{N_2}	S_{HS}	X_{S^0}	S_{SO4}	S_{HCO_3}	X_{Het}	X_A	X_{Sto}	X_{SRB}	X_{SOB}	X_S	X_I	X_{TSS}
	$g_{COD}\cdot mol^{-1}$	-32			0	-64	-48	64	48	0	0	0	160	160	160	160	160		
	M_W ($g\cdot mol^{-1}$)	32	-	-	18	62	28	33	32	96	61	1	-	-	-	-	-	-	-
	i →	1	2	3	4	5	6	7	8	9	10	11	12	13	14	15	16	17	18
j	PROCESSES										STOICHIOMETRIC MATRIX $\nu_{j,i}$								
1	Hydrolysis		0	1	0.010						0.001						-1		-0.75
2	Aerobic storage of COD	-0.15		-1	0.030						0.002			0.85					0.51
3	Anoxic storage of COD			-1	0.030	-0.070	0.070				0.007			0.80					0.48
4	Het. aerobic growth	-0.43			-0.070						-0.005	1		-1.43					0.04
5	Het. anoxic growth				-0.070	-0.30	0.30				0.016	1		-1.85					-0.21
6	Aerobic endogenous respiration	-0.80			0.066						0.005	-1						0.20	-0.75
7	Anoxic endogenous respiration				0.066	-0.28	0.28				0.025	-1						0.20	-0.75
8	Aerobic respiration of X_{Sto}	-1												-1					-0.60
9	Anoxic respiration of X_{Sto}					-0.35	0.35				-0.025			-1					-0.60
10	Autotrophic growth (nitrification)	-18.0			-4.24	4.17					-0.6		1						0.90
11	Auto. aerobic endogenous respiration	-0.80			0.066						0.005		-1					0.20	-0.75
12	Auto. anoxic endogenous respiration				0.066	-0.28	0.28				0.025		-1					0.20	-0.75
13	SRB growth on SO_4^{2-}			-4.55	0.066			0.055		-0.055	0.06				1				0.90
14	SRB growth on S^0			-2.27	-0.002			0.080	-0.080		-0.08				1				-1.65
15	SRB decay		0		0.034						0.002				-1		0.80	0.20	-0.15
16	SOB aerobic growth ($HS^- \rightarrow S^0$)	-1.81			-0.070			-0.18	0.18		0.17					1			6.51
17	SOB aerobic growth ($S^0 \rightarrow SO_4^{2-}$)	-23.0			-0.070				-0.50	0.50	-1.01					1			-15.1
18	SOB anoxic growth ($HS^- \rightarrow S^0$)				-0.070	-0.63	0.63	-0.18	0.18		0.22					1			6.51
19	SOB anoxic growth ($S^0 \rightarrow SO_4^{2-}$)				-0.070	-8.05	8.05		-0.5	0.5	-0.43					1			-15.1
20	SOB decay		0		0.034						0.002					-1	0.80	0.20	-0.15
k	CONSERVATIVES										COMPOSITION MATRIX $\iota_{k,i}$								
1	COD (g_{COD})	-1	1	1		-4.57	-1.71	64	48				1	1	1	1	1	1	1
2	Nitrogen ($g_N\cdot g_{COD}$)		0.01	0.03	1	1	1						0.07	0.07	0.00	0.07	0.07	0.04	0.02
3	Sulphur (mol_S)							1	1	1									
4	Charge (mol_+)				0.071	-0.071		-1		-2		1							
	OBSERVABLE																		
5	TSS [g_{TSS}]								32				0.9	0.9	0.6	0.9	0.9	0.75	0.75 -1

9.10 Calibration and validation of the sewer model

9.10.1 Assumption for the sewer model

The following assumptions and simplifications were made for the sewer model:

- One-dimensional.
- The exposure of parts of the biofilm to the sewer atmosphere during the night is not accounted for.
- The anaerobic processes are not included because these played a minor role in the study reach and consequently data for calibration were lacking.
- The urea hydrolysis is not included because only a limited amount of input data were available.
- The calculation of the boundary layer according to equation (9.15) resulted in AQUASIM in a circular reference. An indirect dependency (a fit of δ_c as $f(Q_{meas.})$) resulted in lengthy calculations. A constant value of 40 µm was therefore used. This has affected the concentrations on the biofilm surface and therewith the rates in the biofilm, but the effect is limited because δ_c varied between 40 (day) and 52 µm (night) as calculated with equation (9.15).

9.10.2 Data for model calibration and validation

Measurement campaigns for the wastewater activity have been conducted while the oxygen uptake rate and COD of the wastewater were monitored.

Pollutographs as model input

Unfortunately, no continuous measurement of the COD-load and the biomass contents of the wastewater that entered the study reach were available. For long-term simulations, a diurnal variation of the COD and other components was determined from the results of several measurement campaigns like those in chapter 5. Figure 9.7 contains the resulting pollutographs. These pollutographs will be used as model input and it will be assumed that the *loads* from the village remained constant. No correction for the weekend was made because *Rümlang* is a town without much industry or large shifts in the population due to many commuters.

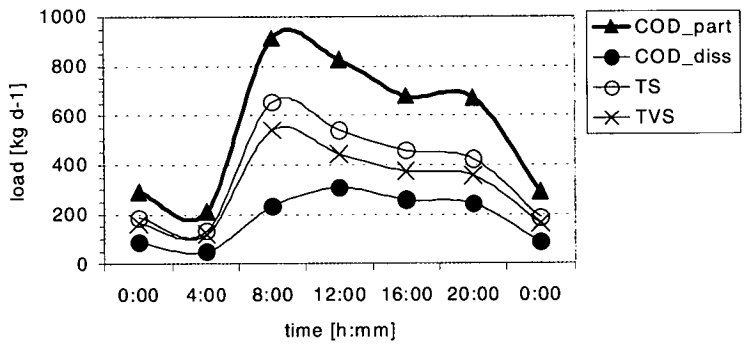

Figure 9.7: The pollutographs which are used as input for the model.

Biological activity in incoming wastewater

The respiration of the biomass in the inflowing wastewater has a significant effect on the oxygen balance. The following relationship between the particulate COD and the estimated X_{Het} was found with the help of batch experiments with wastewater as described in section 8.5.1 (in $g_{COD} \cdot m^{-3}$):

$$X_{Het} = 0.09 \cdot COD_{part.in} - 0.3 g_{COD} \cdot m^{-3} \tag{9.20}$$

Varying erosion rates in the upstream part of the sewer cannot be included and will therefore form a source of error.

Continuously measured in-line data

The discharge, dissolved oxygen concentration and temperature were measured continuously as was described in section 4.4.

Oxygen Uptake Rate data

The wastewater oxygen uptake rate (OUR) was measured during several measurement campaigns during which the COD-concentration was also measured. These data form the major source for calibration and validation.

9.10.3 Calibration

The sewer model was calibrated with the help of a measurement campaign in June 1999 (see also section 8.7). The biochemical parameters and the gas exchange parameters remained unchanged since they had been determined with other experiments. Only the attachment and erosion parameters were estimated.

The attachment is selected such that the biofilm behaves as was observed with the *in situ* measurements: Sufficient S_S for the biofilm respiration is produced but there is no significant release of S_S to the bulk liquid. The erosion is adapted so that the biofilm thickness and composition corresponds to the observations.

The resulting fit and the parameters are shown in figure 9.8 and table 9.9, respectively. The adapted values are those changed as a result of the calibration; the calculated ones were initially determined with the hydrodynamical model and fixed on this value for subsequent calculations. The $\eta_{\mathbb{D}}$ has been kept at one. It has been assumed that the enhanced diffusion as a result of a filamentous biofilm structure compensates for the diffusion limitation due to the biofilm matrix with additional inorganic material.

The calculated active biomass (M_i^{active}) corresponded well with the average biomass density per surface area (γ) that was found with the *in situ* measurements (compare with section 6.4).

9.10.4 Validation

The second measurement campaign with regard to the oxygen balance was used for the validation. The simulation describes the data well as can be seen in figure 9.9.

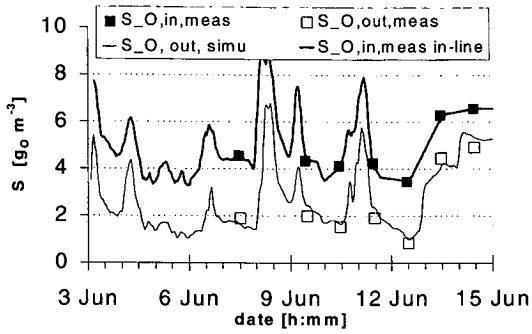

(a) The measured and modelled oxygen concentration.

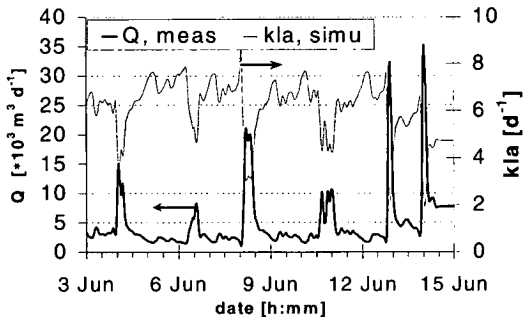

(b) .The measured discharge and the calculated $k_l a$.

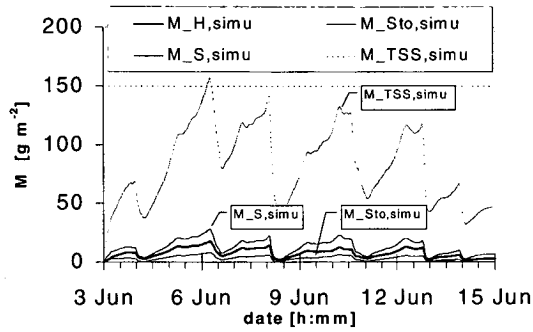

(c) The simulated concentration of solids on the sewer wall.

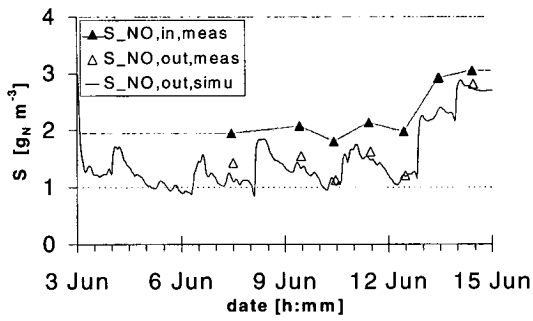

(d) The measured and modelled nitrate concentration.

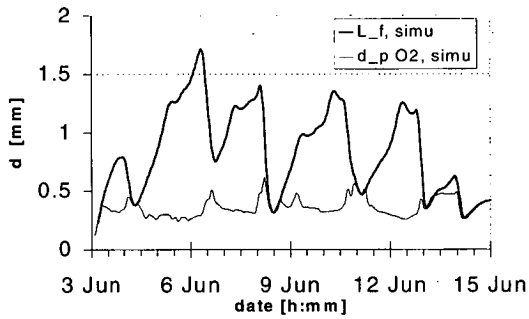

(e) The simulated biofilm thickness (L_f) and oxygen penetration depth ($d_{p,O}$).

Figure 9.8: The calibration of the sewer biofilm model with data from June ($\overline{T}$=18°C).

Table 9.9: The parameter values after the model calibration (see text for explanation).

Parameter (adapted)	*value*	unit	Parameter (calculated)	*value*	unit
$\eta_{\mathbb{D}}$	1.0	-	d_{bound}	40	µm
k_{det}	$4.0 \cdot 10^9$	$g \cdot m^{-5}$	τ_{min}	0.05	$N \cdot m^{-2}$
k_{att}	0.08	d^{-1}			

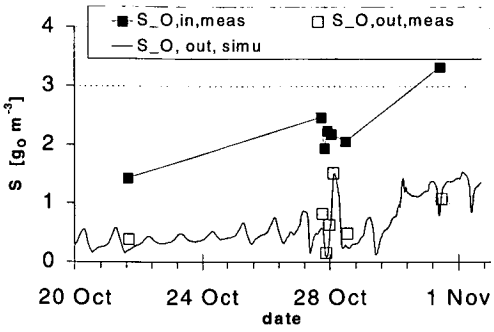

(a) The measured and modelled oxygen concentration.

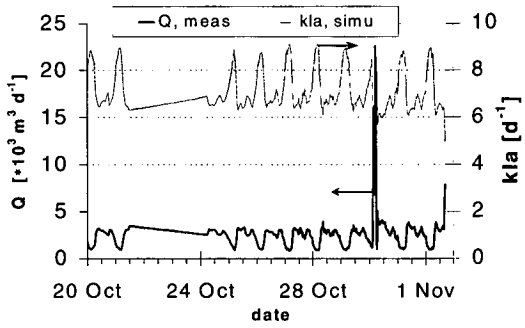

(b) .The measured discharge and the calculated $k_l a$.

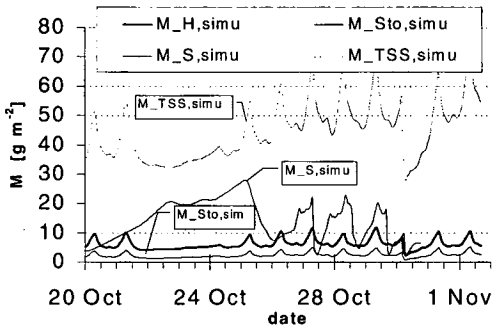

(c) The simulated concentration of solids on the sewer wall.

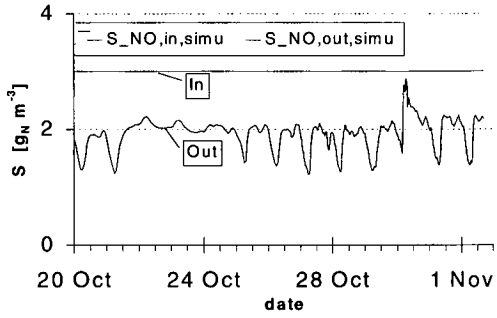

(d) The measured and modelled nitrate concentration.

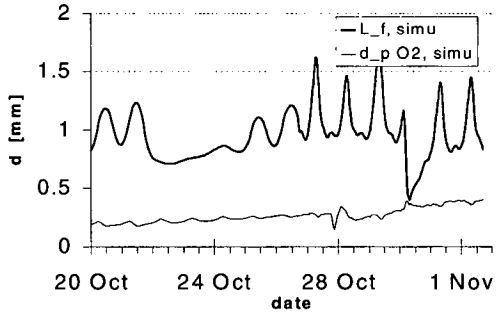

(e) The simulated biofilm thickness (L_f) and oxygen penetration depth ($d_{p,O}$).

Figure 9.9: The validation of the sewer model with data from October ($\overline{T}$=17°C).

9.10.5 Validation with in-line data

Finally, the oxygen concentration during winter conditions was simulated. Discharge, in-line oxygen measurements and temperature served as the only data that were changed. The simulation in figure 9.10 shows that the simulation is satisfactory.

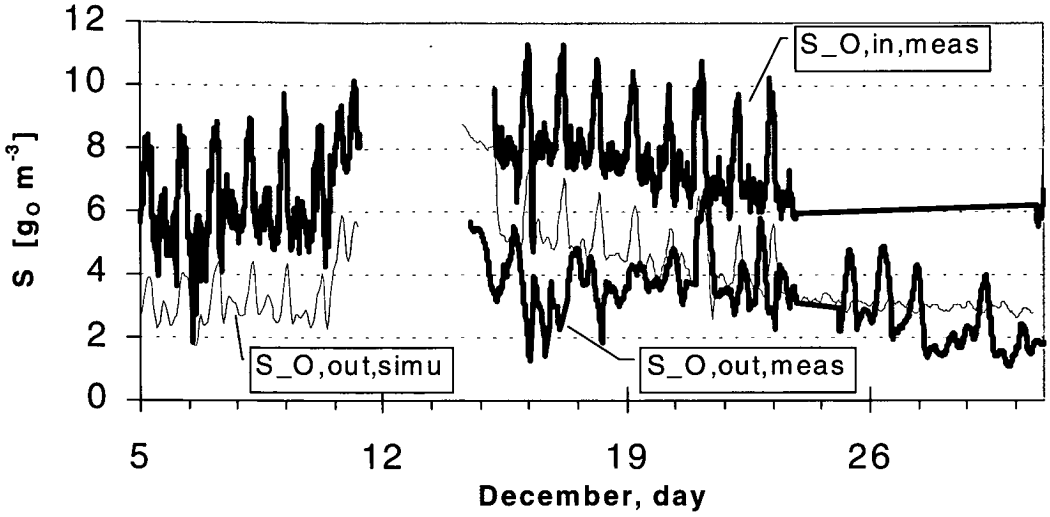

Figure 9.10: The validation of the sewer model with data from December 98 ($\overline{T}$=12° C).

9.11 Conclusions

A deterministic sewer model was presented. The sewer hydrodynamics are calculated with the diffusive wave approach of the Saint Venant equations. The biological processes in the wastewater and the biofilm are based on the ASM 3. The diffusion of components into the biofilm is described with the penetration depth. The new reaeration equation that was presented in chapter 7 is used to calculate the oxygen uptake from the sewer atmosphere. The diffusion of components into the biofilm was described with the penetration depth.

The model was calibrated and validated with literature, laboratory and field data. A model approach for the sulphur cycle that is compatible with the ASM 3 definitions was given. A further extension with fermentation and methanogenesis is feasible. However, these processes were omitted from the full scale sewer model because field data and data from the intact biofilm were lacking; the sewer study reach was practically always aerobic. Laboratory experiments however showed that the concept is valid.

The validation of the sewer model gave good results. The one-dimensional approach of the model ensured that the calculation time remains short. Together with the compatibility in the state variables with the wastewater treatment plant and river models it is possible to include this model in an integrated urban hydrology model.

9.12 Recommendations

- The model was calibrated and validated for only one main sewer. Further research should show to what extend the parameters can be transferred to other sewers.
- The model should be calibrated and validated for anaerobic sewers.
- The attachment and erosion processes require an extensive research effort.

10 Conclusion, interpretation and outlook

10.1 Conclusions

Many goals and questions were mentioned in the introduction. Several of those could be answered but some are still open.

- The sewer is a complex system. It was shown that the compartments (sewer atmosphere, wastewater and biofilm) all interact. It has been proven possible to quantify the major processes in the sewer system: the reaeration through the water surface, the wastewater activity and the biofilm activity. The quantification was mainly based on full-scale field experiments in a sewer with a length of two kilometres. The balancing of dissolved components proved practically useless because the random variations in the wastewater composition were lager than the changes due to conversion processes. The biofilm activity and properties were therefore determined in the sewer. Laboratory experiments with wastewater, suspended biofilm and intact biofilm gave specific additional data.
- The method of determining reaeration rate based on the inert gas sulphur hexafluoride was adapted and calibrated for the sewer system. A new temperature correction and a reaeration equation were presented. The latter also included previously measured data by other researchers and can therefore be used for sewer systems in general.
- The biological wastewater activity was related to the amount of organic particles present. Its growth was limited during the night when the supply of nutrients is much smaller. The overall biomass consists of both eroded biofilm and faecal bacteria, but a distinction between the two could not be made.
- The biofilm served as a particle trap, as a supplier of biomass and contributed to the conversion processes. It was less influenced by the diurnal variation in the substrate supply because it contains entrapped particles that are hydrolysed and bacterial storage material* in order of 5% of the TVS†. The wastewater oxygen concentration was the major factor influencing biofilm growth.
- The biofilm distribution was clearly related to the hydrodynamic conditions. The potential aerobic activity on the sewer wall —which would be released during a rain event— was proportional to the TVS. However, measurements with an *in situ* flow cell showed that the activity of an intact biofilm varied insignificantly along the wetted perimeter. Variations in time of the biofilm activity per area unit were observed. This shows that the biofilm is a dynamic and constantly adapting structure. For example, the fraction of inorganic material increased from 40% for a young biofilm to up to 80% for an older one. It was shown that a sulphur cycle is active but did not have an important effect on the COD balance.
- The different limiting factors for biofilm and wastewater activity resulted in interesting dynamics. During the night, the biofilm can be responsible for 2/3 of the aerobic activity.

*PHA and glycogen
†Total Volatile Solids

However, when the wastewater oxygen concentration approaches zero, its direct contribution becomes negligible. However, in that case it might release easily degradable substrate to the wastewater.

- These results allowed the development of a model with a limited number of adjustable parameters. This model was calibrated and validated with data from a main sewer. The general outcome of this model will be valid for sewers in general. However, care should be taken when using the sewer model for other sewers because the attachment and erosion of particles on the sewer wall are important parameters and are highly influenced by the local conditions.

10.2 Interpretation of the results

Based on literature data, the experiment results described in this work and the model results, the following interpretation of the sewer processes has been developed:

The wastewater contains inorganic and organic components in the dissolved and the particulate form. The composition starts to change as soon as the wastewater leaves the source. Particles break apart due to shear forces. Bacterial enzymes will further dissolve (hydrolyse) the fragments and grow on the products and bacteria will also colonise the wall of sewer pipe and form a biofilm or 'slime layer.' Initially this biofilm is mainly organic but the amount of inorganic material increases over a period of months to up to 80% due to mineralisation processes and the entrapment of inorganic particles.

The biofilm does not grow unchecked. It erodes steadily, losing mainly heterotrophic biomass. This biomass grows on the outside of the biofilm and forms the weakest structure. The eroded biomass will increase the wastewater activity significantly and continue to grow. The biofilm will trap organic particles, which are slowly hydrolysed. But the outer biofilm layers rely on substrate that has been hydrolysed in the wastewater. Nitrate is also degraded, even under aerobic conditions. The rate of degradation is higher than would be expected from a simple layered biofilm model. Oxygen and nitrate have to diffuse through the boundary layer over the biofilm. Therefore, the flow velocity has an effect on the conversion rates.

Nitrifiers grow in biofilm but their growth rate is slow and they are steadily overgrown by heterotrophs, which deprive them of oxygen. As the biofilm thickness increases, the deeper strata will become anaerobic. This creates a niche for sulphur reducing (SRB), methanogenic and other anaerobic bacteria. They will grow on entrapped particles and dead biomass. Fermentative bacteria break down the larger fragments into smaller organic acids and hydrogen on which SRB grow. The hydrogen sulphide that is produced will be oxidised again close to surface by sulphur oxidising bacteria (SOB) when the wastewater is aerobic. The development of the SOB can lead to a symbiosis between SRB and SOB whereby the sulphur cycle runs via elementary sulphur instead of hydrogen sulphide because this more efficient for the bacteria. A pool of elementary sulphur develops and can be found in the film. Methane will also be oxidised and not leave the biofilm in significant quantities as long as the wastewater is aerobic.

A rain event drastically disturbs the system. The weaker biofilm top layer is easily flushed away and a stronger base film remains. Its strength is related to the entrapped sand, zeolite and fats, which function as reinforcements. This base layer contains the anaerobic biomass. The oxygen concentration during and after the rain event is much higher because much of the aerobic biomass has disappeared and the inflow of the oxygen with the water is higher because the discharge remains higher for a few days as a result of the rain event. The anaerobic activity will be affected, but a large number of these bacteria remain alive; it would take months to build

a viable population where there was none but their activity was observed despite a large rain event occurring every few weeks. The conditions for the heterotrophic biofilm biomass are now ideal. The oxygen uptake in the wastewater has dropped because biomass erosion has decreased drastically. Furthermore, the oxygen concentration is high. More substrate from within the biofilm might be available because the anaerobic layer has become (partly) aerobic and inactive. This results in a very fast heterotrophic growth that expresses itself as long filaments. But, these filaments erode more easily. Furthermore, over a period of a few days the discharge falls back to its dry weather value. The long filaments disappear, once again, due to erosion, increased wastewater respiration and decreased oxygen inflow. The biofilm thickness then increases slowly until a steady state is reached or the next rain event occurs.

With all this activity, it will be clear that the wastewater properties will have changed considerably when it finally reaches the wastewater treatment plant.

10.3 Open questions and outlook

At this moment it is to early to develop different scenarios for the sewer system management based on biological processes. The following questions contain aspects that require further research:

- How can the attachment/erosion of particles be quantified? For example, particle tracers like fluorescent micro particles, fluorescently labelled bacteria, coated magnetic nanoparticles or biomass traced with easily detectable rare earth metals could be used.
- Data with regard to the anaerobic processes in the sewer system is required to calibrate these processes in the sewer biofilm.
- What is the effect of the hydrodynamics and inorganic particles on the biofilm structure and strength?
- What is the diurnal variation in the amount of easily degradable material?
- Can the relative contribution of different sources to the wastewater biomass be quantified?

A reliable simulation of the sewer for a wide range of scenarios will be possible when these questions are answered.

Bibliography

Allison, D. (1993). Biofilm associated exopolysaccharides. *Microbiol. Eur.*, **Nov./Dec.**, 16-19.

Almeida, M. C. (1999). *Pollutant transformation processes in sewers under aerobic dry weather flow conditions.* Doctoral dissertation, Imperial College of Science, Technology and Medicine, London, UK.

Almeida, M. C., Butler, D., and Matos, J. S. (2000). Reaeration by sewer drops. *Wat. Sci. Tech. (Submitted)*, **Submitted**.

Alphenaar, P. (1994). *Anaerobic granular sludge, characterization, and factors affecting its functioning.* Doctoral dissertation, Wageningen Agricultural University, Wageningen, The Netherlands.

Anonymous. (1997). *Brittanica CD.* Encyclopedia Brittanica, Inc.

Anonymous. (1998, December 15). *Gewässerschutzverordnung* [Law for the protection of receiving waters]. Bundesamt für Umwelt, Wald und Landschaft (BUWAL), Bern, Switzerland.

Anonymous. (2000). *Mousetrap* (user manual Version 2000). DHI Water & Environment, Hørsholm, Denmark.

APHA. (1985). *Standard methods for the examination of water and wastewater* (16 ed.). Washington DC, USA: Am. Publ. Health. Assoc. (APHA, AWWA, WPCF).

Arvin, E., and Harremoës, P. (1990). Concepts and models for biofilm reactor performance. *Wat. Sci. Tech.*, **22**(1/2), 171-192.

ASCE Standard. (1993). *Measurement of oxygen transfer in clean water* (No. ANSI/ASCE 2-91). ASCE, New York, U.S.A.

Ascher, W. E., Monahan, E. C., Wanninkhof, R., and Bates, T. S. (1991). Correlation of fractional foam coverage with gas transport rates. In S. C. Wilhems and J. S. Gulliver (Eds.), *Selected papers from the second international symposium on gas transfer at water surfaces* (p. 536-548). ASCE, New York, USA.

Balmér, P., and Tagizadeh-Nasser, M. (1995). Oxygen transfer in gravity flow sewers. *Wat. Sci. Tech.*, **31**(7), 127-135.

Banerjee, S. (1992). Turbulent structures. *Chemical Engrg. Sci.*, **47**(8), 1793-1817.

Bennett, C. O., and Myers, J. E. (1962). *Momentum, heat and mass transfer.* McGraw-Hill Book Company, New York, USA.

Bishop, P. L. (1997). Biofilm structure and kinetics. *Wat. Sci.tech.*, **36**(1), 287-294.

Bjerre, H. L., Hvitved-Jacobsen, T., Teichgraber, B., and Schlegel, S. (1998). Modeling of aerobic wastewater transformations under sewer conditions in the Emscher River, Germany. *Wat. Env. Res.*, **70**(6), 1151-1160.

Bland, C. E. G., Bayley, R. W., and Thomas, E. V. (1975). Some observations on the accumulation of slime in drainage pipes and the effects of these accumulations on the resistance to flow. *The public health engineer*, **3**, 21-28.

Boon, A. G., and Lister, A. R. (1975). Formation of sulphide in rising main sewers and its prevention by injection of oxygen. *Prog. Wat. Tech.*, **7**(2), 289-300.

Boon, A. G., Skellett, C. F., Newcombe, S., Jones, J. G., and Forster, C. F. (1977). The use of oxygen to treat sewage in a rising main. *Wat. Pollut. Control*, **76**, 98-112.

Bouwer, E. J. (1987). Theoretical investigation of particle deposition in biofilm systems. *Wat. Res.*, **21**(12), 1489-1498.

Bowman, G. T., and Delfino, J. J. (1980). Sediment oxygen demand techniques: a review and comparison of laboratory and in situ systems. *Wat. Res.*, **14**, 491-499.

Brombach, H. (1982). Zwei Experimente zum Stofftransport im Mischwasserkanal [Two experiments dealing with solids transport in a combined sewer]. *Korrespondenz Abwasser*, **29**(5), 284-291.

Buisman, C. J. N., IJspeert, P., Hof, A., Janssen, A. J. H., Ten Hagen, R., and Lettinga, G. (1991). Kinetic parameters of a mixed culture oxidizing sulfide and sulfur with oxygen. *Biotech. Bioeng.*, **38**, 813-820.

Buisman, C. J. N., IJspeert, P., Janssen, A. J. H., and Lettinga, G. (1990). Kinetics of chemical and biological sulphide oxidation in aquaous solutions. *Wat. Res.*, **245**, 667-671.

Cao, Y. S., and Alaerts, G. J. (1995). Aerobic biodegradation and microbial population in a channel with suspended and attached biomass. *Wat. Sci. Tech.*, **31**(7), 181-189.

Chapra, S. C. (1997). *Surface water-quality modeling.* McGraw-Hill, New York, USA.

Chaudhry, M. A. S., and Beg, S. A. (1998). A review on the mathematical modeling of biofilm processes: Advances in fundamentals of biofilm modeling. *Chem. Eng. Technol.*, **21**(9), 701-710.

Chu, C. R., and Jirka, G. H. (1991). Turbulent velocity and gas concentration measurements in the near-surface layer. In S. C. Wilhems and J. S. Gulliver (Eds.), *Selected papers from the second international symposium on gas transfer at water surfaces* (p. 160-172). ASCE, New York, USA.

Cirpka, O., Reichert, P., Wanner, O., Müller, S. R., and Schwarzenbach, R. P. (1993). Gas exchange at river cascades: Field experiments and model calculations. *Environ. Sci. Technol.*, **27**(10), 2086-2097.

Confer, D. R., and Logan, B. E. (1998). Location of protein and polysaccharide hydrolytic activity in suspended and biofilm wastewater cultures. *Wat. Res.*, **32**(1), 31-38.

Cooney, M. J., Roschi, E., Marison, I. W., Comninellis, C., and Von Stockar, U. (1996). Physiologic studies with the sulfate-reducing bacterium *desulfovibrio desulfuricans*: Evaluation for use in a biofuel cell. *Enzyme and Microbial Technology*, **18**(5), 358-365.

Costerton, J. W., Lewandowski, Z., DeBeer, D., Caldwell, D., Korber, D., and James, G. (1994). Biofilms, the customized microniche. *J. Bacteriology*, **176**(8), 2137-2142.

Cussler, E. L. (1997). *Diffusion: Mass transfer in fluid systems.* Cambridge University Press, Cambridge, United Kingdom. (Cambridge series in chemical engineering)

Danckwerts, P. V. (1951). Significance of liquid-film coefficient in gas adsorption. *Ind. Eng. Chem.*, **43**(6), 1460-.

Dauber, L., Novak, B., Zobrist, J., and Zürcher, F. (1982). *Quellen und Mengen der Schmutzstoffe in Regenabflüssen einer städtischen Mischkanalisation* [Sources and quantities of pollutants of an urban combined sewer during a rain event] (Vol. nr. 927). Dübendorf, Switzerland: EAWAG. (EAWAG Separatum)

Dawson, D. A., and Trass, O. (1972). Mass transfer at rough surfaces. *Int. J. Heat Mass Transfer*, **15**, 1317-1336.

DeBeer, D., Stoodley, P., and Lewandowski, Z. (1996). Liquid flow and mass transport in heterogeneous biofilms. *Wat. Res.*, **30**(11), 2761-2765.

DiToro, D. M., Paquin, P. R., Subburamu, K., and Gruber, D. (1990). Sediment oxygen demand model: methane and ammonia oxidation. *J. Env. Engrg., ASCE*, **116**(5), 945-986.

Dobbins, W. E. (1964). Mechanism of gas adsorption by turbulent liquids. In W. W. Eckenfelder (Ed.), *Advances in water pollution research, proc. int. conf. London, September 1962* (Vol. 2, p. 61-76). Pergamon Press, Oxford, United Kingdom.

Doyle, M. L., and Boyle, W. C. (1986). Translation of clean to dirty water oxygen transfer rates. In W. C. Boyle (Ed.), (p. 48-64). Noyes Publishers, Park Ridge, N.J., U.S.A.

Ehrlich, H. L. (1996). *Geomicrobiology.* Dekker cop., New York.

Elmore, H. L., and West, W. F. (1961). Effect of water temperature on stream reaeration. *J. Sanit. Engrg. Div., ASCE*, **87**(SA6), 59-71.

Fortescue, G. E., and Pearson, J. R. A. (1967). On gas absorption into a turbulent liquid. *Chem. Engrg. Sci.*, **22**, 1163-1176.

French, R. H. (1985). *Open-channel hydraulics.* McGraw-Hill, New York, USA.

Friedmann, B. F., and Blanc, F. C. (1991). Measurement of stream reaeration rate coefficients using propane gas. In S. C. Wilhems and J. S. Gulliver (Eds.), *Selected papers from the second international symposium on gas transfer at water surfaces* (p. 322-332). ASCE, New York, USA.

Fuseler, K., Krekeler, D., Sydow, U., and Cypionka, H. (1996). A common pathway of sulfide oxidation by sulfate reducing bacteria. *FEMS-Microbiology letters*, **144**, 129-134.

Gantzer, C. J., Rittmann, B., and Herricks, E. E. (1991). Effect of long-term water velocity changes on streambed biofilm activity. *Wat. Res.*, **25**(1), 15-20.

Garsdal, H., Mark, O., Dørge, J., and Jepsen, S. E. (1995). Mousetrap: modelling of water quality proceses and the interaction of sediments and pollutants in sewers. *Wat. Sci. Tech.*, **31**(7), 33-41.

Gjaltema, A. (1996). *Biofilm development: Growth versus detachment.* Doctoral dissertation, Delft University of Technology, Delft, The Netherlands.

Green, M., Shelef, G., and Messing, A. (1985). Using the sewerage system main conduits for biological treatment. *Wat. Res.*, **19**, 1023-1028.

Gujer, W., and Boller, M. (1985). Design of a nitrifying tertiary trickling filter based on theoretical concepts. *Wat. Res.*, **20(11)**, 1353-1362.

Gujer, W., Henze, M., Mino, T., and Van Loosdrecht, M. (2000). *Activated sludge model no. 3* (IWA Scientific and Technical Report No. 9). ISBN 1 900222 24 8, ISSN 1025-0913: IWA Publishing, London, UK.

Gujer, W., Henze, M., Mino, T., and Van Loosdrecht, M. C. M. (1999). Activated sludge model no. 3. *Wat. Sci. Tech.*, **39**(1), 183-193.

Gujer, W., Krejci, V., and Fleckseder, H. (1983). Tropfkörper und Tauchtropfkörper bei kleinen Abwasserreinigungsanlagen [Trickling filters und submersed filters at small wastewater treatment plants]. *Gas-Wasser-Abwasser*, **63(7)**, 330-341.

Gujer, W., and Larsen, T. (1995). The implementation of biokinetics and conservation principles in ASIM. *Wat. Sci. Tech.*, **31**, 257-266.

Gutekunst, B. (1988). *Sielhautuntersuchungen zur Einkreisung schwermetallhaltiger Einleitungen* [Sewer biofilm investigations to locate the inflow of heavy metals] (Vol. 49). Doctoral dissertation, ISWW, Karlsruhe, Germany. (Schriftenreihe des ISWW Karlsruhe)

Hager, W. H. (1995). *Abwasserhydraulik* [Wastewater hydraulic]. Springer-Verlag, Berlin, Germany.

Hald, W. (1952). *Statistical theory with engineering applications.* John Wiley and Sons, Inc., New York, USA.

Hamilton, W. A. (1995). Biofilms and microbially influenced corrosion. In H. M. Lappin-Scott and J. W. Costerton (Eds.), *Microbial biofilms* (Vol. 5, p. 171-182). Cambridge University Press, Cambridge, UK.

Hanel, R. (1982). *Der Sauerstoffeintrag und seine Messung beim Belebungsverfahren unter besonderer Beachtung der Viskosität und Oberflächespannung* [The oxygen transfer and its measurement in the activated sludge system with special attention to the viscosity and the surface tension] (Vol. 13). Doctoral dissertation, Institut für Wasserversorgung, Abwasserbeseitigung und Raumplanung der Technischen Hochschule Darmstadt. (WAR)

Hao, O. J., Chen, J. M., Huang, L., and Buglass, R. L. (1996). Sulfate-reducing bacteria. *Critical reviews in environmental science and technology*, **26**(2), 155-187.

Harremoës. (1983). The applicability of biofilm kinetics to rotating biological contactors. In *Rotating biological contactors, International EWPCA-IAWPRC Seminar* (Gesellschaft zur Förderung der Abwassertechnik, e.V. (GFA) Germany ed., p. 43-58). VCH, Deutsche Forschungsgemeinschaft.

Henderson, F. M. (1966). *Open channel flow.* Macmillan, cop., New York, USA. (Macmillan series in Civil Engineering)

Henze, M. (1987). Theories for estimation of fraction of denitrifiers in combined nitrifying-denitrifying treatment plants. *Wat. Res.*, **23**, 1521-1524.

Henze, M. (1992). Characterization of wastewater for modelling of activated sludge processes. *Wat. Sci. Tech.*, **25**(6), 1-15.

Henze, M., Gujer, W., Mino, T., Matsuo, T., Wentzel, M. C., and Marais, G. v. R. (1995). Activated sludge model No. 2. In *IAWQ scientific and technical report no. 3.* IAWQ, London, UK.

Heukelekian, H., and Balmat, J. L. (1959). Chemical composition of particulate fractions of domestic sewage. *Sewage and industrial wastes*, **31**, 413-423.

Hickey, C. W. (1988). Benthic chamber for use in river: Testing against oxygen mass balance. *J. Env. Eng.*, **114**(4), 828-845.

Higbie, R. (1935). On the adsorption of a pure gas into a still liquid during short period of exposure. *Trans. Am. Inst. Chem. Eng.*, **31**, 365-.

Hines, M. E., Visscher, P. T., and Devereux, R. (1997). Sulfur cycling. In C. J. Hurst (Ed.), *Manual of environmental microbiology.*

Hofer, M. (1998). *Bestimmung von SF_6 in Wasser* [Determination of SF_6 in water] (Standard-Arbeitsanweisung No. SAA:1/1). EAWAG, Dübendorf, Switzerland.

Hughes, K., Sutherland, I., and Jones, M. (1998). Biofilms susceptibility to bacteriophage attack: the role of phage-borne polysaccharide depolymerase. *Microbiology*, **144**, 3039-3047.

Huisman, J. L., Burckhardt, S., Larsen, T. A., Krebs, P., and Gujer, W. (2000). Propagation of waves and dissolved compounds in a sewer. *J. Env. Eng., ASCE*, **126**(1), 12-20.

Hunt, J. C. R. (1984). Turbulence structure and turbulent diffusion near gas liquid interfaces. In J. G. Brutsaert W (Ed.), *Gas transfer at water surfaces* (p. 67-82). Reidel, Boston, USA.

Hunter, J. V., and Heukelekian, H. (1965). The composition of domestic sewage fractions. *J. WPCF*, **37**(8), 1142-1163.

ISO. (1983). *Measurement of liquid flow in open channels.* International Organization for Standardization, Geneva, Switzerland. (ISO Standards Handbook 16)

Jähne, B., Heinz, G., and Dietrich, W. (1987). Measurement of the diffusion coefficients of sparingly soluble gases in water. *J. Geophys. Res., C: Oceans*, **92**(C10), 10767-10779.

James, A. (1974). The measurement of the benthic respiration. *Wat. Res.*, **8**, 955-959.

Jensen, N. A. (1995). Emperical modelling of air-to-water oxygen transfer in gravity sewers. *Water Environ. Res.*, **67**(6), 979-991.

Jensen, N. A., and Hvitved-Jacobsen, T. (1990). Tracer measurements of reaeration in gravity sewers. *Wat. Sci. Tech.*, **22**(10/11), 279-282.

Jensen, N. A., and Hvitved-Jacobsen, T. (1991). Method for measurements of reaeration in gravity sewers using radio-tracers. *Res. J. Water Pollut. Control Fed.*, **63**(5), 758-767.

Jørgensen, S. E., Halling-Sørensen, S., and Nielsen, S. N. (Eds.). (1996). *Handbook of environmental and ecological modeling.* CRC Lewis Publishers, cop., Boca Raton, USA.

Kappeler, J., and Gujer, W. (1992). Estimation of kinetic parameters of heterotrophic biomass under aerobic conditions and characterization of wastewater for activated sludge modelling. *Wat. Sci. Tech.*, **25**(6), 125-139.

Keevil, C., Rogers, J., and Walker, J. (1995). Potable-water biofilm. *Microbiol. Eur.*, **3**, 10-14.

King, D. B., and Saltzman, E. S. (1995). Measurement of the diffusion coefficient of sulfur hexafluoride in water. *J. Geophys. Res., Oceans*, **100**(C4), 7083-7088.

Knuth, D. E. (1984). *The TEXbook.* Addison-Wesley, Reading, Mass., USA.

Koch, C. M., and Zandi, I. (1973). Use of pipelines as aerobic biological reactors. *J. WPCF*, **45**, 2537.

Koch, G., M, K., Gujer, W., and Siegrist, H. (2000). Calibration and validation of activated sludge model No. 3 for Swiss municipal wastewater. *Wat. Res., Submitted and accepted.*

Kögel, B., Moser, F., and Pointer, H. (1981). *Grundlagen der Verfahrenstechnik* [Basics of process engineering]. Springer Verlag, Wien.

Kölling, C. (1994). *Finite-Element-Simulation der Geschwindigkeitsverteilung in Kanälen und teilgefüllten Rohrleitungen* [Finite element simulaton of the velocity distribution is channels and partly filled pipes]. Doctoral dissertation, Mitteilungshefte des Lehrstuls für hydraulik und Gewässerkunde der Technischen Universität München, Nr. 60, München, Germany.

Krenkel, P. A., and Orlob, G. T. (1962). Turbulent diffusion and the reaeration coefficient. *J. San. Eng. Div., ASCE*, **88**, 53-83.

Kühl, M., and Barker-Jørgensen, B. (1992). Microsensor measurement of sulphate reduction and sulphide oxidation in compact microbial communities of aerobic biofilms. *Appl. Env. Microbiol.*, **58**(4), 1164-1174.

Lamont, J. C., and Scott, D. S. (1970). An eddy modell of mass transfer into the surface of a turbulent liquid. *A.I.Ch.E. J.*, **16**(4), 513-519.

Lamport, L. (1986). *LATEX: A document preparation system.* Addison-Wesley, Reading, Mass., USA.

Larsen, T. A., and Gujer, W. (1996). Separate management of anthropogenic nutrient solutions (human urine). *Wat. Sci. Tech.*, **34**(3-4), 87-94.

Larsen, T. A., and Harremoës, P. (1994). Combined reactor and microelectrode measurements in laboratory grown biofilm. *Wat. Res.*, **28**(6), 1435-1441.

Lemmer, H., Roth, D., and Schade, M. (1994). Population density and enzyme activities of heterotrophic bacteria in sewer biofilms and activated sludge. *Wat. Res.*, **28**(6), 1341-1346.

Lengeler, J. W., Drews, G., and Schlegel, H. G. (Eds.). (1999). *Biology of prokaryotes.* Thieme, Stuttgart, Germany.

Levenspiel, O. (1972). *Chemical reaction engineering* (2nd. ed.). Wiley, New York, USA.

Levine, A. D., Tchobanoglous, G., and Asano, T. (1985). Characterization of size distribution of contaminants in wastewater treatment and reuse applications. *J. WPCF*, **57**, 805-816.

Lewis, W. K., and Whitman, W. G. (1924). Principles of gas adsorption. *Ind. Engng. Chem.*, **16**(12), 1215-.

MacKay, D., and Yeun, A. T. K. (1983). Mass transfer coefficient correlations for volatilization of organic solutes from water. *Environ. Sci. Technol.*, **17**(4), 211216.

MacKay, D., and Yeun, T. K. (1980). Volatilization rates of organic contaminants from rivers. *Water Pollut. Res. J. Can.*, **15**(2), 83-98.

Manandhar, U. K., and Schroder, H. (1995). Sewage circulating reactor: an approach to recirculating wastewater in sewers. *Environmental Technology*, **16**(3), 201-211.

Marr, A., Nilson, E., and DJ, C. (1963). The maintenance requirement of Escherichia coli. *Ann. NY Acad. Sci.*, **102**, 526-548.

Matthews, P. J. (1976). Growth characteristics of sewer slime. *Envir. Pollut.*, **10**, 79-88.

Maurer, M., Fux, C., and Siegrist, H. (1999). Modelling denitrification in a moving bed of porous carriers from a low-loaded wastewater treatment plant. *Wat. Sci. Tech.*, **39**(7), 251-259.

May, P. (1939). Ist die Sielhaut in Entwässerungsleitungen ein wirksamer Werkstoffschutz? [Is the slime layer an effective protection of the construction material?]. *Gesundheitsingenieur*, **62**(16), 227-230.

McDonald, J. P., and Gulliver, J. S. (1991). Methane tracer technique for gas transfer at hydraulic structures. In S. C. Wilhems and J. S. Gulliver (Eds.), *Selected papers from the second international symposium on gas transfer at water surfaces* (p. 267-277). ASCE, New York, USA.

Montgomery. (1989). In R. H. French (Ed.), *Water quality modeling: Transport and surface exchange in rivers* (Vol. 1, p. 244-). CRC Press, Boca raton, Florida, USA.

Moog, D. B., and Jirka, G. H. (1999). Air-water gas transfer in uniform channel flow. *J. Hydr. Engrg., ASCE*, **125**(1), 3-10.

Müller, G., and Bartocha, W. (1978). Zur Frage der Entstehung von Bakterien über Belebungsanlagen auf Kläranlagen [To the question of the formation of bacteria over the aeration basin in wastewater treatment plants]. *Bundesgesundheitsblatt*, **21**(2), 21.

Nezu, I., and Nakagawa, H. (1993). *Turbulence in open-channel flows.* Balkema, Rotterdam, The Netherlands. (IAHR-AIRH Monograph)

Nielsen, P. H. (1987). Biofilm dynamics and kinetics during high-rate sulfate reduction under anaerobic conditions. *Appl. Environ. Microbiol.*, **53**, 27-.

Nielsen, P. H. (1991). Sulfur sources for hydrogen sulfide production in biofilms from sewer systems. *Wat. Sci. Tech.*, **23**, 1265-.

Nielsen, P. H., Raunkjær, K., Norsker, N. H., Jensen, N. A., and Hvitved-Jacobsen, T. (1992). Transformations of wastewater in sewer systems - a review. *Wat. Sci. Tech.*, **25**(6), 17-31.

Nikuradse, J. (1933). Strömungsgesetze in rauhen Rohren [Hydrodynamic laws in rough channels]. In *Forsch. Gebiet Ing.-Wes.* (Vol. Heft 361). Berlin, Germany.

Norsker, N. H., Nielsen, P. H., and Hvitved-Jacobsen, T. (1995). Influence of oxygen on biofilm growth and potential sulfate reduction in gravity sewer biofilm. *Wat. Sci. Tech.*, **31**(7), 159-167.

Nowell, A. R. M., and Jumars, P. A. (1984). Flow environments of aquatic benthos. *Ann. Rev. Ecol. Syst.*, **15**, 303-328.

Obst, U., and Holzapfel-Pschorn, A. (1988). *Enzymatische Schnelltest für die Wasseranalytik* [Rapid enzymatic test for water analysis] (Vol. 1). Oldenbourg, Wien, Austria.

O'Conner, D. J., and Dobbins, W. E. (1958). Mechanism of reaeration in natural streams. *Trans. Am. Soc. Civil Engr*, **123**, 641-666.

Odom, J. M. (1993). Industrial and environmental activities. In J. M. Odom and R. J. Singleton (Eds.), *The sulphate-reducing bacteria: Contemporary perspectives.* Brock/Springer, New York.

Okabe, S., Itoh, T., Satoh, H., and Watanabe, Y. (1999). Analyses of spatial distributions of sulfate-reducing bacteria and their activity in aerobic wastewater biofilms. *Appl. Environ. Microb.*, **65**, 5107-5116.

Omil, F., Lens, P., Visser, A., Hulshoff Pol, L. W., and Lettinga, G. (1998). Long-term competition between sulfate reducing and methanogenic bacteria in UASB reactors treating volatile fatty acids. *Biotech. Bioeng.*, **57**(6), 676-685.

Owens, M., Edwards, R. W., and Gibbs, J. W. (1964). Some reaeration studies in streams. *Int. J. Air Wat. Poll.*, **8**, 469-486.

Painter, H. A., and Viney, M. (1959). Composition of domestic sewage. *J. Biochem. Technol. Eng.*, **1**, 143-162.

Pan, Y., and Banerjee, S. (1995). A numerical study of free-surface turbulence in channel flow. *Phys. Fluids*, **7**(7), 1649-1664.

Parkhurst, J. D., and Pomeroy, R. D. (1972). Oxygen absorption in streams. *J. San. Eng. Div.*, **98**(SA1), 101-124.

Perry, R. H., Green, D., and Maloney, J. O. (Eds.). (1984). *Perry's Chemical Engineers' Handbook* (6th ed.). McGraw-Hill, New York, USA.

Pescod, M. B., and Price, A. C. (1982). Major factors in sewer ventilation. *J. WPCF*, **54**(4), 385-397.

Petzold, L. (1983). A description of DASSL: A differential/algebraic problem solver. In R. E. Stepleman (Ed.), *Scientific computing* (p. 65-68). IMACS/North Holland, Amsterdam.

Pomeroy, R. D., and Parkhurst, J. D. (1973). Self-purification in sewers. In S. H. Jenkins (Ed.), *Proc. 6th Int. Conf. on Advances in Water Pollution Research, Jerusalem, June 18-23, 1972* (p. 291-306). Pergamon Press.

Ponce, V. M., Li, R. M., and Simons, D. B. (1978). Applicability of kinematic and diffusion models. In *Verification of Math. and Phys. Models in Hydr. Engrg., Proceedings, 26th Annual ASCE Hydraulics Division Specialty Conference, College Park, Maryland, U.S.A.* (p. 605-613).

Preiss, J. (1989). Chemistry and metabolism of intracellular reserves. In J. Pointdexter and E. Leadbetter (Eds.), *Bacteria in nature, structure, physiology and genetic adaptability* (p. 189-258).

Rathbun, R. E., Stephens, D. W., Schultz, D., and Tai, D. Y. (1978). Laboratory studies of gas tracers for reaeration. *J. Env. Engrg Div., ASCE*, **104**(EE2), 215-229.

Raunkjær, K. (1993). *Characterization and transformation of wastewater organic matter in sewer systems.* Doctoral dissertation, Aalborg University, Aalborg, Denmark.

Raunkjær, K., Hvitved-Jacobsen, T., and Nielsen, P. H. (1994). Measurement of pools of protein, carbohydrate and lipid in domestic wastewater. *Wat. Res.*, **28**(2), 251-262.

Raunkjær, K., Hvitved-Jacobsen, T., and Nielsen, P. H. (1995). Transformation of organic matter in a gravity sewer. *Water Environ. Res.*, **67**(2), 181-188.

Reichert, P. (1994). Aquasim - a tool for simulation and data analysis of aquatic systems. *Wat. Sci. Tech.*, **30**(2), 21-30.

Reichert, P. (1998). *Aquasim 2.0 - user manual.* Swiss Federal Institute for Environmental Science and Technology (EAWAG), CH-8600 Dübendorf, Switzerland.

Reiff, H. (1991). *Schmutzstöße infolge Sielhautabtrag* [Pollutant load as a result of slime layer erosion] (Vol. 7). Doctoral dissertation, Fachgebietes Siedlungswasserwirtschaft, Universität Kassel, Kassel, Germany. (Wasser-Abwasser-Abfall)

Reiff, H. (1992). Wachstum und Abtrag der Sielhaut in Mischwasserkanaelen [Growth and erosion of the slime layer in combined sewers]. *Wasser-Abwasser-Abfall*, **9**.

Reye, G., and Bleibtreu, E. (1940). Ist die Sielhaut ein wirksamer Werkstoffschutz? [Is the slime layer an effective protection of construction material?]. *Gesundheits-Ingenieur*, **63**(48), 620-621.

Rittmann, B. E. (1989). Detachement from biofilms. In W. G. Characklis and P. A. Wilderer (Eds.), *Structure and function of biofilms* (p. 49-58). Dalhem workshop report, John Wiley & Sons, New York, USA.

Rittmann, B. E., and McCarty, P. L. (1981). Substrate flux into biofilms of any thickness. *J. Env. Eng. ASCE*, **EE4**, 831-849.

Roeck, C., and Rufer, R. (1994). *Denitrifikationsleistung bei unterschiedlichen Betriebs- und Belastungszuständen* [Denitrification capacity at various conditions of operation and load]. Unpublished master's thesis, IHW at the Swiss Federal Instute of Technology (ETH), Zürich, Switzerland.

Roth, D., Lemmer, H., and Pujol, R. (1994). Biofilms in sewer systems - characterization of the bacterial biocenosis and its metabolic activity. *Wat. Sci. Tech.*, **29**(7), 385-388.

Schlatter, J. W. (1991). *Schwefelhexafluoride als Tracer zum Studium von Mischungsprozesse in Seen* [Sulphurhexafluoride as tracer for the study of mixing processes in lakes]. Doctoral dissertation, Swiss Federal Institute of Technology (EAWAG) and Swiss Federal Institute of Technology Zürich (ETHZ), Zürich, Switzerland.

Schlegel, H. G. (1986). *General microbiology.* The University Press, Cambridge, UK.

Schnur, R. (1940). Ist die Sielhaut in Entwässerungsleitungen ein wirksamer Werkstoffschutz? [Is the slime layer in sewers an effective protection of the construction material?]. *Gesundheits-Ingenieur*, **63**(7), 78-80.

Shanahan, P., Borchardt, D., Henze, M., Rauch, W., Reichert, P., Somlyódy, L., and Vanrolleghem, P. (2000). River water quality model No.1: I. Modelling approach. *Submitted to Wat. Sci. Tech.*

Siegrist, H. (1985). *Stofftransportprozze in festsitzender Biomasse* [Mass transfer processes in attached biomass] (Vol. Nr. 7726). Doctoral dissertation, EAWAG/ETHZ, Zürich, Switzerland.

Siegrist, H., and Gujer, W. (1985). Mass transfer mechanisms in a heterotrophic biofilm. *Wat. Res.*, **19**(11), 1369-.

Skelland, A. H. P. (1974). *Diffusional mass transfer.* Wiley, New York, USA.

Steudel, R. (1996). Mechanism for the formation of elemental sulfur from aqueous sulfide in chemical and microbiological desulfurization processes. *Ind. Eng. Chem. Res.*, **35**, 1417-1423.

Streeter, H. W., and Phelps, E. B. (1925). A study of the pollution and natural purification of the Ohio river. *Bull. U.S. punl. Hlth Serv.*, **No. 146**.

Taghizadeh-Nasser, M. (1986). *Materieöverföring gas vätska i avloppsledningar* [Gas-water mass transfer in sewers] (Vol. Publ. 3:86). Unpublished master's thesis, Clamer Univ. of techn. and Dep. San. Eng., Sweden.

Tanaka, N., and Hvitved-Jacobsen, T. (1998). Transformations of wastewater organic matter in sewers under changing aerobic/anaerobic conditions. *Wat. Sci. Tech.*, **37**(1), 105-113.

Theofanous, T. G., Houze, R. N., and Brumfield, L. K. (1976). Turbulent mass transfer at free, gas-liquid interfaces, with applications to open-channel, bubble and jets flows. *Int. J. Heat Mass Transfer*, **19**, 613-624.

Tijhuis, L. (1994). *The biofilm airlift suspension reactor.* Doctoral dissertation, Delft University of Technology, Delft, The Netherlands.

Tsivoglou, E. C. (1968). Tracer measurement of stream reaeration: II. Field studies. *J. WPCF*, **77**(2), 249-262.

Tsivoglou, E. C., and Neal, L. A. (1976). Tracer measurement of reaeration. iii predicting the reaeration capacity of inland streams. *J. WPCF*, **48**(12), 2669-.

Tsivoglou, E. C., O'Connell, R. L., Walter, C. M., Godsil, P. J., and Logsdon, G. S. (1965). Tracer measurement of atmospheric reaeration - I. Laboratory studies. *J. WPCF*, **37**, 1343-1363.

VandenEnde, F. P., Meier, J., and Van Gemerden, H. (1997). Syntrophic growth of sulfate-reducing bacteria and colorless sulfur bacteria during oxygen limitation. *FEMS Microbiology Ecology*, **23**, 65-80.

Verbanck, M. A. (1995). Capturing and releasing settable solids - the significance of dense undercurrents in combined sewer flows. *Wat. Sci. Tech.*, **31**(7), 85-93.

Visser, A., Hulshof Pol, L. W., and Lettinga, G. (1996). Competition of methanogenic and sulfidogenic bacteria. *Wat. Sci. Tech.*, **33**(3), 99-110.

Vollertsen, J., Almeida, M., and Hvitved-Jacobsen, T. (1999a). Effect of temperature and dissolved oxygen on hydrolysis of sewer solids. *Wat. Res.*, **33**(14), 3119-3126.

Vollertsen, J., and Hvitved-Jacobsen, T. (1999). Stoichiometric and kinetic model parameters for microbial transformations of suspended solids in combined sewers. *Wat. Res.*, **33**(14), 3127-3141.

Vollertsen, J., Hvitved-Jacobsen, T., McGregor, I., and Ashley, R. (1999b). Aerobic microbial transformations of pipe and silt trap sediments from combined sewers. *Wat. Sci. Tech.*, **39**(2), 233-249.

Wanner, O., and Reichert, P. (1996). Mathematical modeling of mixed-culture biofilms. *Biotechnol. Bioeng.*, **49**, 172-184.

Wanninkhof, R., Ledwell, J., and Crusius, J. (1991). Gas transfer velocities on lakes measured with sulfur hexafluoride. In S. C. Wilhems and J. S. Gulliver (Eds.), *Selected papers from the second international symposium on gas transfer at water surfaces* (p. 441-458). ASCE, New York, USA.

Watson, A. J., and Liddicoat, M. I. (1985). Recent history of atmospheric trace concentrations deduced from measurements in the deep sea: application to sulfur hexafluoride and carbon tetrachloride. *Atm. Environ.*, **19**, 1477-1484.

Whitmore, A., and Corsi, R. L. (1994). Measurement of gas-liquid mass transfer coefficients for volatile organic compounds in sewers. *Environmental Progress*, **13**(2), 114-123.

Whittemore, R. C., and Krause, D. K. J. (1991). A gas chromatographic protocol for the measurement of krypton gas in water. In S. C. Wilhems and J. S. Gulliver (Eds.), *Selected papers from the second international symposium on gas transfer at water surfaces* (p. 309-317). ASCE, New York, USA.

Wilcock, R. J. (1984). Methyl chloride as a gas-tracer for measuring stream reaeration coefficients - I. Laboratory studies. *Wat. Res.*, **18**(1), 47-52.

Wöhrle, C., and Brombach, H. (1991). Probenahme im Abwasserkanal [Sampling in the sewer]. *Wasserwirtschaft*, **81**(2), 60-65.

Zhang, T. C., and Bishop, P. (1994). Evaluation of tortuosity factors and effective diffusivities in biofilms. *Wat. Res.*, **28**, 2279-2287.

A Additional Materials and Methods

A.1 Enzyme activity measurements

A.1.1 α- and β-Glucosidases

An adapted method after Obst and Holzapfel-Pschorn (1988) (with thanks to M. Maurer)

Introduction

α-Glucosidase degrades maltose and sucrose (α-glucose-oligomer, products of amylases). β-Glucosidase hydrolyses the disaccharide cellobiose, which is a product of the degradation of cellulose, under the formation of glucose (Schlegel, 1986). Photometric measurement of enzyme activities can be done with the help of nitrophenyl derivates of α-, or β-glucopyranoside as substrate. The enzymatically released *p*-nitrophenol has a yellow colour. The intensity of the colour is linear related to the concentration. The measurements are done under alkaline conditions because the protonated form has a much lower solubility than the deprotonated. The *p*Ks of nitrophenol is 7.6. *p*-Nitrophenol is poisonous to the cell (mutagenic!) Therefore, the maximum final concentration of *p*-nitrophenol should not be higher than 20 mg·L^{-1} to avoid inhibition of the bacterial activity.

Reagents

- **0.02 M MOPS buffer:** 4.1854 g 3-morpholino-propansulphonacid ($C_7H_{15}NO_4S$, pK_S = 7.2), 0.800 g sodium hydroxide (NaOH) and 5.8 g sodium chloride (NaCl) is dissolved in 1 L of sterile filtered demineralised water (e.g. Nanopur). The pH of the solution should be 7.2.
- **0.14 M sodium chloride solution:** 0.818 g sodium chloride (NaCl) is dissolved in 100 mL sterile filtered demineralised water (e.g. Nanopur).
- **Substrate solution:** 25 mg *p*-Nitrophenyl-α-D-glucopyranoside or 25 mg *p*-nitrophenyl-β-D-glucopyranoside is dissolved in 50 mL of buffer (= 500 mg·L^{-1}) and stored cool and in the dark. The substrate concentration should be doubled (1000 mg·L^{-1}) when the enzyme activity is high. This to ensure that enzyme saturation is achieved. The solution can be kept for 24 hours.
- **1 M sodium carbonate solution:** 10.6 g dehydrated sodium carbonate (Na_2CO_3) is dissolved in 100 mL sterile filtered demineralised water (e.g. Nanopur).
- ***p*-Nitrophenol standards:** • *Stock solution 1:* 150 mg *p*-nitrophenol is dissolved in 50 mL sterile filtered demineralised water (e.g. Nanopur). • *Stock solution 2:* to 0.5 mL of stock solution 1, buffer is added to reach a total volume of 50 mL (0.03 g·L^{-1}). The calibration solutions consist of 2 mL sodium chloride solution and the appropriate amount of stock solution 2, filled up with buffer to 4 mL (see table A.1). The standards should undergo the same procedure as the samples.

Table A.1: The composition of the nitrophenol standards.

final nitrophenol conc.		stock sol. 2	buffer
[µM]	[mg·L^{-1}]	[mL]	[mL]
0	0	0	2
26.7	3.75	0.5	1.5
53.9	7.5	1	1
80.9	11.25	1.5	0.5
107.8	15	2	0

Procedure

2 mL of the (raw) sample and 2 mL of the substrate solution are put in a centrifuge tube and are mixed well (vortex stirrer). The photometric blank consist of 2 mL sodium chloride solution and 2 mL substrate solution. The tubes are incubated at room temperature in a shaker for 30 to 240 minutes, depending on the enzyme activity. The reaction is stopped by putting the tubes one minute in boiling water or 1.5 minutes in a heating block at 150°C. Subsequently, the suspended material is removed by centrifuging. Then, 1 mL sodium carbonate solution is added and the absorption is measured immediately at 400 nm against the blank.

A.1.2 Esterases

A adapted method after Obst and Holzapfel-Pschorn (1988) (with thanks to M. Maurer)

Introduction

Fluoresce-indiacetate can be converted by a large number of extracellulair esterases, proteases and lipases from a wide range of organisms as water insoluble substrate. The product of this reaction is apart from acetate the coloured component fluorescein (also known as uranine, pK_{S1} = 2.2, pK_{S2} = 4.4, pK_{S3} = 6.7). This component can be measured photometrically at 490 nm (molar extinction coefficient $e = 8 \cdot 10^4$ $M^{-1} \cdot cm^{-1}$). The enzymatic fluoresce-indiacetate hydrolysis is to a large extent oxygen independent.

Reagents

- 0.02 M MOPS buffer: See page 151.
- 0.14 M sodium chloride solution: See page 151.
- 1 M sodium carbonate solution: See page 151.
- Substrate solution: 100 mg fluoresce-indiacetate is dissolved in 100 mL acetone (quality: *per analysis*) and stored in a closed container at -18°C. This way, the solution can be kept several months.
- Fluorescein standards • *Stock solution 1*: 450 mg fluorescein sodium salt ($C_{20}H_{10}Na_2O_5$, uranine) is dissolved in 250 mL sterile filtered demineralised water (e.g. Nanopur). (=1800 mg·L^{-1}). • *Stock solution 2*: 0.5 mL stock solution 1 is mixed with 250 mL buffer (0.9 mg·mL^{-1} Fluorescein sodium salt = 2.392 mmol·mL^{-1} = 2.39 mM = 900 mg·L^{-1}) The calibration solution consists of 1 mL sodium chloride solution and the appropriate amount of stock solution 2, filled up with buffer to 5 mL (see table A.2).

The standards should undergo the same procedure as the samples.

Procedure

1 mL of the (raw) sample, 4 mL buffer and 40 mL of the substrate solution are put in a centrifuge tube and well mixed (vortex stirrer). The photometric blanks consist of 1 mL (raw) sample with 4 mL buffer and of 40 mL substrate solution with 5 mL buffer. The tubes are incubated at room temperature (20 to 25°C) in a shaker for 30 to 240 minutes, depending on the enzyme activity ($\approx$ 60 minutes for wastewater). The reaction is stopped by putting the tubes in boiling water or in a heating block (1 min 20 sec. at a heating block temperature of 150°C to heat up the solution to 80°C). Subsequently, the suspended material is removed by centrifuging and the absorption is measured at 490 nm against the blank.

A.2 Search for a suitable biofilm substratum

Plates that were installed in the sewer have been used to obtain intact biofilm samples for laboratory measurements (see section 4.3.3). This section describes the tests that were done to find a suitable material and surface treatment.

Polyetheneteraphthalate (PET) , polycarbonate (PC), Polypropylene (PP) and stainless steel (AISI Type 316; Composition in Wt. %: C = 0.08, Cr = 17, Fe = 65, Mn = 2, Mo = 2.5, Ni = 12, P = 0.045, S = 0.03, Si= 1) were tested. The surface was either treated mechanically or chemically. The physical treatments should give the biofilm the opportunity to anchor itself into cavities. The treatment consisted of sanding with different types of commercial products (see table A.3). The surfaces were treated in horizontal and vertical direction. The chemical treatments were based on the hypothesis that an oxidised surface would have a stronger physical-chemical interaction with the bacteria. The surfaces were oxidised with a mixture of concentrated sulphuric acid and dichromate, with hot hypochloric acid or by arch oxidation. A further chemical treatment was the carbonisation of the surface. The plates were subdivided in four sections that received either chemical or physical surface treatments or no treatment. The suitability of a certain material-surface treatment combination was tested by determining the amount of biofilm formed on the surface after three weeks in the sewer. Table A.4 gives an overview of the results.

Polypropylene (PP) was the least suitable material because the biofilm easily loosened from the surface. The best results were obtained with polycarbonate (PC), treated with a rotating steel brush (type *B*). The difference between the sanding products was astonishing, because

Table A.2: The mixing ratio for the fluorescein standards.

final fluorescein conc.		Stock sol. 2	Buffer
[μM]	[mg·L^{-1}]	[mL]	[mL]
0	0	0	4
1.91	0.68	1	3
3.83	1.35	2	2
5.74	2.03	3	1
7.65	2.7	4	0

Table A.3: Overview of the surface treatment for different materials.

Identification	Name	diameter [mm]	Material	Brand and Model nr.
A	*sanding nylon*	75	Nylon, K80	COOP 153640
B	*shaft brush*	23	Steel, 0.3 mm	COOP 610004
C	*shaft brush*	50	Brass, 0.2 mm	COOP 153643
D	*shaft brush*	75	SiC 80	Bosch 2 608 622 051
E	*sandpaper*	60	Size '120'	Bosch 2 609 200 185

Table A.4: The biomass growth on plate material (thickness: 1 mm) with different surface treatments. For A to E see table A.3.

Material: **PC** Method	$m_{organic}$ g/m^2	Material: **PP** Method	$m_{organic}$ g/m^2	Material: **PET** Method	$m_{organic}$ g/m^2
Aceton	36	A	38	Aceton	51
H_2SO_4/Cr_2O_4	44	B	43	H_2SO_4/Cr_2O_4	33
A	30	B	44	A	41
B	32	C	42	B	35
B	40	D	27	B	40
D	18	E	28	D	38
Untreated	16	Untreated	23	Untreated	31
Stainless Steel, untreated		28 g/m^2			

no apparent differences in the surface roughness could be observed with the naked eye. The chemical treatments did not enhance the biofilm formation much in comparison to the untreated surface. The plasma oxidation and carbonisation yielded good results, but these treatments were expensive, laborious and the treatable area was small. Polyetheneteraphthalate (PET) was unsuited because it deformed under sewer conditions.

It could be concluded from these tests that polycarbonate (PC) plates roughened with brush *B* (see table A.3) gave the best results. Consequently, this set-up was used for the experiments.

A.3 Sewer *in situ* flow cell

A.3.1 Design of the measurement chamber

The design of the measurement chamber for the *in situ* activity measurement is shown in figure A.1. A rubber gasket with a large deformation capacity along the outer edge of the cell isolated the medium in the cell from the surrounding wastewater. Another, thinner and more flexible gasket was fixed around the measurement area to avoid water exchange with dead zones. The pressure required to held the flow cell in place and to get a tight connection is delivered by an extendable bar pressed against the other side of the sewer pipe; a similar construction as was used for the biofilm sample box (see right hand side in figure 4.2).

The recirculated water entered the cell under an angle of 90°(see figure 4.9 for the complete system) which forced the water to divert itself over the whole width of the inflow section. The biofilm under the inlet section is protected from the flow by a tinplate. The flow is equalised

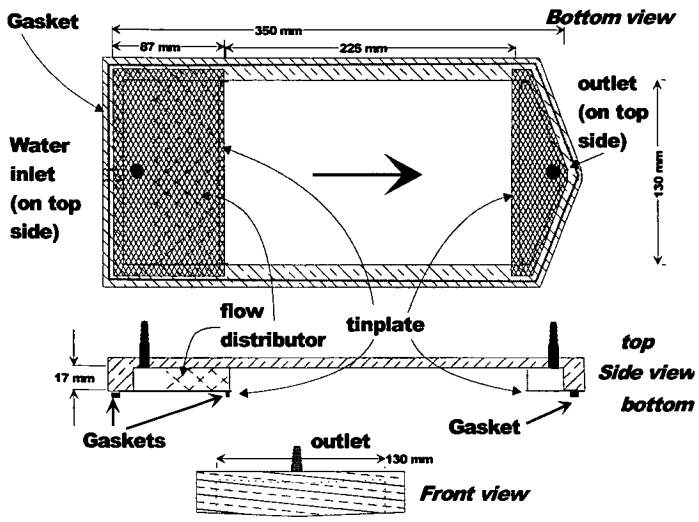

Figure A.1: Dimensions of the in situ flow cell for use in a 0.9 m diameter sewer pipe.

further as it passes through four perforated stainless steel plates. The height difference between the measurement chamber and the biofilm due to the gasket is bridged with the slightly ramped cover plate of the inflow section. The actual measurement chamber is smooth. The water leaves the chamber through a perforated steel plate. This causes a small pressure drop that prevents that the streamlines convert to the outlet pipe before the end of the chamber.

A.3.2 *In situ* flow cell supporting system

The water circulation was maintained by a pump that could be used submersed as well as dry (Type LC-3CP-MD submersible, March Manufacturing, Glenview, Illinois, USA; 30 $L \cdot s^{-1}$). A degassing connection has been made to the pump chamber. Furthermore, this pump was equipped with a cooling coil around the motor through which a part of the pumped water is circulated. However, this would have heated up the medium, which is undesirable. The coil has therefore been disconnected. During an experiment water was pumped through the coil for cooling*. The wastewater that flows over the system withdrew enough heat to maintain a temperature within two degrees of the wastewater temperature. Therefore, no additional cooling was applied.

The system further contained an impeller type flow meter (model A103LM100NA1, Great Plains Industries, Inc., Wichita, KS, USA), a regulation valve, a connection for an oxygen/temperature sensor, a septum for sample withdrawal or substrate addition, a reaeration connection and a several degassing connections. The tubing materials were hard and soft PVC.

In situ flow cell operation

The operation of the *in situ* flow cell was not trivial because *all* air should be removed from the system before the actual measurement could start. Entrapped air would have led to a slower

*By smartly connecting some tubing it was even possible to use the water height difference imposed by the obstruction of the water by the *in situ* flow cell and the water drag force to maintain a water flow through the coil.

decrease in the dissolved oxygen concentration than the actual oxygen uptake, because the 0.2 $mg_{ox} \cdot mL_{air}{}^{-1}$ of oxygen would have dissolved in the medium.

The flow cell was installed by carefully placing it on the sewer wall and exerting pressure by extending the bar. Subsequently, the system was filled with the medium through a connection on the flow cell. The air was removed as much as possible through the degassing connections. The medium pump was stopped to observe whether a drop of the water level in a vertical degassing tube would occur. This would have indicated that the gasket had not closed of properly. This was mostly caused by an uneven sewer wall or trapped solids. The pump was started with the regulation valve closed. The regulation valve is slowly opened until the desired flow rate is reached. The medium was pumped into the system again until all remaining air was removed. This also removed suspended biomass that might have been released during installation of the cell. The degassing tubes remained open during the experiment to equalise the pressure. The data from the dissolved oxygen meter (Oxi197S, WTW, Weilheim i. OB, Germany) were stored in a logger (Squirrel 1200, Grant Instruments (Cambridge) Ltd., Shepreth, Cambridgeshire, UK) and plotted as a visual control and backup.

Samples could be withdrawn through the septum. Medium had to be added if more than 10 mL of sample was taken.

A.4 Biofilm Flow Cell (BFC) and supporting system

Figure A.2 shows the measurement chamber of the BFC. The only differences in comparison with the *in situ* measurement chamber is that the biofilm in the BFC is flat and that the amount of biofilm is double because a plate can be installed on either side.

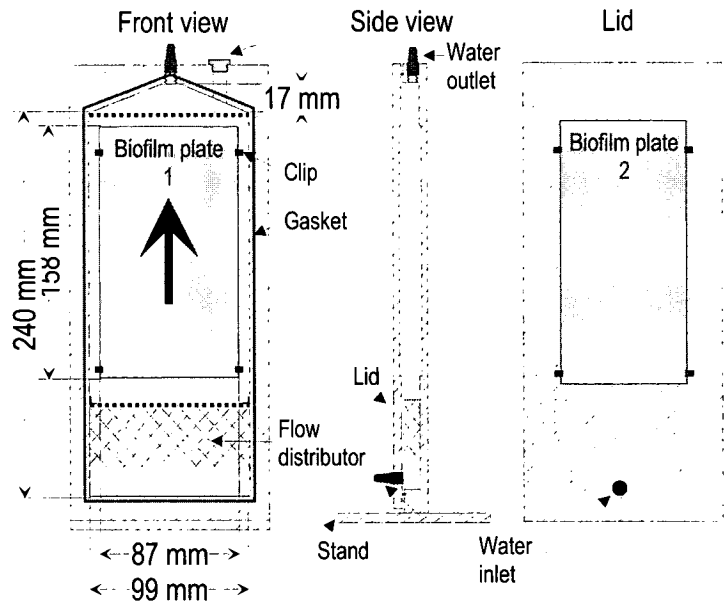

Figure A.2: Drawings with the dimensions of the biofilm flow cell for laboratory use.

Operation of the laboratory BFC

The oxygen sensor was calibrated as described in appendix A.6 and installed. Plates with biofilm were obtained according to the method described in section 4.3.3. One or two of these plates were carefully taken from the wastewater they were stored in and allowed to drain by putting them upright for two minutes. The biofilm amount was then determined by weighing. The release of water was proportional with time, as figure A.3 shows. After being wetted again to prevent dehydration, they were carefully put in the BFC. The system was filled up with the medium (mostly centrifuged wastewater) and the recirculation pump was started with the regulation valve closed. This valve was then slowly opened. Medium was recirculated with the peristaltic pump outside the system where air bubbles could escape.

The pressure in the top of the system was equalised with the surrounding pressure by opening the top valve (see figure 4.10). Otherwise, contraction or expansion of the medium due to temperature changes would have disturbed the reaeration.

The controller program determined how long the three-way valve would have to be open based on the measured oxygen flow, the system volume and the desired increase in the oxygen concentration. There were no problems with the accumulation of other gases because pure oxygen was used. Gas bubbles were formed only when large amounts of nitrogen were produced during certain denitrification experiments.

A.5 SF_6 gas exchange experiment methodology

A.5.1 Preparation and addition of the tracers

Water (0.25 to 0.5 l.) was saturated with gaseous 99.5% SF_6 (Carbagas, Rümlang, Switzerland) and carefully mixed with 30 L of water containing sodium bromide (NaBr, 300 $kg_{Br} \cdot m^{-3}$) as a tracer to quantify sewer discharge and groundwater infiltration. This mixture was pumped continuously into the sewer. After 30 min., a tracer pulse (rhodamine or plain salt) for sampling synchronisation was added.

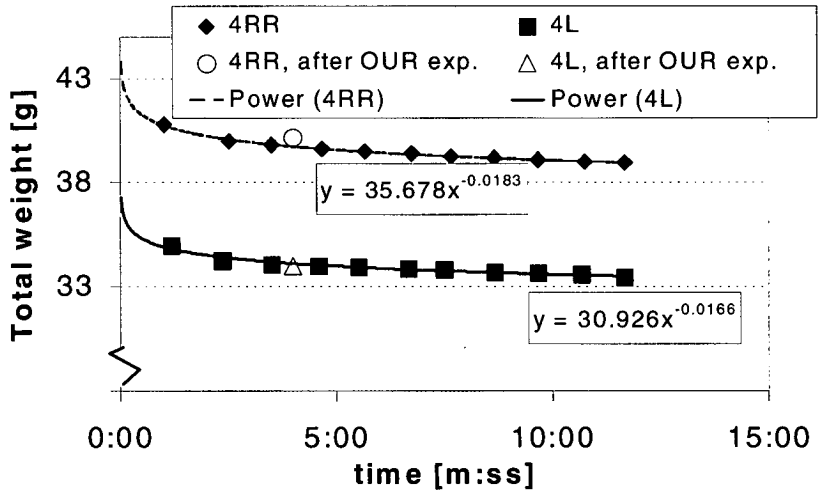

Figure A.3: The weight-loss of the biofilm plates as a function of time.

A.5.2 Sampling for the SF_6 method

Sampling was conducted at two to three sites 10 min. after the maximum of the tracer pulse had passed. At time intervals of one or two minutes a 250 mL sample was carefully scooped from the wastewater and brought to the surface. From this water, duplicate samples of 25 mL were taken in 50 mL glass syringes (Ultrafit, Henke, Germany) leaving no headspace*. The glass syringes were stored under water until analysis, which occurred within 24 hours after sampling.

A.5.3 Analysis of SF_6

The samples were analysed on a simple gas chromatograph as described by Hofer (1998). First, the syringes with the 25 mL sample were filled up to 50 mL with 99.999% nitrogen (Carbagas, Rümlang, Switzerland) to create a headspace with the same volume as the sample. The head-space was equilibrated with the water by shaking vigorously for 30 seconds and then contained over 99% of the SF_6. The gas was injected into the sample loop (1 mL) through a 5 cm tube filled with magnesium perchlorate (Merck no. 5874) to remove water vapour that would otherwise inactivate the zeolite. Heating the column to $\approx$ 150°C for a few hours while flushing with nitrogen could however regenerate the zeolite. The 1.8 m steel column (Ø=1/8") was filled with 5Å, 80/100 mesh washed zeolite (Alltech, Socolabo SA, Lausanne, Switzerland). The carrier gas was 99.999% nitrogen. The zeolite separated the SF_6 from oxygen for which the detector, based on the electron capture principle (model ECD 800, Fisions, Brechbühler AG, Schlieren, Switzerland) also has a high affinity. The ECD is extremely sensitive to halogenated compounds, which makes it possible to analyse the samples without any sample preconcentration. The detector output was processed by a HP 3396A integrator (Hewlett Packard (Schweiz) AG, Urdorf/Zürich, Switzerland). The analytical conditions are listed in table A.5. The retention time of SF_6 and oxygen under these conditions are $\approx$ 0.5 and 1.2 minutes, respectively. Care should be taken with hydrogen sulphide, which can occur in anaerobic water. This might interfere with the analyses when the separation is insufficient. The linear range reaches from the detection limit of 0.03 to 180 $ng{\cdot}L^{-1}$. The reproducibility of duplicate measurements was 15% for concentrations around 0.07 $ng{\cdot}L^{-1}$ and became $< 5\%$ at concentrations $>$ 1 $ng{\cdot}L^{-1}$.

Four standards have been made gravimetrically by Carbagas and stored in 5 L. pressure containers (0.065, 0.541, 6.581 65.813 $ng{\cdot}L^{-1}$). The exact concentration has been determined by comparing with dilutions of 0.1 ppm SF_6, the lowest concentration that can still be made accurately.

The bromide concentration was measured in the samples after the SF_6 had been measured.

*Bubble inclusion must be avoided because bubbles can contain $\approx$ 200 times more SF_6 by volume than the equivalent amount of water. Furthermore, oxygen can interfere with the analysis.

Table A.5: SF_6 analysis operating conditions.

Column	Gas flow	$\approx$ 30	$mL{\cdot}min^{-1}$
	Temperature	25 or 40	°C
Detector	Temperature	350	°C
	Voltage	50	V
	Pulse width	1	µs
	Current	1.5	nA

A.6 Application and calibration of the oxygen meters

The dissolved oxygen meter Oxi 196 (WTW, Weilheim i. OB, Germany) has a Clark-type* Polarographic Oxygen Sensor (POS) type CellOx 196. The sensor of the newer and much more accurate types OXI 197 and OXI 340 have a CellOx 325 sensor, which has a gold cathode and a lead anode. As far as known, the membrane has remained unchanged.

Both the older and the newer cells are of the amperometric type: the oxygen flux through the membrane imposes a directly proportional current through the electrodes. Therefore, there is no signal, when there is no oxygen (zero-current free). This implies that a one-point calibration is sufficient. The manufacturer supplies a calibration and storage vessel 'OxiCal-SL' which has a small sponge and a cover of silicone, which is oxygen permeable, to ensure that the oxygen concentration and humidity at the membrane surface are influenced only by the temperature and the air pressure. These two variables are measured in the sensor and in the meter, respectively.

The calibration with the OxiCal vessel led to acceptable results. However, the method proved to be susceptible to temperature changes which could easily occur during the preparation for a field experiment. The reason is that the measurement cell changes its temperature with a rate different from the two build-in temperature sensors. Furthermore, on some occasions differences between several oxygen sensors was observed when they were placed in a stirred vessel after 'OxiCal-SL' calibration†. Errors in the order of 0.5 $mg{\cdot}L^{-1}$ or 5% have been observed. The calibration should therefore be checked by putting the sensors in an aerated and stirred vessel with demineralised water, whereby care should be taken that no air bubbles get trapped under the membrane. In this case the conditions are as close as possible to the actual measurement conditions. The meters can also be calibrated while in the water. An important advantage of calibrating this way is that the temperature equilibrium is reached much quicker.

The water velocity over the sensor membrane must be sufficiently high (> 0.1 $m{\cdot}s^{-1}$). Otherwise, the oxygen flux through the thicker boundary layer will leads to a lower oxygen concentration on the membrane surface which results in a lower read-out.

A weak point of the WTW dissolved oxygen meter is the membrane that gets damaged easily, especially when the protection ridges are cut away. However, these ridges on the membrane caps should at least be rounded of to prevent that coarse material gets trapped on the sharp edges. The air pressure sensor is a weak point in the meters themselves. A malfunction means that the calibration will be wrong. Systematic errors of several percents can be introduced this way. They can be identified by comparing the oxygen concentration after calibration with other meters or by directly comparing the measured air pressure, as is possible on the Oxi 340 models.

A.7 Other materials and methods

A.7.1 Alkalinity, TSS and TVS

The alkalinity was determined by titrating a sample volume between 20 and 70 mL with hydrochloric acid to pH 4.3 using a Mettler-Toledo titrator with autosampler (Mettler Toledo, Greifensee, Switzerland).

*The electrodes are a platinum cathode and a silver anode coated with silver chloride. The measuring cell contains a potassium chloride solution as electrolyte and is closed of with a gas permeable membrane with a thickness of ≈ 1 μm. All oxygen that passes through the membrane will be reduced when a polarisation voltage of -0.8 V is applied to the electrodes.

†This was not due to ground loops or other interferences.

The wastewater total suspended solids (TSS) and total volatile solids (TVS) were determined by centrifuging 100 mL sample and then filtering the sample through a pre-dried Whatman GF/F glassfibre filter (effective pore width 0.7 µm). The filter was dried at 110°C and weighed after cooling in an exsiccator. The centrifuging step had the function of precipitation most of the particles, so that the supernatant could be filtered easily. The pellet was flushed onto the filter at the last moment. This procedure saved time, but most of all increased the accuracy, because the sample volume could be more than doubled. The TVS was found be incinerating the filter at 550°C for at least two hours. A dried filter, which went through the same treatment, served as a reference for the weight loss of the filter material (typically 2%).

A.7.2 Sewer biofilm TSS and TVS

The samples that were obtained with the methods described in section 4.3.2 and section 4.3.1 contain a high concentration of biofilm biomass. Because the purpose of a biofilm is to form a protecting matrix for bacteria, it has a strong tendency to form conglomerate again during analyses even after previous vigorous stirring. This rapidly clogs filters. Therefore, the biofilm total suspended solids (TSS) and total volatile solids (TVS) were partly determined according to the method for wastewater as described in section A.7.1.

A biofilm sample was put in one or more centrifuging tubes and was centrifuged until the liquid was clear (typically three minutes at 3000 g). The liquid was decanted and the pellet was flushed into a porcelain dish with a jet from a water bottle containing demineralised water and the tube was rinsed. The dish was dried at 110°C and weighed after cooling in an exsiccator, which gave the TSS. The amount of TVS was determined be incinerating the dish at 550°C until loose ashes remained. This typically took five hours. The dish was weighed after cooling in an exsiccator. No correction was necessary for a weight loss of the porcelain dish.

A.7.3 Sewer biofilm density

It was possible to determine the biofilm density in the samples taken with the sewer balloon method (see section 4.3.1). For this, the biofilm sample together with any water that might have separated from it, were put into a measuring flask (V_{flask} = 10 or 25 mL) with a known weight (m_e, in gram). The weight of the flask with biofilm (m_b) was determined and it was filled to its calibration mark with demineralised water whereby attention was paid that no air bubbles remained trapped. The full flask was weighed again (giving m_f). Subsequently, the TVS and TSS were be determined as described above, although centrifuging was normally not necessary due to the smaller amount of water.

Deducting m_e from m_b yields the sample weight that results with the sampled area in the wet biofilm mass per area unit. The volume of the biofilm follows from (under the assumption that water has a density of 10^3 kg·m^{-3}):

$$V_{biof} = V_{flask} - V_{water} = V_{flask} - (m_f - m_b) \tag{A.1}$$

where V_{water} = amount of demineralised water added (mL).

The biofilm density $\rho_{biofilm}$ (kg·m^{-3}) is then easily calculated as:

$$\rho_{biofilm} = TSS/V_{biof} \tag{A.2}$$

It will depend very much no the biofilm structure how accurate this method is. A strong smooth biofilm will give much better results then a filamentous, fluffy biofilm.

A.7.4 Chemical Oxygen Demand

The Chemical Oxygen Demand (COD) measurement was based on a digestion with potassium dichromate in concentrated sulphuric acid for 2 h at 150°C. The applied test tubes were manufactured by Hach Company (Loveland, CO, USA). In the low range test (test no. 435), the decrease in yellow dichromate is measured at 620 nm. In the high range test (test no. 430), the green coloured product is determined at 420 nm. The test tubes were measured several times on a Hach DR/2000 spectrophotometer to find the lowest (test no. 430) or highest (test no. 435) reading to rule out the influence of impurities on the wall or in the glass. The standard deviations were 3 and 2 % respectively.

A.7.5 Nitrogen Components with FIA

Nitrite (NO_2^-), nitrate NO_3^- and ammonium (NH_4^+) were quantified with flow injection analysers that are based on colorimetric methods (ASIA, Ismatec AG, Glattbrugg, Switzerland).

The nitrite method was based on the reaction of sulphanylamide with nitrite. The resulting diazonium salt formed an azo dye with N-(naphthyl)-ethylenediamine that was measured at 559 nm. Nitrate was first reduced to nitrite with a cadmium reducer in the flow path and then measured as mentioned above. The ionchromatograph (see section A.7.6) has been used to analyse nitrite and nitrate when this machine was used to measure other anions.

The ammonium method was based on the colour change of a pH indicator. The analyser mixed the sample with sodium hydroxide to raise the pH. Subsequently, the sample flew over a polypropylene membrane with the pH indicator on the other side. The ammonia that diffused through the membrane caused a colour change that was measured at 605 nm. The reproducibility was $\leq 4\%$ for all methods in the range from 0.1 to 15 $mg_N \cdot L^{-1}$.

Total nitrogen was analysed by first digesting the sample with 4mass% potassium peroxic disulphate and 0.7mass% sodium hydroxide for 2 h at 121°C, neutralising the sample and measuring nitrogen as nitrate by flow injection analysis. The reproducibility was 2%.

A.7.6 Ionchromatographic analysis of anions

The anions Cl^-, Br^-, NO_2^-, NO_3^-, SO_4^{2-} and PO_4^{3-} were analysed on a Dionex DX300 (Dionex Corporation, Sunnyvale, CA, USA) with an electrochemical self regenerating suppressor and conductivity detector. Initially, an AS11 column (4 mm diameter) and a hydroxide eluent with a gradient from 1 to 10 mM were used at a flowrate of 1 $mL \cdot min^{-1}$. Later, the column was replaced with an AS12 (4 mm) and an isocratic carbonate eluent at a flowrate of 1.5 $mL \cdot min^{-1}$ (2.7 mM Na_2CO_3 and 0.3 mM $NaHCO_3$). This gave more stable results because there were fewer problems with the current setting of the suppressor. The chromatograms were processed with the software AI450 Model 1 from the Dionex corporation. The reproducibility of the measurements was $\leq 2\%$ in the range from 2 to 50 $mg \cdot L^{-1}$.

A.7.7 Analysis of urea

The urea analysis is derived from a common method used in medicine and is based on the difference in the ammonium concentration of samples with and without added urease. The urease enzyme catalyses the hydrolysis of urea to ammonium and carbon dioxide according to the following equation:

$$NH_2 - CO - NH_2 + H_2O \longrightarrow 2\,NH_3 + CO_2$$

Solutions

The following solutions are required:

- **Urease stock solution (a)** 400 mg urease are dissolved in 100 mL buffered, 50% glycerine solution (b). This solution can be kept for several months at 4°C, as long as it does not become turbid.
- **buffered, 50% glycerine solution (b)** 162 g Glycerine are weighed in a 250 mL measuring flask, 25 mL of the buffer solution (c) is added and the whole is filled up with distilled water.
- **0.5 M Buffer/complexing agent solution (c)** 1.0 g titriplex (Merck, no.8418), 34 g KH_2PO_4 and 44.5 g $Na_2HPO_4 \cdot 2H_2O$ are dissolved in 1000 mL distilled water.
- **urease analysis solution (d)** 10 mL urease solution (a) are diluted to 100 mL with the buffer/complexing solution (c). This solution can be kept for one week at 4°C.

Procedure

- **Incubation:**
  - 0.5 mL urease analysis solution (d) is mixed with 5 mL sample.
  - The mixture is incubated at room temperature for at least 30 min.
  - The ammonium concentration is measured subsequently (range 0.2-10 $mg_N \cdot L^{-1}$).

  Remark: Concentrations between 10 and 200 $mg_N \cdot L^{-1}$ can be analysed by diluting the incubated sample. Samples with higher concentrations before the measurement because otherwise the buffer capacity and the amount of enzyme are insufficient.
- **Ammonium measurement:** The ammonium concentration is measured in the samples with and without added urease as described in section A.7.5. The samples are preferably measured in a random order to avoid a possible influence of drift of the analyser on the final results.
- **Calibration:** The urease analysis solution effects the amount of ammonium that is found when the standard calibration procedure is used*. Therefore, the standards for urea of 0, 2, 4, 6, 8 and 10 $mg_N \cdot L^{-1}$ went through the same procedure as the samples and were mingled in a random order with the samples on the autosampler.
- **Hydrolysis check:** Two samples with 0.6 and 10 $mg_N \cdot L^{-1}$ as urea went through the same procedure as the samples and were also mingled with the samples. These served as a check for the activity of the urease analysis solution.

A standard addition of urea to wastewater showed that this matrix did not influence the measurements.

*The standards are not on the autosampler but in five separate bottles. With the help of a six-way valve, the software selects either the sample or one of the standards.

B Oxygen Uptake Monitor program

B.1 Introduction

This appendix describes the program that was written to control the respiration rate measurement. The classical respiration rate measurement with an oxygen electrode is an easy and valuable tool to acquire data about the activity in mixed culture systems like activated sludge. The experimental procedure is described in section 4.5.

Initially, the readings from the oxygen meter were written on a recorder and the data were processed by hand with a pencil and ruler. Later, dedicated 'oxygen monitors' were developed, for example by Hitec microsystems (UCT Chemical Engineering, Kaapstad, South Africa). This machine automatically started the aeration when the oxygen concentration sank below a preset value until it reached an upper value. The oxygen concentration would then fall due to the biological activity in the sample and the machine would calculate the slope once the oxygen concentration would reach the lower oxygen limit and the aeration would start again. The calculated respiration rates were stored internally and could be read from the machine via the serial port.

This saved the manual reaeration and laborious processing of the data. An advantage is that the UCT machine can work stand-alone. However, with the present low prices for computer hardware and the abundance of written-off PC that is of no importance anymore.

An important disadvantage of this machine was its inflexible hardware. It was designed for oxygen meters with a 4-20 mA output and only the connection of a specific type of electronic temperature transducer was possible. Furthermore, the programming was difficult and the oxygen concentrations and results were not on-line available in graphical form.

A new respirometer system was therefore developed. The program and surrounding hardware that are presented here are a further development of the UCT oxygen monitor. The new system has to following features:

- The oxygen concentration and temperature are read from a (dissolved) oxygen meter (either analog via a analog/digital converter card or digital via the standard serial ports of the PC). These data are stored on the hard disk and plotted on the screen.
- The average respiration rate during the cycle is continuously updated.
- The Oxygen Uptake Rate (with standard deviation) is calculated from the oxygen data between free selectable oxygen concentrations. Furthermore, the average temperature, the time that aeration started and ended and the time that the high and low boundaries were reached are also stored. These data are also written to disk (as a standard text file) and plotted on the screen.
- When the low oxygen boundary is reached, an output signal is produced which can be used to control the aeration valve. This signal stays active until another adjustable boundary is reached which can either be lower or higher than the upper boundary for the OUR determination (useful for switching between aeration with pure oxygen and air).

- The program can control up to six independent respiration experiments at the same time.

Some additional equipment is necessary to make a complete system. Of course there are the computer and the oxygen meter. When the oxygen meter has a serial output, it can be attached directly to the computer (at the moment the program can read the data from a WTW OXI 340). The easiest option to control a valve is by using a relay card which is attached to the printer port. Some more investment is necessary when only an analog output is available. I used a National Instruments Lab PC+ card. This firm is expensive, but they are good. This card can read the analog data and has digital output (among others) which can control a relay via an amplifier. Probably cards from other manufactures can also be used as long as they have drivers that are compatible with LABVIEW. A screen shot of the program is shown in figure B.1.

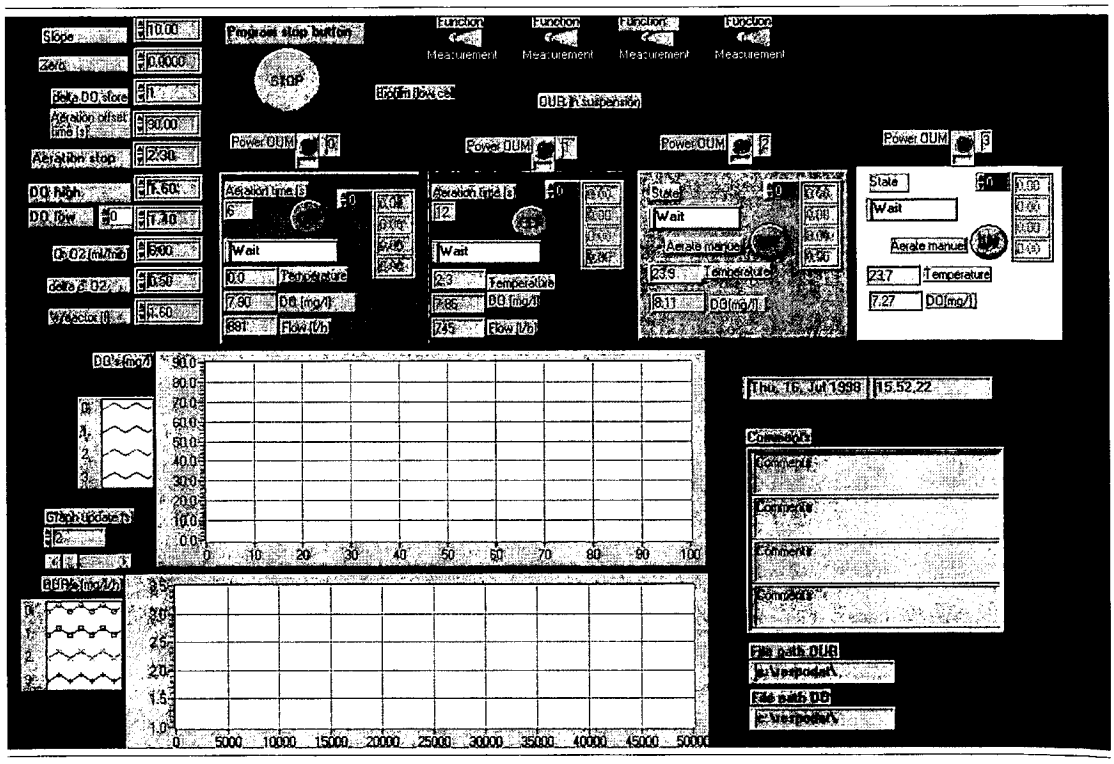

Figure B.1: A screen shot of the Oxygen Uptake Monitor program.

C Additional data

C.1 Oxygen balances

The data of the oxygen balance measurements in June and October 1999 are listed in table C.1

C.2 Ammonium concentration changes - Urea hydrolysis

over a sewer section (see section 5.5) might seem surprising for an aerobic system with a high (biofilm) biomass residence time. Nitrification plays a negligible role, because the nitrifying bacteria are constantly overgrown by heterotrophic bacteria that deprive the nitrifiers of oxygen (see section 2.5.2). The degradation of proteins as a source of ammonium was also negligible because the protein concentration changes were insignificant (results not shown). Therefore, the hydrolysis of urea must have caused the increase. An artifact due to hydrolysis during analysis was excluded because the samples were measured randomly.

A measurement campaign for ammonium and urea changes in the *Rümlang* sewer section (see section 5.3.1) was conducted to verify the hypothesis that urea hydrolysis is responsible for the ammonium concentration increase. The results as shown in figure C.1 indicated that the urea concentration dropped with 2.2 $g_N \cdot m^{-3}$ or 45% over the length of the section. The question then arises whether the hydrolysis occurs in the wastewater or in the biofilm, where the biomass concentration is much higher.

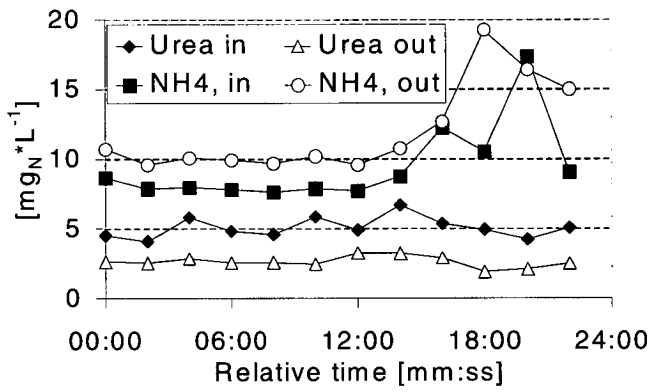

Figure C.1: Changes in the urea and ammonium concentrations in the Rümlang sewer section (T_{water} = 14°C).

Table C.1: The results of the hydrodynamic and the respiration rate measurements for oxygen balances in June and October 1999. $L_{sect.}$=1906 m

Description	Unit	7/6	9/6	10/6	11/6	12/6	13/6	14/6	22/10	28/10	28/10	28/10	29/10	29/10	01/11
t_{start}	(h:mm)	10:50	10:00	10:00	10:00	10:40	10:20	10:00	15:20	17:09	19:39	22:08	0:40	11:38	9:18
τ	(h:mm)	1:09	1:09	1:12	1:08	1:09	0:58	0:51	1:20	1:23	1:19	1:24	1:39	1:22	1:08
Q	($m^3 \cdot s^{-1}$)	0.054	0.055	0.043	0.055	0.061	0.095	0.120	0.03	0.0235	0.0315	0.0229	0.0111	0.0312	0.0321
$\overline{T}$	(°C)	16.3	16.1	16.2	16.2	16.7	16	15.7	17.1	16.7	17.5	17.4	16.5	16.9	16.7
$\overline{u}$	($m \cdot s^{-1}$)	0.455	0.457	0.438	0.464	0.46	0.543	0.619	0.383	0.379	0.402	0.374	0.318	0.387	0.461
A_{cr}	(m^2)	0.118	0.12	0.098	0.119	0.132	0.174	0.195	0.078	0.062	0.078	0.061	0.035	0.08	0.070
α	(-)	1.025	1.034	0.955	1.028	1.072	1.199	1.256	0.878	0.806	0.878	0.803	0.656	0.887	0.841
P_w	(m)	0.92	0.93	0.86	0.92	0.96	1.08	1.13	0.79	0.73	0.79	0.72	0.59	0.8	0.76
A_w	(m^2)	1759	1773	1638	1763	1839	2057	2154	1454	1382	1507	1377	1125	1522	1442
R_h	(m)	0.128	0.129	0.114	0.128	0.137	0.161	0.172	0.099	0.0855	0.0991	0.0849	0.0592	0.1008	0.0920
w	(m)	0.77	0.77	0.73	0.77	0.79	0.84	0.86	0.692	0.649	0.693	0.647	0.549	0.698	0.671
d_m	(m)	0.153	0.156	0.133	0.154	0.167	0.208	0.227	0.113	0.096	0.113	0.095	0.064	0.115	0.104
u^*	($m \cdot s^{-1}$)	0.034	0.034	0.032	0.034	0.035	0.038	0.039	0.03	0.028	0.03	0.028	0.023	0.03	0.029
Fr	(-)	0.37	0.37	0.38	0.38	0.36	0.38	0.41	0.36	0.39	0.38	0.39	0.4	0.36	0.46
$\overline{S_{O,in}}$	($g_{O_2} \cdot m^{-3}$)	4.57	5.57	6.57	7.57	8.57	9.57	10.57	1.43	2.47	1.94	2.24	2.18	2.06	3.33
Inflow	($kg_{O_2} \cdot d^{-1}$)	21.2	26.5	24.3	36.0	45.0	78.3	110	3.7	5.0	5.3	4.4	2.1	5.5	9.2
$\overline{S_O}$	($g_{O_2} \cdot m^{-3}$)	3.2	4.2	5.2	6.2	7.2	8.2	9.2	0.9	1.65	1.05	1.44	1.85	1.28	2.20
S_O^*	($g_{O_2} \cdot m^{-3}$)	9.39	9.42	9.41	9.39	9.31	9.45	9.49	9.23	9.3	9.15	9.17	9.34	9.27	9.31
$k_l a_{O_2}^{T=20°C}$	(d^{-1})	8.4	8.3	9.1	8.4	7.9	7	6.7	10	11.1	10	11.1	13.9	9.9	10.8
$k_l a_{O_2}^{T=\overline{T}°C}$	(d^{-1})	7.7	7.6	8.3	7.7	7.3	6.3	6.0	9.3	10.25	9.5	10.4	12.8	9.2	10.0
Reaeration	($kg_{O_2} \cdot d^{-1}$)	10.6	9.0	6.5	5.5	3.8	2.6	0.6	11.2	9.3	11.4	9.4	6.4	11.2	9.4
$\overline{S_{O,out}}$	($g_{O_2} \cdot m^{-3}$)	1.9	2.9	3.9	4.9	5.9	6.9	7.90	0.39	0.83	0.16	0.64	1.52	0.49	1.08
Outflow	($kg_{O_2} \cdot d^{-1}$)	8.8	13.8	14.4	23.3	31.0	56.4	82.2	1.01	1.69	0.45	1.27	1.46	1.32	2.98
$OUR_{WW,in}^{T=21°C}$	($g_{O_2} \cdot m^{-3} \cdot d^{-1}$)	58.3	35.2	44.6	33.9	66.4	15.2	9.7	113	86.7	185	101	61.6	125.2	78.3
$OUR_{WW,out}^{T=21°C}$	($g_{O_2} \cdot m^{-3} \cdot d^{-1}$)	54.2	41.1	67.9	38.4	86.1	19.2	11.9	147	185	218	114	42.8	136.6	105
$\overline{OUR_{WW}^{T=18°C}}$	($g_{O_2} \cdot m^{-3} \cdot d^{-1}$)	56.3	38.1	56.3	36.1	76.3	17.2	10.8	130	136	202	107	52.2	131	91.6
$\overline{OUR_{WW}^{T=T_{sewer}}}$	($g_{O_2} \cdot m^{-3} \cdot d^{-1}$)	49.2	48.6	48.7	49.1	50.7	48	47.2	95.8	97.5	153	81.3	36.7	95.1	65.5
OUR_f	($kg_{O_2} \cdot d^{-1}$)	11.0	11.1	9.1	11.1	12.8	15.9	17.5	13.8	11.5	22.9	9.5	2.4	14.6	8.7

A wastewater sample and an intact biofilm sample as described in section 4.3.3 were therefore collected. The wastewater and biofilm samples were measured in a CSTR-type respirometer and the biofilm flow cell system as described in section 4.7. The temperatures were 18 and 19°C respectively. The pH was 7.6. Extra urea up to a concentration of $\approx 10\ g_N \cdot m^{-3}$ was added.

The biofilm activity — after correction for the medium of centrifuged wastewater that had an activity of $14\ g_N \cdot m^{-3} \cdot d^{-1}$ — was $8.8\ g_N \cdot m^{-2} \cdot d^{-1}$. The raw wastewater activity was 35 $g_N \cdot m^{-3} \cdot d^{-1}$. The effect of the biofilm on the urea concentration change in the wastewater can be determined with the ratio of the biofilm-area to the wastewater-volume. This ratio was on average $12\ m^2 \cdot m^{-3}$ during daytime in the *Rümlang* sewer. The biofilm activity is therefore equivalent to a hydrolysis of $106\ g_N \cdot m^{-3} \cdot d^{-1}$ in the wastewater.

The laboratory experiment corresponds well with the field measurement when the observed residence time during the field measurement of 72 minutes is taken as time basis for the laboratory experiment. A hydrolysis of 3.3 (biofilm) + 1.8 (wastewater) = $5.2\ g_N \cdot m^{-3}$ is found. This is larger than in the field where $2.2\ g_N \cdot m^{-3}$ was found. This is partly caused by the difference in temperature of 4°C. Furthermore, the biofilm mass transfer could have played a role because the urea concentration in the laboratory experiment was 50% higher than in the sewer.

It can be concluded that the biofilm as well as the wastewater contribute similar to the urea hydrolysis. Furthermore, the separate measurement of the biofilm and the wastewater activity under controlled laboratory conditions yielded results comparable with those observed in the field.

C.3 Easily degradable substrate in sewer

The amount of easily degradable substrate in the wastewater has been determined with a respiration method based on mixing the wastewater with starved activated sludge as described by Kappeler and Gujer (1992). Allylthiourea (ATU) was added to suppress nitrification. The results in table C.2 make clear that no clear change occurred over the length of the *Rümlang* sewer. The average S_S was $8\ g_{COD} \cdot m^{-3}$.

Table C.2: The concentration easily degradable substrate S_S at RS5002 (in) and RS3096 (out)

Date		20-05-97	22-05-97	27-05-97	16-06-97
S_S	in	8.2	5.3	8.4	12.6
($g_{COD} \cdot m^{-3}$)	out	8.1	7.1	6.7	24.6*
S_S:COD_{total}†	in	2.1%	2.1%	1.8%	3.1%
	out	1.6%	1.5%	1.5%	7.3%
S_S:$COD_{dissolved}$†	in	5.0%	3.5%	4.5%	7.0%
	out	3.7%	2.8%	3.7%	12.3%
NH_4^+	in	-	27.2	23.4	-
(mg_N/L)	out	-	31.5	34	-
NO_3^-	in	-	1.3	1.1	-
(mg_N/L)	out	-	0.7	0.7	-
NO_2^-	in	-	0.243	0.162	-
(mg_N/L)	out	-	0.142	0.115	-

*: The pumping station had been left switched on to investigate the effect on the wastewater composition. In the pumping station the undiluted and anaerobic wastewater stands for approx. 30 min.
†: The ratio of S_S to total or dissolved COD

Seite Leer /
Blank leaf

D Dynamic biological sewer model

D.1 The simulation tool Aquasim

The sewer model was implemented with the simulation and data analysis software for aquatic systems, AQUASIM (Reichert, 1994, 1998), version 2.0a_β1 (see http://www.aquasim.eawag.ch for topical details on this program). Within a spatial configuration consisting of compartments and links of the available types, this program allows its users to define any state variables and transformation processes and to perform simulations, parameter estimations and sensitivity analyses. In order to solve the partial differential equations numerically, in a first step this program discretises the space derivatives. In a second step, the spatially discretised partial differential equations are integrated in time with the implementation DASSL (Petzold, 1983) of the implicit (backward differencing) variable-step, variable-order GEAR integration technique. The sum of weighted squares of the deviations between model results and measurements, given as the goodness of fit is evaluated with the help of the χ^2-criterion (Hald, 1952):

$$\chi^2(\mathbf{p}) = \sum_{i=1}^{n} \left(\frac{f_{meas,i} - f_i(\mathbf{p})}{\sigma_{meas,i}} \right)^2 \tag{D.1}$$

where $p = (p_1 \cdots p_m)$ = the array of m parameters, $f_{meas,i}$ = the measured and $f_i(p)$ the calculated value corresponding to a data point, $s_{meas,i}$ = standard deviation of $f_{meas,i}$. The goal during a parameter estimation is to minimise the value of equation (D.1) by changing the model parameters.

D.1.1 The sewer modelled as a river

At present, AQUASIM contains six compartments. The hydrodynamics of the sewer system can be modelled well with the river section, which is specially designed for open channel flow. In contrast to the MOUSE program AQUASIM allows an user defined friction slope equation which is necessary to accurate model dynamic processes (Huisman *et al.*, 2000). The following implementations of the required variables are used to specify the bed geometry:

- **cross sectional area:** $A_{cr} = 1/4 \cdot D^2 \cdot (\alpha - \sin(\alpha) \cdot \cos(\alpha)) + d_{press} \cdot w_{slot}$

  where d_{press} = water height in the so-called Preissmann slot and w_{slot} = the width of the Preissmann slot. The 'Preissmann slot' is a technique to maintain a free water surface throughout the surcharged system and thereby continues to use the same methodology as for open-channel flow conditions.easy method to allow for the numerical simulation of pipe flow under pressure in models meant for open channel flow.
- **Perimeter:** $D \cdot \alpha$
- **Surface width:** $D \cdot \sin(\alpha)$
- **Friction slope:** Equation (3.10), which is based on Darcy-Weisbach, is used.

D.1.2 Calculation of the stoichiomatrix matrix

The stoichiometric coefficients of the biological model (see section 9.9) were calculated with the equations listed in the tables D.1 to D.3.

Table D.1: Calculation of the stoichiometric coefficients for the dynamic sewer model. Definitions: $\alpha_{SO_4} = 64\ g_O \cdot mol_S^{-1}$, $\alpha_{S^0} = 48\ g_O \cdot mol_S^{-1}$, $\alpha_{NO_3} = -4.57\ g_O \cdot g_N^{-1}$, $\alpha_N = -1.71\ g_O \cdot g_N^{-1}$.

	State variable→ unit→	S_O $g_{O_2} \cdot m^{-3}$	S_I $g_{CSB} \cdot m^{-3}$	S_S $g_{CSB} \cdot m^{-3}$	S_{NH} $g_N \cdot m^{-3}$
	$g_{COD} \cdot mol^{-1}$ M_W ($g \cdot mol^{-1}$)	-32 32	-	-	0 18
1	Hydrolysis		$+f_{S_I}$	$1 - f_{S_I}$	$+i_{NX_S} - i_{NS_S} \cdot (1 - f_{SI}) - f_{SI} \cdot i_{NSI}$
2	Aerobic storage of COD	$Y_{Sto,O} - 1$		-1	$+i_{NS_S}$
3	Anoxic storage of COD			-1	$+i_{NS_S}$
4	Aerobic growth	$-\left(\frac{1}{Y_H} - 1\right)$			$-i_{NBM}$
5	Anoxic growth				$-i_{NBM}$
6	Aerobic endogenous respiration	$-(1 - f_{X_I})$			$+i_{NBM} - i_{NX_I} \cdot f_{X_I}$
7	Anoxic endogenous respiration				$+i_{NBM} - i_{NX_I} \cdot f_{X_I}$
8	Aerobic respiration of X_{Sto}	-1			
9	Anoxic respiration of X_{Sto}				
10	Nitrification	$\frac{-(-\alpha_{NO_3} - Y_A)}{Y_A}$			$-\frac{1}{Y_A} - i_{NBM}$
11	Aerobic endogenous respiration	$-(1 - f_{X_I})$			$+i_{NBM} - i_{NX_I} \cdot f_{X_I}$
12	Anoxic endogenous respiration				$+i_{NBM} - i_{NX_I} \cdot f_{X_I}$
13	Growth on SO_4^{2-}			$\frac{-1}{Y_{SRB,SO_4}}$	$\frac{+i_{NS_S}}{1/Y_{SRB,SO_4}} - i_{NBM}$
14	Growth on S^0			$\frac{-1}{Y_{SRB,S^0}}$	$\frac{+i_{NS_S}}{Y_{SRB,S^0}} - i_{NBM}$
15	SRB Decay		$+f_{S_I}$		$+i_{NBM} - i_{NX_S} \cdot (1 - f_{X_I} - f_{S_I}) - i_{NX_I} \cdot f_{X_I} - i_{NS_I} \cdot f_{S_I}$
16	Aerobic growth ($HS^- \rightarrow S^0$)	$\frac{(\alpha_{S^0} - \alpha_{SO_4})}{Y_{SOB,HS}} + 1$			$-i_{NBM}$
17	Aerobic growth ($S^0 \rightarrow SO_4^{2-}$)	$1 - \frac{\alpha_{S^0}}{Y_{SOB,S^0}}$			$-i_{NBM}$
18	Anoxic growth ($HS^- \rightarrow S^0$)				$-i_{NBM}$
19	Anoxic growth ($S^0 \rightarrow SO_4^{2-}$)				$-i_{NBM}$
20	SOB Decay		$+f_{S_I}$		$+i_{NBM} - i_{NX_S} \cdot (1 - f_{X_I} - f_{S_I}) - i_{NX_I} \cdot f_{X_I} - i_{NS_I} \cdot f_{S_I}$

Table D.2: Calculation of the stoichiometric coefficients for the dynamic sewer model, continuation.

	S_{NO} gN ·m^{-3}	S_{N_2} gN ·m^{-3}	S_{HS} mol ·m^{-3}	X_{S^0} mol·m^{-3}	S_{SO4} mol·m^{-3}	$S_{HCO_3^-}$ mol m·m^{-3}
	-64	-48	64	48	0	0
	62	28	33	32	96	61
1						$\frac{1}{14}\cdot\left(i_{NX_S} - i_{NS_S}\cdot(1-f_{S_I}) - f_{S_I}\cdot i_{NS_I}\right)$
2						$\frac{1}{14}\cdot i_{NS_S}$
3	$-\frac{1-Y_{Sto,\,NO}}{2.86}$	$+\frac{1-Y_{Sto,\,NO}}{2.86}$				$-\frac{1}{14}\cdot\left(-\frac{1-Y_{Sto,\,NO}}{2.86} - i_{NS_S}\right)$
4						$-\frac{1}{14}\cdot i_{NBM}$
5	$+\frac{1-\frac{1}{Y_{HNO}}}{2.86}$	$+\frac{\frac{1}{Y_{HNO}}-1}{2.86}$				$\frac{1}{14}\cdot\left(-i_{NBM} - \frac{1-\frac{1}{Y_{HNO}}}{2.86}\right)$
6						$\frac{1}{14}\cdot(i_{NBM} - i_{NX_I}\cdot f_{X_I})$
7	$-\frac{1-f_{X_I}}{2.86}$	$\frac{1-f_{X_I}}{2.86}$				$\frac{1}{14}\cdot\left((i_{NBM} - i_{NX_I}\cdot f_{X_I}) + \frac{1-f_{X_I}}{2.86}\right)$
8						
9	$-\frac{1}{2.86}$	$\frac{1}{2.86}$				$-\frac{1}{14}\cdot\frac{1}{2.86}$
10	$\frac{1}{Y_A}$					$-\frac{1}{14}\cdot\left(i_{NBM} + \frac{2}{Y_A}\right)$
11						$\frac{1}{14}\cdot(i_{NBM} - i_{NX_I}\cdot f_{X_I})$
12	$-\frac{1-f_{X_I}}{2.86}$	$\frac{1-f_{X_I}}{2.86}$				$\frac{1}{14}\cdot\left(i_{NBM} - i_{NX_I}\cdot f_{X_I} + \frac{1-f_{X_I}}{2.86}\right)$
13			$\frac{1-Y_{SRB,\,SO_4}}{\alpha_{SO_4}\cdot Y_{SRB,\,SO_4}}$		$\frac{-1-Y_{SRB,\,SO_4}}{\alpha_{SO_4}\cdot Y_{SRB,\,SO_4}}$	$\frac{1}{14}\cdot\left(\frac{i_{NS_S}}{Y_{SRB,\,SO_4}} - i_{NBM}\right) + \frac{1-Y_{SRB,\,SO_4}}{\alpha_{SO_4}\cdot Y_{SRB,\,SO_4}}$
14			$\frac{1-Y_{SRB,\,S^0}}{(\alpha_{SO_4}-\alpha_{S^0})\cdot Y_{SRB,\,S^0}}$	$\frac{-1-Y_{SRB,\,S^0}}{(\alpha_{SO_4}-\alpha_{S^0})\cdot Y_{SRB,\,S^0}}$		$-\frac{1}{14}\cdot\left(\frac{i_{NS_S}}{Y_{SRB,\,S^0}} - i_{NBM}\right) - \frac{1-Y_{SRB,\,S^0}}{(\alpha_{SO_4}-\alpha_{S^0})\cdot Y_{SRB,\,S^0}}$
15						$\frac{1}{14}\cdot(i_{NBM} - i_{NX_S}\cdot(1-f_{X_I}-f_{S_I}) - i_{NX_I}\cdot f_{X_I} - i_{NS_I}\cdot f_{S_I})$
16			$-\frac{1}{Y_{SOB,\,HS}}$	$\frac{1}{Y_{SOB,\,HS}}$		$-\frac{1}{14}\cdot i_{NBM} + \frac{1}{Y_{SOB,\,HS}}$
17				$-\frac{1}{Y_{SOB,\,S^0}}$	$\frac{1}{Y_{SOB,\,S^0}}$	$-\frac{1}{14}\cdot i_{NBM} - \frac{2}{Y_{SOB,\,S^0}}$
18	$-\frac{\left(\frac{\alpha_{SO_4}-\alpha_{S^0}}{Y_{SOB,\,HS}}-1\right)}{\alpha_N-\alpha_{NO_3}}$	$\frac{\left(\frac{\alpha_{SO_4}-\alpha_{S^0}}{Y_{SOB,\,HS}}-1\right)}{\alpha_N-\alpha_{NO_3}}$	$-\frac{1}{Y_{SOB,\,HS}}$	$\frac{1}{Y_{SOB,\,HS}}$		$-\frac{1}{14}\cdot\left(i_{NBM} - \left(\frac{\frac{\alpha_{SO_4}-\alpha_{S^0}}{Y_{SOB,\,HS}}-1}{\alpha_N-\alpha_{NO3}}\right)\right) - \frac{1}{Y_{SOB,\,HS}}$
19	$-\frac{\left(\frac{\alpha_{S^0}}{Y_{SOB,\,S^0}-1}\right)}{\alpha_N-\alpha_{NO_3}}$	$\frac{\left(\frac{\alpha_{S^0}}{Y_{SOB,\,S^0}-1}\right)}{\alpha_N-\alpha_{NO_3}}$		$-\frac{1}{Y_{SOB,\,S^0}}$	$\frac{1}{Y_{SOB,\,S^0}}$	$-\frac{1}{14}\cdot\left(i_{NBM} - \left(\frac{\frac{\alpha_{S^0}}{Y_{SOB,\,S^0}}-1}{\alpha_N-\alpha_{NO3}}\right)\right) - \frac{2}{Y_{SOB,\,S^0}}$
20						$\frac{1}{14}\cdot(i_{NBM} - i_{NX_S}\cdot(1-f_{X_I}-f_{S_I}) - i_{NX_I}\cdot f_{X_I} - i_{NS_I}\cdot f_{S_I})$

Table D.3: Calculation of the stoichiometric coefficients for the dynamic sewer model, continuation.

	X_H	X_A	X_{Sto}	X_{SRB}	X_{SOB}	X_S	X_I	X_{TSS}
	$g_{CSB} \cdot m^{-3}$	$g_{CSB} \cdot m^{-3}$	$g_{CSB} \cdot m^{-3}$	$g_{CSB} \cdot m^{-3}$	$g_{CSB} \cdot m^{-3}$	$g_{CSB} \cdot m^{-3}$	$g_{CSB} \cdot m^{-3}$	$g \cdot m^{-3}$
	160	160	160	160	160			
	-	-	-	-	-	-	-	-
1						-1		$-i_{TSSX_S}$
2			$+Y_{Sto,O}$					$+i_{TSSX_{Sto}} \cdot Y_{Sto,O}$
3			$+Y_{Sto,NO}$					$+i_{TSSX_{Sto}} \cdot Y_{Sto,NO}$
4	1		$-\frac{1}{Y_H}$					$+i_{TSSBM} - 1/Y_H \cdot i_{TSSX_{Sto}}$
5	1		$-\frac{1}{Y_{HNO}}$					$+i_{TSSBM} - 1/Y_{HNO} \cdot i_{TSSX_{Sto}}$
6	-1						$+f_{X_I}$	$-i_{TSSBM} + i_{TSSX_I} \cdot f_{X_I}$
7	-1						$+f_{X_I}$	$-i_{TSSBM} + i_{TSSX_I} \cdot f_{X_I}$
8			-1					$-i_{TSSX_{Sto}}$
9			-1					$-i_{TSSX_{Sto}}$
10		1						$+i_{TSSBM}$
11		-1					$+f_{X_I}$	$-i_{TSSBM} + i_{TSSX_I} \cdot f_{X_I}$
12		-1					$+f_{X_I}$	$-i_{TSSBM} + i_{TSSX_I} \cdot f_{X_I}$
13				1				$+i_{TSSBM}$
14				1				$+i_{TSSBM} - (\alpha_{SO_4}/2)/Y_{SRB,S^0}$
15				-1		$1 - f_{X_I} - f_{S_I}$	$+f_{X_I}$	$-i_{TSSBM} + i_{TSSX_S} \cdot (1 - f_{X_I} - f_{S_I}) + i_{TSSX_I} \cdot f_{X_I}$
16					1			$+i_{TSSBM} + 32/Y_{SOB,HS}$
17					1			$+i_{TSSBM} - (\alpha_{SO_4}/2)/Y_{SOB,S^0}$
18					1			$+i_{TSSBM} + (\alpha_{SO_4}/2)/Y_{SOB,HS}$
19					1			$+i_{TSSBM} - (\alpha_{SO_4}/2)/Y_{SOB,S^0}$
20					-1	$1 - f_{X_I} - f_{S_I}$	$+f_{X_I}$	$-i_{TSSBM} + i_{TSSX_S} \cdot (1 - f_{X_I} - f_{S_I}) + i_{TSSX_I} \cdot f_{X_I}$

E Applied constants and definitions

E.1 Biomass

An average biomass* composition of $C_5H_7NO_2$ is assumed, which results in a molecular mass of 113 $g_{X_X} \cdot mol_{X_X}^{-1}$. The amount of COD is 5·32 + 7·1 + 1·14 + 2·16 = 160 $g_{COD} \cdot mol_{X_X}^{-1}$. Consequently, the COD of biomass is 1.42 $g_{COD} \cdot g_{X_X}$.

E.1.1 Temperature dependency of wastewater biomass

The temperature dependency of wastewater biomass is commonly described as:

$$\mu_{Het}^{max,T=T} = \mu_{Het}^{max,T=20°C} \cdot e^{[\beta_{T,Het} \cdot (T-20)]} \tag{E.1}$$

where $\mu_{Het}^{max,T=T}$ and $\mu_{Het}^{max,T=20}$ = maximum heterotrophic specific growth rate at T and 20°C, respectively ($g_{COD} \cdot g_{COD}^{-1} \cdot d^{-1}$), and $\beta_{T,Het}$ = temperature coefficient for heterotrophic growth (-). The constant $\beta_{T,Het}$ = 0.078 has been determined experimentally with wastewater from *Rümlang* in the range from 9 to 25°C.

E.2 Water properties

The dynamic viscosity, η (Pa·s), is (Perry *et al.*, 1984, p. F-51):

$$\eta = 0.1 \cdot 10^{\left[\frac{1301}{998.333+8.1855\cdot(T-20)+0.00585\cdot(T-20)^2} - 3.30233\right]} \text{ between 0–50°C} \tag{E.2}$$

The water density, ρ ($kg \cdot m^{-3}$), is (Perry *et al.*, 1984, p. F-11):

$$\rho = -1.62 \cdot 10^{-5} \cdot (3.98-T)^3 - 0.005799 \cdot (3.98-T)^2 + 0.024738 \cdot (3.98-T) + 1000 \tag{E.3}$$

The kinematic viscosity, ν ($m^2 \cdot s^{-1}$), can be calculated as:

$$\nu = \frac{\eta}{\rho} \tag{E.4}$$

E.3 Physical properties of oxygen

The saturation concentration of oxygen in pure water is given by (Montgomery, 1989)

$$S_O^* = \frac{468}{31.6 + T(°C)} \text{ at 1 atm} \tag{E.5}$$

*Biomass is expressed as X_X

Siegrist (1985) used the following temperature dependency for oxygen diffusion through water ($m^2 \cdot s^{-1}$):

$$\mathbb{D}_{O_2}^{T=T} = \mathbb{D}_{O_2}^{T=25} \cdot e^{[0.036 \cdot (T-25)]} \tag{E.6}$$

$$= 2.4 \cdot 10^{-9} \cdot e^{[0.036 \cdot (T-25)]} \tag{E.7}$$

Partial pressure of water in water saturated air (Pa) (Perry *et al.*, 1984):

$$p^*_{H_2O} = 0.04178 \cdot T^3 + 1.321 \cdot T^2 + 43.17 \cdot T + 615.4 \tag{E.8}$$

E.4 Physical properties of sulphur hexafluoride (SF_6)

Diffusion coefficient of SF_6 in water ($m^2 \cdot s^{-1}$) (King and Saltzman, 1995):

$$D_{SF_6} = 2.9 \cdot 10^{-6} \cdot e^{1.93 \cdot 10^{-4} / \mathcal{R} \cdot T_K} \tag{E.9}$$

where: $\mathcal{R}$ = ideal gas constant (8.31441 $J \cdot mol^{-1} \cdot K^{-1}$) and T_K = temperature (K).

$$\mathbf{Sc}_{SF_6} = 3016.1 - 172.00 \cdot T + 4.4996 \cdot T^2 - 0.047965 \cdot T^3 \tag{E.10}$$

where: **Sc** = Schmidt number and T = temperature (°C).

Additional information concerning SF_6 (Watson and Liddicoat, 1985)

- The atmospheric background concentration is 2 ppt.
- The increase of SF_6 in atmosphere is 0.1 ppt/yr.

F Curriculum Vitae

6 Januari 1969	Born in Heerjansdam, The Netherlands
1975–1981	Primary school in Heerjansdam
1981–1987	Secondary school in Zwijndrecht
1987–1993	Chemical Engineering at the Delft University of Technology. Specialisation in bioprocess technology. Graduation thesis on the 'Dynamics of Nitrifying Biofilms in the Biofilm Airlift Suspension Reactor'
1993–1994	project co-worker in the Norwegian firm 'EnviroNor.' Development of a process for the cleansing of heavy metal polluted drainage water from old mines with sulpate reducing bacteria
1995	project co-worker at the Shell Laboratories in Rijswijk, The Netherlands
1996–2000	Doctoral studies the the Swiss Federal Institute of Environmental Science and Technology (EAWAG) in Dübendorf, Switzerland and the Swiss Federal Institue of Technology Zurich (ETHZ), Switzerland.

Seite Leer /
Blank leaf

Nomenclature

VARIABLES

a	empirical exponent	(-), page 15
a	specific exchange surface area	($m^2 \cdot m^{-3}$), page 12
A_{cr}	cross sectional area	(m^2), page 16
A_f	wetted biofilm area	(m^2), page 12
$a_{reaer.}$	proportionality constant of the reaeration equation (7.30)	(-), page 80
A_{shaft}	area of the shaft in the horizontal plane	(m^2), page 90
A_S	interfacial area	(m^2), page 70
a_f	specific biofilm area	($m^2 \cdot m^{-3}$), page 121
$b_{reaer.}$	proportionality constant of the reaeration equation (7.30)	(-), page 80
$b_{NO,Sto}$	anoxic resp. rate for X_{Sto}	(d^{-1}), page 128
$b_{NO,Aut}$	anoxic endogenous resp. rate of X_{Aut}	(d^{-1}), page 128
$b_{NO,Het}$	anoxic endogenous resp. rate of X_{Het}	(d^{-1}), page 128
$b_{O,Aut}$	aerobic endogenous resp. rate of X_{Aut}	(d^{-1}), page 128
$b_{O,Het}$	aerobic endogenous resp. rate of X_{Het}	(d^{-1}), page 128
$b_{O,Sto}$	aerobic resp. rate for X_{Sto}	(d^{-1}), page 128
c	proportionality constant	(-), page 72
c_2	system constant	($s^{1/2} \cdot m^{-1}$), page 72
$c_{b,g}$	gas-phase bulk concentration	($kg \cdot m^{-3}$), page 71
$c_{b,l}$	liquid-phase bulk concentration	($kg \cdot m^{-3}$), page 70
c_l^*	equilibrium concentration of solute in liquid phase	($kg \cdot m^{-3}$), page 70
$\mathbb{D}_{O,f}$	biofilm oxygen diffusion	($m^2 \cdot s^{-1}$), page 53
D	pipe diameter	(m), page 15
d_{max}	maximum water depth	(m), page 16
d_{mean}	mean water depth	(m), page 13
$d_{p,i}$	penetration depth	(m), page 122
Da	Dalton, unit of mass, equal to $1/12$ the mass of the carbon-12 atom	(-), page 60
$d_{endlevel}$	water height at the end of the section	(m), page 92
E_x	axial dispersion coefficient	($m^2\ s^{-1}$), page 14
E_y	lateral dispersion coefficient	($m^2\ s^{-1}$), page 14
f	friction factor, calculated after Prandtl-Colebrook	(-), page 15
$f_i(p)$	calculated value corresponding to a data point	, page 169
$F_{COD,diss.}$	dissolved COD-load at the section start	($kg_{COD} \cdot d^{-1}$), page 107
$F_{COD,tot.}$	total COD-load at the section start	($kg_{COD} \cdot d^{-1}$), page 107
$f_{meas,i}$	the measured value corresponding to a data point	, page 169
f_{X_i}	fraction of total COD	(-), page 125
g	gravitational acceleration = 9.81	($m \cdot s^{-2}$), page 15
g_z	gravitational acceleration in the flow direction	($m \cdot s^{-2}$), page 17

h	water depth	(m), page 14
H_g	Henry coefficient related to gas phase	($Pa \cdot m^3 \cdot mol^{-1}$), page 70
H_l	Henry coefficient related to liquid phase	$(kg \cdot m^{-3})_{gas}/(kg \cdot m^{-3})_{liquid}$, page 70
h_{offset}	distance between channel insert and outlet	(m), page 87
J_i	flux of compound i into the biofilm	($g \cdot m^{-2} \cdot d^{-1}$), page 121
k^*	dimensionless wall roughness	(-), page 15
K_2	stream reaeration	(s^{-1}), page 71
$k_l a$	reaeration coefficient	(s^{-1}), page 12
k_l	liquid-phase mass transfer velocity	($m \cdot s^{-1}$), page 12
k_s	equivalent sand roughness	(m), page 15
k_{att}	specific attachment rate	(d^{-1}), page 124
k_{det}	specific detachment rate	($g \cdot m^{-5}$), page 124
k_g	gas-phase mass transfer velocity	($m \cdot s^{-1}$), page 70
K_i	half-saturation constant of component i	($g \cdot m^{-3}$), page 121
$k_l^{\mathbf{Sh}}$	k_l based on the Sherwood number	($m \cdot s^{-1}$), page 72
$K_{O,f}$	biofilm oxygen half saturation constant	($g_{O_2} \cdot m^{-3}$), page 53
$k_{o,l}$	overall mass transfer velocity related to the liquid-phase	($m \cdot s^{-1}$), page 70
k_H	hydrolysis rate constant	($g_{S_S} \cdot g_{X_{Het}} \cdot d^{-1}$), page 128
K_{NO}	saturation constant for S_{NO}	($g_{NO_3^- - N} \cdot d^{-1}$), page 128
K_O	saturation constant of S_O for X_{Het}	($g_{O_2} m^{-3}$), page 128
$K_{O,Aut}$	saturation constant of S_O for X_{Aut}	($g_{O_2} m^{-3}$), page 128
K_S	saturation constant for S_S	($g_{COD} \cdot d^{-1}$), page 128
K_{Sto}	saturation constant for X_{Sto}	($g_{X_{Sto}}$), page 128
k_{Sto}	storage rate constant	($g_{S_S} \cdot g_{X_{Het}} \cdot d^{-1}$), page 128
K_X	hydrolysis saturation constant	($g_{X_S} \cdot g_{X_{Het}}$), page 128
L	characteristic length	(m), page 72
L_f	biofilm thickness	(m), page 121
l_l	length scale for lateral mixing	(m), page 13
l_v	length scale for vertical mixing	(m), page 13
L_f^*	dimensionless biofilm thickness	(-), page 121
$L_{sect.}$	section length	(m), page 13
L_0	reference channel length	(m), page 14
m	exponent of $\mathbf{Re}^*$	(-), page 75
M_x	molecular mass of the solute	($g \cdot mol^{-1}$), page 71
m_x	weight of a flask where x is: e =empyt, b = with biofilm, f =full	(g), page 160
$m_{X_{S^0}}$	initial concentration of elementary sulphur	($mol_S \cdot m^{-3}$), page 125
$\widehat{M_i}$	input variable	, page 107
M_i	amount of a particulate species i on the surface	($g \cdot m^{-2}$), page 123
$\widehat{M_{i,j}}$	randomised value of input variable M_i	, page 107
M_{TSS}	amount of TSS on the surface	$g \cdot m^{-2}$, page 123
MW_S	molecular weight of sulphur	$g \cdot mol^{-1}$, page 123
M_{X_X}	amount of bacterial biomass X_X on the surface	($g_{COD} \cdot m^{-2}$), page 121
$M_{X_X}^{active}$	fraction of active biomass	($g_{COD} \cdot m^{-3}$), page 121
n	constant which depends on the turbulence level at the interface	(-), page 72
p	$= (p_1 \cdots p_m)$, the array of m parameters	, page 169
P_w	wetted perimeter	(m), page 15

p_x	partial pressure of a solute in the atmosphere	(Pa), page 71
$p^*_{H_2O}$	Partial pressure of water in water saturated air	(Pa), page 174
Pr	Probability	(%), page 40
$\overline{Q}$	average discharge	($m^3 \cdot s^{-1}$), page 12
Q	discharge	($m^3 \cdot s^{-1}$), page 12
Q_{DW}	dry weather discharge	($L \cdot s^{-1}$), page 35
$Q_{gw,inf}$	groundwater infiltration	($m^3 \cdot s^{-1}$), page 12
$q^{max}_{S_i}$	max. specific substrate uptake rate	($g_S \cdot g_X{}^{-1} \cdot d^{-1}$), page 121
$\sum r_O$	the sum of the oxygen fluxes in the mass balance	($kg \cdot d^{-1}$), page 107
r	pipe radius	(m), page 16
r	random replacement times at a mean frequency	(s^{-1}), page 74
r^2	correltation coefficient	(-), page 67
$r^{att}_{X_i}$	attachment rate of any particle j	($g \cdot m^{-3} \cdot d^{-1}$), page 124
R_h	hydraulic radius	(m), page 15
$r''^{meas}_{O,f}$	measured biofilm oxygen uptake rate per surface area	($g_{O_2} \cdot m^{-2} \cdot d^{-1}$), page 53
$r''_{O,f}$	biofilm oxygen uptake rate per surface area	($g_{O_2} \cdot m^{-2} \cdot d^{-1}$), page 12
$r^{bal}_{O,f}$	biofilm activity determined with the oxygen balance	($kg \cdot d^{-1}$), page 109
$r_{O,w}$	conversion rate by suspended biomass	($g_{O_2} \cdot m^{-3} \cdot s^{-1}$), page 12
$r_{O,m}$	oxygen mass transfer rate	($kg \cdot m^{-3} \cdot s^{-1}$), page 72
$r^{meas}_{O,f}$	measured biofilm activity	($kg \cdot d^{-1}$), page 110
$r^{meas}_{O,w}$	measured wastewater activity	($kg \cdot d^{-1}$), page 110
r_i	consumption rate of substrate i	($g \cdot m^{-3} \cdot d^{-1}$), page 121
$r^{det}_{X_i}$	detachment rate of i	, page 123
S^*_i	dimensionless limiting substrate concentration	(-), page 121
S_0	sewer slope	($m \cdot m^{-1}$), page 77
S_i	concentration of compound i	($g \cdot m^{-3}$), page 12
S^f_i	substrate concentration in the active layer of the biofilm	($g \cdot m^{-3}$), page 121
$s_{meas,i}$	standard deviation of $f_{meas,i}$	, page 169
$S_{O,gw}$	groundwater oxygen concentration	($g_{O_2} \cdot m^{-3}$), page 12
S_O	oxygen concentration	($g_{O_2} \cdot m^{-3}$), page 12
S^*_O	oxygen saturation concentration	($g_{O_2} \cdot m^{-3}$), page 12
$S^{surf.}_O$	oxygen concentration at the biofilm surface	($g_{O_2} \cdot m^{-3}$), page 53
S^{base}_O	oxygen concentration at the base of the biofilm	($g_{O_2} \cdot m^{-3}$), page 53
S_f	friction slope	($m \cdot m^{-1}$), page 14
S^s_i	concentration of component i on the biofilm surface	($g \cdot m^{-3}$), page 122
$r^{chemox}_{S^{2-}_{tot}}$	chemical oxidation rate of sulphide	($mol \cdot m^{-3} \cdot d^{-1}$), page 118
S_{tot}	total sulphide concentration	($mol \cdot m^{-3}$), page 118
T	temperature	(°C), page 75
T_K	absolute temperature	(K), page 70
T_m	measurement temperature	(°C), page 53
T_{ref}	reference temperature	(°C), page 75
t	time	(s), page 12
T_{sin}	wave period of sinusoidal perturbation	(s), page 14
u	velocity	($m \cdot s^{-1}$), page 77
u^*	shear velocity	($m \cdot s^{-1}$), page 13
$\bar{u}$	average velocity	($m \cdot s^{-1}$), page 12

$\bar{u}_x$	cross-sectional average axial velocity	($m \cdot s^{-1}$), page 15
V	volume	(m^3), page 71
V_{dead}	dead volume in a reactor	(m^3), page 30
V_{flask}	measuring flask volume	(mL), page 160
V_{water}	amount of demineralised water added	(mL), page 160
w	surface width	(m), page 12
x	longitudinal coordinate	(m), page 12
X_i^f	biomass concentration active for component i in the biofilm	($g \cdot m^{-3}$), page 121
X_{part}	particulate fraction ($>$ 0.7μm) of total wastewater COD	($g_{COD} \cdot m^{-3}$), page 103
X_X	biomass concentration where subscript X indicates the type of biomass: Het, Aut etc.	($g_{COD} \cdot m^{-3}$), page 54
z_f	distance from the biofilm substratum	(m), page 122
Z_j	vector of random numbers with a standard normal distribution	, page 107

GREEK SYMBOLS

α	angle between water surface and vertical line through pipe center	(rad), page 16
$\alpha_{k_l a}$	ratio of $k_l a$ under practical conditions to that in clean water	(-), page 72
β	ratio of solubility under practical conditions to that in clean water	(-), page 72
$\beta_{T,Het}$	temperature coefficient for heterotrophic growth	(-), page 173
Γ	empirical resistance coefficient	($m^a \cdot s^{-1}$), page 15
γ	biomass density in biofilm	($g_{COD} \cdot m_f^{-3}$), page 53
$\overline{\Delta}$	the average difference between points of two pollutographs	($g_x \cdot m^{-3}$), page 40
Δh	water level change	($m \cdot s^{-1}$), page 90
δ	boundary layer thickness	(m), page 32
δ_c	depth of concentration boundary layer	(m), page 122
Δ	difference between all 'out' and all 'in' terms	($kg_{O2} \cdot d^{-1}$), page 105
ε	near-surface turbulent energy dissipation rate	($J \cdot s^{-1}$), page 74
η	dynamic viscosity	(Pa·s), page 15
$\eta_{\mathbb{D}}$	factor describing biofilm diffusion reduction or enhancement	(-), page 121
η_f	effectiveness factor for the biofilm activity	(-), page 121
η_{NO}	the anoxic reduction factor for growth	(-), page 126
θ	exponential temperature coefficient	(-), page 75
$\iota_{k,i}$	matrix with the composition of the compounds in the model	(...), page 127
μ_{Aut}^{max}	autotrophic max. growth rate	(d^{-1}), page 128
$\mu_{Het,f}^{max}$	max. specific growth rate of heterotrophic biofilm biomass	($g_{COD} \cdot g_{COD}{}^{-1} \cdot d^{-1}$), page 53
μ_{Het}^{max}	maximum heterotrophic growth rate	($g_{COD} \cdot g_{COD}^{-1} \cdot d^{-1}$), page 13
$\mu_{Het}^{max,T=T}$	maximum heterotrophic specific growth rate at T	($g_{COD} \cdot g_{COD}^{-1} \cdot d^{-1}$), page 173
ν	kinematic viscosity = η/ρ	($m^2 \cdot s^{-1}$), page 15
$\nu_{j,i}$	stoichiometric coefficient for compound i and process j	(-), page 121
ν_O	stoichiometric parameter for oxygen	($g_{O_2} \cdot g_{COD}{}^{-1}$), page 53
ρ	liquid density	($kg \cdot m^{-3}$), page 15
σ	the standard deviation based on a sample	(-), page 40
$\widehat{\sigma_{M_i}}$	estimated (relative) standard deviation for the variable M_i	, page 107
$\widehat{\sigma_{OB}}$	estimated absolute standard deviation of the oxygen balance	($kg \cdot d^{-1}$), page 107
$\hat{\tau}$	dimensionless wave period of unsteady flow	(-), page 14
τ_c	time constant for reactions	(d), page 13

τ_f	standard biofilm depth dimension	(m), page 121
τ_{min}	minimal shear stress under dry weather conditions	($N \cdot m^{-2}$), page 123
τ_r	residence time	(s), page 12
τ_w	average wall shear stress	($N \cdot m^{-2}$), page 17
ϕ	biofilm modulus	(-), page 121
$\phi^{meas}_{COD,diss}$	flux of dissolved COD	($kg \cdot d^{-1}$), page 110
$\phi^{meas}_{COD,tot}$	flux of total COD	($kg \cdot d^{-1}$), page 110
ϕ_m	mass flux across interface	($kg \cdot s^{-1}$), page 70
ϕ_O	oxygen flux	($kg_{O_2} \cdot d^{-1}$), page 12
ξ	fill grade of the channel	(-), page 18

DIMENSIONLESS NUMBERS

Fr	Froude number: ratio of inertial and gravitational forces in fluid motion	(-), page 77
$\mathbf{Fr}_0$	steady uniform Froude number	(-), page 14
Re	Reynolds number: ratio of inertial force to viscous force	(-), page 15
Re*	shear Reynolds number	(-), page 73
Sc	Schmidt number: ratio of mass transport by turbulence and by diffusion	(-), page 72
Sh	Sherwood number: ratio of overall mass transfer to the molecular diffusivity	(-), page 72

SUB-, SUPERSCRIPTS AND OTHERS

Aut	Autotrophic biomass	, page 9
CWW	centrifuged wastewater	, page 55
$\mathbb{D}$	diffusion coefficient	($m^2 \cdot s^{-1}$), page 72
DOC	Dissolved Organic Carbon, here defined as < 0.7 µm	($g_C \cdot m^{-3}$), page 102
DO	Dissolved Oxygen	($g_{O_2} \cdot m^{-3}$), page 100
f_T	temperature factor for k_l	(-), page 75
Het	heterotrophic biomass	, page 54
i	compound	, page 121
j	process	, page 121
k	conservative	, page 127
PE	People Equivalents	, page 45
$\mathcal{R}$	ideal gas constant = 8.31441	($J \cdot K^{-1} \cdot mole^{-1}$), page 70
RW	river water	, page 55
S_S	easily degradable substrate	($g_{COD} \cdot m^{-3}$), page 42
SS_{res}	residual sum of squares	, page 97
SOB	sulphur oxidising biomass	, page 59
SRB	sulphur reducing biomass	, page 59
TSS	total suspended solids	(g), page 23
TVS	total volatile solids	(g), page 23
$\sum F_O$	the sum of a (redundant) oxygen balance	($kg \cdot d^{-1}$), page 107

Index

S_S, 45, 167
α, 16, 20
α-glucosidases, 151
$\alpha_{k_l a}$, 71, 78, 92
β-glucosidases, 151
MOUSETRAP, 113
MOUSE, 113
AQUASIM, 54, 125, 131
  description, 169
  river section compartment, 169
in situ flow cell, 31, 53
  chamber design, 154
  operation, 155
  results, 53, 54
χ^2-criterion, 169
H_2S, 58

abrasion, 10, 46, 55, 65
Activated Sludge Model No. 3, *see* ASM 3
additional oxygen balances, 107
alkalinity, 40, 43, 115, 159
allylthiourea, 167
ammonium, 8, 165
  conversion, 42
analysis
  nitrogen Components, 161
anions
  analysis, 161
ASM 2, 126
ASM 3, 45, 60, 65, 113–135
  denitrification, 126
  hydrolysis, 124
attachment, 113, 124, 138
  rate equation, 124
ATU, 126, 167
autosamplers, 38

benthic activity measurement, 30
BFC-system, *see* biofilm flow cell
biofilm
  in situ respiration, 104, 106
in situ activity measurement, 30, 154–156
aerobic activity, 53
attachment, 124
biomass, 115
COD, 67
denitrification, 8, 65
density measurement, 160
detachment, 123
distribution, 10, 16
enzyme activity, 151
erosion, 6, 10, 102, 103, 106, 111, 123
erosion, rain event, 51
flow cell, 33–34, *see* biofilm flow cell, 156–157
growth & decay, 10
growth and activity, 50
heterotrophic activity, 125
hydrolysis, 45
hydrolysis measurement, 62
in sewer, 6
morphology, 6, 46
nitrification, 8
overall activity, 30
plate material, 25
properties, 67
sampling, 22
sampling of intact biofilm, 24
sampling with 'biofilm box', 24
sampling with sewer balloon, 23, 160
SEM photo, 6, 46
spatial distribution, 9
storage material, 57
substratum, 25, 31, 122, 153
suspended, 125
  denitrification, 126
  nitrification, 126
total suspended solids, 160
total volatile solids, 160
TSS, 67

TVS, 67
wetted area, 16
biofilm flow cell, 25, 62, 64, 66, 67, 167
biofilm respiration, 107
biological model, 115
biomass
temperature dependency, 173
biomass load, 103
boundary layer, 53, 72, 85, 120, 122, 131, 138
mass transfer models, 72
bromide, 36, 81, 82, 105
bursts, 17, 75, 97

catastrophic events, 10
centrifuged wastewater, 54
Chemical Oxygen Demand, see COD, 161
ciliates, 10
COD
analysis, 161
conversion, ii, 8, 42, 110
degration, ii
dissolved, 42
total, 42
conversion
COD
sewer, aerobic, 109
current problems, 1

Darcy-Weisbach equation, 15
denitrification, 8, 11, 42, 45, 65, 122, 125, 126, 157
dense undercurrent, 20, 39, 42
dentrification, 110
quantification, 66
detachment
rate equation, 123
deterministic sewer model, 113
diffusive wave, 14, 115
discharge, 22
dispersion, 22, 81, 82
axial, 14
lateral, 13
numerical, 92
dissolved oxygen, 43
diurnal variation, 101
wastewater respiration, 101

DO, 43, 100
DOC, 60, 101
Doppler Ultrasound, 27
dry weather flow, 107

easily degradable substrate, *see* S_S
effectiveness, 120–122
elementary sulphur, 43, 58, 125
empirical equation, 14, 75
empirical resistance coefficient, 15
endogenous respiration, 120
enzyme activity, 151
equivalent sand roughness, 15
erosion, 10, 138
esterases, 152

fast sampling, 42, 81
Fe-sulphur cycle, 9
FIA, 161
film theory, 75, 97
FISH, 9, 58, 119
flow equations, 14
flow measurement, 87
dilution method, 27
Doppler ultrasound, 27
friction factor, 15
friction slope, 14
Froude number (**Fr**), 14, 78
full scale experiments
gas exchange, 93
full-scale experiment
in situ sewer biofilm respiration rate, 53
biofilm erosion, 51
continuous wastewater respiration, 101
gas exchange calibration experiments, 85
sewer oxygen balance, 99
sewer residence time, 36
substrate limitation, 64
wastewater composition changes, 38
full-scale experiments
additional oxygen balances, 107

gas exchange, 69–98, 114
'Verbindungskanal', 87
'Schwamendinger Dorfbach', 86
calibration experiments, 85
conversion, 82

direct method, 80
empirical equations, 77
full scale experiments, 93
indirect method, 80
measurement methods, 80
modelling calibration experiment, 91
new reaeration equation, 80
stream reaeration, 77
sulphur hexafluoride, 81
temperature influences, 75
gas exchange measurements
comparasion with literature data, 93
gas-liquid mass transfer, 70
boundary layer models, 72
length scales, 73
Sherwood number, 72
turbulence, 73
water quality, 71
glycogen, 45, 57
goals, 1
goodness of fit, 169
grazing, 10
groundwater infiltration, 43, 82, 90, 97, 99, 105, 107

heterotrophic biomass, 8, 9, 13, 103, 114, 116, 125, 128
hydraulic radius, 15
hydrodynamic model, 115
calibration, 115
hydrodynamics, 13
Saint Venant equations, 14, 115
secondary currents, 17, *see* SC
shear stress distribution, 17
velocity distribution, 17
hydrogen sulphide, 8, 11, 58, 138, 158
hydrolysis, 10, 42, 45, 57, 116, 124, 128
enzyme quantification, 61
measurement, 60
modelling, 124
sewer biofilm, 62

ideal gas constant, 174
in situ
area to volume ratio, 32
in-line data, 132
in-line measurements, 26
sensor calibration, 27
sensor protection, 26
ionchromatography, 161

kinematic viscosity, 15
kinematic wave, 14
krypton, 80, 81

longitudinal oxygen variations, 100

mass transfer models, 72
surface renewal, 74
mass transfer velocity
gas-phase, 70
liquid-phase, 12, 70
material and methods, 21–34, 151–162
methane, 82
methane producing bacteria, 117
production by sewer biofilm, 58
methanogenic bacteria
in sewer biofilm, 58
methodology, 2
model, 113–135
activity incoming wastewater, 132
biofilm thickness, 123
calibration, 131, 132
dynamic, 13
goals, 114
hydrodynamic, selection, 13
parameter identification, 125
recommendations, 135
results, 125
results wastewater, 125
sulphur cycle, 126
validation, 131, 132
validation w. inline data, 134
wastewater biomass, 115
Monte Carlo simulation, 106

NH_4^+
analysis, 161
nitrate, 101, 118, 122
conversion, 40
nitrate respiration, 42, 102
nitrification, 8, 42, 101, 114, 116, 125, 126, 128, 165
nitrifiers, 126
nitrite

conversion, 42
nitrogen cycle, 8
NO_2^-
analysis, 161
NO_3^-
analysis, 161

open channel hydrodynamics, *see* hydrodynamics
OUR, 28, 33, 54, 59, 63, 66, 67, 100, 109, 131
data, 132
outline, 2
oxygen
longitudinal variations, 100
physical properties, 173
sewer balance, 12
oxygen balance, 132

parameter identification, 125
particles, 46, 48, 51, 57, 64, 83, 101, 113
addition, 64
attachment and erosion, 114
PC, 25, 153
penetration depth, 58, 113, 135
penetration theory, 75, 97
PET, 154
PHA, 45
PHB, 57
phosphate
conversion, 42
physical properties
oxygen, 173
sulphur hexafluoride, 174
pipe radius, 16
polycarbonate, 25, 153
polyetheneteraphthalate, 153, 154
Polypropylene, 153
PP, 153
Prandtl-Colebrook equation, 15
proteins, 8

rain event, 51
biofilm erosion, 51
reaeration, 70
reaeration equation, 77
parameter estimation, 97
Remigen–Villigen, 36
residence time, 22, 115, 185
residual sum of squares, 97
respiration activity, suspended biomass, 27
respiration measurement
biomass growth, 100
continuous, 101
respiration rate measurement
biofilm, 53
biomass load, 103
wastewater, 100
Reynolds number, 72
Reynolds number (**Re**), 15, 72, 122
Rhodamine, 22
rhodamine, 81, 157
Rumlang–Oberglatt, 35

Saint Venant equations, 14, 135
salt, 22, 36, 64, 157
sampling
autosamplers, 38
conclusions field sampling, 43
fast, 21
manual, 39
sample quantity, 22
sewer balloon, 23
synchronisation, 21, 81
SC, 17, 46
Schmidt number (**Sc**), 72, 74, 81, 97, 174
secondary currents, *see* SC
SEM, 46, 119
photo, 6, 46, 47
sewer
as reactor, 11
biomass load, 103
denitrification, 65
history, 3
mass balance, 12, 99
residence time, 36
substrate limitation, 64
system description, 4
trickling filter comparison, 56
sewer balloon, 23, 52
sewer biofilm, 6
longitudinal distribution, 48
processes, 8
radial distribution, 46
sewer model, 169

implementation, 125
kinetic constants, 128
stoichiometric matrix, 130
stoichiometric parameters, 129
sewer model structure, 114
sewer oxygen balance, 99–111
data collection, 104
results, 105
validation, 103
SF_6, *see* sulphur hexafluoride
shear Reynolds number (**Re***), 73–75, 80, 97
shear stress, ii, 10, 11, 17, 18, 20, 46, 50, 123
distribution, 17
shear velocity, 15
Sherwood number (**Sh**), 72, 122
site description, 35
sloughing, 10
SOB, 59, 116, 118, 129
interactions with SRB, 118
SRB, 59, 116, 117, 119, 127, 129
interactions with SOB, 118
stoichiometric matrix, 127, 170
storage material, 57, 62, 68, 137
substrate
easily degradable, *see* S_S
sulphide oxidation, 119, 125
sulphur cycle, 8, 43, 58, 113, 117, 126
activity measurement, 59
sulphide oxidation, 118
sulphur reduction, 117
sulphur pool, 119
sulphur hexafluoride, 70, 81
addition, 157
additional information, 174
analysis, 158
biofilm absorption, 83
experimental procedure, 82
Henry coefficient, 83
physical properties, 174
pulse or step addition, 83
sampling, 158
sewer measurements, 93
sulphur oxidising bacteria, *see* SOB
sulphur reducing bacteria, *see* SRB
sulphur reduction, 117, 118, 125
chemical, 118
surface reaeration, 12, 106
surface reaeration rates, 105
suspended biomass, 27
symbiosis, 119

total COD, 5, 40, 42, 123, 125
tracer, 105, 115
addition, 157
dispersion, 82
gas, 80
inert salt, 81
krypton, 80
methods, 21
radioactive, 81, 82
trickling filter, 11, 45, 56
biofilm, 56
trickling filter biofilm, 56
tritium, 81
TSS, 23, 24, 45, 46, 48, 53, 123, 160
turbulence, 17, 18, 24, 29, 32, 39, 48, 70, 73
TVS, 23, 24, 45, 46, 48, 53, 160

urea, 8
analysis, 161
hydrolysis, 42, 131, 165

volatile organic compounds (VOC), 69

wall roughness, 36, 115
wastewater
age, 37
composition, 5
measurement of changes, 38
wastewater respiration, 100
diurnal variation, 101
wastewater respiration rate measurement
batchwise, 28
continuous, 28
water
partial pressure, 174
wetted perimeter, 15
WWTP, 1, 11, 21, 22, 27, 57, 114, 128